8C

Foundation Performance of a Tower Silo

by

Getahun Haile, B.A.Sc (Cum Laude)

University of Ottawa (1975)

Thesis submitted to the School of Graduate Studies in partial fulfillment of the requirements for the degree of Master of Applied Science in Civil Engineering.

Department of Civil Engineering

University of Ottawa

Ottawa, Canada, 1977

to my parents and the people of Ethiopia

ABSTRACT

A large rigid circular raft has been instrumented to study its foundation performance in the Leda Clay of the Ottawa region. The raft which supports a tower farm silo has a diameter of 13.7 m (45 ft) and a thickness of 1 m (3.28 ft). Comprehensive laboratory and field measurements were performed. All the laboratory tests including, CIU triaxial and oedometer, as well as the field vane shear strength tests were carried out by the staff of NRC, DBR. The other measurements which included: normal contact pressure distributions, settlement and pore-water pressures at various depths and the deflection of the raft were carried out by the University of Ottawa in cooperation with NRC, DBR.

The measurements have been analyzed and where possible the results of the analysis compared to theory and to case records. In addition, the load settlement data for six square footings and four test plates also in Leda Clay, have been analyzed; and the results compared to those for the silo raft. The plate and footing measurements were carried out by the Geotechnical Group of the University of Ottawa at Algonquin College, Woodroffe Campus, in Ottawa.

The outcome of the research programme includes the following: a) recommended ranges of E_u/S_u values applicable to most foundation elements founded in Leda Clay of the Ottawa area; b) settlement distribution curves which appear to be a characteristic of the clay, and c) design recommendations concerning normal contact pressures and

the modulus of subgrade reaction. All the above recommendations apply when the soil is loaded below its preconsolidation stress.

Finally, a list of suggestions for further research work is brought forward.

ACKNOWLEDGEMENTS

The author is indebted to all those who have helped directly or otherwise in the preparation and the completion of this project. Of all a very special thanks is extended to Dr. J. D. Scott, Professor and Thesis Advisor, for his guidance. His invaluable advice and deep interest in the project are very much appreciated.

Dr. M. Bozozuk, Research Officer with the National Research Council, Division of Building Research (NRC, DBR), also a project advisor is thanked for making the field and laboratory soil test results and the photographs available.

Thanks are also due to Dr. D. H. Shields for making me interested in geotechnical engineering through his lectures and to Dr. A. P. S. Sèlvadurai for his suggestions.

The owners of Carl Fraser and Sons Ltd. are thanked for their cooperation in the project.

The assistance of Mr. R. Moore, in the instrumentation and data collection is greatly appreciated. Mr. A. Laberge, senior technician at NRC, DBR is to be thanked for his help and cooperation throughout the project.

Miss Lise Jerome, a real friend, is thanked for her continual encouragement, for reading and typing most of the first draft. Also, the comments of Mr. Hussien Abu-Sitta, who read the first draft, are greatly appreciated.

The author is extremely grateful to Mrs. Wanda Storto who so expertly did the typing of the final draft.

The financial assistance of the Ministry of Agriculture and Food of Ontario and Ontario Harvestore Systems Ltd. is greatly acknowledged.

TABLE OF CONTENTS

LIST OF FIGURES

Figure		Page

LIST OF TABLES

SYMBOLS

LATIN LETTERS

A = Pore-water pressure coeffient.

B = Pore-water pressure coefficient.

c = Cohesion.

C_o = Coefficient.

D = Depth to founding level.

E_c = Elastic modulus of concrete.

E_f = Elastic modulus of footing.

E_H = Elastic modulus in the horizontal direction.

E_s = Elastic modulus of soil.

E_u = Undrained modulus of clay.

E_v = Elastic modulus in the vertical direction.

F_2 = Adhesion factor (function of Poisson's ratio).

f = Initial shear stress ratio.

H = Layer depth also layer thickness.

I_p = Settlement influence factor (elastic theory).

K = Stiffness coefficient.

K_o = Coefficient of earth pressure at rest.

k = Modulus of subgrade reaction.

$\overline{K}_z, K_\theta, K_r$ = Ratios of vertical, tangential and radial stresses to average stress.

k_1 = Subgrade modulus for a test plate.

m_f = Poisson's number for footing = $\frac{1}{\nu_f}$

m_s = Poisson's number for soil = $\frac{1}{\nu_s}$

m_v = Coefficient of volume compressibility $(\frac{mm^2}{kN})$.

$\overline{M}_z, \overline{M}'_z$ = Functions for calculating elastic settlement.

N_c, N_q, N_γ = Bearing capacity factors.

$p(r)$ = Contact pressure distribution.

P or P_1 = Concentrated load.

Q = Total footing load = average pressure times area.

q or q_a = Average applied pressures (allowable).

q_{ep} = Elasto-plastic stress at the edge of footing (Zeevaert's notation).

q_u = Ultimate bearing pressure.

q_y = Foundation pressure to cause first yield.

R = Radius.

R_e = Equivalent radius for rectangular footing.

r = Distance measured from the centre of a circular footing.

r_1 = Distance measured from the centre of footing to the point of transition from elastic to plastic contact pressure.

s = Shear strength of soil, also total settlement.

S_w = Weighted vane shear strength.

S_u = Shear strength from field vane, also initial settlement.

$\overline{S}_u$ = Arithmetic average of vane shear strength for undrained settlement.

T = Total load (plastic portion).

t = Thickness of foundation.

u = Pore-water pressure.

U = Degree of consolidation.

V = Total load (elastic portion).

w	= Elastic settlement.
y	= Notation used for settlement in the theory of subgrade modulus.
z	= Any depth below foundation.

GREEK LETTERS

β	= Ratio of depth to radius (z/R).
γ_1	= Unit weight of soil above founding level.
γ_2	= Unit weight of soil below founding level.
δ	= Elastic settlement.
ε	= Strain.
η	= Ratio of stress anisotropy.
ξ	= Ratio of radial distance to radius of raft (r/R).
κ_1	= Shape factor (bearing capacity equation).
κ_2	= Depth factor (bearing capacity equation).
μ	= A semi-empirical correction factor for 3-D effects in calculating consolidation settlement.
ν	= Poisson's ratio in general.
ν_1	= Effect of horizontal strain on horizontal strain.
ν_2	= Effect of horizontal strain on vertical strain.
ν_3	= Effect of vertical strain on horizontal strain.
ν_s, ν_f	= Poisson's ratio of soil and footing, respectively.
ρ	= Theoretical consolidation settlement.
ρ_{oed}	= Consolidation settlement from one dimensional oedometer result.
σ_1	= Major principle stress.
σ_3	= Minor principle stress.

σ'_{ho} = Horizontal effective stress.

σ'_{vo} = Vertical effective stress.

σ_r = Radial stress.

σ_z = Vertical stress.

σ_{zD} = Effective vertical stress at founding level.

σ_θ = Tangential stress.

CHAPTER 1

INTRODUCTION

1.1 Statement of Problem

Due to the relatively high cost involved, instrumentation of structures for geotechnical use has not been a routine practice. It is, however, well recognized by soils engineers and researchers that the need for instrumentation to study the actual performance of structures is growing. Today, geotechnical engineering has reached a stage where theoretical solutions based on ideal soil media can be found for most of the common design problems. The accuracy and reliability of these mathematical models can only be determined when enough field measurements reflecting the response of foundation soils to load are made.

The present state of foundation engineering is such that tower silos like any other structures can adequately be designed with respect to bearing capacity and settlement using standard techniques. However, the problem with farm silos is that the use of the standard factor of safety of 3 for bearing capacity may make the design uneconomical. This is because unlike most structures, silos can tolerate relatively large settlements both from the point of view of structural integrity and aesthetics. Most farm silos in Canada are constructed either from pre-cast concrete staves or cast-in-place concrete and are founded on circular ring footings. The live load (silage or haylage) in such structures is transferred to the subsoil in the following two modes:

1) by friction along the walls of the silo which transfers the load to the annular footing,
2) by the portion of the live load bearing directly on the ground in the annular space of the footing.

Hence to be able to use a lower factor of safety, it is important to know the proportions of the live load transfer mentioned above.

The original research proposal was to instrument a standard concrete silo with a ring foundation having a factor of safety of 3 against bearing capacity failure. Instead, the owner chose to buy a "Harvestore" metal silo which had to be founded on a large stiff raft in order to obtain the same factor of safety for bearing capacity. Therefore, the opportunity to instrument a ring foundation was not available. However, the project presented an excellent large scale model to study the performance of a rigid raft foundation in Leda Clay where the maximum soil pressure would be below the preconsolidation pressure. Such rigid circular footings have applications in the following structures; large silos, large chimneys, nuclear reactors, water towers and sometimes as column supports for buildings and bridges.

The instrumentation involved the measurement of settlements and pore-water pressures at different depths below the raft and normal contact pressures at eight different points. The differential settlement of the raft was also measured.

This thesis presents the field measurement results, analysis and discussion of some of these results and comparisons in light of previous work reported in the geotechnical literature and other sources.

1.2 Objectives of the Study

The principal objectives of the research were:

1) to analyze the compressibility of the clay at different pressure levels and depths and also to investigate the ratios of deformation modulus to the vane shear strength values at different depths and load levels and to compare these results with available data in the geotechnical literature and other sources,
2) to determine the distribution of contact pressures and to compare these with theory and measurements in the literature and other sources,
3) to show by field measurements if theoretical methods of calculating settlement give results that are in agreement with observed values.

1.3 Outline of Thesis

Following is a chapter-by-chapter summary of the content of this thesis.

CHAPTER 2 - The theory of contact stress distribution is introduced. By combining Boussinesq's elastic contact stress distribution with plastic flow along the edges, two formulae for estimating the elasto-plastic contact pressure distribution across a rigid circular raft are introduced. Moreover, other simple techniques available in the literature for estimating contact stresses are explored. Some criteria for determining the rigidity of a circular raft and the main factors that affect contact pressure distribution are presented. Finally, some case records and one of the most commonly used elastic theories known as the Winkler model or the theory of subgrade reaction for calculating contact pressures is introduced. The content of the chapter is summarized.

CHAPTER 3 - A short exposé of foundation settlement, its importance and the difficulty associated in making an accurate determination of it are presented. Some of the important factors that affect settlement are introduced. In particular important topics namely, immediate, consolidation and the critical depth of settlement are dealt with. Case records are also given. At the end, highlights of the chapter are given in a summary.

CHAPTER 4 - Given are the location of the project and the site description. A discussion of the pertinent geological history of the area with emphasis on the pleistocene geology is presented. In particular the geotechnical properties of the soil from borehole data are outlined. Also included in this chapter are descriptions of the size and geometry of the raft and that of the silo itself.

CHAPTER 5 - This chapter contains laboratory calibrations and field installation of instruments. Also, the principles on which some of these instruments work and their accuracy are discussed. The instruments include; two types of piezometers, hydraulic contact pressure cells, deep settlement gauges, bench mark and surface settlement points.

CHAPTER 6 - Here instrument readings are presented in graphical forms. Estimation of silo load from pressure cell readings and its accuracy are discussed. Variation of settlement and pore water pressures with applied load, time and depth are presented. The results of consolidated undrained (CIU) triaxial tests and oedometer tests carried out at the National Research Council, Division of Building Research Laboratory are presented.

CHAPTER 7 - Measured contact stress distributions are compared with theoretical predictions and with work by other researchers. Settlement estimates using laboratory modulus and oedometer results are calculated and their accuracy discussed. Moreover, the distribution of settlements calculated from these laboratory results are compared with the actual measured distributions. The actual settlement distribution is compared with that for other foundation elements in a similar clay deposit. The ratios of undrained modulus to average shear vane strength are calculated and compared to other calculations in similar soil. The last section presents the subgrade modulus calculation for the raft and makes comparison with other values.

CHAPTER 8 - A short summary covering the important points in the thesis is given. Furthermore, on the basis of observations and calculations performed during this study, conclusions and recommendations for further work are brought forward.

CHAPTER 2

CONTACT PRESSURE DISTRIBUTION UNDER A RIGID CIRCULAR RAFT IN ELASTIC SOIL

2.1 General

Contact pressure is the term used to describe the normal and shear stresses that exist between the bottom of a foundation and the supporting soil. The knowledge of this quantity enables foundation designers to accurately determine the shear and moments that are taken by the foundation structure. In general the contact pressure depends on:

a) the rigidity of the footing

b) the roughness of the bottom of the footing

c) the thickness of the compressible layer and its soil properties

d) the magnitude of the loading

e) the type of loading, i.e., concentrated, line or uniformly distributed

f) the size of the footing

g) the depth of the footing

Because of their relative importance factors (a) to (c) inclusive are discussed in detail in the subsequent sections of this chapter. The effect of the load intensity becomes significant only when the ultimate bearing pressure is approached; also for a circular <u>rigid</u> footing the type of loading is immaterial provided that there is no eccentricity induced. The last two factors become relevant only in the case of deep foundations with small cross-sectional area.

In this thesis shear stresses are not taken into consideration and therefore, the term contact pressure is used to denote only the normal pressure.

In order to make the theory easily understandable, a qualitative description of the shape of the contact pressure distribution for two ideal cases follows.

The discussion below assumes a smooth interface between the load and the soil, as well as an infinite medium thickness. If a flexible uniform load is applied to a perfectly elastic medium, "elastic clay", the settlement assumes the shape of a shallow bowl. This is because the vertical stress increase in the medium is higher below the centre than it is below the edges. In order to maintain a uniform settlement some of the applied load must be moved away from the centre toward the edges. This shape of load distribution which gives uniform settlement would look exactly the same as the contact pressure distribution under a rigid footing of the same loaded area (Figure 2.1.1(a)).

On the other hand if a perfectly non-cohesive dry sand is subjected to a flexible uniform load, there will be more settlement at the edges than at the centre. In such soils for settlement to take place relative grain movements are necessary. Since below the centre of the loaded area, the confining stress and therefore the frictional resistance against relative grain movements is higher, the

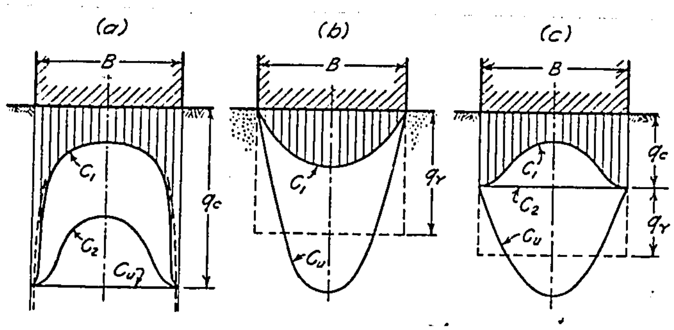

q_c, q_γ = limiting edge stress (ultimate bearing capacity)

C_1 = elastic contact pressure curve

C_2 = elasto-plastic contact pressure curve

C_u = ultimate contact pressure curve

B = size of footing

FIGURE 2.1.1 DISTRIBUTION OF NORMAL CONTACT PRESSURE ON BASE OF SMOOTH RIGID FOOTING SUPPORTED BY: (a) REAL, ELASTIC MATERIAL; (b) COHESIONLESS SOIL; (c) SOIL HAVING INTERMEDIATE CHARACTERISTICS.
(AFTER TERZAGHI AND PECK, 1948).

medium compresses less than at the edges. To make the vertical displacement uniform some of the applied load must be transferred from the edges to the centre; the resulting load distribution would be similar to the contact pressure distribution under a rigid footing resting on a medium of ideal sand (Figure 2.1.1(b)).

What happens as the load is increased indefinitely? In the first case the soil starts to yield at the edges; and as the load is increased further this plastic zone migrates to the centre until the whole area is plasticized, the pressure distribution becomes uniform and collapse impends due to plastic flow of the subgrade. In the case of a rigid footing resting on an ideal sand, however, the pressure keeps increasing at the centre but approaches zero at the edges at all load levels. Hence at failure the distribution can be approximated by a triangle with its apex below the centre of the footing. All these stages are illustrated in Figure 2.1.1

In solving practical problems, however, one has to deal with soils that are neither perfectly elastic nor purely cohesionless. Hence, one would expect real soils to behave somewhere in between the above two ideal cases. Moreover, when all the other factors that affect contact pressures are considered, the theoretical treatment of the subject for real soils becomes very complex.

However, in the past a number of mathematical models have been developed to estimate the contact pressure distribution at the base of a rigid footing on elastic soils. These theories therefore are only approximate for real soils, but are very useful for engineering applications. Some of these techniques are discussed below.

2.1.1 Effect of Rigidity on Contact Pressure

The effect of increasing the stiffness of a raft founded on an elastic soil is to increase the reaction near the edges and to decrease its value near the centre. However, the influence of raft stiffness on moments, deflections and differential settlements is more critical than its effect in altering the shape of the contact pressure distribution curves. For example, highly flexible rafts suffer excessive differential settlements, whereas very rigid ones may be subject to excessive bending moments. For the very ideal case of a circular foundation on an elastic medium of great depth, Borowicka's (1936) work shows (Figure 2.1.1.1) the variation of contact pressure distribution curves for different stiffnesses. It can be seen from the figure that for zero stiffness the pressure distribution becomes uniform and that for infinite stiffness the pressure at the centre drops to 50 percent of the average applied pressure while the value at the edges approaches infinity. However, it is discussed later in this thesis that soils have limited strength and therefore infinite edge stresses cannot exist.

2.1.2 Effect of Roughness on Contact Pressure

Except in simple cases, the effect of roughness has always been neglected in analysis of contact pressure simply because of the

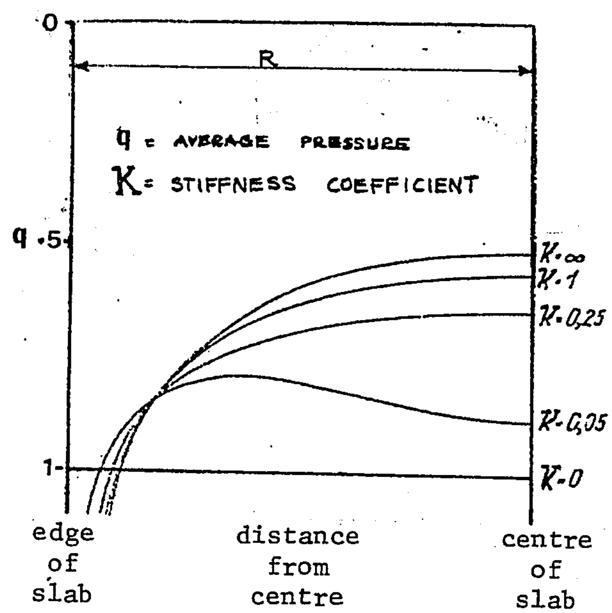

FIGURE 2.1.1.1 THEORETICAL NORMAL CONTACT PRESSURE DISTRIBUTIONS UNDER AN ELASTIC CIRCULAR SLAB WITH A UNIFORM LOAD OF 1 kg/cm^2. (AFTER BOROWICKA, 1936).

complexity of the problem. Among the few closed form solutions for foundations on elastic soil that are available, the latest is that given by Hooper (1974). The author gives equations for the normal and shear stresses on the base of foundations as functions of Poisson's ratio and a certain integration parameter. Although the evaluation of the integrals requires the use of numerical techniques like the Gaussian quadrature, the equations show that for $\nu = 0.5$ the shear stress becomes zero and the normal stress gives results similar to the elastic solutions for smooth surfaces. This conclusion is supported by works of other researchers, such as Parks (1956) and Brown (1969b). In fact according to Yamaguchi et al (1968), the contact stresses are similar for both smooth and rough surfaces for $\nu = .3$, $.4$ and $.5$. This conclusion is shown in Table 2.1.2.1. This table which contains numerical solutions of the general equation given by Hooper, shows that at the centre of the footing there is only a 2% decrease in the contact pressure when ν is increased from .375 to 0.5, which could easily be neglected for all practical purposes.

Recently, the use of the finite element technique has made the problem much simpler, since in the analysis, the shear stresses due to roughness can be introduced as simple horizontal forces at the nodes of the elements selected. Such a technique was recently used by Carrier and Christian (1973) to check the effect of roughness for homogeneous and non-homogeneous (E-linearly increasing with depth) soils. For the homogeneous case, the authors confirmed the conclusion reached by Yamaguchi et al (1968) and after checking the effect of even

Rigid punch on homogeneous half-space: computed values of $p(r)/q_a$ for adhesive contact after Spence (1973)

p	ξ							
	0	0.15	0.35	0.55	0.65	0.75	0.85	0.925
0	0.577	0.584	0.614	0.684	0.746	0.848	1.042	1.391
0.125	0.553	0.560	0.589	0.657	0.719	0.820	1.014	1.370
0.25	0.530	0.536	0.565	0.632	0.693	0.792	0.987	1.347
0.375	0.510	0.516	0.544	0.610	0.670	0.768	0.962	1.326
0.5	0.500	0.506	0.534	0.599	0.658	0.756	0.949	1.316

$\xi = r/R$

r = any distance along the radius

R = is the radius of the foundation

TABLE 2.1.2.1 Effect of Poisson's ratio on normal contact pressure distribution across a rigid circular footing (from Hooper (1974)).

lower Poisson ratios they concluded that for $\nu \geq .3$ the effect of roughness is small enough to be neglected. This effect is even smaller for the non-homogeneous case.

Another very interesting finding is that reported by Lee (1973) and quoted by Brown (1969b). He shows that for a rough footing, the moment decreases as the Poisson ratio decreases being 27% less for a rough than for a smooth footing at $\nu = 0$. Hence, for footings on saturated clays where $\nu = 0.5$ immediately after application of the load, the moment should decrease as consolidation progresses. This in effect means that it is safer to design for a smooth raft than for a rough one. Although the above finding is for a strip footing, it is believed, that circular foundations should behave similarly.

2.1.3 Effect of Compressible Layer Thickness and Soil Properties on Contact Pressure

In most cases footings are constructed on soil medium of finite thickness, underlain by a hard stratum or bedrock. By using numerical techniques and digital computers Poulos (1968) and Brown (1969a) among others have studied the effect of layer depth on contact pressures. Figure 2.1.3.1 is a result of such analysis carried out by Poulos for a Poisson's ratio of 0.4. It is easily seen that when the depth of the compressible layer approaches zero the contact pressure becomes uniform and when H/R approaches infinity, the pressure at the centre assumes 50 percent of the average pressure as expected from elastic theory. In any case the effect of layer thickness on contact pressures is only significant for shallow sediments ($H/R \lesssim 1$) as shown in the figure. Hence, for all practical purposes $H/R \gtrsim 2$ can

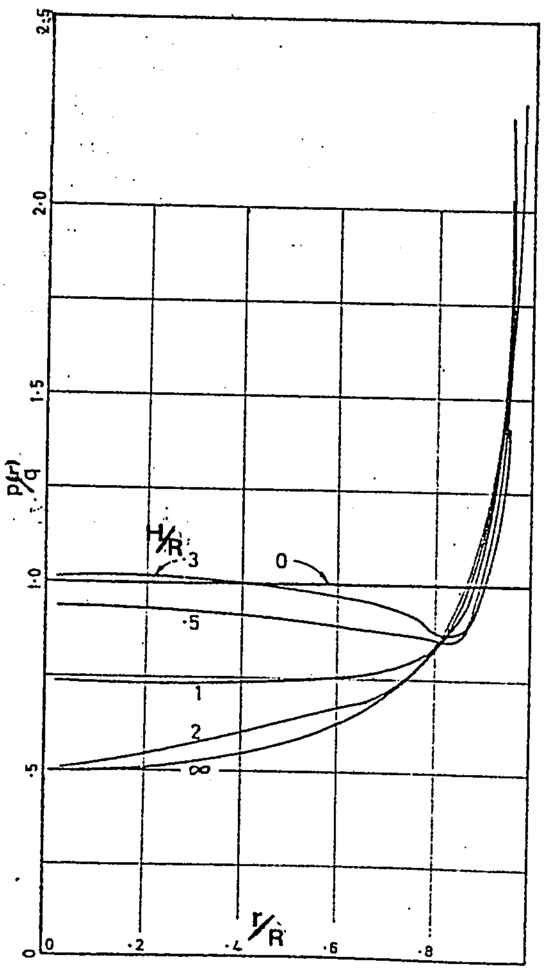

q = average pressure
p(r) = contact pressure
H = layer depth
R = radius of foundation

Figure 2.1.3.1 Effect of layer depth on contact pressure ($\nu_s = 0.4$), after Poulos (1968).

be approximated by the infinite half-space case.

Some of the factors which affect contact pressures, such as, homogeneity and the simplest non-homogeneous cases have been discussed in Section 2.1.2. The other influencing factor that requires a closer scrutiny is the Poisson ratio as related to layer thickness. Again as investigated by Poulos (1968), the effect of Poisson's ratio becomes noticeable only for shallow layer thickness, ($H/R < 1.0$). Examination of Figure 2.1.3.2 shows that at the centre the pressure increases as the Poisson ratio increases while the reverse trend is seen close to the edges. This trend is similar to the half-space case as shown in Table 2.1.2.1, however the magnitudes of the variations differ. For example, when $H/R = .3$ and $\nu = 0.5$, Poulos (1968) found that the stress at the centre is 20 percent larger than the average pressure. However, this tendency decreases as H/R is decreased approaching the uniform case for a footing resting on a hard stratum.

2.2 Criteria for Relative Rigidity of Raft

The rigidity of a circular raft depends on a number of factors. Among these are: the elastic modulus and the Poisson ratio of both the footing and the soil, the size of the footing and its thickness. For footings resting on soft normally consolidated clays one can assume a rigid case without being in any noticeable error. For the general case of a circular footing resting on any soil Equation 2.2.1 given by Hooper (1974) can safely be used to determine its relative stiffness.

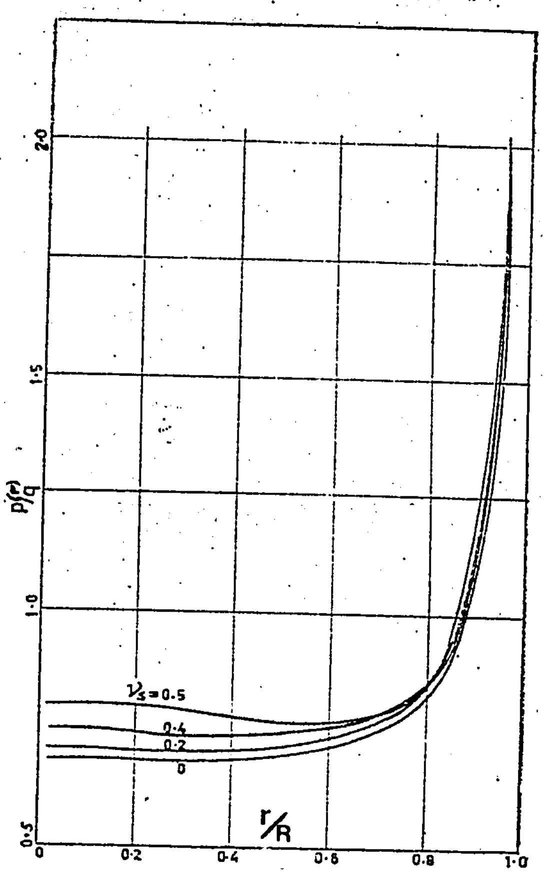

q average applied pressure
p(r) normal contact pressure
R radius of foundation
r distance from center of foundation.
H layer thickness

Figure 2.1.3.2 Effect of Poisson's ratio of layer on contact pressure distribution (H/R = 1), after Poulos (1968).

$$K = \frac{E_c(1-\nu_s^3)}{E_s} (\frac{t}{R})^3 \qquad 2.2.1$$

where E_s, ν_s represent the elastic constants of the homogeneous soil layer

E_c, t represent the elastic modulus and the thickness of the raft respectively

K stiffness

According to the author, K = 0 represents a very flexible raft whereas K ≥ 100 stands for a very rigid die. Since the formula does not include the effect of reinforcement, pretensioning and other stiffeners, the user should rely on his own judgement to decide on the final degree of stiffness of the footing in question. It is also worth noting that the elastic constants of the soil depend on the stress levels and also on the degree of consolidation. A more general solution, which takes into consideration the Poisson ratio of the footing as well as all the variables given in Equation 2.2.1, is Borowicka's (1936) result, Equation 2.2.2. To use the formula, Equation 2.2.2

$$K = (\frac{1}{6}) (\frac{m_s^2-1}{m_f^2-1}) (\frac{m_f^2}{m_s^2}) (\frac{E_f}{E_s}) (\frac{t}{R})^3 \qquad 2.2.2$$

where $m_s = \frac{1}{\nu_s}$; $m_f = \frac{1}{\nu_f}$

ν_s, ν_f = Poisson's ratio for soil and footing respectively

is first evaluated and the result compared to the contact pressures calculated for different stiffnesses which are given in Figure 2.1.1.1. For concrete, the Poisson's ratio to be used is in the range of 0.1 to 0.15.

2.3 Theoretical Methods For Estimating Contact Pressures Distribution

The simplest equation for estimating the contact pressure distribution under a rigid circular die is that defined by 2.3.1. This is the famous Boussinesq's

$$p(r) = \frac{q_a}{2(1-\xi^2)^{1/2}} \qquad 2.3.1$$

where q_a = average applied pressure

$\xi = r/R$, ratio of radial distance to the radius of the die.

solution for a smooth circular die resting on the surface of a homogeneous and isotropic elastic half-space. A close look at this equation shows that when $\xi = 0$, the contact pressure assumes a value which is 50 percent of the average pressure, whereas at $\xi = 1$, the stresses assume infinite value. However, no material including soils can withstand such infinite stresses without yielding. Hence any solution that is of practical use should take this plastic flow into consideration. Nevertheless, because of the non-linear load deformation behaviour of soils, a general elasto-plastic solution involves the integration of systems of non-linear differential equations (Shirokov et al, 1970), (Huang, 1968).

The Russians have reported success with some theories that explain the non-linear behaviour of soils. One such work is that reported by Shirokov et al (1970). In this paper the authors assume the shear deformation relationship to be non-linear while the volumetric compression of the soil occurs according to a linear relationship. Using this assumption they arrive at contact pressure and deformation equations for different soils. However, the problem with such an approach is that somehow the modulus of volumetric compression and the shear rigidity modulus have to be either estimated or evaluated in laboratories, which is not an easy task. Other elasto-plastic closed form solutions include a recent paper by Selvadurai (1976). The author uses a bi-linear elasto-plastic model. This is achieved by assuming the Winkler springs to be connected by a shear plate which deforms non-linearly.

Recently the use of numerical methods employing digital computers has simplified the problem. For example, Carrier and Christian (1973) and Hooper (1974) give results using the finite element method. The technique is so powerful that effects of footing roughness, Poisson's ratio as well as non-homogeneity can easily be considered. Another simpler numerical technique is the method of superposition of sectors introduced by Poulos (1968). In this method the circular rigid plate is divided into a number of concentric annuli and on each annulus, a uniform pressure is assumed - which is the contact pressure of the annulus. By using the sector method (Poulos, 1967b) the vertical displacement of each annulus is calculated. Since for a rigid plate the settlement is uniform, by equating the displacements of the annuli, a set of simultaneous equations is obtained, the solution of which gives the contact pressure distribution. The author reports that 10 annuli and 144 sectors give results that are good enough for all practical purposes. However, even these techniques have not fully solved the high stresses that exist at the edges of the die. Next, two more methods which are both simple and also applicable to practical problems are discussed in detail. These are semi-empirical elasto-plastic solutions proposed by Zeevaert (1972) and Schultze (1961).

2.3.1 Zeevaert's Method (1972)

In this method, Boussinesq's solution is assumed to be applicable in the elastic range as given by Equation 2.3.1.1

$$p(r) = C_o \frac{q_a}{(1-\xi^2)^{1/2}} \qquad 2.3.1.1$$

where C_o = is a constant to be determined. At the edges, because of the visco-plastic behaviour of the soil, the stress will have a finite value represented by q_{ep}. Since for equilibrium the sum of the downward vertical forces must be equal to the sum of the upward vertical forces, we can write the following equation:

$$\Pi R^2 q_a = \int_{r_1}^{R} q_{ep}(2\Pi r)dr + \int_{o}^{r_1} p(r)2\Pi r\, dr \qquad 2.3.1.2$$

where, r_1 = distance from centre of footing to the edge of the plastic zone.

After integration we obtain,

$$q_a = q_{ep}\,(1-\xi_1^2) + 2C_o q_a[1-\sqrt{1-\xi_1^2}] \qquad 2.3.1.3$$

where $\xi_1 = \frac{r_1}{R}$

Further algebraic manipulations give

$$C_o = \frac{1}{2-\sqrt{1-\xi_1^2}} \tag{2.3.1.4}$$

and

$$\frac{q_a}{q_{ep}} = 2\sqrt{1-\xi_1^2} - (1-\xi_1^2) \tag{2.3.1.5}$$

The author, based on experimental and theoretical work gives Equation 2.3.1.6 to evaluate the limiting edge stress:

$$q_{ep} = \frac{3}{2} s + \sigma_{zD} \tag{2.3.1.6}$$

where s = the shear strength of the soil

σ_{zD} = the effective vertical stress at founding level = $\gamma' D$ (if there is no surcharge).

For sensitive sediments of a preconsolidated type, the author suggests that the smallest of the values given by Equation 2.3.1.6 and the preconsolidation pressure be used. Once q_{ep} is selected, q_a/q_{ep} can be calculated and by entering this value in Figure 2.3.1.1 ξ_1 can be obtained. Then using ξ_1, Figure 2.3.1.2 gives the constant C_o, after which the stresses at any distance from the centre can easily be calculated.

2.3.2 Derivation of Contact Pressure Distribution for a Rigid Circular Footing

Schultze (1961) proposed an elasto-plastic solution by combining Boussinesq's elastic solution with the general bearing capacity

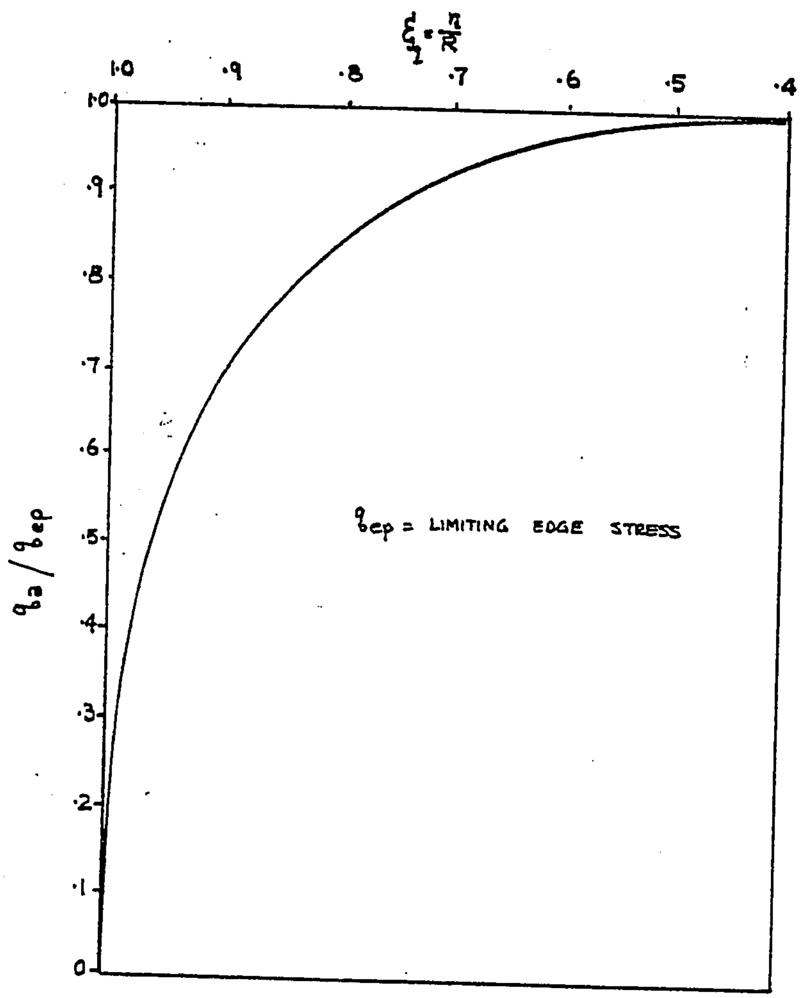

FIGURE 2.3.1.1 q_a/q_{ep} VS ξ_1, FOR SOLVING EQUATION 2.3.1.2 (AFTER ZEEVAERT, 1972)

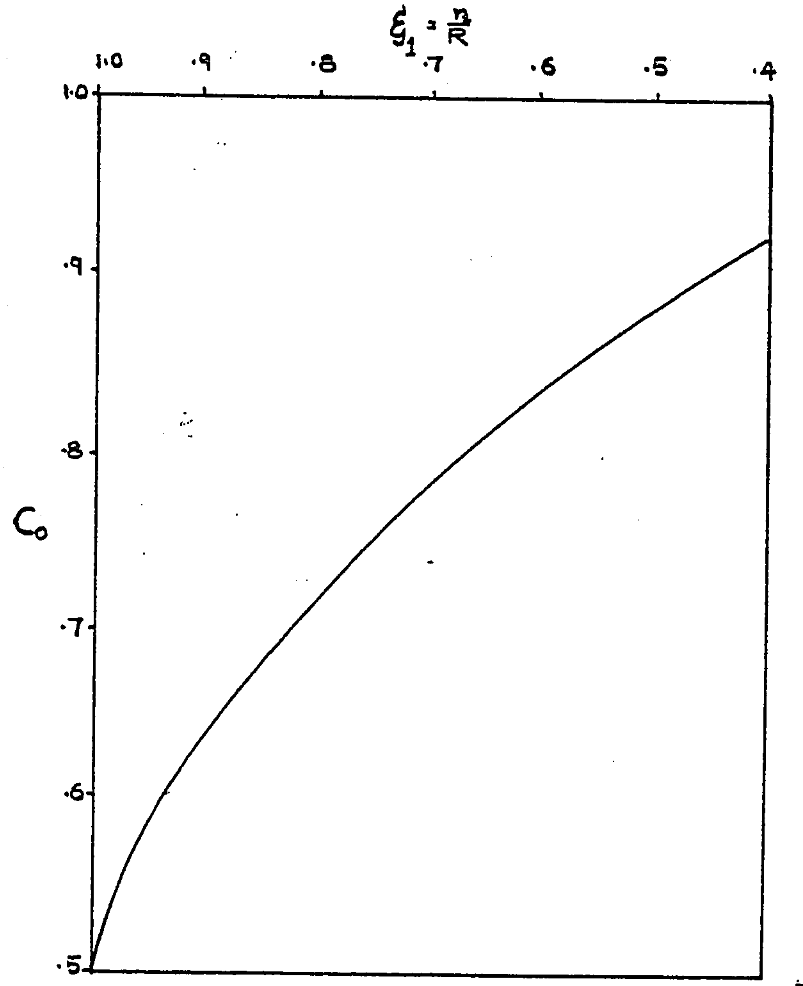

FIGURE 2.3.1.2 C_o vs ξ_1, FOR SOLVING EQUATION 2.3.1.2 (AFTER ZEEVAERT, 1972)

formula given by Prandtl and Buisman; Equation 2.3.2.1.

$$p(r) = \kappa_1 c N_c + \gamma_1 N_q D + 4R\kappa_2 \gamma_2 N_\gamma \left(1 - \frac{r}{R}\right) \qquad 2.3.2.1$$

where $p(r)$ = the normal stress distribution

N_c, N_q, N_γ = bearing capacity factors

c = cohesion

γ_1, γ_2 = unit wt. of soil above and below the footing level

R = radius of footing

D = depth of footing

κ_1, κ_2 = shape and depth factors

r = distance from the centre

The author solves the equation only for a strip footing. However, the method is not restricted to such footings alone. Hence, a solution of the problem based on Schultze's hypothesis follows. The solution starts by assuming that at the transition point from fully elastic to fully plastic state, the stresses must be the same. Hence by equating these stresses at the transition point, we get:

$$\frac{P_1}{2\pi R^2 \sqrt{1-\left(\frac{r_1}{R}\right)}} = \kappa_1 c N_c + \gamma_1 D N_q + 4R\kappa_2 \gamma_2 N_\gamma \left(1 - \frac{r_1}{R}\right) \qquad 2.3.2.2$$

where P_1 = Elastic portion of total load carried by footing.

Referring to Figure 2.3.2.1, we note that the distribution is composed of a parabola in the elastic range and a trapezoid in the plastic range. Because of the symmetrical nature of the problem, it is only required to get the pressure distribution along one radius.

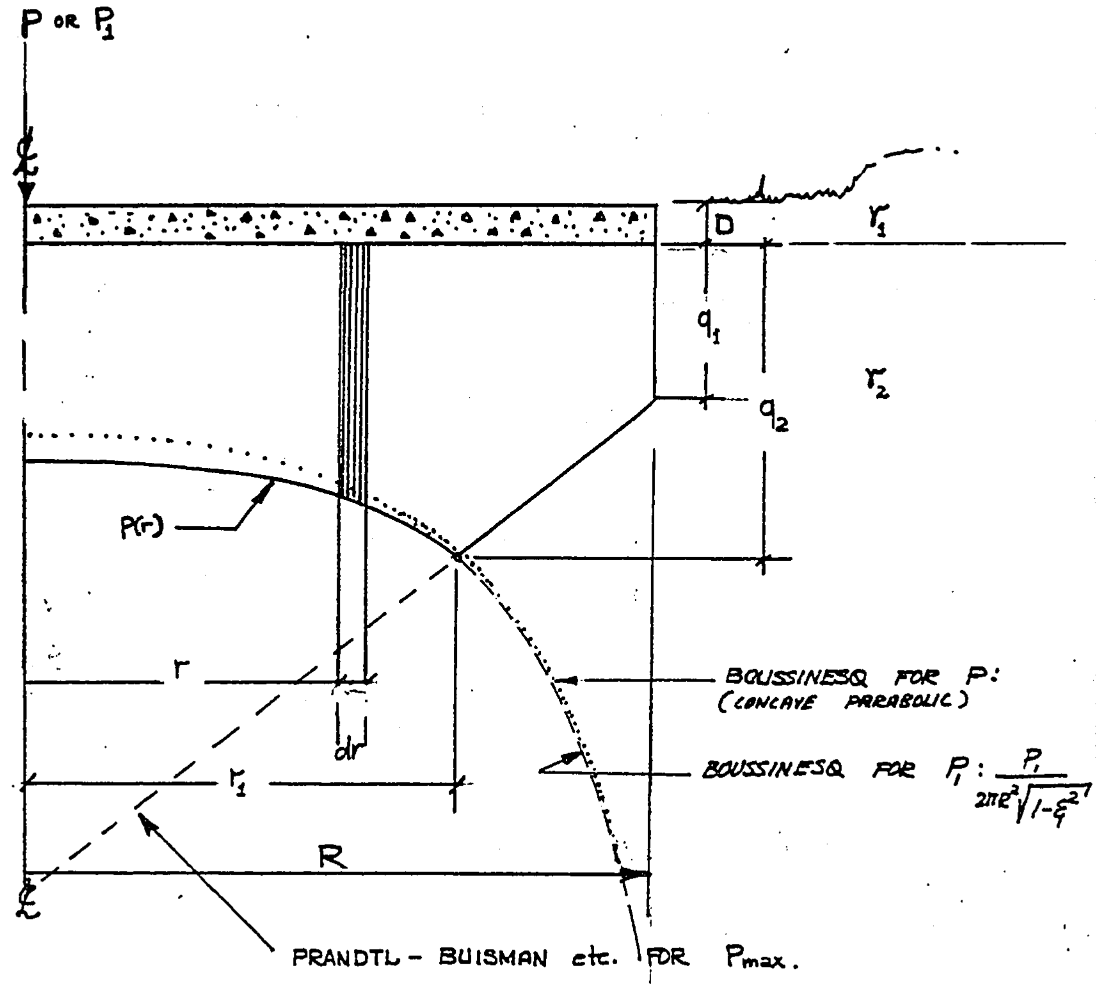

$$q_1 = k_1 c N_c + \gamma_1 D N_q + 4 R k_2 \gamma_2 N_\gamma \left(1 - \frac{r_1}{R}\right)$$

$$q_2 = k_1 c N_c + \gamma_1 D N_q$$

FIGURE 2.3.2.1 ELASTO- PLASTIC CONTACT PRESSURE DISTRIBUTION ON THE BASE OF A SMOOTH CIRCULAR FOOTING.

Letting, the total load carried by the footing = Q

the elastic portion = V

the plastic portion = T

Then $\frac{Q}{2} = \frac{V}{2} + \frac{T}{2}$

where, $\frac{V}{2} = \frac{1}{2}[2\Pi \int_{o}^{r_1} p(r) r \, dr]$, where p(r) is given by Equation 2.3.1

$$\frac{T}{2} = \frac{1}{2}\int_{r_1}^{R} [\kappa_1 cN_c + \gamma_1 DN_q + 4R\kappa_2\gamma_2 N_\gamma \; (1 - \frac{r}{R})] 2\Pi r \, dr$$

For intermediate steps, the reader is referred to Appendix A. After performing the integration and some algebraic manipulation, we get

$$\frac{V}{2} = \frac{P_1}{2}[1 - \sqrt{1-\xi_1^2}] \qquad 2.3.2.3$$

and

$$\frac{T}{2} = \frac{C_1}{2}(1-\xi_1^2) + \frac{C_2}{6}[3(1+\xi_1)(1-\xi_1)^2 - 2(1-\xi_1^3) + 3(1-\xi_1)(\xi_1+\xi_1^2)] \qquad 2.3.2.4(a)$$

where $\xi_1 = \frac{r_1}{R}$

$$C_1 = (\kappa_1 cN_c + \gamma_1 DN_q)\Pi R^2 \qquad 2.3.2.4(b)$$

$$C_2 = 4\Pi R^3 \kappa_2\gamma_2 N_\gamma \qquad 2.3.2.4(c)$$

From Equation 2.3.2.2 we have

$$\frac{P_1}{2} = \Pi R^2 \sqrt{1-\xi_1^2}\,(\kappa_1 cN_c+\gamma_1 DN_q) + \Pi R^2 \sqrt{1-\xi_1^2}(4R\kappa_2\gamma_2 N \; (1 - \frac{r_1}{R}))$$

Simplifying we get

$$\frac{P_1}{2} = C_1(1-\xi_1^2)^{1/2} + C_2(1-\xi_1)^{3/2}\,(1+\xi_1)^{1/2} \qquad 2.3.2.5$$

Substituting for P_1 from Equation 2.3.2.5 into Equation 2.3.2.3 and adding the result to Equation 2.3.2.4(a), we get:

$$\frac{Q}{2} = C_1 f_{C1}(\xi_1) + C_2[g_{C2}(\xi_1) + h_{C2}(\xi_1) + k_{C_1}(\xi_1)] \qquad 2.3.2.6$$

where $$f_{C1}(\xi_1) = (1-\xi_1^2)^{1/2} - 0.5\ (1-\xi_1^2) \qquad 2.3.2.7$$

$$g_{C2}(\xi_1) = (1-\xi_1)^{3/2}\ (1+\xi_1)^{1/2} \qquad 2.3.2.8$$

$$h_{C2}(\xi_1) = -\ 0.5\ (1+\xi_1)(1-\xi_1)^2 \qquad 2.3.2.9$$

$$k_{C2}(\xi_1) = -\ \frac{1}{6}[2(1-\xi_1^3) + 3(1-\xi_1)(\xi_1 + \xi_1^2)] \qquad 2.3.2.10$$

Once Q is known Equation 2.3.2.6 can be solved by trial and error until the value of ξ_1 which makes the two sides of the equation equal is obtained. To facilitate this procedure Figure 2.3.2.2 gives plots of Equations 2.3.2.7 to 2.3.2.10 inclusive against the dimensionless parameter ξ_1. Having selected the correct ξ_1 value, then r_1 can easily be calculated. Next the contact pressure distribution is plotted for any factor of safety using the following procedure. Use Boussinesq's formula given by the left hand side of Equation 2.3.2.2 to plot the elastic portion of the pressure distribution from the centre of the raft to r_1, then from r_1 to the edge use Equation 2.3.2.1 to obtain the trapezoidal plastic portion. It is interesting to note that since for undrained clay $N_\gamma = 0$, the shape of the pressure distribution becomes similar to that given by Zeevaert (1972).

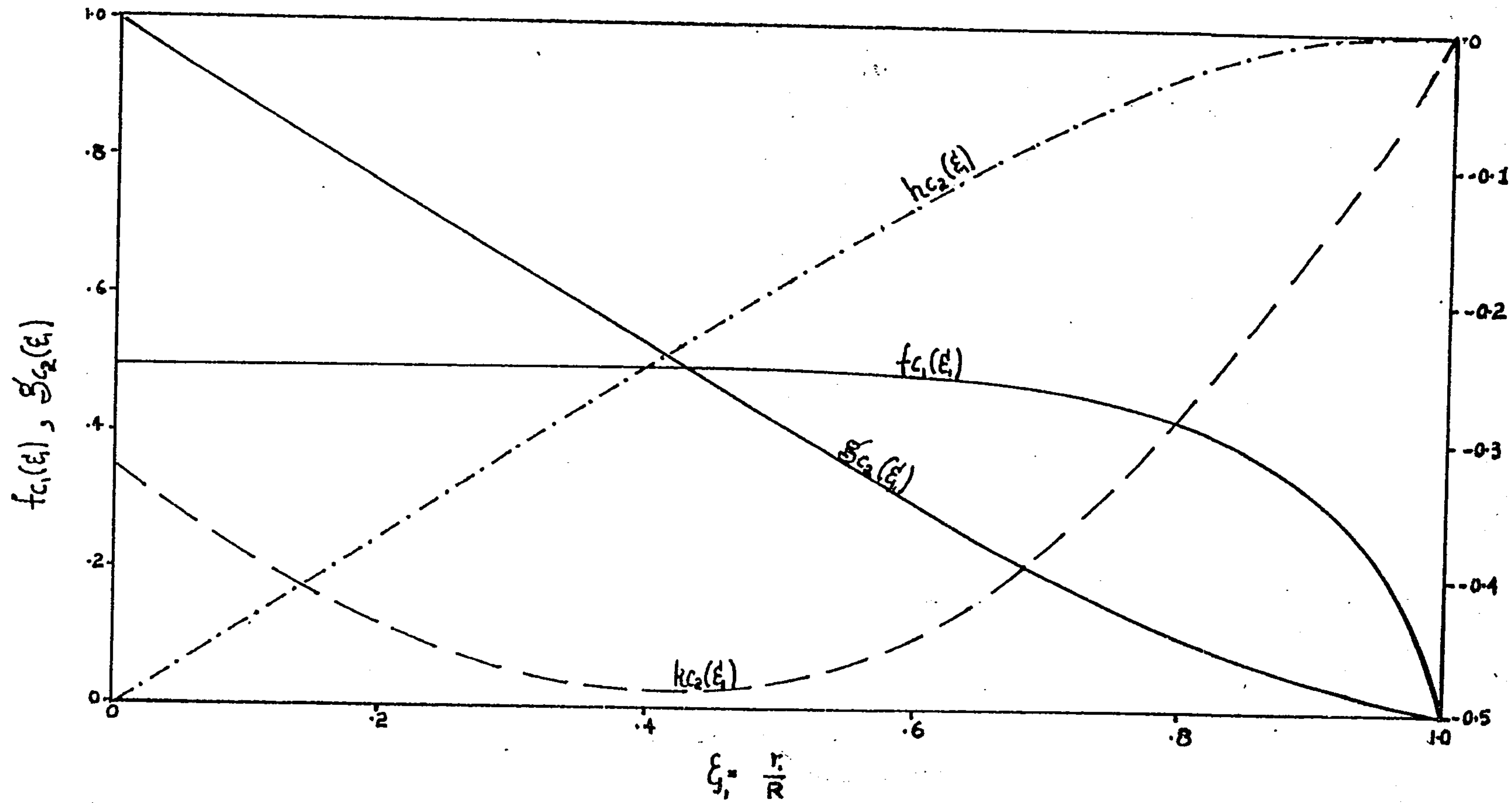

FIGURE 2.3.2.2 VALUES OF $f_{c_1}(\xi_1)$, $g_{c_2}(\xi_1)$, $h_{c_2}(\xi_1)$ and $k_{c_2}(\xi_1)$ VS ξ_1 FOR CALCULATING NORMAL CONTACT PRESSURE DISTRIBUTION UNDER A RIGID CIRCULAR RAFT.

2.4 The Concept of Subgrade Reaction - The Winkler Model

The theory of subgrade reaction is based on the assumption that the reaction pressure between the raft and the foundation material is dependent solely on and directly proportional to the foundation displacement at that point. The assumption is usually known as the Winkler hypothesis and is given by Equation 2.4.1

$$k = \frac{q_a}{y} = \text{const} \qquad 2.4.1$$

where k = the modulus or coefficient of subgrade reaction

q = the unit contact pressure at a given point

y = the settlement at that point

The method has been found acceptable when applied to a large flexible raft or for an infinite beam on an elastic foundation, Brown (1969a), Vesic (1961) and Carrier et al (1973). For a symmetrically loaded rigid raft, however, because of the uniformity of the settlement, the theory becomes misleading since Equation 2.4.1 gives a uniform contact stress distribution. But we know that a uniform pressure gives zero bending moments which is not the case for a rigid raft, thus using Equation 2.4.1 would lead to erroneous conclusions.

For design, the coefficient of subgrade reaction is obtained by performing plate load tests or from geotechnical literature. One of the main problems with the test is that it cannot account for the consolidation settlement of saturated clays, and therefore the result is somewhat inaccurate. Furthermore, all of the other factors that are listed in Section 2.1 also apply to the modulus of subgrade reaction.

Once the plate test results are obtained, the subgrade modulus for the prototype footing is determined by semi-empirical formulae. For stiff clay where it can be assumed that the deformation characteristic is independent with depth, Terzaghi (1955) proposed Equation 2.4.2

$$k = \frac{k_1}{D} \text{ or } \frac{k_1}{B} \qquad 2.4.2$$

where k_1 = subgrade modulus for the plate

B = size of square or strip footing

D = diameter of footing

In order to obtain k_1, a plot of average pressure against deformation is made. Then the subgrade modulus is taken as being the tangent modulus of the curve. Provided the applied load is less than 50 per cent of the ultimate bearing stress, the method gives reasonable values. For beams on an elastic foundation, which this thesis does not cover, the reader is referred to Vesic's (1961) work. His empirical equations appear to be more reliable than Terzaghi's (1955), since they account for the elastic properties of both the footing and the subgrade.

In his second edition, Bowles (1977), proposes Equation 2.4.3 for a rapid

$$k = 36\ q_a\ (\text{KCf})$$
$$k = 120\ q_a\ \text{kN/m}^3 \qquad 2.4.3$$

evaluation of the coefficient of subgrade reaction; and claims this simple formula to be as reliable as all the other methods. He arrived at the equation by assuming that the settlement that is associated with an allowable bearing pressure is in the order of 1 inch. The derivation of Equation 2.4.3 is as follows

let q_u = the ultimate bearing pressure

$$q_a = \frac{q_u}{F.S.}, \text{ where F.S.} = 3$$

$$\delta = \text{settlement} = 1''$$

Then from the definition of subgrade modulus we have

$$k = \frac{q_u}{\delta}$$

substituting for δ in feet and $q_u = 3q_a$ then

$$k = \frac{3q_a}{1/12} = 36\, q_a (\text{KCf}) .$$

2.5 Field Measurements of Contact Pressure in the Literature

For future comparison purposes some field investigations reported in the literature are introduced. Only measurements in similar soil and loading conditions to this project are presented. One such work is that discussed by Gaumy (1970) in a Master's thesis. The instrumentation was carried out in Leda Clay (Chapter 4) at the Woodroofe Avenue site of the Algonquin College of Applied Arts and Technology, Ottawa. For the test a rigid square footing with sides measuring 3.1 m (10 ft) was constructed. To measure the contact pressure a total of five vibrating wire load cells were utilized. Loading was carried out using a hydraulic jack and a tendon anchored in the bedrock.

The soil profile and a plan view of the footing showing the location of the load cells are given in Figures A1 and A2, respectively.

Using readings of 3 cells along the diagonal from the centre to the corner of the footing and 3 cells along the centre line of the footing from the centre to the mid-point of the edge, Gaumy (1970) presents plots of contact pressures at various load levels (Figures 2.5.1 and 2.5.2). Although, around the centre, the distributions are similar (cell no. 2 is used in both plots), there is a great disparity near the edges between the two plots. The total load measured by the load cells, and using the distributions shown was close to the applied load. Therefore, it appears that for this square footing the contact pressure was very high at the corners of the footing and smallest at the mid-point of the edge of the footing. At the centre of the footing it changed from 100% to 75% of the average applied load as the load level was increased.

The second case record reported by Eden et al (1973) involves a large raft foundation for a 15 storey apartment building also in Ottawa, Canada. Here 10 "Gloetzl" hydraulic load cells, similar to the ones discussed in this project (Chapter 5) are used. A copy of the soil profile and a schematic plan of the foundation showing the location of the load cells are given in Figure A5.

The reinforced concrete raft has a thickness of .91 m (3 ft). Because of the effect of shear walls and also the floors above, the writers consider this to be a very rigid structure. Diagrams showing the measured contact pressure distributions and those assumed for design are given in Figure 2.5.3. It is seen from these plots that the general trend is for pressure to increase from the centre to the edges

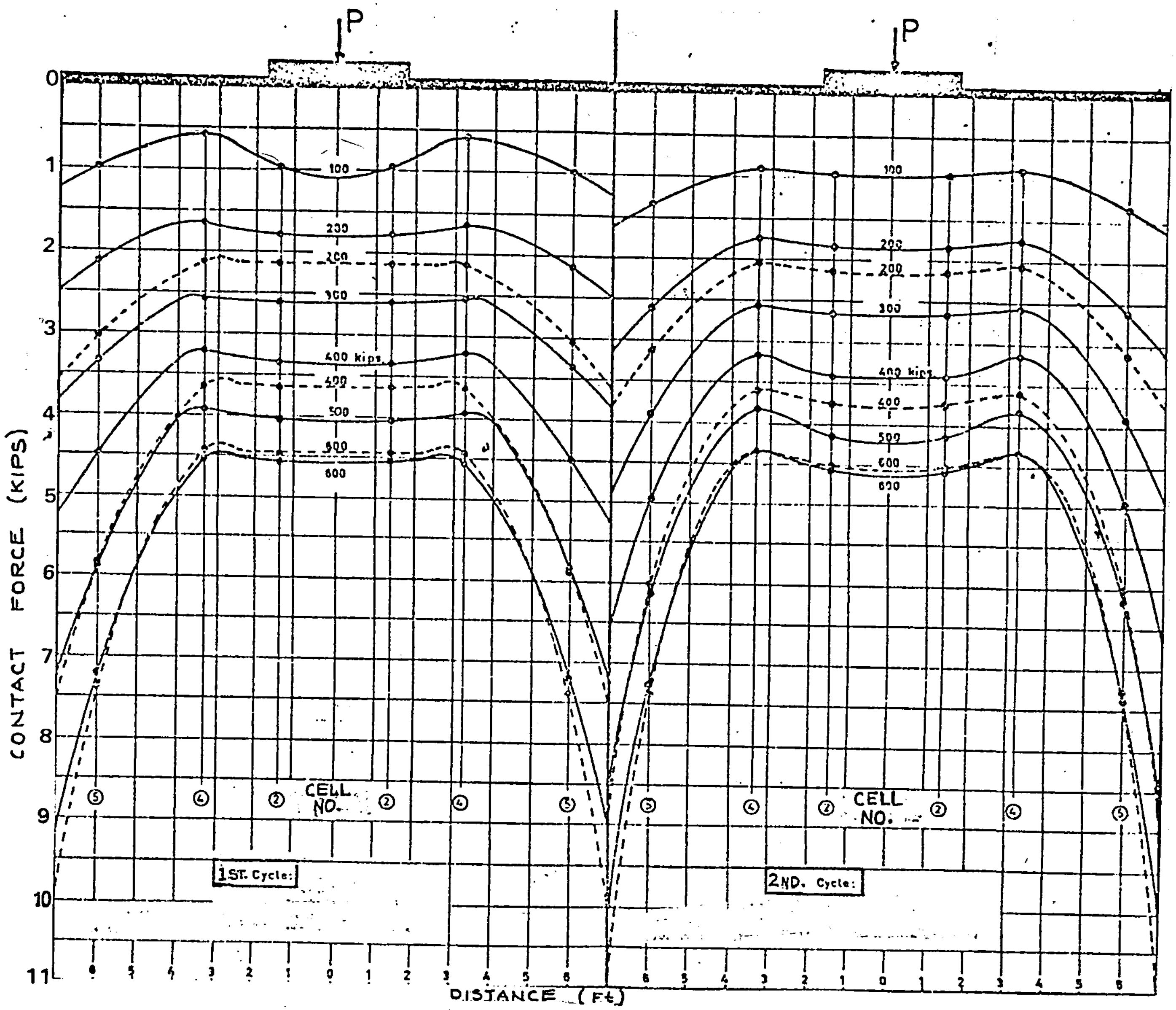

FIGURE 2.5.1 CONTACT PRESSURE DISTRIBUTIONS UNDER TEST FOOTING IN THE DIAGONAL DIRECTION. (After **Gaumy** ,1970)

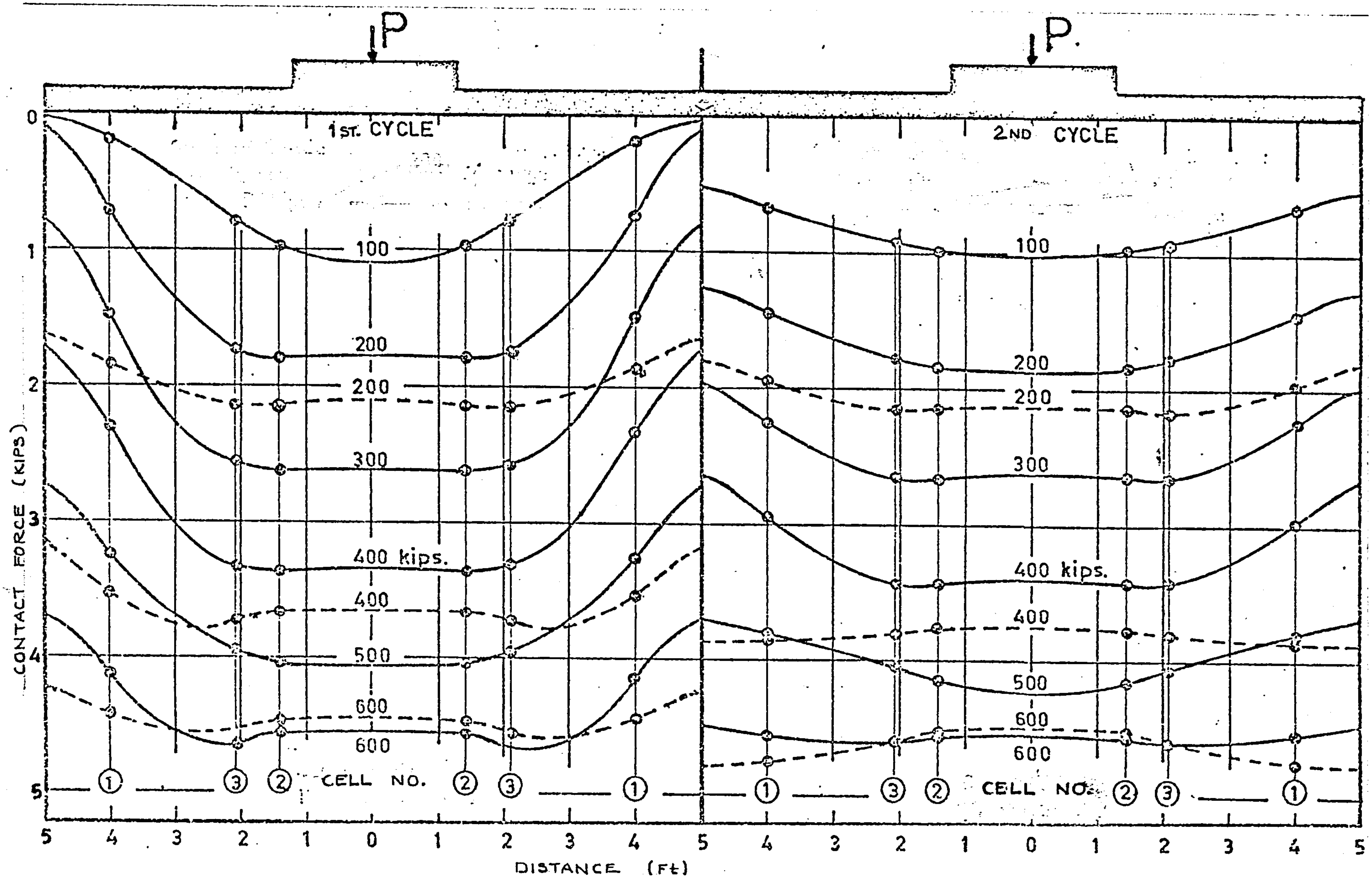

FIGURE 2.5.2 CONTACT PRESSURE DISTRIBUTIONS UNDER TEST FOOTING ACROSS FOOTING ALONG THE CENTRE LINE. (After **Gaumy** ,1970)

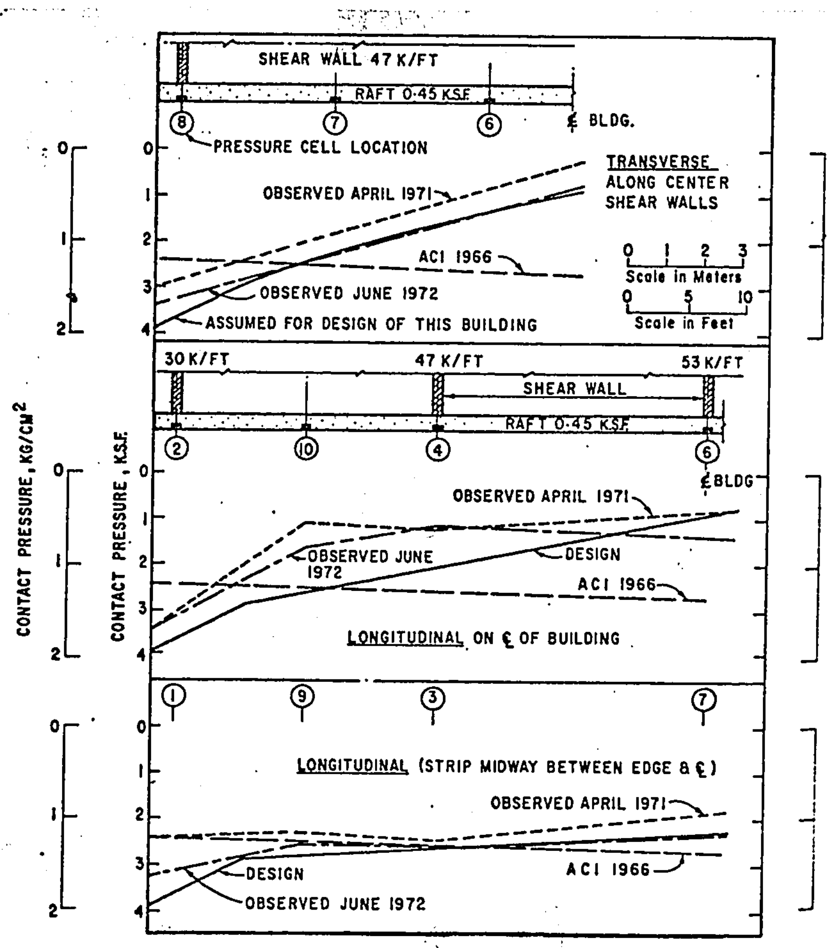

FIGURE 2.5.3 MEASURED CONTACT PRESSURES UNDER A RIGID RAFT FOR A 15-STOREY APARTMENT BUILDING. (AFTER EDEN ET AL, 1973).

as expected from theory, however since the contribution to the rigidity of the raft by the shear walls is non uniform, the contact pressure distributions plotted along the three directions are not exactly similar.

To complete the list, load test results performed in Osaka, Japan are included. The work was done by Takenaka et al (1971) at a subway construction site on homogeneous marine clay deposit having a thickness of 10 m (32.8 ft). The deposit which is about 100,000 years old derives its preconsolidation stress from aging. It has the following average geotechnical properties: liquid limit = 107.1, plastic limit = 44.5 and a natural water content of 81.2 percent.

Contact pressure measurements were carried out under a rigid circular footing with a diameter of 3 m (6.56 ft). A total of five hydraulic cells consisting of rubber tubes and pressure gauges were used. The authors give no explanation about the design of the cells. The load cells were evenly spaced across the centre of the footing. Loads were applied using hydraulic jacks. Reaction was provided by an H-beam spanning across anchored H-piles. Figure 2.5.4 shows the layout of the load cells as well as the resulting contact pressure distribution curves. Here, for a reason the writers could not explain, the distributions are completely different from that predicted by elastic theory. A discussion about such phenomenon is given in Chapter 7.

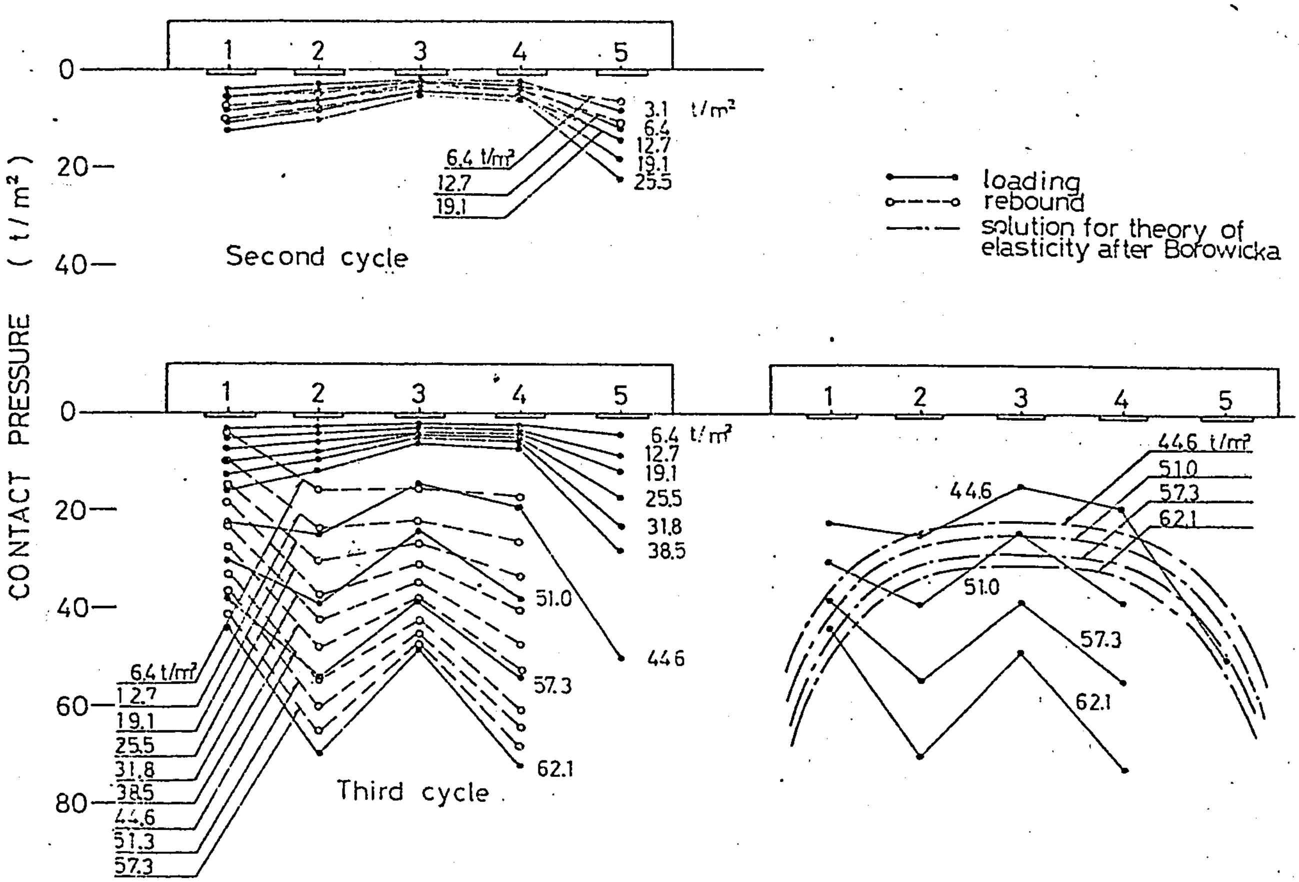

FIG. 5. The Distribution of Contact Pressure.

FIGURE 2.5.4 CONTACT PRESSURE MEASUREMENTS IN MARINE CLAY. (AFTER TAKENAKA, 1971).

2.6 Summary of Important Points

Contact pressure depends on a number of variables of which the most important ones are rigidity, roughness and thickness of the soil medium. Theoretically at relatively low applied pressure levels, the contact pressure distribution under the base of a rigid footing resting on an elastic soil such as clay assumes the shape of a bowl, with the maximum stresses near the edges, while the same footing resting on a non-cohesive sand gives rise to a parabolic pressure distribution having zero stresses near the edges. On the other hand, real soils tend to behave somewhere in between.

In the case of elastic soils, the effect of higher rigidity is to increase the edge stresses relative to the average pressure. This stress can only increase to a certain limiting value after which plastic yielding takes place. For most practical applications, theory shows that for Poisson's ratio greater than or equal to .3, the effect of base roughness on contact pressure distribution is very negligible. Except for a very shallow clay deposit, where the thickness is less than the diameter of the footing, the effect of layer thickness on contact pressure distributions is also very small. For most problems, if the stratum is greater than the diameter of the footing the assumption of semi-infinite half space which is the basis for most theories is acceptable.

By assuming a limiting edge stress equal to the ultimate bearing capacity or the preconsolidation pressure, elasto-plastic equations for calculating contact pressures are presented. Also, two techniques for calculating the modulus of subgrade reactions are given.

Three case histories of contact pressure measurements are introduced. This is done so that the measured values in this project could be compared both to theoretical predictions and to similar field data by other researchers. In the first two cases the distributions show that the pressure is higher at the edges than at the centre. In the last case the distributions are different from that given by elastic theory.

CHAPTER 3

SETTLEMENT OF A RIGID RAFT IN CLAY

3.1 General

The total vertical displacement of a rigid raft in clay is composed of undrained and consolidation settlements, and can be approximately represented by Skempton's (1957) well known formula:

$$S_{Tt} = S_u + U\mu\, S_{oed} \qquad 3.1.1$$

$$S_{TF} = S_u + \mu\, S_{oed} \qquad 3.1.2$$

where S_{Tt} = total settlement after time t ($U < 1.0$)

S_{TF} = total settlement at the end of primary consolidation ($U = 1.0$)

S_u = undrained settlement

S_{oed} = consolidation settlement estimated from oedometer test results

U = degree of consolidation

μ = a semi-empirical correction factor for 3-dimensional effect (see Section 3.6)

Equation 3.1.1 gives the total settlement at any time for a degree of consolidation less than 100 percent, whereas Equation 3.1.2 gives the value after the process of consolidation is completed. Estimates of the two components are usually made by doing field or laboratory tests. Detailed discussions of the two components are found in Sections 3.5 and 3.6.

Actually it has been observed that there is a third component of settlement due to secondary compression, or creep. Its magnitude must also be evaluated in foundation design. Generally, however, its magnitude at stress levels below the preconsolidation pressure is small enough that it can be neglected. In Leda Clay (see Chapter 4), creep settlements are large at stress levels approaching or over the preconsolidation pressure.

Since by definition, a rigid footing does not suffer any deflection, it must experience a uniform settlement. However, as shown by Giroud (1972) (Figure 3.1.1), there is a deviation from uniformity as the influence of rigidity diminishes with depth up to $z/R = 1.5$. For $z/R \geq 1.5$, the settlement distribution within the cylindrical soil column defined by the footing becomes approximately uniform again. Also shown in this figure is the settlement distribution with depth below selected points across the footing. The above calculated settlements are of theoretical interest only, since they are based on a rigid die resting on an ideal elastic half-space. In general, the total settlement and its distribution with depth depend on a number of variables. Some of the important factors are:

a) foundation size, rigidity and roughness;

b) foundation depth;

c) thickness of the compressible layer;

d) non-homogeneity, anisotropy and local yield.

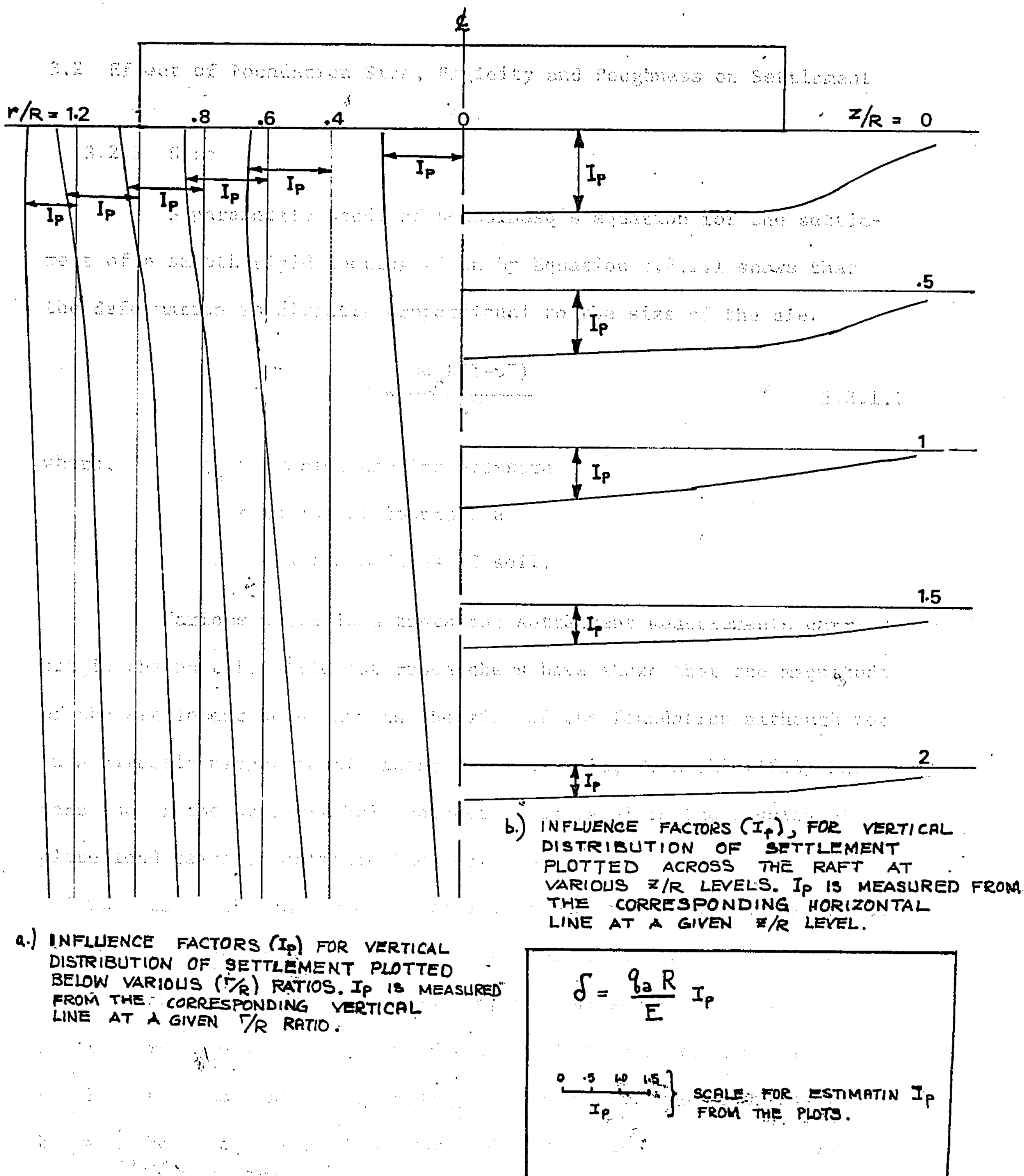

FIGURE 3.1.1 DISTRIBUTIONS OF ELASTIC SETTLEMENT BELOW A RIGID CIRCULAR FOOTING FOR $\nu = .3$ AND INFINTE LAYER THICKNESS. BASED ON GIROUD'S (1972) WORK.

3.2 Effect of Foundation Size, Rigidity and Roughness on Settlement

3.2.1 Size

A parametric study of Boussinesq's equation for the settlement of a smooth rigid footing given by Equation 3.2.1.1 shows that the deformation is directly proportional to the size of the die.

$$\delta = \frac{\Pi q_a R(1-\nu^2)}{2E} \qquad 3.2.1.1$$

where, q_a = average applied pressure

R = radius of foundation

E = elastic modulus of soil.

Various plate load tests and settlement measurements carried out in the past by different researchers have shown that the magnitude of the settlement does vary as the size of the foundation although not in a directly proportional manner. For example, Terzaghi (1955) has made use of the pressure bulb concept to extrapolate the results of plate load tests to estimate the performance of larger footings. Unfortunately, the author was unable to locate more classical material dealing with the subject. A recent experiment carried out by Chin (1969) shows that a dimensionless mathematical model relating the applied pressure, the cohesion, the size of the footing and the settlement is possible. His model also shows that the relationship between the size of the foundation and the settlement is non-linear. However, since his finding was based on small footings (24 cm dia.), the reliability of the approach is questionable.

3.2.2 Rigidity

It is known from elastic theory that under similar conditions a rigid footing experiences less settlement and distortion than a flexible one. The reason for this behaviour is best explained by comparing the stress distribution with depth below rigid and flexible footings of similar size resting on an elastic medium. Figure 3.2.1, prepared from Giroud's (1972) calculations shows the vertical stress distribution below the centre and the edge for the two footings. Also given in the figure is a table containing the radial and tangential stresses for the two cases. Using stress distribution theory, one can write Equation 3.2.2 to estimate the elastic settlement of footings on homogeneous and isotropic soil medium.

$$\delta = \frac{H}{E}[\sigma_z - \nu(\sigma_\theta + \sigma_r)] \qquad 3.2.2.1$$

where σ_z = the vertical stress

σ_θ = the tangential stress

σ_r = the radial stress

H = layer depth.

When $\nu = 0$ then the settlement depends on σ_z alone since H and E are assumed constant. But we can also see from Figure 3.2.1 that below the centre, the vertical stress is higher for a flexible footing than for a rigid one, which results in a higher settlement. However, at the edges the reverse is true. The differential compression of the soil beneath the rigid footing is therefore less.

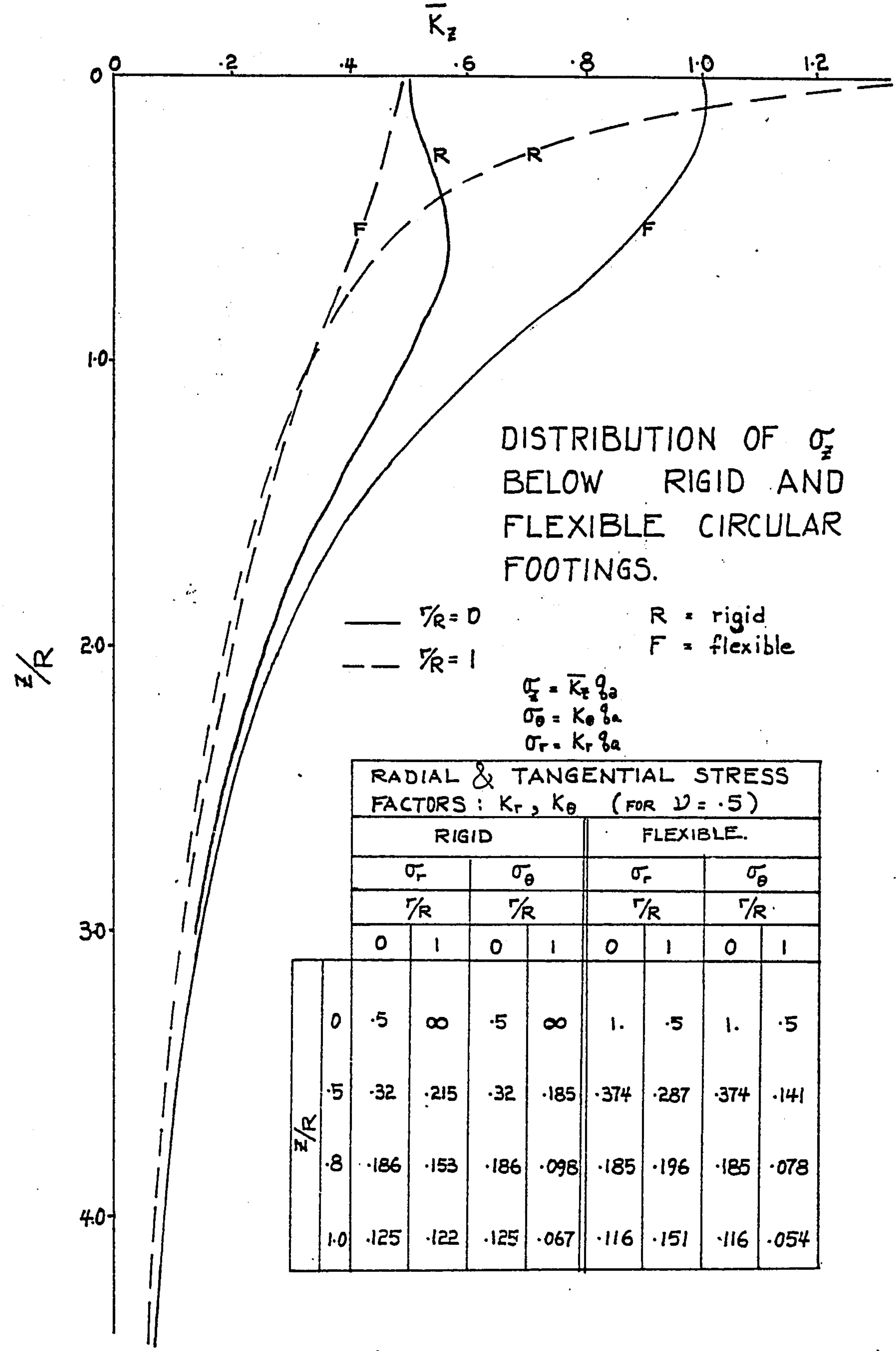

$\sigma_z = \overline{K}_z q_a$
$\sigma_\theta = K_\theta q_a$
$\sigma_r = K_r q_a$

RADIAL & TANGENTIAL STRESS FACTORS : K_r, K_θ (FOR $\nu = \cdot 5$)

	RIGID				FLEXIBLE			
	σ_r		σ_θ		σ_r		σ_θ	
	r/R		r/R		r/R		r/R	
z/R	0	1	0	1	0	1	0	1
0	·5	∞	·5	∞	1.	·5	1.	·5
·5	·32	·215	·32	·185	·374	·287	·374	·141
·8	·186	·153	·186	·098	·185	·196	·185	·078
1·0	·125	·122	·125	·067	·116	·151	·116	·054

FIGURE: 3·2·1 (PLOTTED FROM GIROUD'S TABLES, 1972)

Now let us examine the case where ν is greater than zero. For the discussion $\nu = 0.5$ is selected since the expressions for the radial and tangential stresses are simpler to calculate. Under the centre of the footings, the table in Figure 3.2.1 shows that for both cases, due to symmetry, the radial and tangential stresses are the same, hence Equation 3.2.2.1 becomes

$$\delta = \frac{H}{E}[\sigma_z - 2\nu\sigma_r] \qquad 3.2.2.2$$

and for $\nu = 0.5$

$$\delta = \frac{H}{E}[\sigma_z - \sigma_r] \qquad 3.2.2.3$$

Equation 3.2.2.3 gives the settlement as being proportional to the difference between the vertical and radial stresses. Since this stress difference is the greatest in the flexible case, then the centerline deformation is always larger than that of a rigid footing. However, even though there is a difference in the magnitude of the settlement distribution below a flexible and a rigid one, the curves are almost similar when plots of percent settlement with depth are made for the two cases (see Figure 3.2.2)

3.2.3 Roughness

In Section 2.1.2 it was pointed out that for $\nu \geq .3$, the effect of roughness on contact pressure is minimal; this is applicable to the settlement as well. Although in general the displacement of a rough footing is smaller than a smooth one, Carrier and Christian (1973) conclude that only when $\nu < .3$ does the difference become significant. The above conclusion applies both to homogeneous and

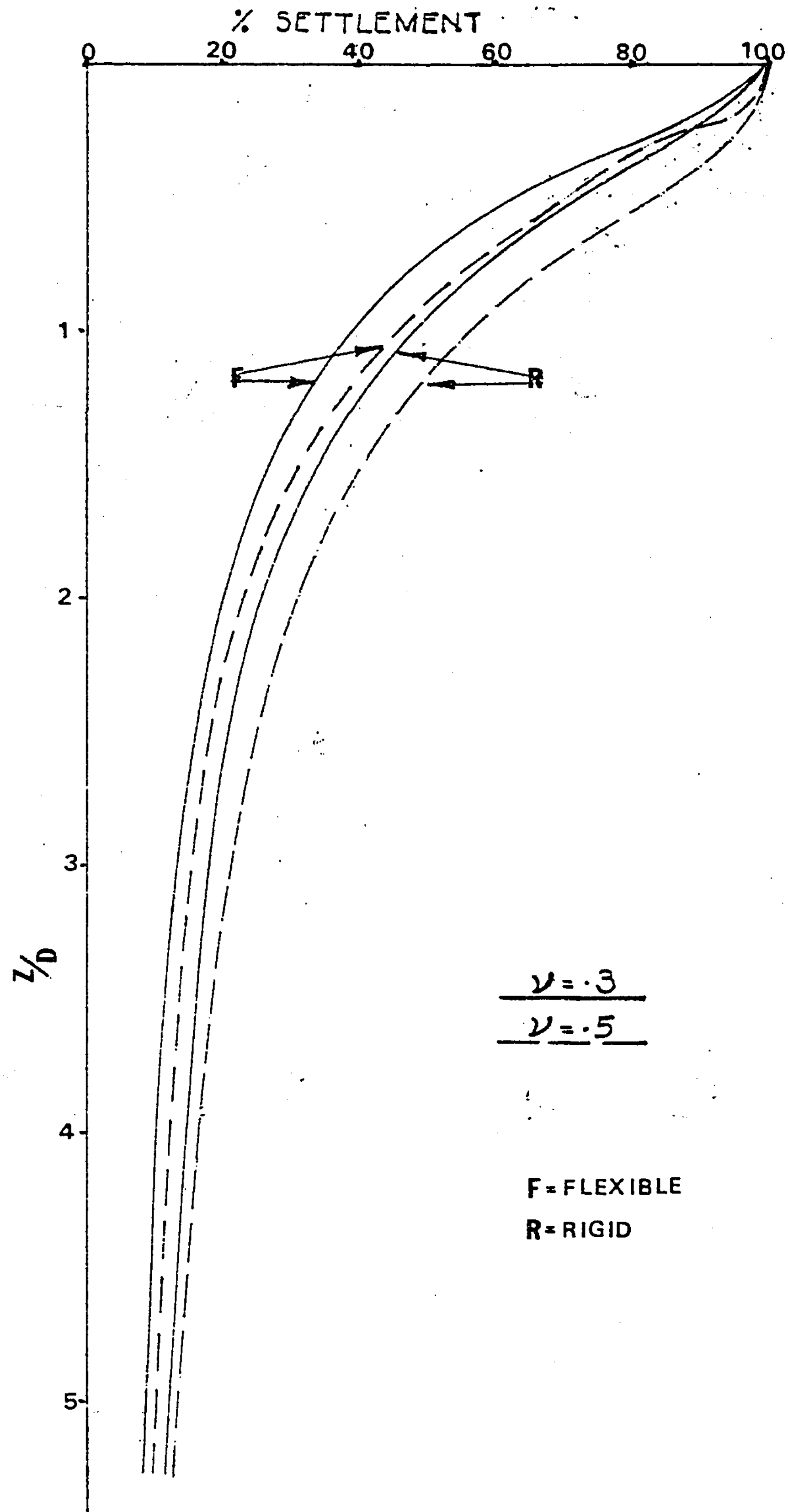

FIGURE 3.2.2 THEORETICAL ELASTIC SETTLEMENT DISTRIBUTIONS UNDER THE CENTER OF CIRCULAR AND SQUARE FOOTINGS.

heterogeneous (E linearly increasing with depth) deposits. The maximum difference for the homogeneous case is about 10 per cent and occurs when $\nu = 0$; and for the non-homogeneous medium, the effect is even smaller. Since clayey soils tend to fall between these two limits, for the purpose of calculating immediate settlement using $\nu \geq .4$, the assumption of a smooth surface is justified. Hooper (1974) gives Equation 3.2.3.1

$$\rho = \frac{\Pi}{2} F_2 \frac{(1-\nu^2)}{E} q_a R \qquad 3.2.3.1$$

where

$$F_2 = \frac{1-2\nu}{(1-\nu)\ln(3-4\nu)} \qquad 3.2.3.2$$

which is similar to Boussinesq's (Equation 3.2.1.1), except here a factor is included to account for the adhesion at the footing-soil interface. We note that when $\nu = 0.5$, $F_2 = 1$ which makes Equation 3.2.3.1 the same as Equation 3.2.1.1. Also when $\nu = 0$, $F_2 = 0.91$ indicating that the settlement in the adhesive case is 9 percent less than the smooth one, which agrees well with results of Carrier and Christian (1973), based on finite element solutions. The above conclusion is also supported by Davis et al (1973) and Schiffman (1969).

3.3 Effect of Foundation Depth and Thickness of Compressible Layer on Settlement

It is well known that most of the elastic solutions assume that the footing rests on top of an ideal elastic medium. This is because this geometry offers the simplest boundary conditions. In practice, however, footings are cast at some depth in the ground in order to protect the structure against erosional damages due to wind and rain;

and mainly to avoid frost heave problems. The effect of foundation depth is to decrease the settlement provided the compressibility of the soil does not increase with depth. There are at least two explanations for the above phenomenon. Excavation processes for construction of footings unload the underlying soil. So when a load is applied to the footing, there should only be a very small settlement due to recompression provided the total applied pressure of footing, backfill, and load is less than or equal to the overburden pressure removed due to the excavation.

The second reason for a lower settlement with increasing foundation depth is that the theoretical vertical stress concentrations below the footing are somehow lower. Using photoelastic models Skopek (1961) discovered that provided the elastic mass above the footing can take some tensile stresses, there is in fact a reduced vertical stress concentration compared to the case where the footing rests at zero depth. Hence, the stress reduction appears to be more noticeable in saturated clays than in non-cohesive soils since only the former can take any tensile stresses. Figure 3.3.1 is the result of the photoelastic stress analysis conducted by Skopek.

As mentioned previously with respect to contact pressures, the thickness of the compressible layer also affects the magnitude and distribution of settlement. For example the elastic theory based on the semi-infinite ideal half-space can only be used if the clay deposit is thick enough compared to the size of the footing. The error involved in assuming an infinite layer depends on the Poisson

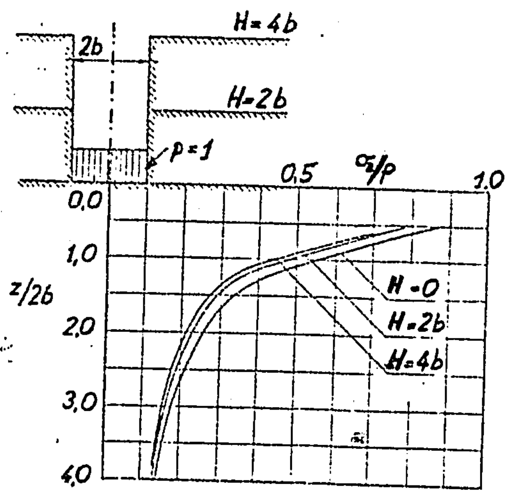

$b = \frac{B}{2}$

Figure 3.3.1 Distribution of vertical stress along the axis of a uniform load as a function of depth determined from photoelastic tests, after Skopec (1961).

ratio selected. If we assume $\nu = 0.5$, we find that for H/R = 6, there is a 21 percent error in the calculated settlement in assuming an infinite thickness. The relationship between vertical displacement of a rigid circle and the relative thickness of the layer are shown in Figure 3.3.2 for four Poisson's ratios and cover a wide range of H/R ratios. In order to cover the entire range of H/R, Poulos (1968) plots the displacement factor, Ip against H/R from H/R = 0 to 1 and against R/H for H/R = 1 to ∞. As shown in the figure, the effect of layer thickness is to make the elastic settlement less than that estimated by the semi-infinite case. This is because, when there is a rigid base at a shallow depth the stresses causing displacement tend to concentrate within a shallow layer below the footing, while in the case of semi-infinite half space the stress distribution penetrates much deeper. A detailed treatment of the subject is given by Burmister (1956) in his two layer rigid base soil system.

3.4 Effect of Non-Homogeneity, Anisotropy and Local Yield on Settlement

3.4.1 Non-Homogeneity and Anisotropy

Because of its simplicity, the assumption of homogeneous and isotropic elastic medium has in the past been extensively used to generate theoretical solutions for most soil mechanic problems. By homogeneity it is meant that the properties of the soil do not change from point to point whereas isotropy implies that at a given point the properties do not vary with direction. A material can be homogeneous and isotropic, homogeneous and anisotropic, heterogeneous and isotropic

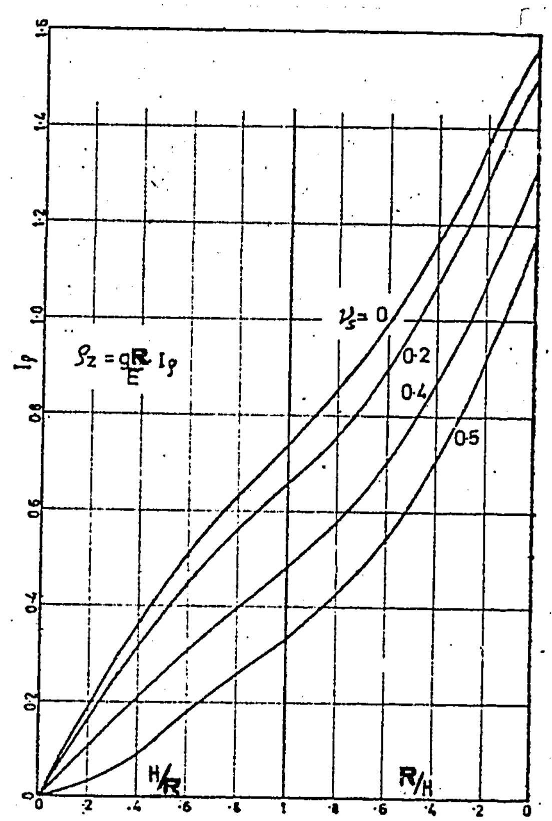

I_p = settlement influence factor

ν_s = Poisson's ratio of soil

R = radius of foundation

H = thickness of soil

FIGURE 3.3.2 INFLUENCE FACTORS FOR VERTICAL DISPLACEMENT OF A RIGID CIRCLE (AFTER POULOS, 1968).

or heterogeneous and anisotropic. In geotechnical engineering we find the last one to be the most frequently occurring, although it is case one which has received much theoretical attention. However, simple cases of heterogeneity have been successfully solved. These include two or three horizontal layered systems and the case where either the elastic modulus or the cohesion linearly increases with depth. Layered system problems have been tackled by Burmister (1956) and others whereas a recent work on the second type of heterogeneity is given by Hooper (1974). The theoretical treatment of stress anisotropy is a very complex problem and therefore only very little practical material is available to engineers. One such work is the solution of stress and displacements in a homogeneous cross-anisotropic soils given by Barden (1963). Since by definition a material exhibiting cross-anisotropy is given by five elastic constants, the reliability of the theory will depend on the accuracy of determining these values. The elastic constants are:

E_V = the elastic modulus in the vertical direction

E_H = the elastic modulus in the horizontal direction

Poisson's ratios

ν_1 = effect of horizontal strain on horizontal strain

ν_2 = effect of horizontal strain on vertical strain

ν_3 = effect of vertical strain on horizontal strain.

To accurately estimate these parameters very sophisticated laboratory and sampling techniques are necessary which is not warranted for everyday engineering application. With regards to settlement the vertical stress, σ_z is more important than the other stresses. Since Poisson's ratios are more difficult to determine than the elastic modulus, the author suggests that estimating these constants but accurately measuring E_H and E_V will give a fairly accurate distribution of σ_z, from which settlements can be calculated. Figure 3.4.1.1 shows the distribution of σ_z for different values of η and also the range of the three Poisson's ratios (shaded area) when the medium is subjected to a point load. It is interesting to note that the distribution at $\eta = 1$ corresponds to the isotropic case given by Boussinesq and therefore shows no dependency on the Poisson ratio.

Hooper (1974), after studying the simplest type of heterogeneity (E_u increasing with depth) concludes that some of the important effects on settlement are:

1) to localize surface displacement in the region of the loaded area,
2) to increase the consolidation component of raft displacement, and
3) to reduce differential raft displacements for uniformly applied loads.

The effect of anisotropy is to give the soil medium a greater load spreading capacity at a shallower depth. According to Barden (1963), many undisturbed deposits of over-consolidated clays possess an anisotropy between 1 and 3 and therefore Boussinesq's theory will always over-estimate the settlement. Although, the degree of anisotropy is not very well known, it might be one of the possible reasons why footings resting on the desiccated crust of Leda Clay settle less than theoretically estimated, Mitchell et al (1972).

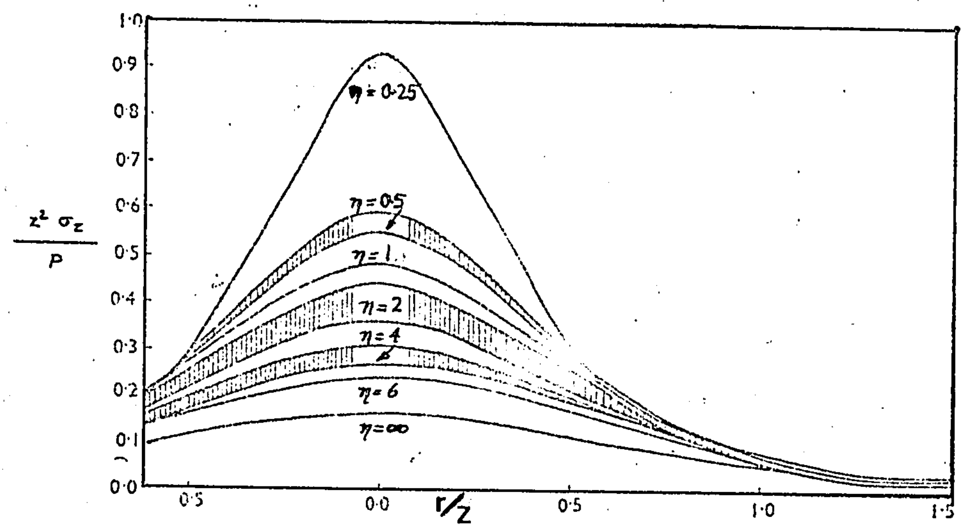

Stress anisotropy, $\eta = \frac{E_H}{E_V}$

FIGURE 3.4.1.1 $(\sigma_z)/(P/z^2)$ VERSUS r/z FOR DIFFERENT LEVELS OF STRESS ANISOTROPY, η. THE HATCHED AREAS INDICATE THE RANGE IN WHICH THE STRESS DISTRIBUTION FELL WITH THE DIFFERENT VALUES OF ν_1, ν_2 and ν_3 THAT COULD EXIST AT THAT PARTICULAR η VALUE. (AFTER BARDEN, 1963).

3.4.2 Local Yield

When the applied pressure approaches the ultimate bearing capacity of the soil, then undrained settlements calculated using elastic formulae will always be underestimated. This is because of the formation of locally contained plastic flow in the soil mass. According to d'Appolonia et al (1971), the factor of safety at which first local yielding occurs depends on the initial shear stress ratio given by Equation 3.4.2.1

$$f = \frac{\sigma'_{vo} - \sigma'_{ho}}{2S_u} = \frac{(1-K_o)}{2S_u}\sigma'_{vo} \qquad 3.4.2.1$$

where f = the initial shear stress ratio

$\sigma'_{vo}, \sigma'_{ho}$ = the initial vertical and horizontal effective stresses, respectively

S_u = undrained shear from field vane

K_o = the coefficient of earth pressure at rest.

Using elastic theory Davis and Poulos (1968) derived the following equations to estimate, from the initial shear stress ratio, the foundation pressure to cause first local yield, q_y:

$$q_y = \Pi(1-f)S_u \text{ for } 0 \le f \le 1$$
$$q_y = \Pi(1-f^2)S_u \quad -1 \le f \le 0 \qquad 3.4.2.2$$

Although Equations 3.4.2.2 were derived for a uniformly loaded strip foundations D'Appolonia et al (1971) have found out that the formulae can be used for circular rigid footings as well. Knowing the ultimate bearing capacity and Equations 3.4.2.2, the minimum factor of safety before local yield occurs can be calculated. If the actual factor of safety against bearing capacity is smaller than the minimum required to cause local yield, then settlement can be calculated using elastic theory, otherwise local plastic flow should always be accounted for. For a detailed discussion on how to consider local yield in settlement calculations, the reader is advised to refer to the paper by d'Appolonia et al (1971) as well as that by Davis and Poulos (1968). It is worth mentioning at this point that the type of local yield at the edges of rigid footings even with low load levels does not have a significant effect on the elastic load displacement behaviour of the soil

3.5 Immediate or Undrained Settlement

When a saturated clay is subjected to a rapidly applied load, it deforms without any volume change and this settlement which is a form of shear deformation is called immediate or undrained settlement. There is very little or no pore water pressure dissipation associated. There are at least two reasons why we want to know this quantity: First of all, immediate settlement being related to the undrained stability of the foundation may give an indication about the integrity of the structure. Secondly, depending on the nature of soil, geometry of loading and thickness of the layer, immediate settlement may constitute a large portion of the final vertical deformation.

Undrained settlement is calculated either directly from elastic displacement theory or by integration of strains in the soil media using elastic stress distribution theory. In any event, it can only be determined by a three dimensional strain approach since saturated soil can experience settlement under one-dimensional strain only when drainage occurs. Its reliability depends among other variables on:

a) the accuracy of the elastic equation used, i.e., whether or not the elastic model used is applicable to the particular problem at hand,

b) the accuracy of laboratory and field stiffness values that enter it,

c) the attention given to the effect of local yield.

One of the main difficulties associated with the estimation of immediate settlement is the difficulty in assessing the undrained modulus, since this quantity varies with the stress level in the soils. A few researchers have tried to model this non-linear stress strain behaviour. However, as mentioned in the previous chapter, because of their complexities, the methods have not received a wide acceptance among practicing engineers. Among the elastic solutions that are available in the literature, Giroud's (1972) solution for the ideal semi-infinite elastic half-space is the most complete. Using cylindrical coordinates, the author gives formulae for estimating stress and strains at any point below a rigid circular footing including points at $\xi > 1$. The vertical displacement is given by:

$$w = \frac{(1+\nu)q_a R}{E} [\overline{M}_z + (1-2\nu)\overline{M}'_z] \qquad 3.5.1$$

where $\overline{M}_z = \beta\overline{N}'_z + \overline{M}'_z$

$$\overline{M}'_z = \frac{1}{2}\,\text{Arc sin}\,\frac{2}{\sqrt{\beta^2 + (1+\xi)^2} + \sqrt{\beta^2 + (1-\xi)^2}}$$

$$\overline{N}'_z = \frac{\text{Sin}\,\phi/2}{2\,\sqrt[4]{A}}$$

$$A = (\xi^2 + \beta^2 - 1)^2 + 4\beta^2$$

$$\phi = \text{Arc tan}\,\frac{2\beta}{\xi^2 + \beta^2 - 1}$$

$$\xi = r/R$$

$$\beta = z/R$$

In the book, which is included in the list of references, $\overline{M}_z$ and $\overline{M}'_z$ are found tabulated for ξ ranging from zero to 12 and β ranging from zero to 10, making the calculation of settlement much too easy. We notice that when $\xi = \beta = 0$, then $\overline{M}'_z = \overline{M}_z = \frac{\Pi}{4}$. When these values are substituted in Equation 3.5.1 it reduces to Boussinesq's solution which was given by Equation 3.2.1.1.

3.6 Consolidation Settlement

Consolidation settlement is the result of plastic deformation and void-ratio reduction of a soil mass which in turn are functions of time and pore-water pressure. As mentioned in Section 3.1, there is no practical mathematical model for the plastic deformation also known as secondary consolidation, hence this discussion will concentrate on the important primary component. Although, there is a large difference between the initial pore pressure distributions beneath a flexible and a rigid circular footings, the rate of consolidation is generally the same; with the rigid plate tending to settle at a slightly slower rate, Poulos (1968). It is therefore, valid to assume a uniform loading when estimating the consolidation settlement of a rigid raft. The quantity is usually estimated from standard oedometer tests, which is a one-dimensional model. However, this method has only very limited applications, since in the field there is lateral straining as well as pore pressure dissipation in the radial direction. The condition of no lateral strain is approximately true for at least two practical cases:

a) that of a thin layer of clay lying between rigid beds of sand and rock,

b) that of a loaded area of horizontal extent which is great compared with the thickness of the underlying clay.

When the lateral strain is negligible except at the edges of the footing, the excess pore water pressure can be estimated by Skempton's (1957) formula as:

$$u = B[\Delta\sigma_3 + A(\Delta\sigma_1 - \Delta\sigma_3)] \qquad 3.6.1$$

where u = the excess pore-water pressure

$\Delta\sigma_1, \Delta\sigma_3$ = vertical and lateral stresses respectively

A, B = are pore pressure coefficients which are constant for the soil

The coefficient A depends on the stress history of the clay whereas B varies mainly with the degree of saturation. Hence, neglecting lateral straining, the general approximate consolidation settlement for a deep clay deposit is given by Equation 3.6.2

$$\rho_c = \int_o^z m_v u \, dz \qquad 3.6.2$$

Since for saturated clay B = 1, substituting for B as well as for u, and rearranging the terms we get

$$\rho_c = \int_o^z m_v \Delta\sigma_1 [A + \frac{\Delta\sigma_3}{\Delta\sigma_1} (1-A)] dz \qquad 3.6.3$$

And from the oedometer test, the one dimensional settlement is given by

$$\rho_{oed} = \int_o^z m_v \, \Delta\sigma_1 \, dz \qquad 3.6.4$$

where ρ_c, ρ_{oed} = the general and the oedometer settlements

m_v = the coefficient of volume compressibility

Knowing the stress history or the coefficient A, a correction can be applied to Equation 3.6.4 to estimate the consolidation settlement from oedometer tests without having to evaluate Equation 3.6.3. Such a correction factor is given in a graph form for A ranging from zero to 1.2 and thickness of soil to width of footing ratio varying from .5 to 4 by Skempton and Bjerrum (1957). However, since the determination of A requires careful laboratory testing, the correction factor in the way presented by the above authors is not useful for most design offices. A more practical approach is to correlate the overconsolidation ratio (which is easily calculated from oedometer tests) and the depth of the compressible layer to the correction factor. One such correlation prepared by Leonards (1976) is reproduced in Figure 3.6.1. This correction factor, first introduced in Equation 3.1.1 is just a ratio of Equation 3.6.3 to 3.6.4.

The simplest method of estimating the oedometer settlement is from void ratio or strain versus log pressure curves. The method is found commonly discussed in almost all soil mechanics text books.

3.7 The Concept of Active Zone of Settlement

Deep settlement measurements have in the past indicated that the deformation of the subsoil is damped out after a certain critical depth.* The space occupied by the soil above this depth is referred to as the active zone of settlement. According to Stefanoff et al (1973) and Burmister (1956), the depth of the active zone of settlement depends on:

1) the size and shape of the foundation area
2) the average foundation pressure
3) the basic contact stress distribution pattern
4) the magnitude and distribution of the overburden and the excavation stresses
5) the type of soil and the thickness of the compressible layer.

By far the most detailed laboratory and field work carried out to date is that by Shvets and Kulchitskii (1970). The tests covered a wide range of variable soil types and the footings consisted of 5000 cm^2 metal and 10,000 cm^2 concrete dies. Although the critical depth

*The critical depth of deformation is defined as the boundary below which the percent settlement due to the applied load is not significant.

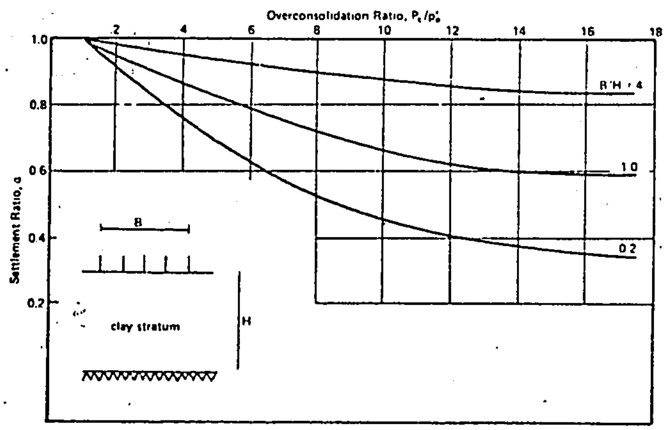

FIGURE 3.6.1 CORRECTION FACTORS FOR THREE DIMENSIONAL EFFECTS TO BE APPLIED TO SETTLEMENT CALCULATIONS FROM STANDARD OEDOMETER TESTS. (AFTER LEONARDS, 1976).

depended on the characteristics of the soil, in general the field tests showed that it lay between 1.5 to 2.0 D. There are a number of advantages to knowing this depth, and the two important ones are: It makes it easier to select or derive a mathematical model that simulates the problem best. And, secondly it will help estimate the minimum depth of boring required. There are available design methods which help the soils engineer in the selection of the critical depth of settlement. In fact the Russian Construction and Standards Regulation (SNiP) has recognized the existence of this depth and gives rules for estimating it. The practice is to take the point below the loaded area where the stress due to the applied load is less than or equal to a certain fraction of the effective overburden pressure. This fraction varies from .2 to .5. It is believed that elastic theory when used in conjunction with the active zone of settlement has the same effect as considering the more complex non-linear behaviour of soils. It should be noted that the method is just a design technique and not an exact theory. However, it will give reliable settlement results provided that the deformation properties of the soil do not get worse with depth.

Incidentally, Burmister (1956) had recognized this concept and even proposed a method for estimating the critical depth.*

*According to Burmister, the critical depth is that at which the foundation stress becomes less than 20 percent of overburden stresses for granular soils and 10 percent of overburden stresses for clay soils. This rule recognizes the fact that the pressure bulb penetrates deeper in clay than it does in granular soils. It should be remembered that his work applies to flexible footings only.

3.8 Settlement Data and Analyses by Other Researchers

In this section, raw settlement data as well as results of analyses found in the geotechnical literature and elsewhere are presented. Once again only results of investigations in similar clays are given. Some of these data are being reported for the first time to be used in a comparative analysis in Chapter 7. The comparison to be made is between three sizes of loaded surfaces all located in the same clay formation; and they are: the large circular raft, six similar size square footings and four load test plates. All the test plates and the instrumentation of the square footings were performed by the geotechnical group of the Department of Civil Engineering of the University of Ottawa. The site is the Woodroffe Campus of the Algonquin College of Applied Arts and Technology (see map, Figure 4.1.1). Moreover, the soil profile is the same as that reported by Gaumy (1970) Figure A1. In all cases, the settlements were measured with respect to a deep seated bench mark.

3.8.1 Plate Load Tests and a Full-Scale Footing Test Performed at the Algonquin College Campus, Ottawa

This information is well documented in a thesis for a Master of Applied Science degree in geotechnical engineering by Hanna (1976). The full-scale footing test was carried out to assess the performance of the actual footings to support a new extension building. However, the main purpose for the plate load tests which were carried out four years after the completion of the building was to investigate if they could have been used for the actual footing design instead of performing a relatively expensive full-scale footing test. Figure 3.8.1.1 shows the relative locations of the test footing, the site for the plate load tests and the five interior instrumented footings, to be discussed in the next section. The figure also gives the elevations of the original ground and the underside of the footings and plates.

3.8.1.1 Plate Load Tests

The plate tests included both vertical and horizontal loadings in a specially prepared trench close to the test footing level. Since the thesis is only concerned with vertical deformation, only the results of the vertical load tests will be examined. The plates have diameters of 46 cm (18 in.). Deep settlement gauges were installed at 90-degree intervals at a distance of R/2 from the centre. The gauges made of 9.5 mm (3/8 in.) diameter wood drill bits welded to extension rods, were installed at depth of 1R, 2R, 3R and 4R, where R is the radius of the plate; and settlement readings were taken with a dial gauge accurate to .03 mm (.001 in.). For more detail concerning settlement gauges the reader is referred to Chapter 5 of this thesis. In the test three types of loading procedures were followed. The first two, which will be discussed below were designed to study the elastic deformation of the soil while the third one was for studying creep. In the first two procedures a constant loading rate of 0.1 mm per min. (.004 in/min) was used. The first type (tests V2/1, V3/1) involved

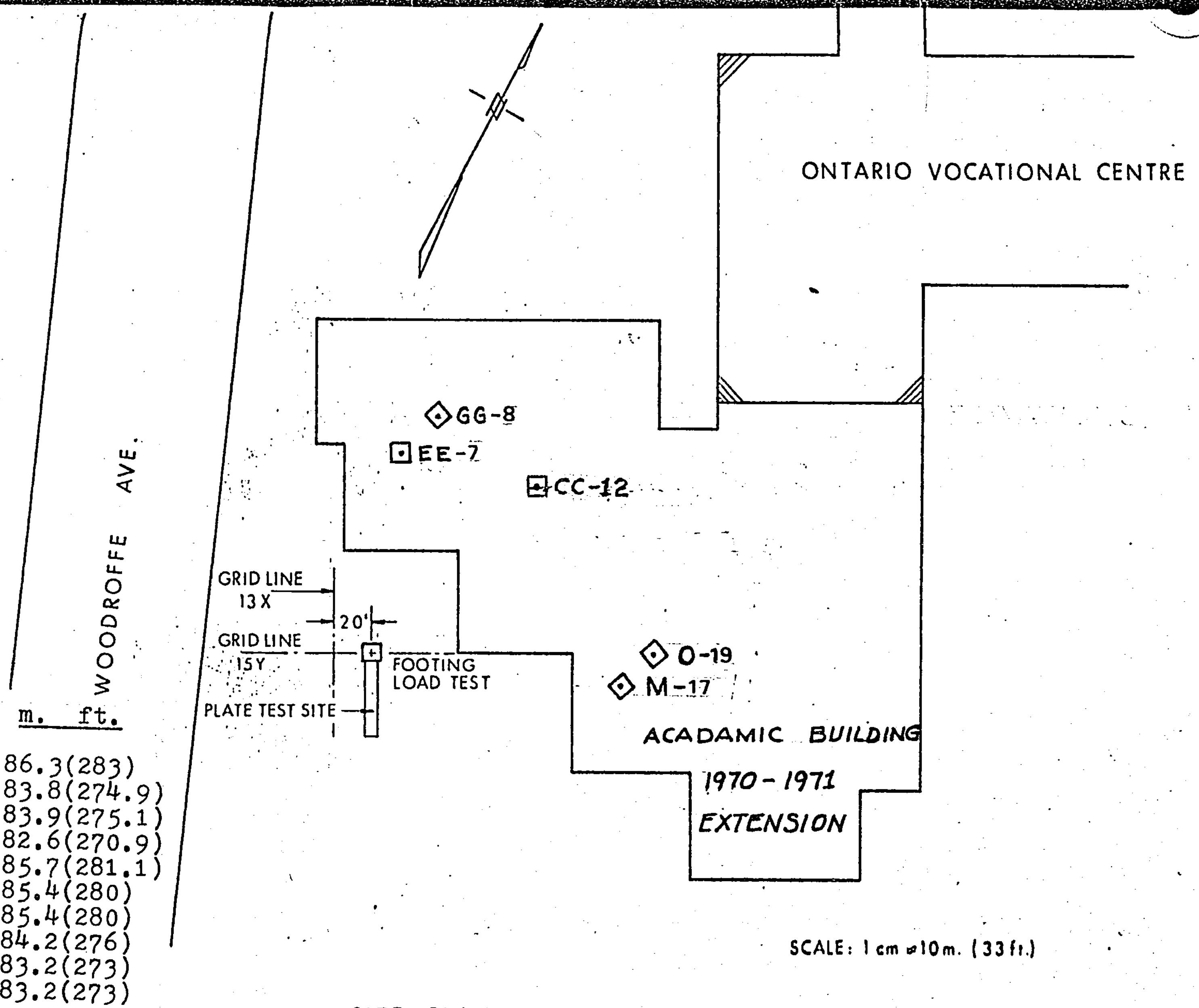

ELEVATIONS	m. ft.
Orig. ground	86.3(283)
V2/1	83.8(274.9)
V2/2	83.9(275.1)
V3/1	82.6(270.9)
Test Footing	85.7(281.1)
M-17	85.4(280)
0-19	85.4(280)
CC-12	84.2(276)
EE-7	83.2(273)
GG-8	83.2(273)

SITE PLAN

FIGURE 3.8.1.1 ALGONQUIN COLLEGE OF APPLIED ARTS AND TECHNOLOGY, WOODROFFE CAMPUS. Hanna, 1976 keeping the pressure at a given load until the settlement rate became .03 mm/min (.001 inches/min.) while in the second case (tests V2/2 and V3/2), the plates were subjected to frequent loading and unloading. The settlement of the soil below each gauge at various pressure levels is given in Figures 3.8.1.1.1 to 3.8.1.1.4 inclusive. Moreover, to show the similarity in the results of the two test procedures, Figures A4 and A5 give the results of the total settlement at various pressure levels.

3.8.1.2 Full-Scale Footing Test

The test footing is the same one used by Gaumy (1970) to study the distribution of contact pressures (Section 2.5). Deep settlements at various levels below the footing were measured by means of spiral gauges (Chapter 5) installed at depths of .25B, .5 B, B and 1.5 B, where B is the width of the footing. Two sets of gauges were installed: one set near the centre and another near the edges (see Figure A2). The load settlement curves for both locations below each settlement gauges are given in Figures 3.8.1.2.1 and 3.8.1.2.2 inclusive.

3.8.2 Algonquin College Building Footings

As mentioned earlier, the footings for the structure were designed based on the results of the full-scale footing tests. However, five of these footings were also instrumented to study both short and long term load settlement behaviour of the soil. Although,

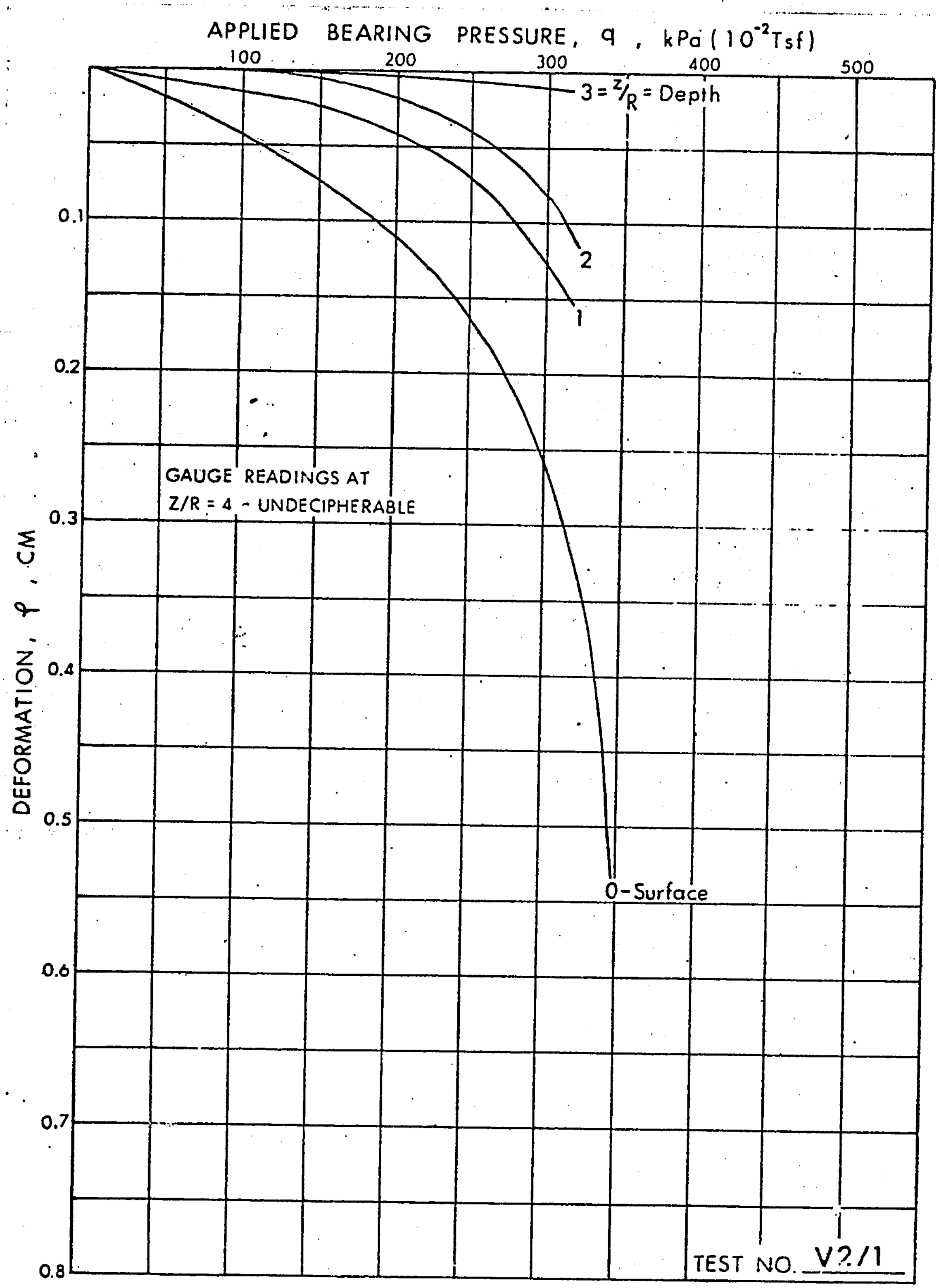

TOTAL DEFORMATION AND DEFORMATION AT VARIOUS DEPTHS BELOW LOADED SURFACE.

FIGURE 3.8.1.1.1. (After Hanna, 1976)

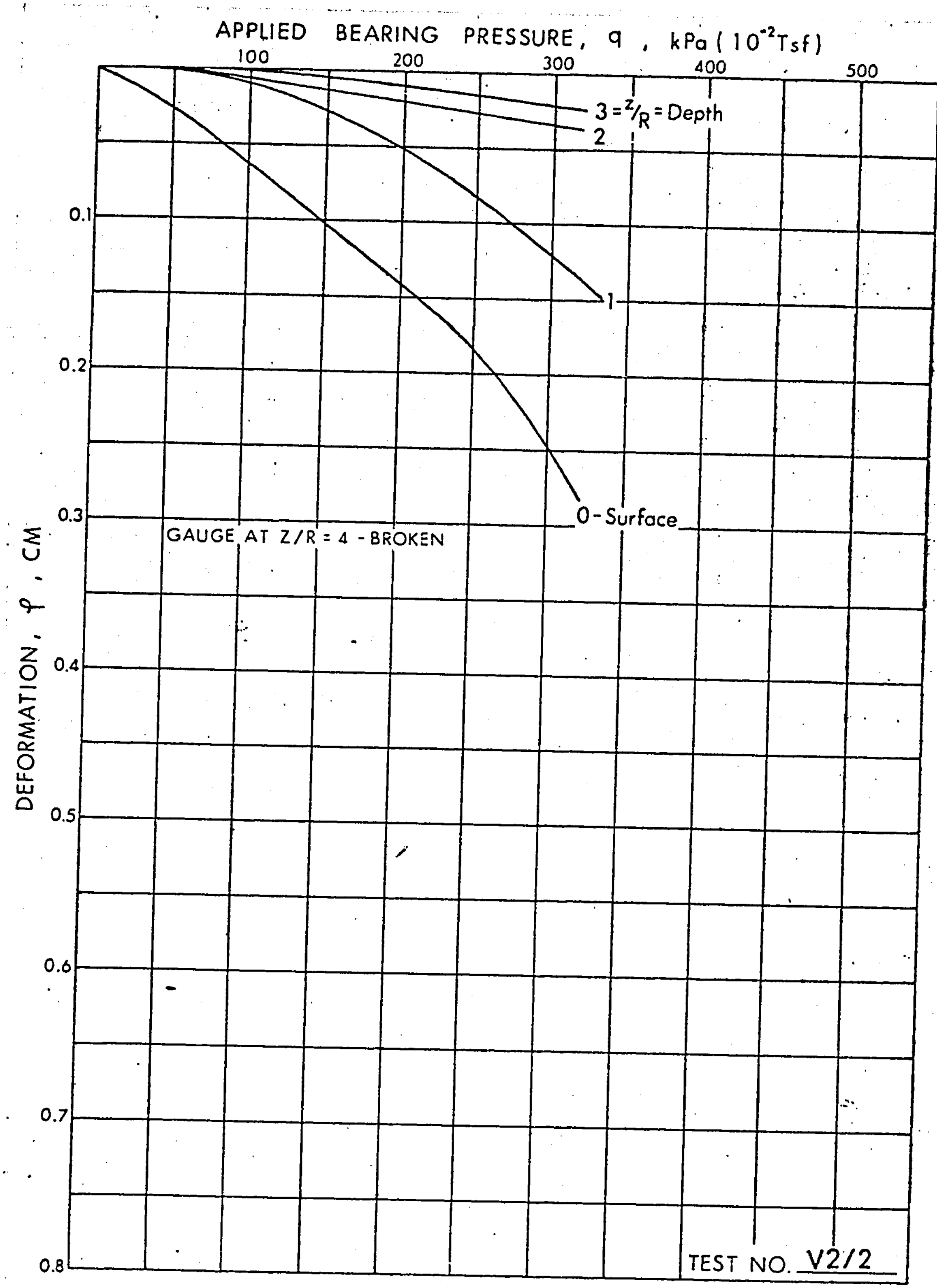

TOTAL DEFORMATION AND DEFORMATION AT VARIOUS DEPTHS BELOW LOADED SURFACE.

FIGURE 3.8.1.1.2 (After Hanna, 1976)

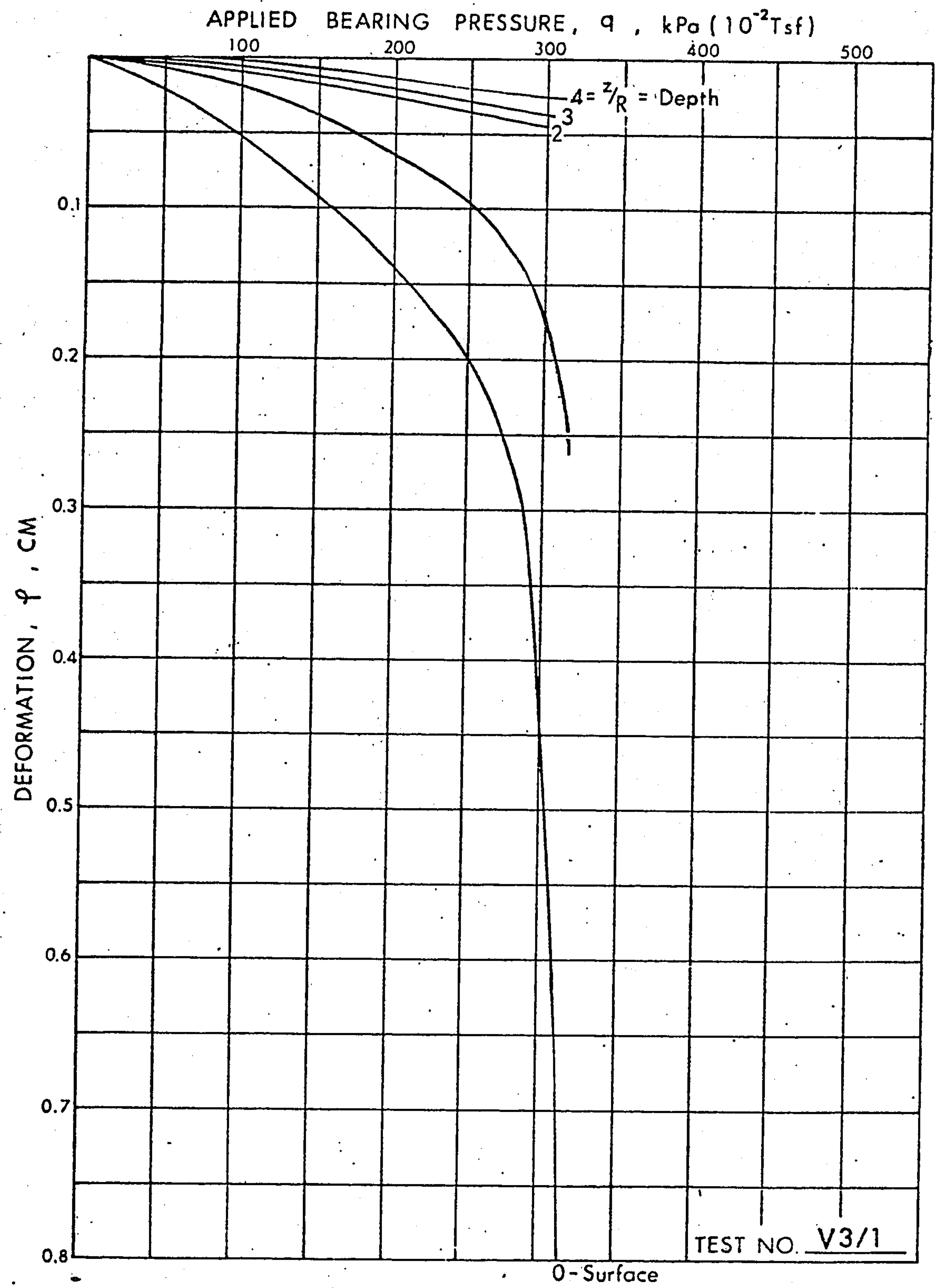

TOTAL DEFORMATION AND DEFORMATION AT VARIOUS DEPTHS BELOW LOADED SURFACE.

FIGURE 3.8.1.1.3 (After Hanna, 1976)

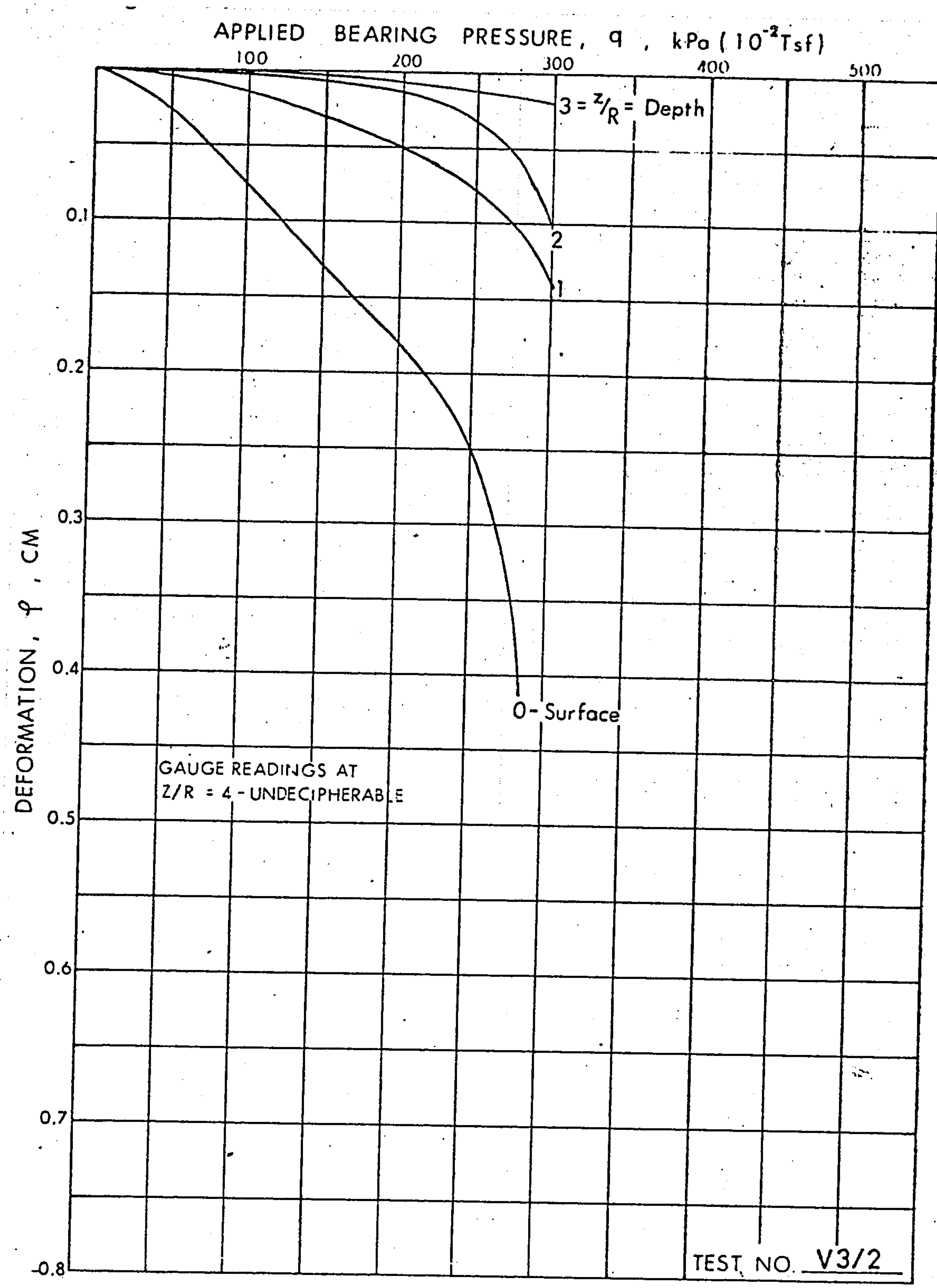

TOTAL DEFORMATION AND DEFORMATION AT VARIOUS DEPTHS BELOW LOADED SURFACE.

FIGURE 3.8.1.1.4 (after Hanna, 1976)

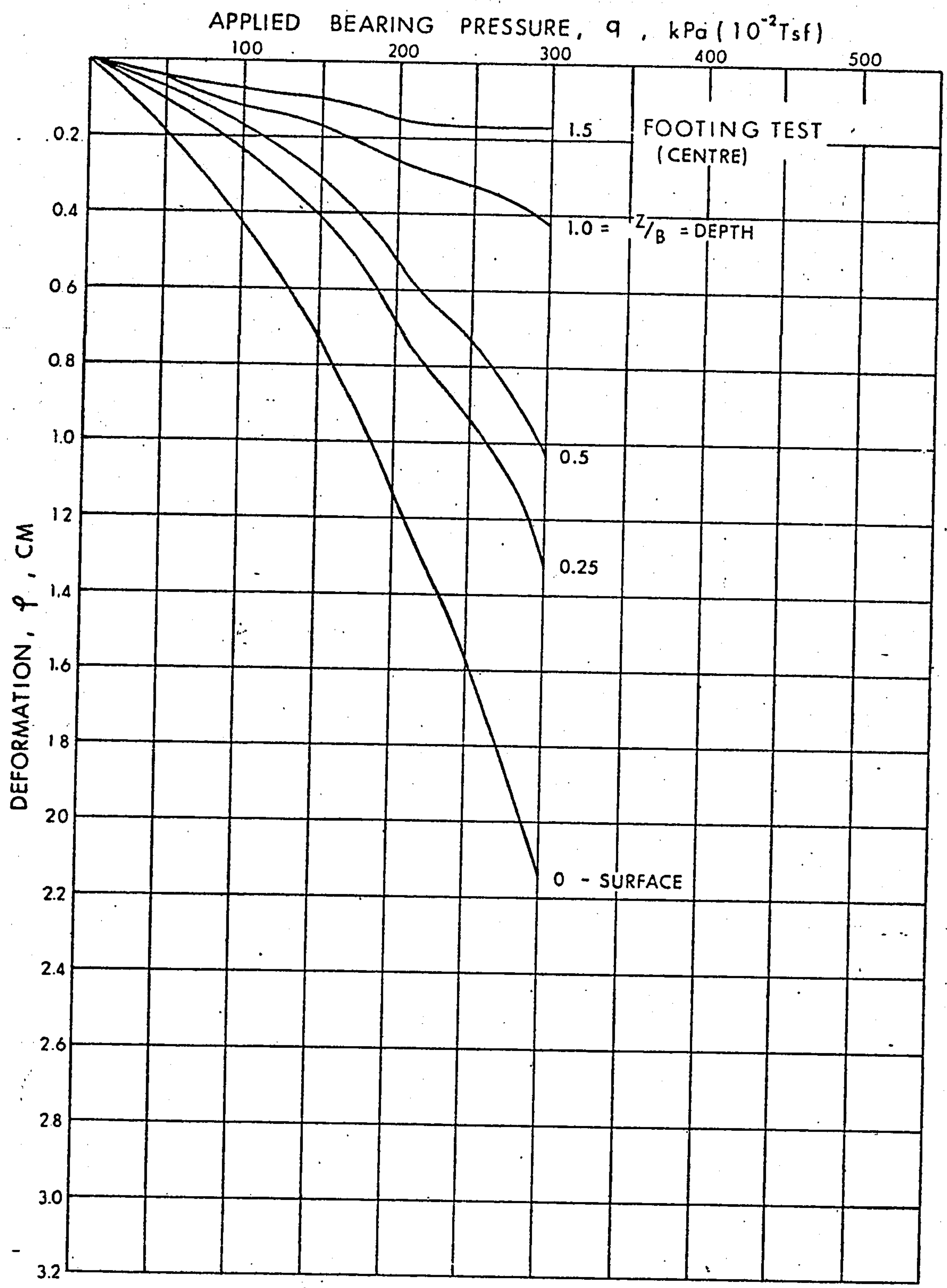

TOTAL DEFORMATION AND DEFORMATION AT VARIOUS DEPTHS BELOW LOADED SURFACE.

FIGURE 3.8.1.2.1 (After Hanna,1976)

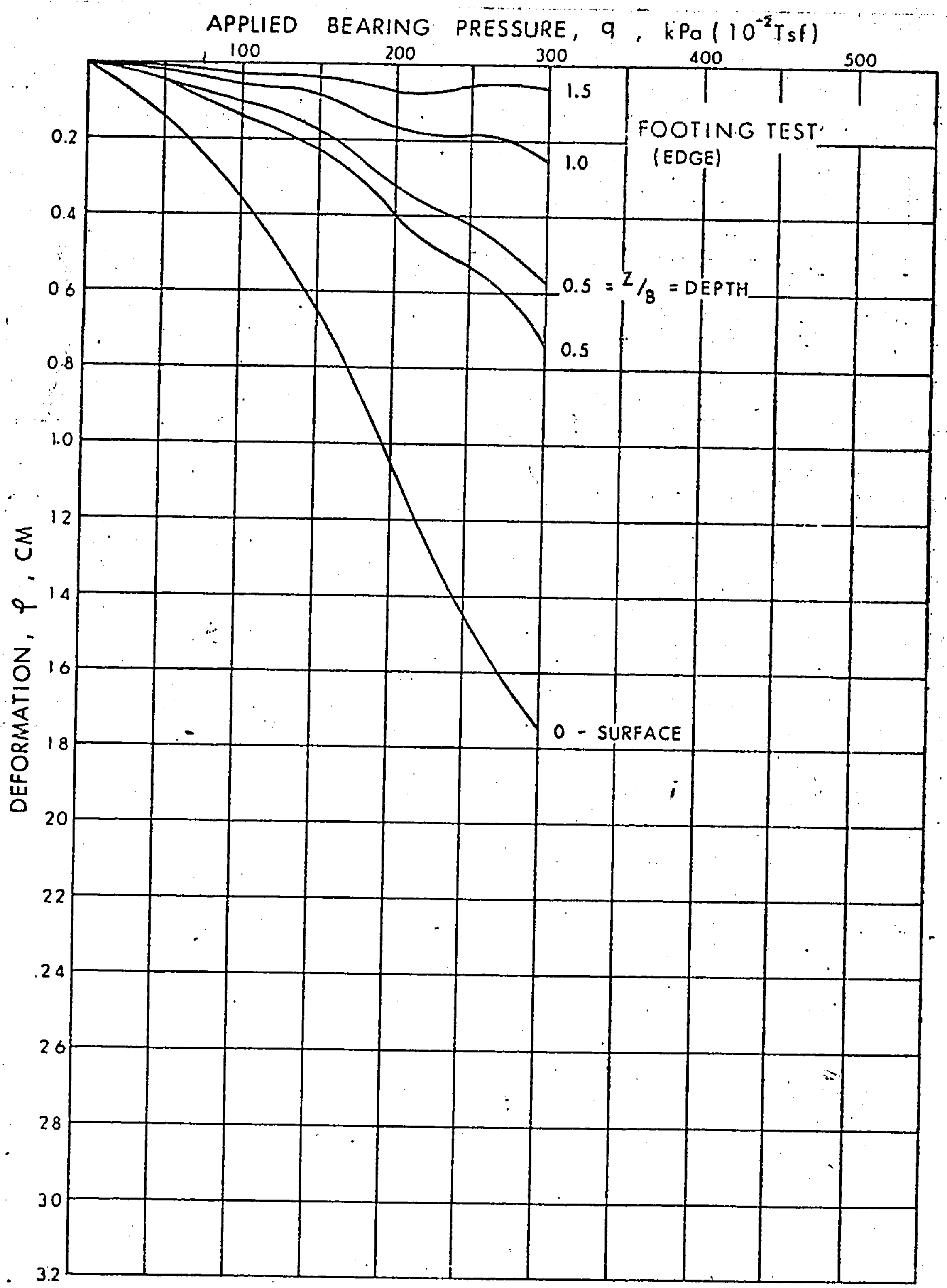

TOTAL DEFORMATION AND DEFORMATION AT VARIOUS DEPTHS BELOW LOADED SURFACE.

FIGURE 3.8.1.2.2 (After Hanna, 1976)

the load settlement data for footings M-17 and GG-8 have previously been presented by Bauer et al (1976), the data for all the five footings is being presented for the first time for further analysis in Chapter 7. Figures 3.8.2.1 to 3.8.2.5 inclusive give, the load settlement curves, the size and elevation of the footings as well as the location of the deep settlement gauges. The depth of the settlement gauges are indicated on the corresponding load settlement curves.

3.8.3 E_u/S_u Values in the Literature

In Chapter 1, it was mentioned that one of the objectives of this thesis was to study the distribution of E_u/S_u ratios of the soil with depth and with changes in the applied presure. To date, the most detailed work done on the subject is that of D'Appolonia et al (1971). The authors chose their suggested values for various soil types after examining a sufficiently large number of case records. For their analysis the authors used the semi-infinite elastic half-space model and a Poisson ratio of 0.5. Table 3.8.3.1 lists the results of their calculations for the various case records. It is suggested in the text that for lean inorganic clay of moderate to high sensitivity a value of E_u/S_u between 1000 and 1500 will give reliable settlement estimate. It will be seen later (Chapter 4), the soil discussed in this project falls in the above clay category.

3.9 Summary of Important Points

Theories indicate that for elastic soils, the settlement varies directly with the size of the footing. Limited load tests in the

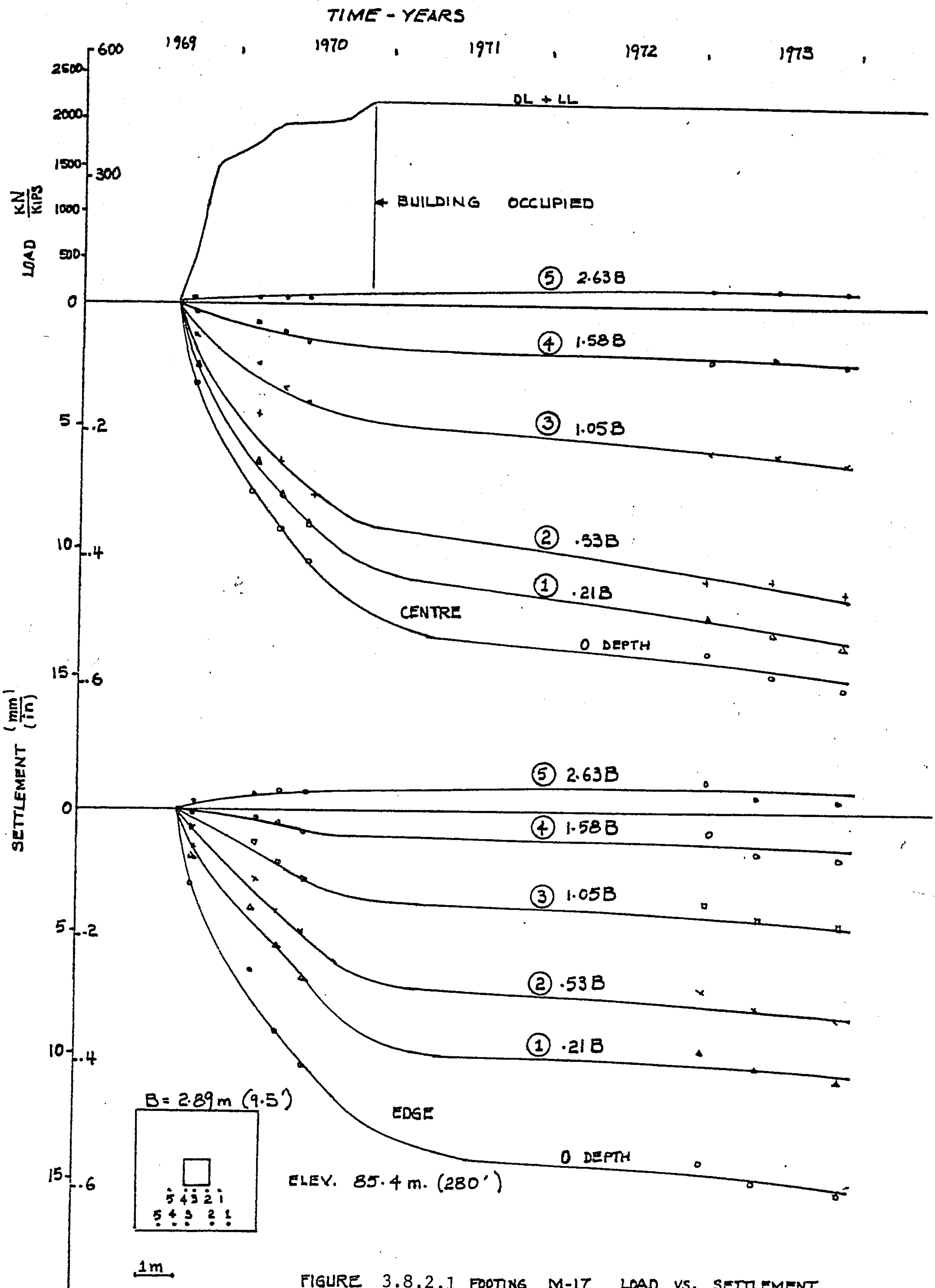

FIGURE 3.8.2.1 FOOTING M-17 LOAD VS. SETTLEMENT.

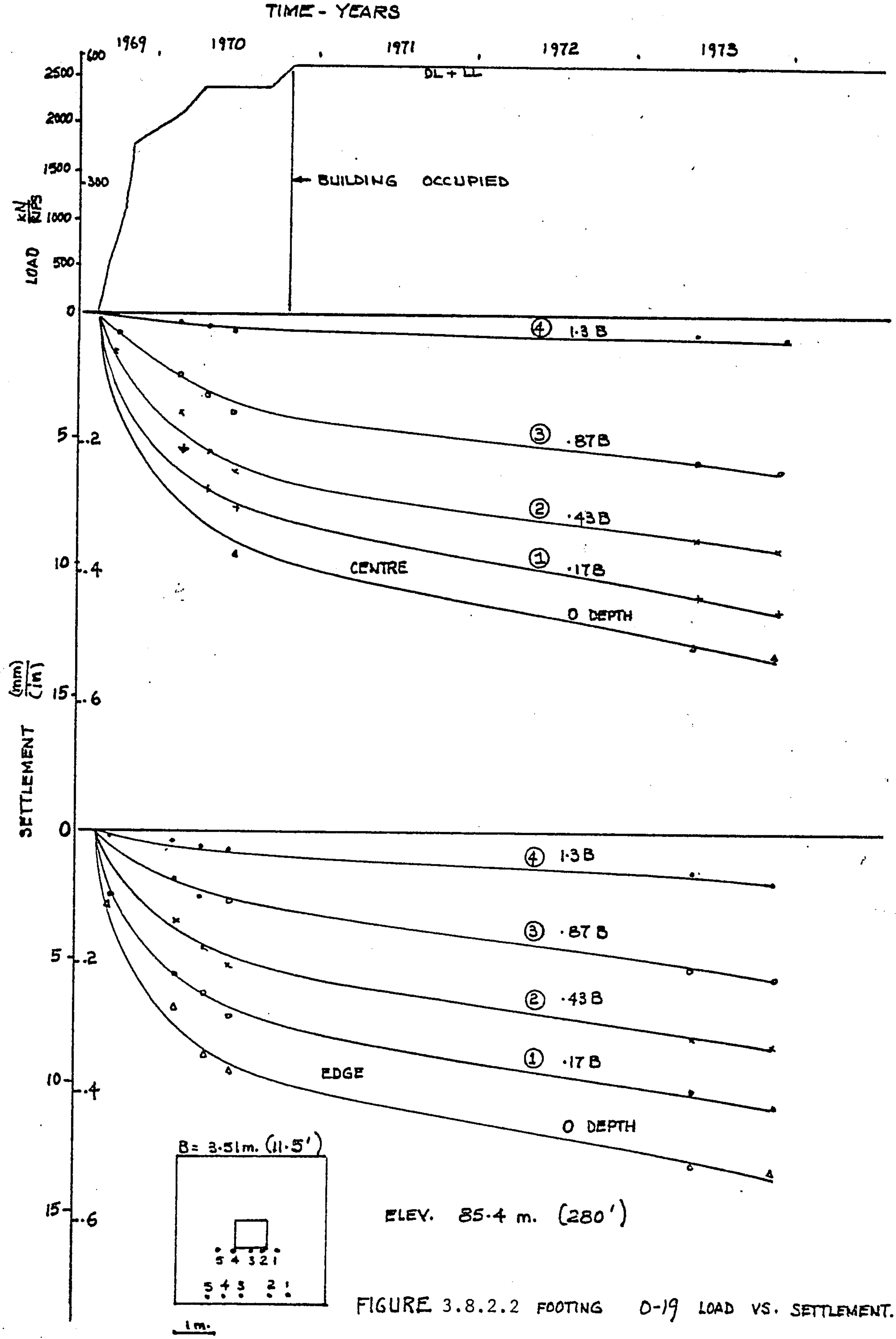

FIGURE 3.8.2.2 FOOTING O-19 LOAD VS. SETTLEMENT.

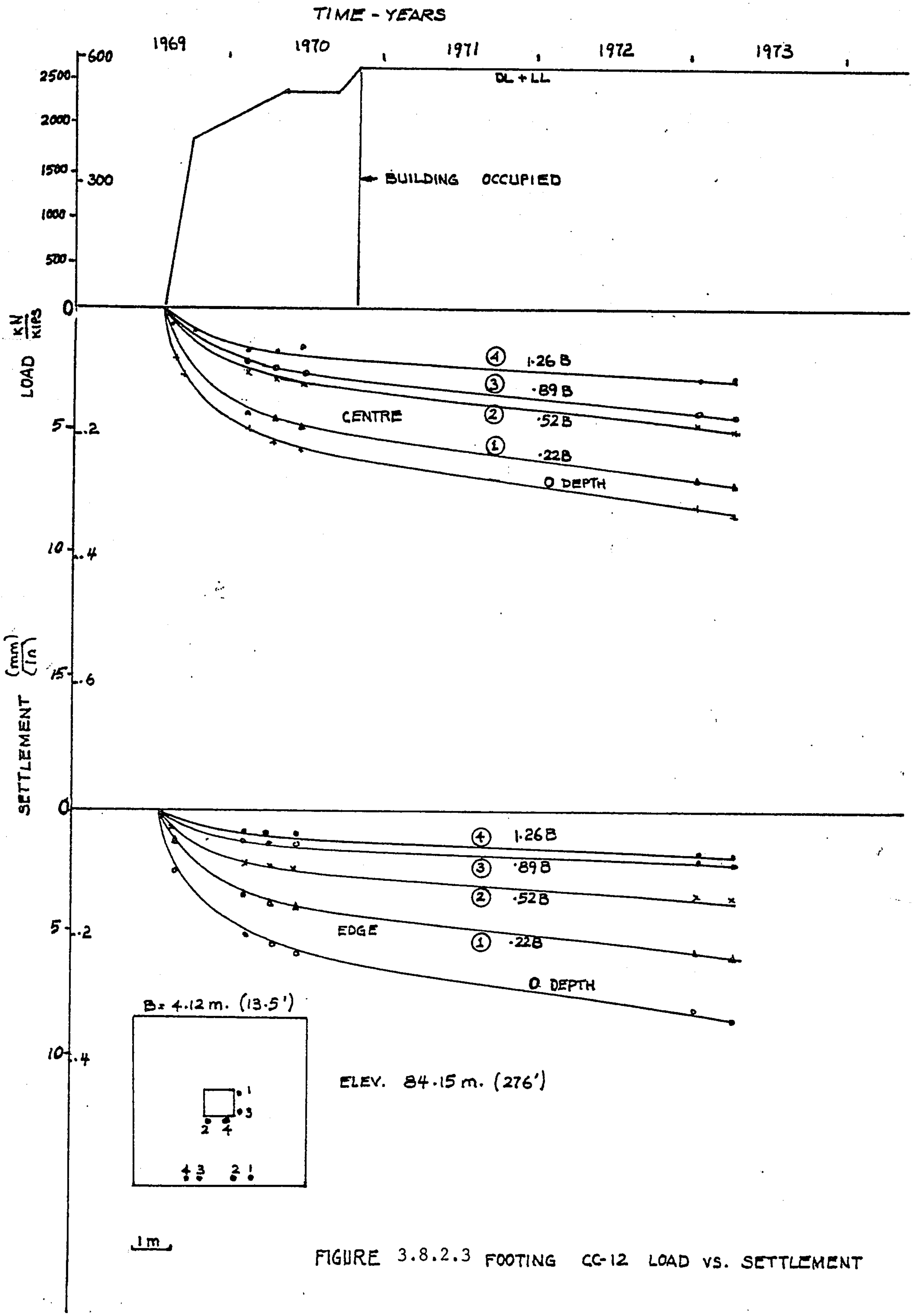

FIGURE 3.8.2.3 FOOTING CC-12 LOAD VS. SETTLEMENT

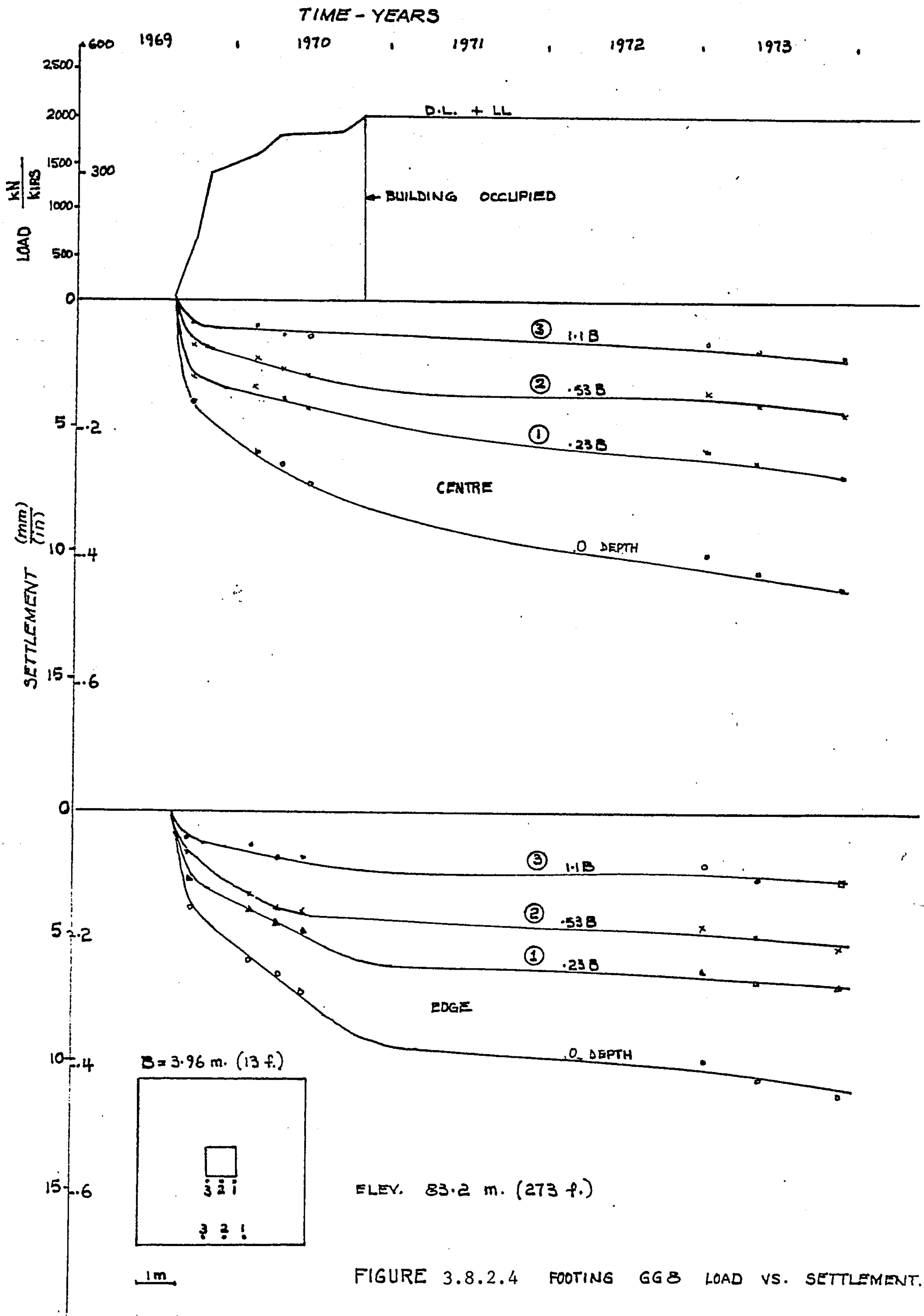

FIGURE 3.8.2.4 FOOTING GG8 LOAD VS. SETTLEMENT.

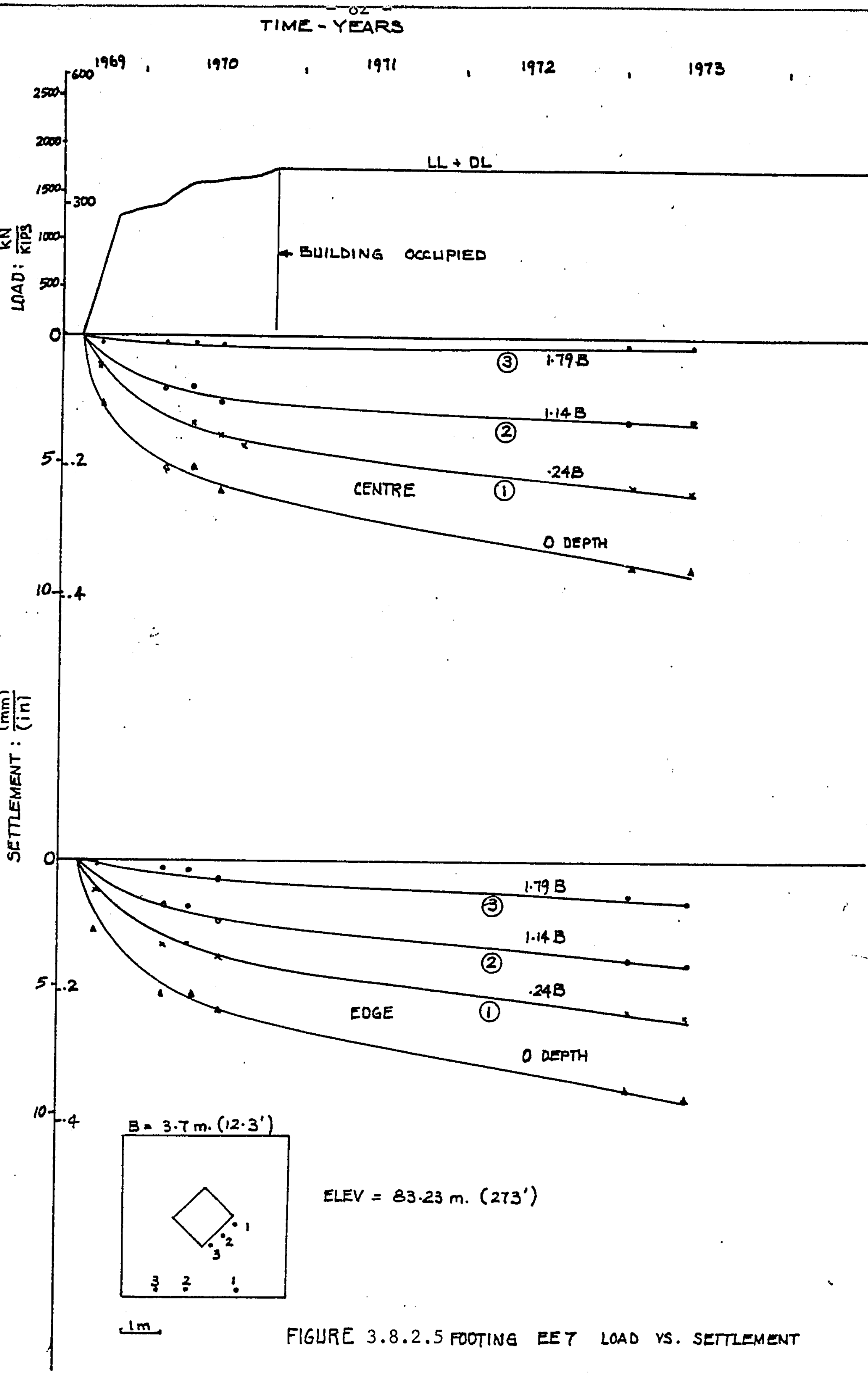

FIGURE 3.8.2.5 FOOTING EE7 LOAD VS. SETTLEMENT

$(E_u)_{field}$, in tons per sq m	E_u/S_u	Source of S_u	Reference	Case #	Location and structure	Clay Properties: PI, as a percentage	Sensitivity S_t	OCR
(6)	(7)	(8)	(9)	(1)	(2)	(3)	(4)	(5)
7,600	1,200	CIU	Simons (1963)	1	Oslo-nine storey bldg	15	2	3.5
990	1,000	Field Vane		2	Asrum I-circular load test	16	100	2.5
	1,200	CIU	Hoeg, et al. (1969)					
880	1,000	Field Vane		3	Asrum II-circular load test	14	100	1.7
	1,100	CIU	Hoeg, et al. (1969)					
1,300	1,200	Field Vane		4	Mastemyr-circular load test	14		1.5
	1,700	Bearing Capacity	Clausen (1969)					
3,000	2,000	Field Vane	Haley & Aldrich, Inc.	5	Portsmouth-highway embankment	15	10	1.3
	1,700	Bearing Capacity	Ladd (1969)					
10,000	1,600	Field Vane	MIT	6	Boston-highway embankment	24	5	1.5
	1,200	CK_oU						
13,000	2,500	Field Vane						1.0
	1,500	CK_oU						
3,200	1,400	Field Vane		7	Drammon-circular load test	28	10	1.4
	1,100	CK_oU	NGI					
2,200	400	Field Vane		8	Kawasaki-circular load test	38	6±3	1.0
		CIU	MIT					
5,000	800	CIU	Lambe (1962)	9	Venezuala-oil tanks	37	8±2	1.0
100-200	80-160	UU and Bearing Capacity	Ladd, et al. (1969)	10	Maine-rectangular load test	33±2	4	1.5-4.5

Table 3.8.3.1 Case Studies of Initial Settlement (after D'Appolonia et al (1971))

literature also show this dependency of settlement on the size of the footing, however, the relationship is far from linear.

Since the stress in the soil medium below the centre of a footing is higher when the load is flexible than when it is rigid, under similar conditions, the former footing settles more than the later one. In general, theory shows that footing roughness reduces settlement, however, for all practical applications for Poisson's ratio equal or larger than 0.3, the difference between the behaviour of the smooth and the rough footings is negligible. The depth of the foundation as well as the thickness of the compressible layer are more important than the above factors. An increase in foundation depth and a decrease in the compressible layer thickness results in a reduced settlement.

The effects of soil non-homogeneity are: to localize surface displacement, increase the contribution due to consolidation and to reduce differential settlement under uniform loads. Similarly, increasing stress anisotropy gives the soil a lateral load spreading capacity; the result is a relatively smaller vertical settlement. For normal designs where the factors of safety is equal to or greater than 3, effect of local yield is negligible.

Methods for calculating immediate and consolidation settlements as well as a discussion on the active zone of settlement are given. Knowledge of the active zone of settlement is very important for predicting the deformation of the soil with some confidence.

To make the analysis of elastic settlement distribution and E_u/S_u ratios with depth and applied pressure more complete, load settlement data for four plates and six square footings are introduced. Also, a detailed study of E_u/S_u values for various clay soils studied by D'Appolonia et al (1971) is introduced. A range of E_u/S_u values between 1000 and 1500 is recommended for the type of clay which this thesis is concerned with.

CHAPTER 4

SITE DETAILS

4.1 General

The site where the instrumentation was carried out was previously investigated by the National Research Council (NRC), Division of Building Research (DBR). The investigation involved field and laboratory tests to find the cause of the failure of a large concrete silo, supported on a ring foundation, that had overturned the previous year due to weak foundation. The site was chosen since it offered the opportunity to study the behaviour of farm silo foundations in Leda Clay. This interest has stemmed from the fact that there have been a number of other silo failure problems in this same soil.

When the owner decided to build a new silo to replace the one that had failed, the site once again became available for further research work. The National Research Council recommended a safe design bearing capacity value of 1750 psf for the new structure. In return, the owner allowed the instrumentation of the new structure, which was jointly carried out by NRC, DBR and the Geotechnical Group of the University of Ottawa. The main reason for studying the behaviour of the new silo was to obtain field data which would make future designs of ring foundations in similar soils relatively more reliable; without having to use uneconomically high factors of safety.

However, the choice by the owner to build a "Harvestore" metal silo which had to be founded on a large stiff raft foundation, to achieve a factor of safety of 3 against bearing capacity failure, caused the subject of the research to be changed to the study of the performance of a rigid raft in Leda Clay.

4.1.1 Location

The site of the project shown in Figure 4.1.1 is located some 11 km (6.1 mi) south of the Queensway on Richmond Road, in Richmond, Carleton County, at an elevation of about 107 m (315 ft). The structure was founded about 6 m (20 ft) west of a concrete silo that had overturned in September 1975 (Figure 4.1.2). The location for the new silo was chosen to make sure that its foundation would not be affected by the clay that was disturbed due to the overturning of the previous one. A field soil investigation was carried out by technicians of the National Research Council, Division of Building Research in October 1975. The test hole was made some 45-60 m (150 to 200 ft) in the corn field north of the silo. The geotechnical properties of the soil are presented later in this chapter.

4.1.2 Geological Background

Although, the bore holes did not go deep enough, bedrock is expected to be at a depth of not more than 30 to 60 m (100 to 200 ft) overlying glacial till, Karrow (1960). Wells that have been drilled around this area showed the depth of bedrock to be 30 m (100 ft).

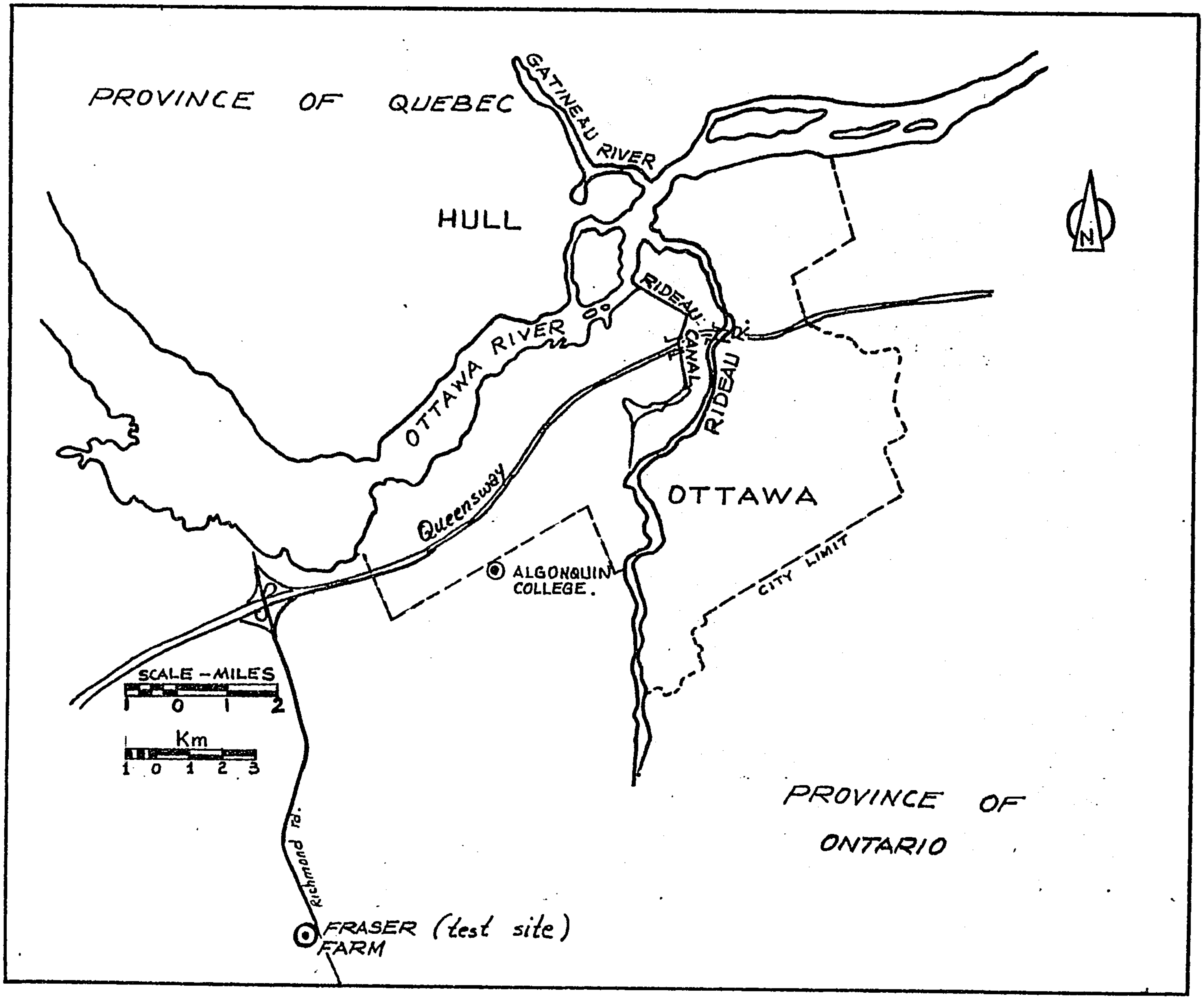

FIGURE 4.1.1. MAP SHOWING LOCATION OF PROJECT.

Figure 4.1.2.2 Large concrete silo after overturning.

Height = 32.3 m. (106 ft.), diameter = 9.14m. (30 ft.)
Wall thickness = 152 mm (6 in.)
Footing: Unreinforced ring foundation

I.D. = 7.62 m (25 ft.)

O.D. = 11.9 m. (39.0 ft.)

Thickness = 55.9 to 61 cm. (22-24 in.)

According to Gadd (1962), the bedrock should mainly be Palezoic limestone, assuming of course, the site is not one of the exceptional cases where sandstone and shale are the predominant bedrock features.

In a recent geological map No. 316/5 entitled 'Distribution of Sensitive Clay Deposits and Associated Landslides in the Ottawa Valley', Fransham et al (1976) classify the surficial soil by map unit 1. This map unit covers all sensitive clay with silt of marine origin, mainly Leda Clay, and some reworked or redeposited clay of freshwater region. Gadd (1962) defines the surface material in this area as mottled clay probably of fresh water origin that has been redeposited in river channels cut into the Leda Clay by an ancestor of the Ottawa River. The sensitive clay which will be explained in the next section was deposited in a marine environment during the submergence of the Champlain Sea by salt water. The extent of this area is shown shaded in Figure 4.1.2.1.

4.1.3 Leda Clay Formation

Ottawa is located some 250 km (400 mi) inside the most recent episode of continental glaciation which advanced across the broad St. Lawrence Valley (see Figure 4.1.2.1). The advancing ice mass caused the area to undergo substantial amounts of crustal movements under its heavy weight. During this period non-marine sediments at least 66,500 ± 1600 years old were deposited. These make up the glaciolacustrine sediments and till that are commonly found at the bottom of the clay deposit.

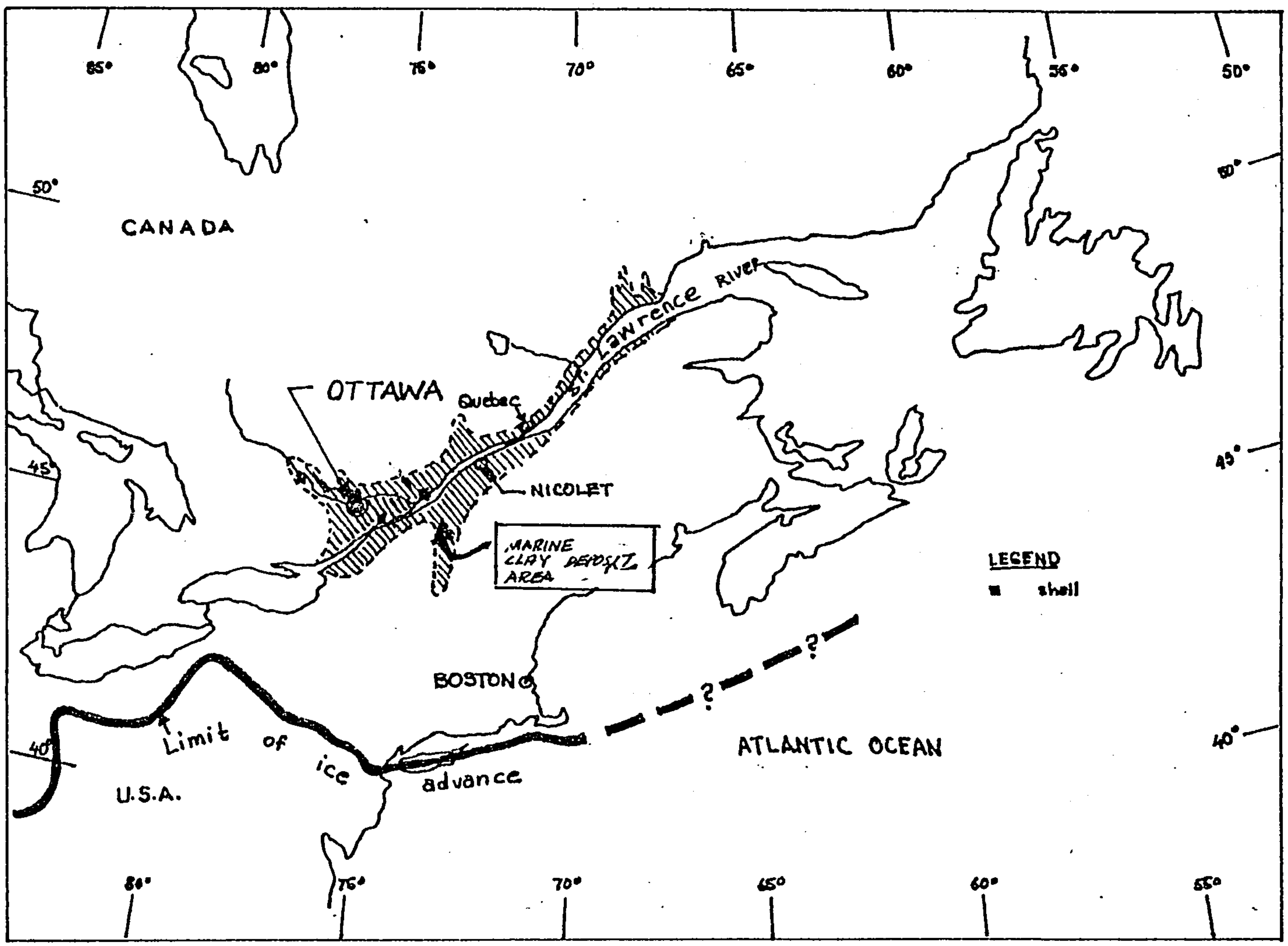

FIG. 4.1.2.1. EXTENT OF "CLASSICAL" WISCONSIN GLACIATION OF NORTH AMERICA. (AFTER T.C. KENNEY, 1964)

Around 12,400 ± 160 B.P. (Before Present) the glacier retreated and the Champlain Sea in the resulting depression was invaded by brackish water when part of the ice barrier in the region of Quebec City gave way. Recent studies by Gadd (1975) show that the Wisconsin Ice margin moved forward and retreated, probably several times in the saline water of the Champlain Sea as early as 12,400 ± 160 B.P. and as recently as 11,200 ± 170 B.P. It is in this body of marine water and subsequently in fresh water that 'Leda Clay' which is a fine sediment composed of clay to silt facies was deposited. The name came from the predominant fossil found in the deposit, which was originally believed to be leda glacialis. Recently, Gadd (1975) has pointed out that the correct identification of the fossil is Portlandia arctica. He recommends, however, the name Leda Clay be retained for the following reasons:"'Leda Clay' has become widely known, particularly among engineers and it has wider scope than the alternative names including the words 'Champlain Sea'".

Speculative trends indicate that the sensitive clay deposits in the Ottawa Valley can be divided into four distinct stratigraphic units, Fransham et al (1976). These units from the oldest to the youngest are:

1. Varved clay facies
2. Deep-water marine clay facies
3. Prograding delta facies
4. Shoaling prograding delta facies.

The varved clay facies is generally under 2 meters in thickness and therefore not very important in foundation engineering. This older clay layer was deposited in the fresh water environment of glacial lakes. It is composed of alternating fine and coarse bands of clay. This layer is not found exposed at the surface.

The deep water marine clay was deposited in brakish water when the area was invaded by salt water. The thickness of this layer is known to vary between 3 and 30 meters. The clay is easily identified by its dark grey color and also by marine shells in it.

The prograding delta facies was deposited in almost the same environment as the deep water marine clay, except in this case there was some fluctuation in the depositional environment due to variation in current and material supply (Fransham et al, 1976). The clay is either red-grey banded or light and grey banded. It has a thickness ranging between 13 and 50 m.

The shoaling prograding delta facies unit was deposited at the final stage of the Champlain Sea when the marine environment was very shallow. This facies is not common everywhere; however it can attain a thickness of up to 15 m. It is believed that this facies was subjected to channel erosion by an ancestor of the Ottawa River. The channels were subsequently refilled with redeposited Leda Clay and other fluvial sediments.

Depending on the location of the site, most structures are usually founded in one of the latest three stratigraphic units. Some of the properties of these layers are given in Table 4.1.3.1. One notes from the table that, they all have almost the same specific gravity; which is an indication that they were deposited from the

Unit	Thickness (m)	Specific gravity	Bulk density kg/m^3	Natural Water content %	Liquid Limit %	Plastic Limit %	Clay Size %	Silt Size %	Sand Size %
Varved clay facies	2-8	2.79	1920	36.4	33.2	18.6	32	45	23
Deep-water marine clay facies	3-30	2.79	1730	50.2	47.4	24.6	62	37	1
Prodelta facies	13-50	2.79	1720	55.5	53	24	70	30	0
Shoaling prograding delta-silty material	<15	2.79	1760				14	82	4
Shoaling prograding delta-clayey material	<15	2.80	1830	48.5	44	25	50	50	0

TABLE 4.1.3.1 Average Index Properties of Sensitive Marine Clay of the Champlain Sea. [After Fransham P.B. and Gadd N.R. (1976)].

same material source. Another important property they all have in common is their natural water content which is larger than their liquid limit. This is a common property of sensitive clays.

4.1.4 Description of the Soil at the Site

All the field and laboratory data about the soil at the site was compiled by the technicians of the National Research Council, Division of Building Research. Based on the above complete data, a detailed description of the soil follows.

The soil profile together with water contents, Atterberg limits and the undrained shear strength is given in Figure 4.1.4.1. The depths shown are from the original ground surface. For the first 2 m (6.5 ft) a small vane was utilized but for the remaining depth the NGI (Norwegian Geotechnical Institute) standard vane was employed. This vane which is 110 mm (4.33 in) high and 54 mm (2.13 in) wide has a square end. Samples for laboratory triaxial and consolidation tests were collected using the NGI piston sampler which has an inside diameter of 53.98 mm (2.125 in).

The top 3 m (10 ft) consists of a brown silty clay containing some angular stones, sand and even some organic material. Below 3 m the silty clay predominates, however the color changes from mottled to grey at a depth of 19 m. The top 3 m appears to be the fluvial sediments deposited in channels cut into the Leda Clay. From 3 m to 19 m the Leda Clay may be the prograding delta facies. Below 19 m the Leda Clay appears to be the deep marine facies.

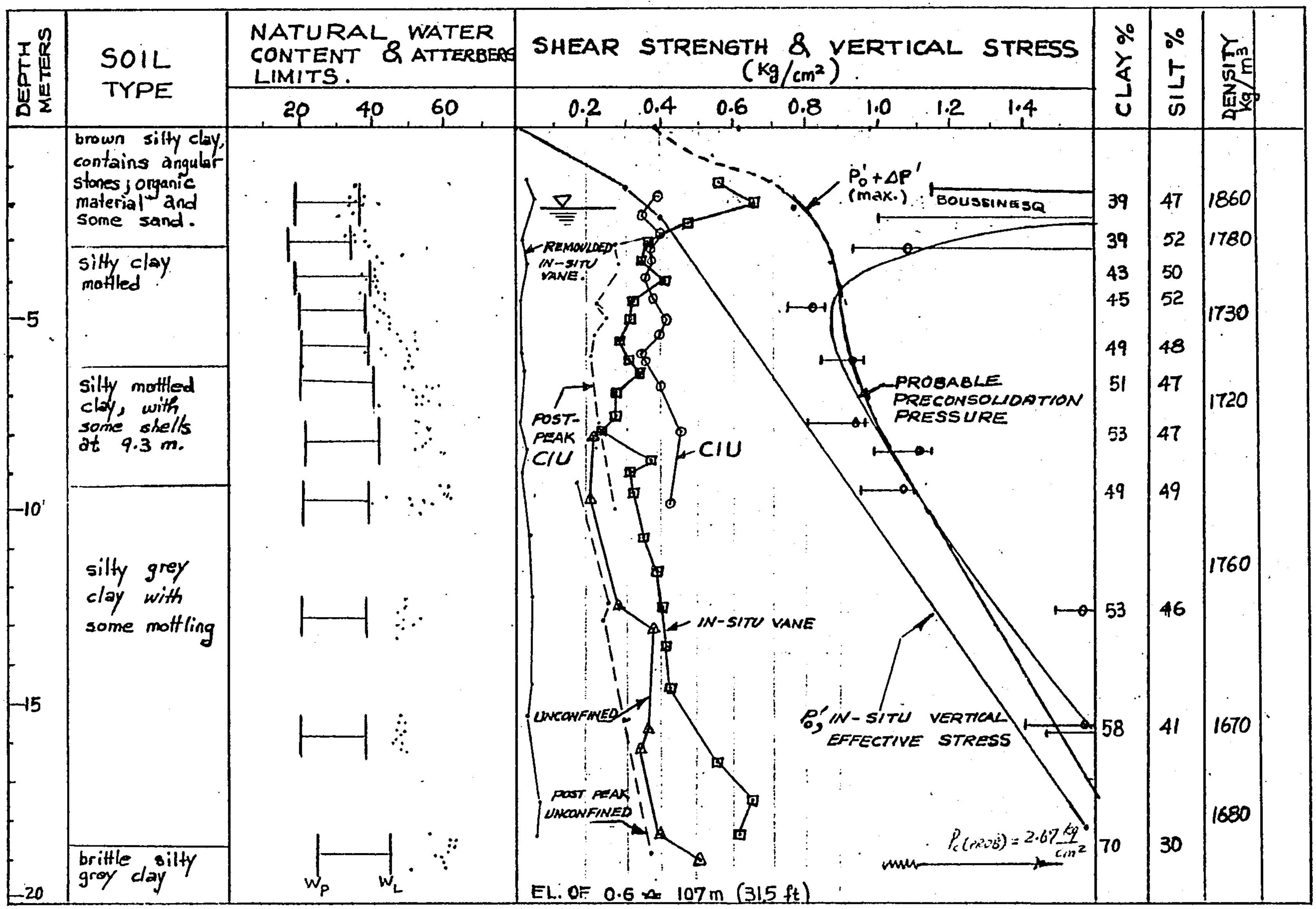

FIGURE 4.1.4.1 SOIL PROFILE

At the time of sampling, which was the first week of October, 1975, the watertable was at a depth of 2 m (6.5 ft) below the original ground surface.

The average plasticity index is about 20 and in most cases, the natural water content is higher than the liquid limit. The representative liquidity index and sensitivity are 1.40 and 22, respectively.

Other information given in Figure 4.1.4.1 include, the clay and silt content, the unit weight, the in situ vertical effective stress and also the most probable preconsolidation pressure obtained from oedometer tests. Moreover, the distribution of incremental vertical stress due to the net maximum applied load is also shown. The calculation was done below r/R = 0.67, which is also the radial location of the deep settlement gauges from the centre of the raft. The distribution is based on Giroud's (1972) solutions. For more discussion on this see Chapter 6.

From the distribution of the most probable preconsolidation pressure, the thickness of the crust appears to be about 4.5 m (14.8 ft). This top layer is overconsolidated by about 1.0 kg/cm^2 whereas the underlying firm clay is overconsolidated by only about 0.2 kg/cm^2. In terms of overconsolidation ratio (OCR), the average for the crust is about 3.5 while that for the sublayer varies from a minimum of 1.2 to a maximum of 1.5. Although not plotted in Figure 4.1.4.1 the last consolidation test shows a stiffer soil below 19.1 m (62.6 ft) (see Chapter 6).

During the installation of the instruments, the following additional information was observed: a) piezometers and deep settlement gauges were pushed through the crust by two persons with no difficulty, even though for the deeper gauges and piezometers additional help was needed to overcome the increasing side friction, b) an augered hole at the bottom of the excavation left overnight was used to measure the depth of the ground water table which was 35 cm (1.2 ft) below the bottom of the excavation or 98 cm (3.2 ft) below the original ground surface. This shows that the water table at the time of construction was about 1 m (3.28 ft) lower than at the time of field sampling. Due to rain the previous day and subsequent sunshine the following two days, the bottom of the excavation was noticeably drier in some spots than others. This was noticed when beds for the load cells were prepared. As a result the beds for some of the load cells were more softer than the others.

4.2 Size and Geometry of the Tower Silo

The silo, manufactured and installed by Ontario Harvestore Systems Ltd. has an inside diameter of 7.62 cm (25 ft) and a height of about 26.1 m (85.5 ft) excluding the roof. The raft was founded at a shallow depth of 0.72 m (2.35 ft). After the excavation was completed, the reinforcing rods, the load cells as well as twelve 51 mm, 2 in (I.D.) galvanized steel sleeves for the installation of piezometers and deep settlement gauges were securely put in their place (Figure 4.2.1(a), 4.2.1(b)). The main concrete foundation has a diameter of 13.7 m (45 ft) and a thickness of 1 m (3.28 ft). On top of this a

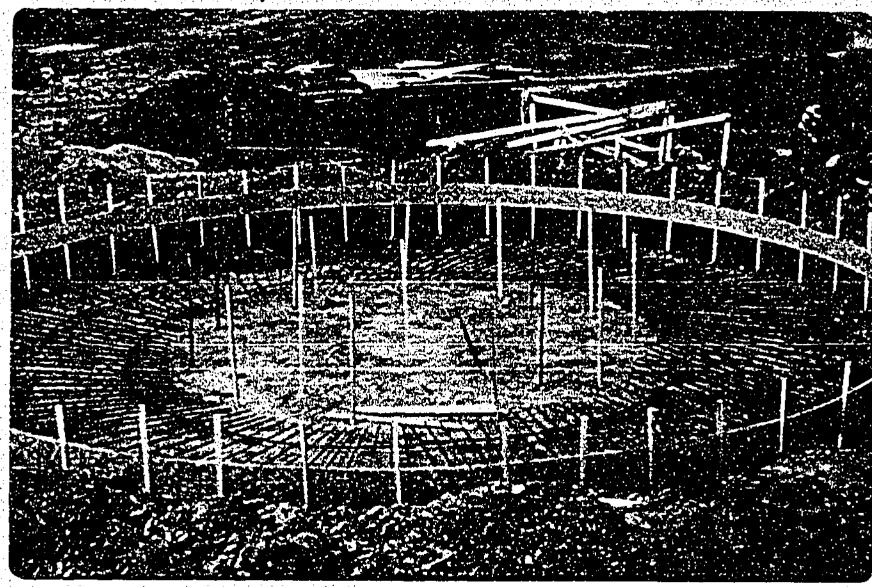

Figure 4.2.1(a) Foundation bed with reinforcing steel and formwork in place.

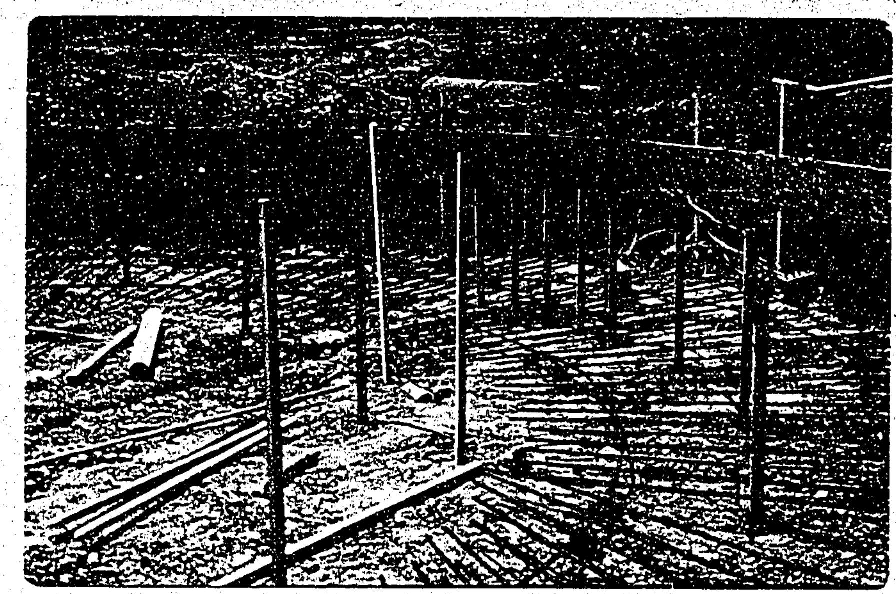

Figure 4.2.1(b) 51 mm., 2 in. (I.D.), galvanized steel sleeves secured in place. They were used to install the piezometers and the settlement gauges. [illegible]

smaller concrete pedestal with a diameter of 7.6 m (25 ft) and a thickness of 92 cm (3 ft) was poured inside a permanent form, which serves as the base anchor for the structure (Figure 4.2.2(a), 4.2.2(b)). A plan view of the foundation structure indicating actual dimensions, spacing of reinforcing steel and also the locations of the sleeves is given in Figure 4.2.3.

After the concrete had set, the complete silo was assembled in about 3 days. The Harvestore System is built from the top down. First, the roof section is assembled, then each succeeding ring of sheets is bolted at ground level and raised up with synchronized jacks. Figures 4.2.4(a) and 4.2.4(b) show the system being built, while Figure 4.2.4(c) gives a picture of the completed structure.

Figure 4.2.2(a) First ring of sheets bolted in place, to serve as the base anchor for the structure. Notice, in the background portion of the silo that collapsed previously.

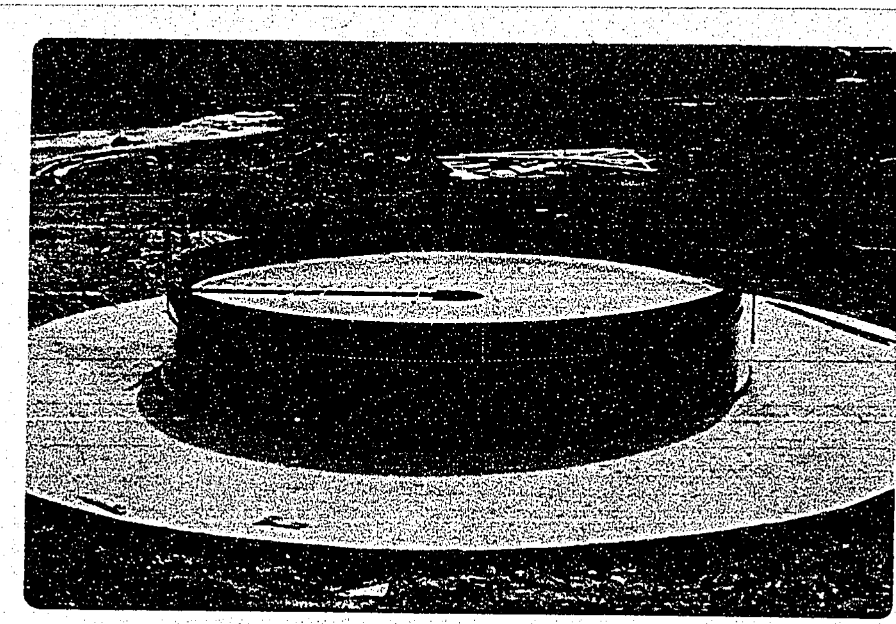

Figure 4.2.2(b) Concrete pedestal poured on top of large raft. Also shown is the trough for the unloader conveyer system.

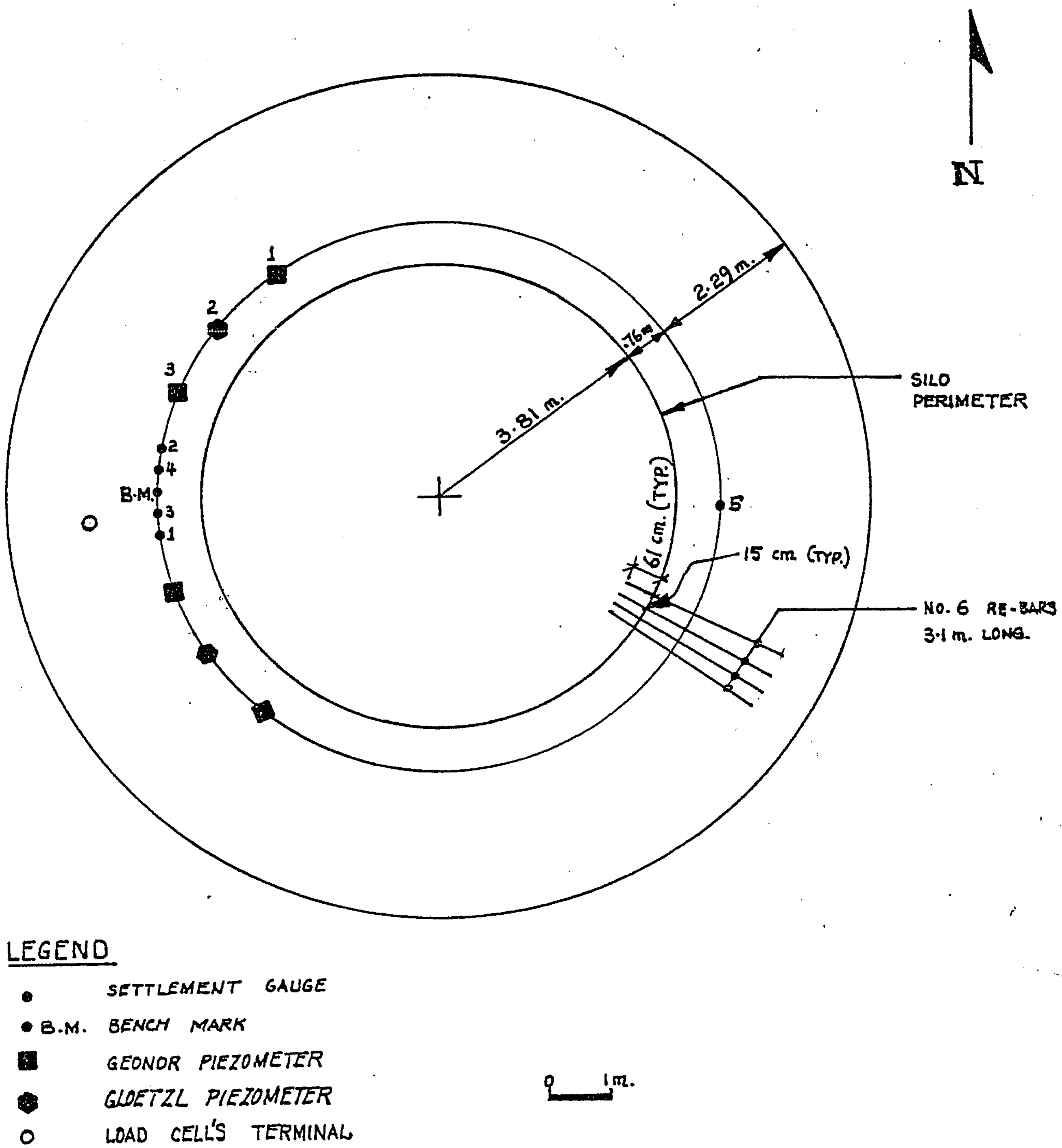

FIGURE 4.2.3 PLAN OF RAFT WITH LAYOUT OF INSTRUMENT SLEEVES AND REINFORCING DETAILS.

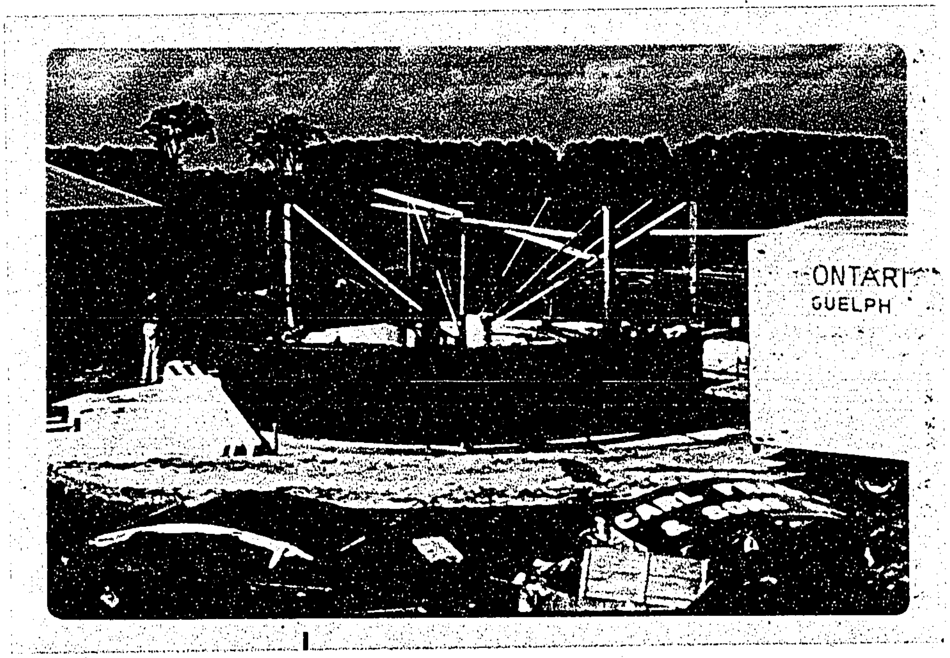

Figure 4.2.4(a) Synchronized jacks ready to start assembly. In the foreground are shown curved sheet components.

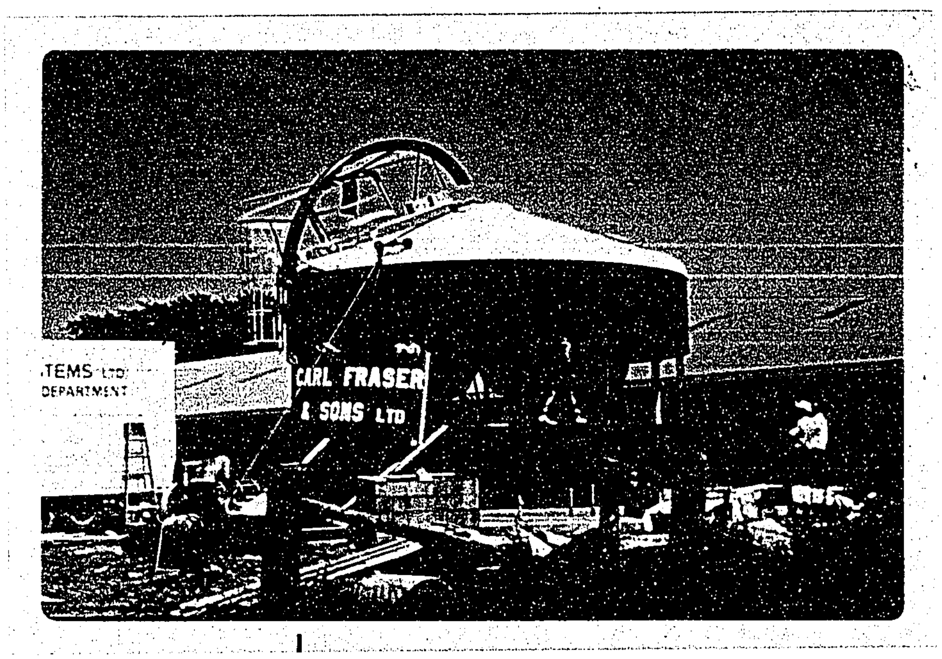

Figure 4.2.4(b) Roof and other accessories already installed. Structure gradually being built from top down.

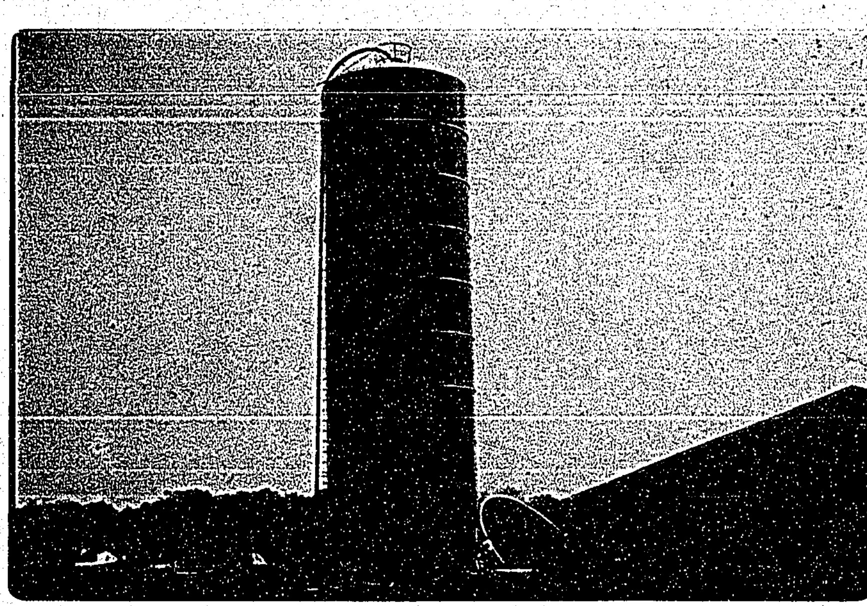

Figure 4.2.4(c) Tower silo completely erected. Height excluding, the roof = 26.1 m. (85.5 ft.). (Portion of the collapsed concrete silo is seen in the background.)

CHAPTER 5

INSTRUMENTATION

5.1 General

The principal reason for instrumenting the structure was to gather actual field performance data, which would provide relatively reliable criteria for the successful design of other similar structures in Leda Clay. Moreover, field measurements would also help in assessing the accuracy of theoretical calculations based on laboratory tests. Just as important is the contribution that such information makes to the knowledge of geotechnical engineering. Measurements carried out not necessarily in the order of importance included: normal contact pressures, pore-water pressures, the compression of the soil at various depths, and deflection or curling of the raft.

The following instruments were used to make the above measurements:

<u>Measurement</u>	<u>Instrument Used</u>
Normal contact pressures	8 hydraulic load cells (Glötzl cells) installed along 3-radii
Pore-water pressure	2 pneumatic (Glötzl) and 4 open stand pipe (Geonor) piezometers at various depths below raft
Compression of subsoil	5 deep settlement gauges made by welding bracing auger bits at the end of standard 1/4 in (6.4 mm) pipes. With the exception of one pair, all gauges are at different elevations below the raft. For reference, a deep seated bench mark was also installed.

Some of the Inst. used.

Curling of raft	24-levelling points installed around two circumference on the apron of the raft. These points are 2.59 cm (1 in) concrete nails installed with an ordinary hammer.

5.2 Contact Pressure Cells

Contact pressure cell, often referred to as a load cell, is a name given to a device which measures the reactive total stress that exists at the interface of the bottom of a footing and the subgrade. By strategically locating a number of cells along a radius or across the width of a footing, measurement of the total pressure distribution can be obtained. If the effective pressure is sought, the pore-water pressure should also be measured at the same points. In general, the more the number of cells used, the more accurate the distribution becomes. Load cells can be designed to measure shear, normal or a combination of the two stresses. However, since in the design of raft foundations, boundary shear stresses play a very minor role, this investigation only deals with normal contact pressure cells.

According to Hanna (1973), when an earth pressure cell is introduced into a mass of soil, the stress field in the vicinity of the cell is modified owing to the redistribution of stresses; and as a result, the stress recorded by the cell is different from the actual one. Recognition of this problem has initiated considerable research work in the field of load cell design. A summary of such work by a few researchers and their design recommendations to obtain reliable pressure measurements is well presented by Hanna (1973). The design guidelines deal mainly with the flexibility of the diaphragm and the aspect ratio which is the ratio of half the thickness to the length or diameter of the cell. For example, Tory and Sparrow quoted by Hanna (1973) conclude that the best performance occurs when the cell diaphgram is very stiff relative to the soil and when the cell is as flat as possible. Basically there are at least two types of load cells: electrical and hydraulic. In the electrical type, the pressure acting on the diaphragm is measured by either a vibrating wire or a rosette of strain gauges. The principle of the hydraulic load pressure cell which was used in this project is now explained in detail.

The Glöetzl cell was selected because of its relatively low cost, ruggedness for field use and the simplicity of its operation. It is worth mentioning that since the cells were used to measure contact pressures, error due to modifications of the stress fields in the cells' vicinity does not occur. ..., Hanna (197[illegible]

5.2.1 Operation of the Gloetzl Cell

The cell used for this project is rectangular in shape, with the following dimensions: length = 30.48 cm (12 in.), width = 20.32 cm (8 in.) and a thickness = 5/16" (7.9 mm). The principle of operation is best explained by referring to Figure 5.2.1.1. When the sensing pad is subjected to an external load, the oil pressure in the pad and that in the bypass assembly increase by the same amount as the applied normal stress. In order to measure the unknown normal stress, a small and constant volume of oil is pumped through the pressure line; when this

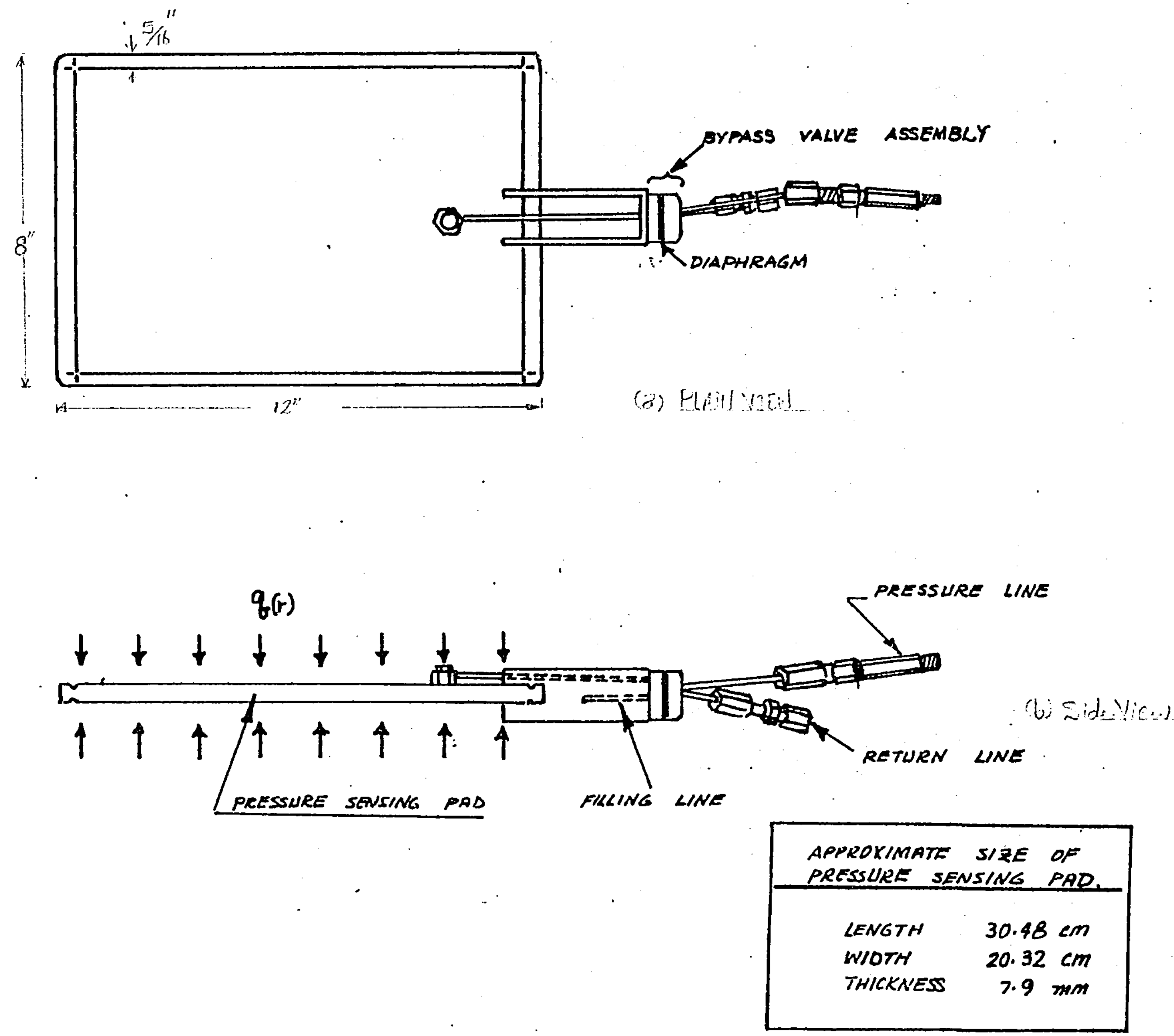

FIGURE 5.2.1.1. GLOETZL EARTH PRESSURE CELL [NOT TO SCALE]

pressure equals that in the sensing pad, the pressure diaphragm in the bypass valve assembly deflects permitting oil to pass through an orifice into the return line. The pressure reading at the moment the diaphragm deflects equals the normal stress to which the sensing pad is subjected. In most applications the reading instrument is at a different elevation from the load cell; which means that the hydrostatic pressure, negative or positive, should be added to the gauge readings to determine the actual contact pressure. This requires that the elevation difference between the gauge or the transducer and the bypass assembly be accurately known; moreover the specific gravity of the hydraulic fluid usually oil, should also be available. Furthermore, if there is a substantial temperature difference between the reading instrument and the cells, this should be recorded and a correction applied. Since there is no theoretical formula for temperature correction, the correction should be determined in the laboratory and kept in a tabulated or graphical form to be used in the field. It is also worth noting that the load cells come prestressed, the prestressing is done so that the measurement of high contact pressures is possible. Hence the net resultant contact pressure is equal to the gauge pressure plus the hydraulic head (elevation difference between cell and gauge times specific gravity of liquid) plus the algebraic temperature correction minus the prestress.

5.2.2 Calibration and Installation

The calibration was carried out at the NRC, DBR Laboratory in a large metal autoclave using air as the pressure medium. The results of the laboratory calibration for the eight load cells are found in Appendix B. It is seen from these plots that the relationship is linear.

Because of the limited budget available, only eight load cells were thought feasible. This meant that in order to get a very satisfactory result, the location of the cells had to be selected in such a way that fairly representative pressure distribution curves could be obtained. A preliminary field visit and weather information revealed the existence of a fairly strong wind which occasionally blows from the west. It was then decided to put a few cells along this direction so that the additional pressure due to the wind could be monitored. Next, to avoid favouring only a single direction, two more rows (strings) of load cells were arbitrarily chosen (Figure 5.2.2.1). Cell number 4 was originally planned to be placed at the centre. However, since it interfered with construction surveying, it had to be moved to the position shown in the diagram.

Once the layout plan is prepared, the field installation is straightforward. To ensure a good contact between the pressure sensing pads and the soil, the cells were installed in small rectangular pits prepared manually (Figures 5.2.2.2(a) and 5.2.2.2(b)). Then each load cell was connected to a common return line; the individual pressure lines and the common return line were all bundled and brought to a level above the expected top elevation of the raft foundation, along a small ditch (Figure 5.2.2.3(a)) and through the 102 mm, 4 in. (I.D.) asbestos concrete pipe sleeve (Figure 5.2.2.3(b)). Following the completion of

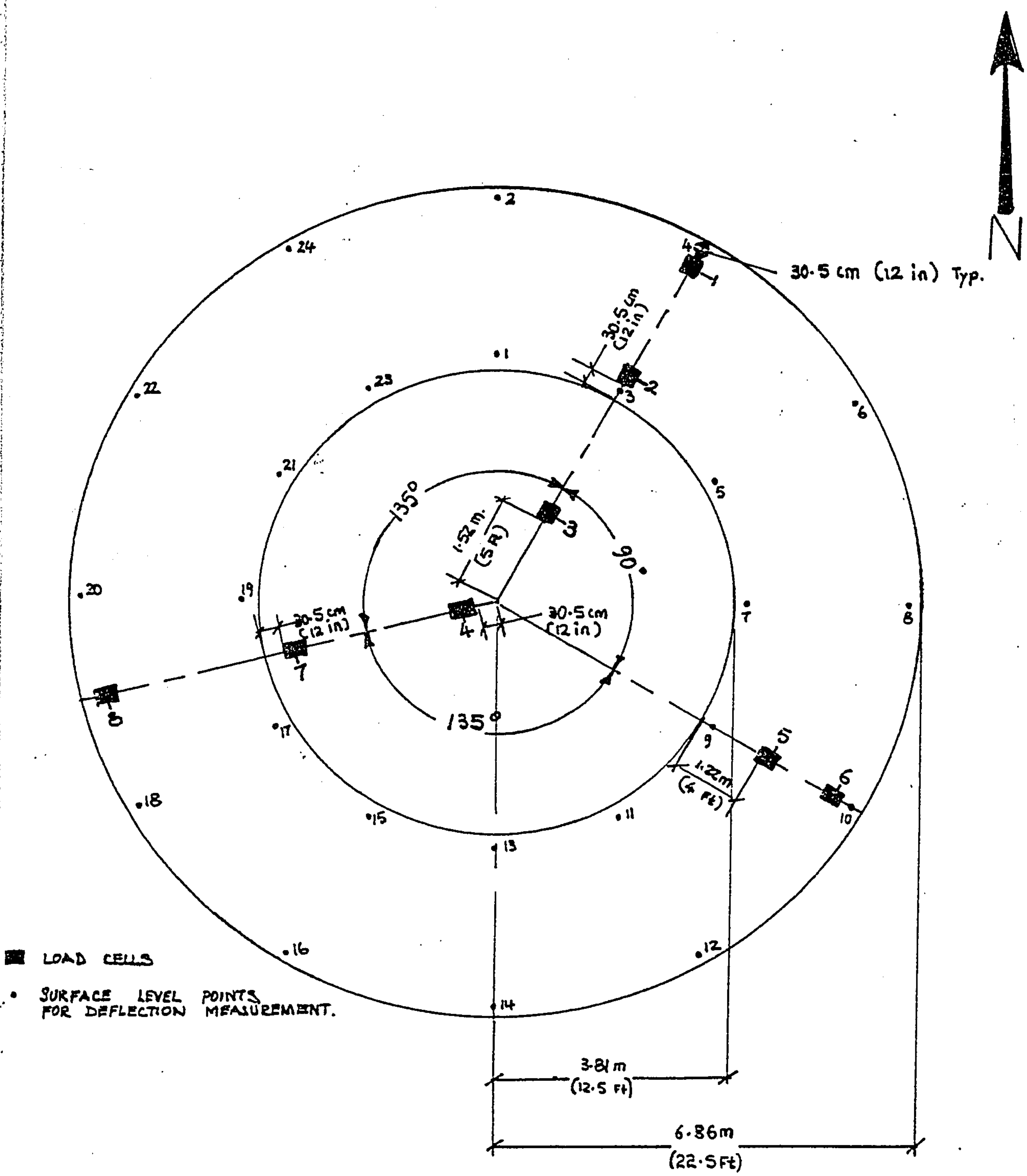

FIGURE. 5.2.2.1 LAYOUT OF LOAD CELLS AND DEFLECTION POINTS.

Figure 5.2.2.2(a) Rectangular pit being prepared to assure adequate contact between cell and soil.

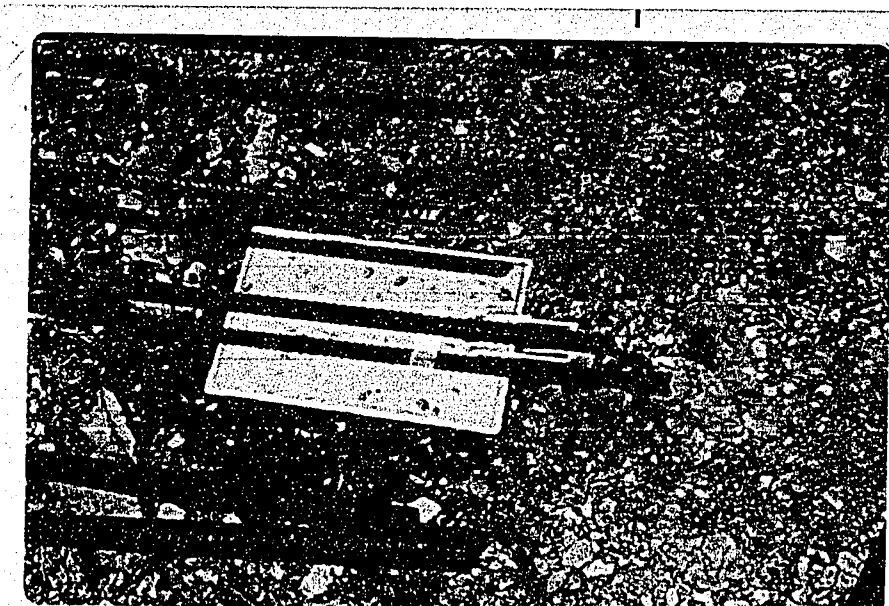

Figure 5.2.2.2(b) Load cell properly installed.

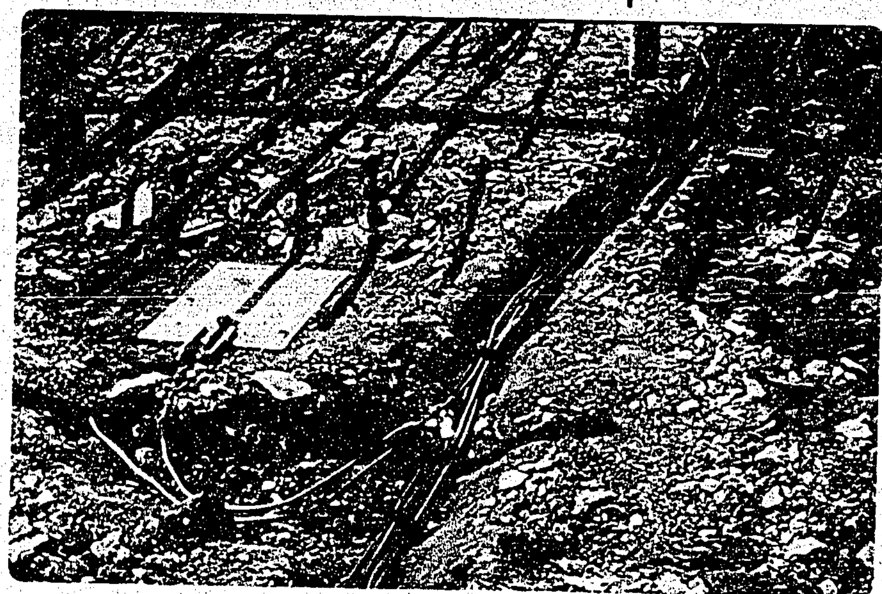

FIGURE 5.2.2.3(a) TYPICAL LOAD CELL CONNECTED TO A PRESSURE AND A COMMON RETURN LINES.

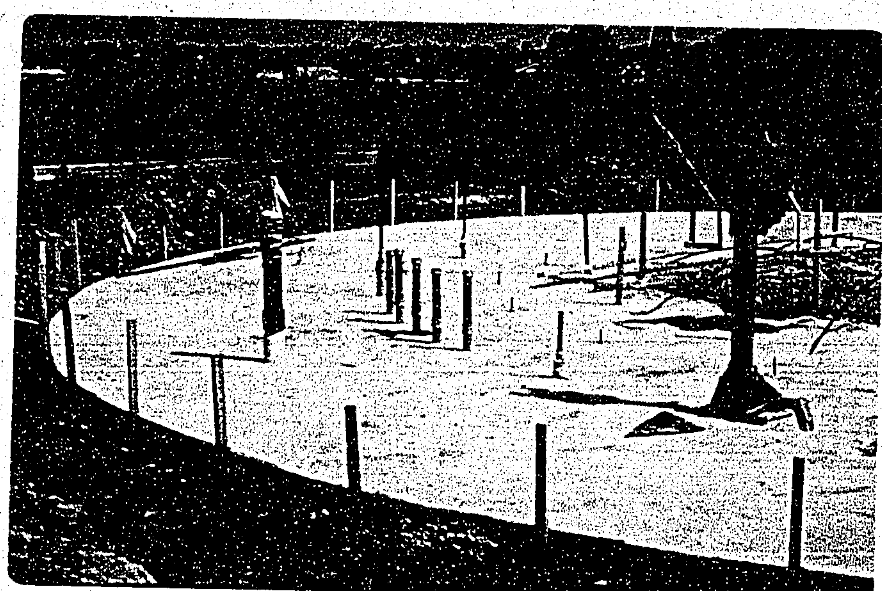

FIGURE 5.2.2.3(b) 102 mm (4 in) DIAMETER ASBESTOS CONCRETE SLEEVE PROTECTING THE LOAD CELL HYDRAULIC LINE TERMINALS. TO THE RIGHT ARE SHOWN FIVE METAL SLEEVES HOUSING THE SETTLEMENT GAUGES AND THE DEEP B.M. WHICH IS IN THE MIDDLE. NOTICE ALSO IN THE FOREGROUND TO THE RIGHT THE "BORROS" RACK JACK ANCHORED AGAINST A METAL, SLEEVE READY FOR THE INSTALLATION OF ONE OF THE PIEZOMETERS. (THIS JACK HAS A CAPACITY OF 5 TONS).

the circuits, the lines were filled with the recommended hydraulic fluid and all joints checked against possible leakage, while at the same time field prestress readings were conducted (Figure 5.2.2.4). The hydraulic fluid used is that recommended by the manufacturer and is a mixture of 90 percent kerosene and 10 percent 10-weight non-detergent motor oil. The readout instrument (Figure 5.2.2.5) consists of a small oil reservoir, a hand pump and a Bourdon pressure gauge and a pressure transducer, not shown in the diagram. The instrument has two outlets for pressure lines, these are terminals (13) and (15). The procedure for reading the pressure in a single load cell is as follows. Connect the pressure line of the load cell to terminal (13) and the return line to terminal (1). Close valve (C) but leave valve (D) open. Next, shut pressure bleed-off valve (B) and crank up the pump at a very low but constant rate. Bypass pressure is reached when further introduction of oil into the line is no longer accompanied by a slight increase in pressure; this is easily controlled by visual observation of the Bourdon gauge.

To facilitate quick field readings, soon after the raft was poured, the pressure and return lines were made to terminate in a permanently installed Switch-Manifold unit, protected in small metal box housing. The unit allows the readout instrument to be connected only to one pressure and return lines and by shutting or closing valve switches, individual cell readings can be quickly taken.

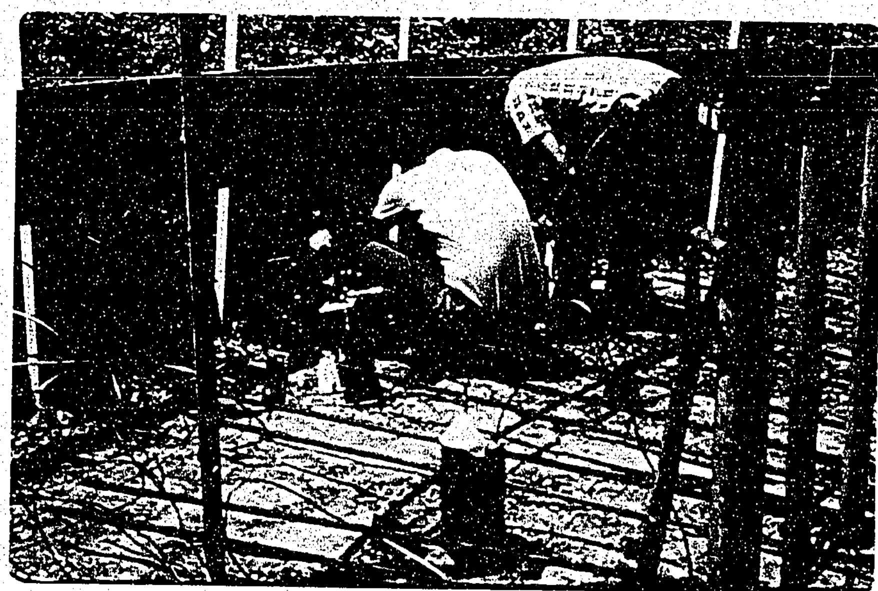

Figure 5.2.2.4 Technicians taking cell pressure readings under zero load.

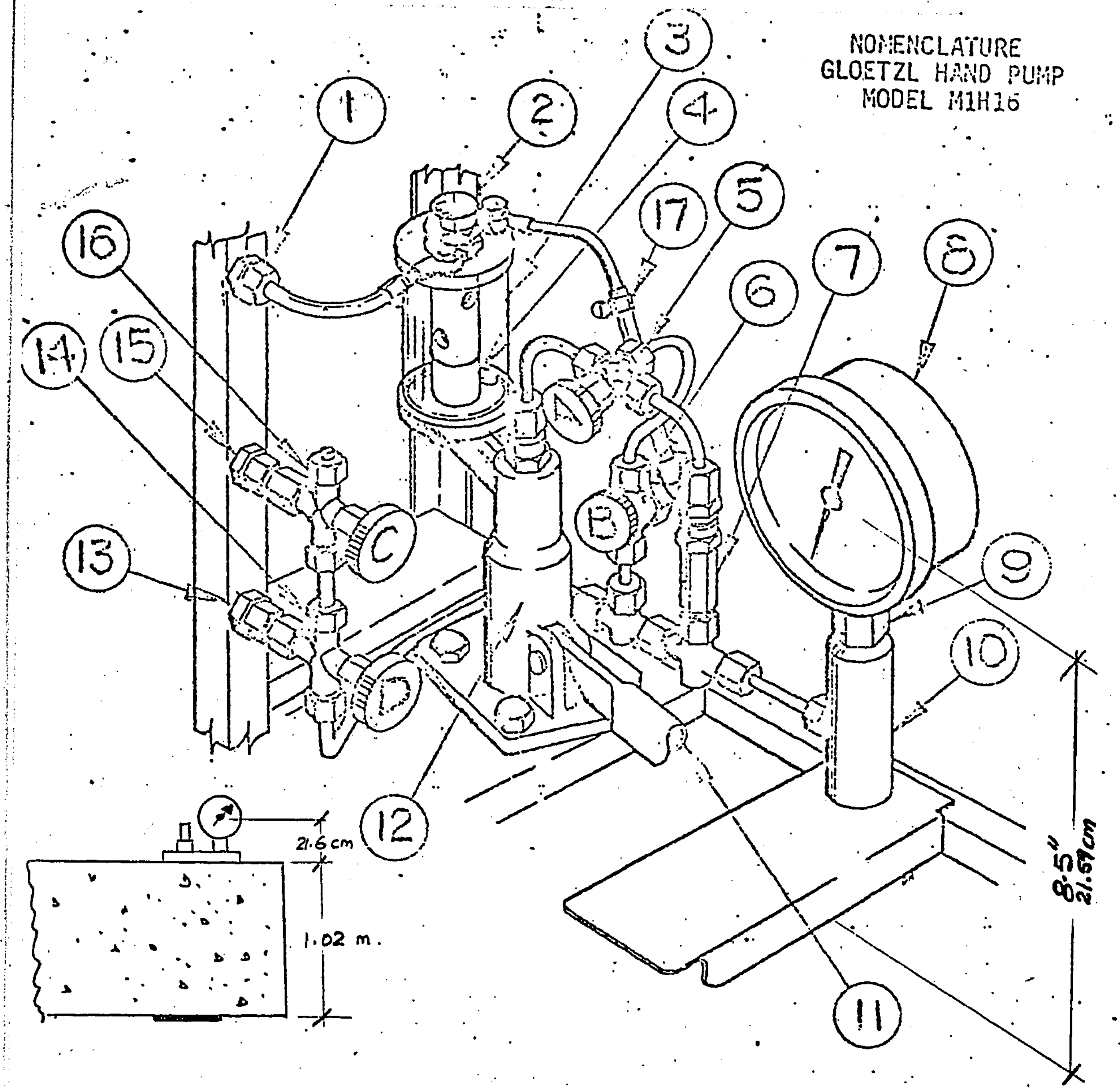

1	Return Line Inlet	10	Manometer Stand
2	Filler Cap	11	Pump Handle
3	Reservoir	12	Pump Housing
4	Primary Filter	13	Pressure Line Outlet (D) (Transducer)
5	Main Control Valve (A)	14	Pressure Line Valve (D)
6	Pressure Bleed Off Valve (B)	15	Pressure Line Outlet (C) (Bourden Gauge)
7	Throttle Valve	16	Pressure Line Valve (C)
8	Manometer	17	Pressure Bleed Off Line (From B)
9	Manometer Adapter		

FIGURE 5.2.2.5 GLOETZL HAND PUMP FOR LOAD CELL READINGS.

5.3 Piezometers

5.3.1 General

The purpose of installing piezometers at different depths below a foundation is to measure the pore-water-pressure distribution in the soil layer. Knowledge of the field pore pressure makes the prediction of the primary consolidation settlement more accurate. Moreover, since for a given surface load the excess pore water pressure decreases with depth, by strategically locating the piezometers, the critical depth of settlement can also be estimated. This depth would correspond to the position of the deepest piezometer, where the increse in pore pressure due to the applied load is insignificant. It was mentioned in Section 3.6 that Skempton's (1954) equation could be used to estimate the pore pressure resulting from loading the compressible layer. The difficulty when using this equation arises in accurately assessing the pore pressure coefficients and also the incremental normal and lateral stresses. The other advantage of piezometers is that they can be used as a means of either construction control, stability checking or both.

According to Hanna (1973), for satisfactory results a piezometer should satisfy the following requirements. (a) Record accurately the pore pressures in the ground with a known range of error. (b) Cause as little interference as possible to the load response of the surrounding soil medium. (c) should respond quickly to pressure changes in the surrounding soil and, (d) should be rugged, durable and fairly affordable. Today there are a variety of piezometers which are commercially available to the engineer. Basically, there are about four major types: the open standpipe, the porous tube, the electrical, and the pneumatic (gas or fluid). The porous tube and the pneumatic piezometers, which were used in this project, are discussed in the paragraphs to follow.

5.3.2 The GEONOR Porous Bronze Tip Piezometer

This piezometer gets its name from the manufacturer GEONOR A/S. The instrument consists of a hollow stem on the lower end of which is screwed a conical point. Three sinterized bronze filters are mounted on the stem (Figure 5.3.2.1). The top of the filter stem is provided with external "E-rod" threads for connection to the extension tubing. For the piezometer tube itself, 6.35 mm, 0.25 in (I.D.) plastic tubing is usually used. The plastic tubing is screwed inside the top of the piezometer stem and sealed by a rubber "O" ring which is compressed by a gland nut. For extension, the manufacturer recommends the use of diamond core drill (E) rods. However, if cost becomes a factor an ordinary galvanized or black pipe of the same diameter as the tip can be used by welding a thread adapter piece at the top of the filter stem. The water level in the piezometer tube is measured with the help of an electric circuit which is completed when a thin co-axial cable, lowered down the piezometer tube, reaches the water surface. If the pressure head is very high a Bourdon gauge or a transducer can be installed. For winter operation where the water level in the tube is expected to rise above the frost line, anti-freeze liquid should be employed. The manufacturer gives the following

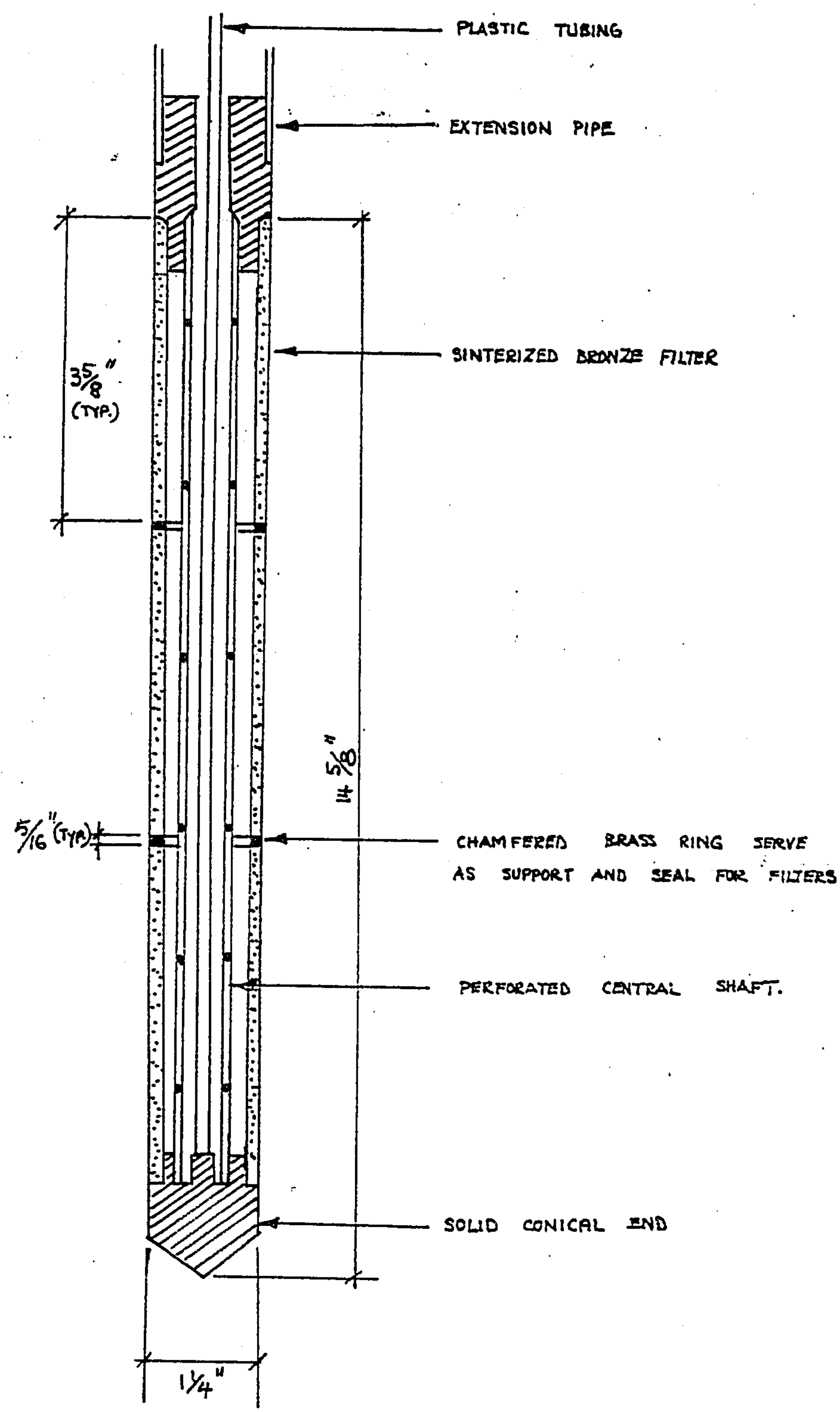

1 in = 2.54 cm. (N.T.S)

FIGURE 5.3.2.1 THE GEONOR POROUS BRONZE TIP PIEZOMETER formula for making the antifreeze for a temperature as low as -27°C: glycerine (5.5 ℓ), alcohol (5.5 ℓ), water (10 ℓ) and concentrated suphur acid (4 cc), the mixture should yield about 20 liter anti-freeze-liquid.

5.3.3 Pneumatic Piezometer (Glöetzl)

The Glöetzl pore pressure cell (Model P3SFLAG) consists of a bypass valve assembly, a microporous ceramic filter, a pressure line and a return line (Figure 5.3.3.1). It has a diameter of 30 mm (1.2 in) and a length of about 54 mm (2.1 in) excluding the threads. The principle on which it works is very similar to that of the Glöetzl load cells. The operating medium is compressed nitrogen from a cylinder. To take pore pressure readings, a flow of compressed nitrogen is admitted into the pressure line; when this gas pressure equals the pore water pressure, the diaphragm deflects allowing the gas to bypass. The flow of gas is maintained for 1 to 3 minutes; when the reading remains unchanged the pore pressure value has been reached. Unlike the hydraulic load cells, correction due to the elevation difference between the pressure gauge and the piezometer is not necessary since the specific gravity of nitrogen is very small. However, errors due to the rate of gas flow can be very significant, especially if the lines are extremely long. To keep this error to a minimum, the readout instrument is equipped with two sensitive pressure gauges so that when the reading of the unknown pressure is taken on one, the other serves for the adjustment of a certain maximum differential pressure that must be maintained across the two gauges. The slower the rate of flow the

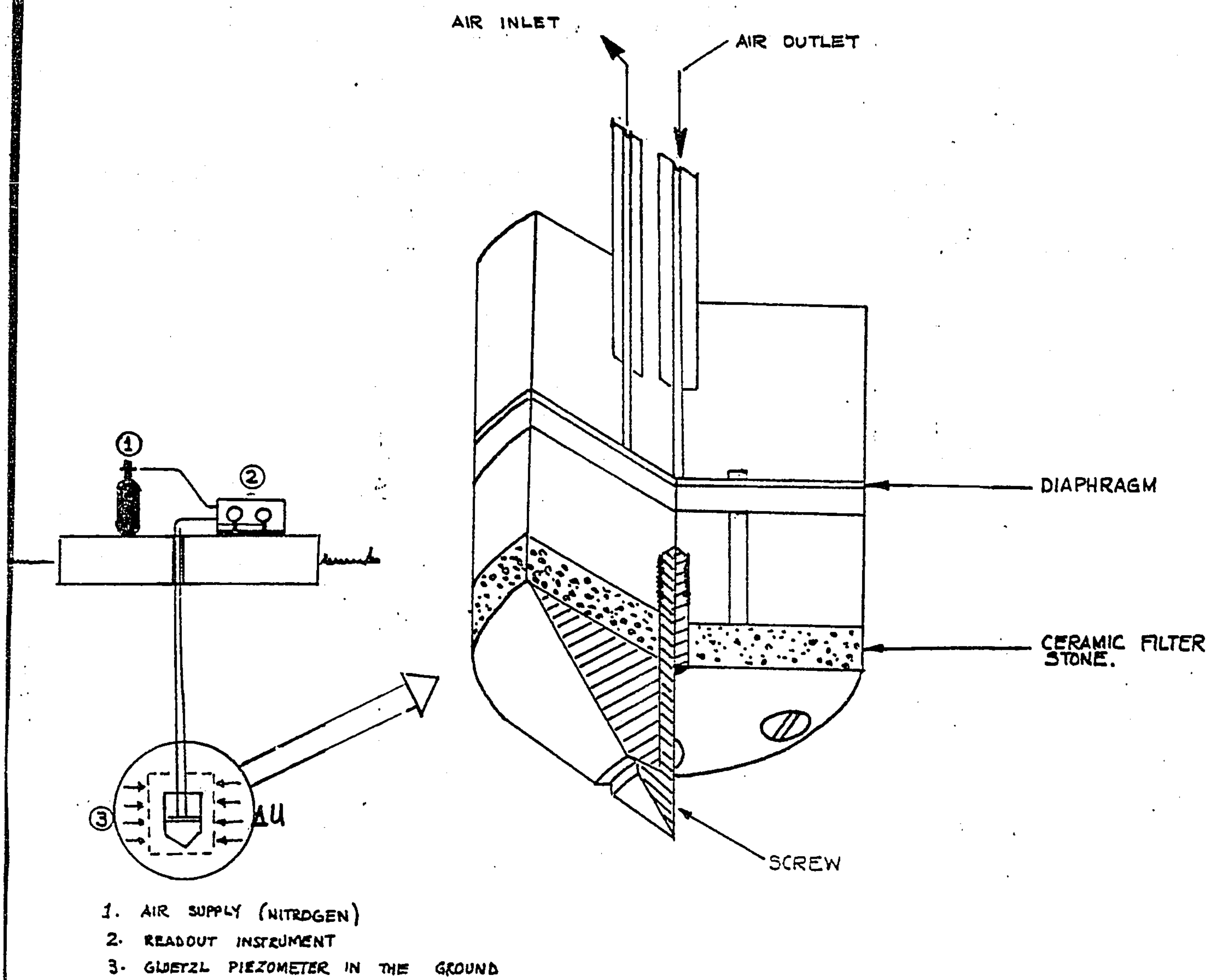

FIGURE :5.3.3.1 THE GLOETZL PNEUMATIC PIEZOMETER (SCHEMATIC) more accurate the pressure readings; however, for very long pressure lines this technique can take several minutes for reading just one piezometer. For most applications the recommended pressure differential is 0.1 kg/cm^2. The operation of the readout instrument is best understood by referring to Figure 5.3.3.2(a). For very long pressure lines and other differential pressures, the manufacturer provides graphs of filling time versus known pressure for different lengths and pressure differentials. One such curve is reproduced in Figure 5.3.3.2(b). Notice the significant increase in pressure loss when the differential pressure is increased from 0.1 to 0.4 kg/cm^2.

Before field installation the two Gloetzl piezometers used for the project were calibrated in water using a triaxial cell; these curves are found in Appendix B.

5.3.4 Comparison Between Piezometers

The main difference between the two piezometers lies on how fast they react to pore pressure changes. In the case of the pneumatic piezometer a very small volume change is required, whereas in the Geonor-type a greater volume change has to take place before equilibrium is reached which means the time lag is substantially longer. For the pneumatic piezometer, since the volume change required for most civil engineering application is so small, that the manufacturers do not commonly give this information. However, in the case of the Geonor piezometer, the volume change needed to respond to a certain increase in pore-water pressure can easily be calculated as illustrated by the following examples:

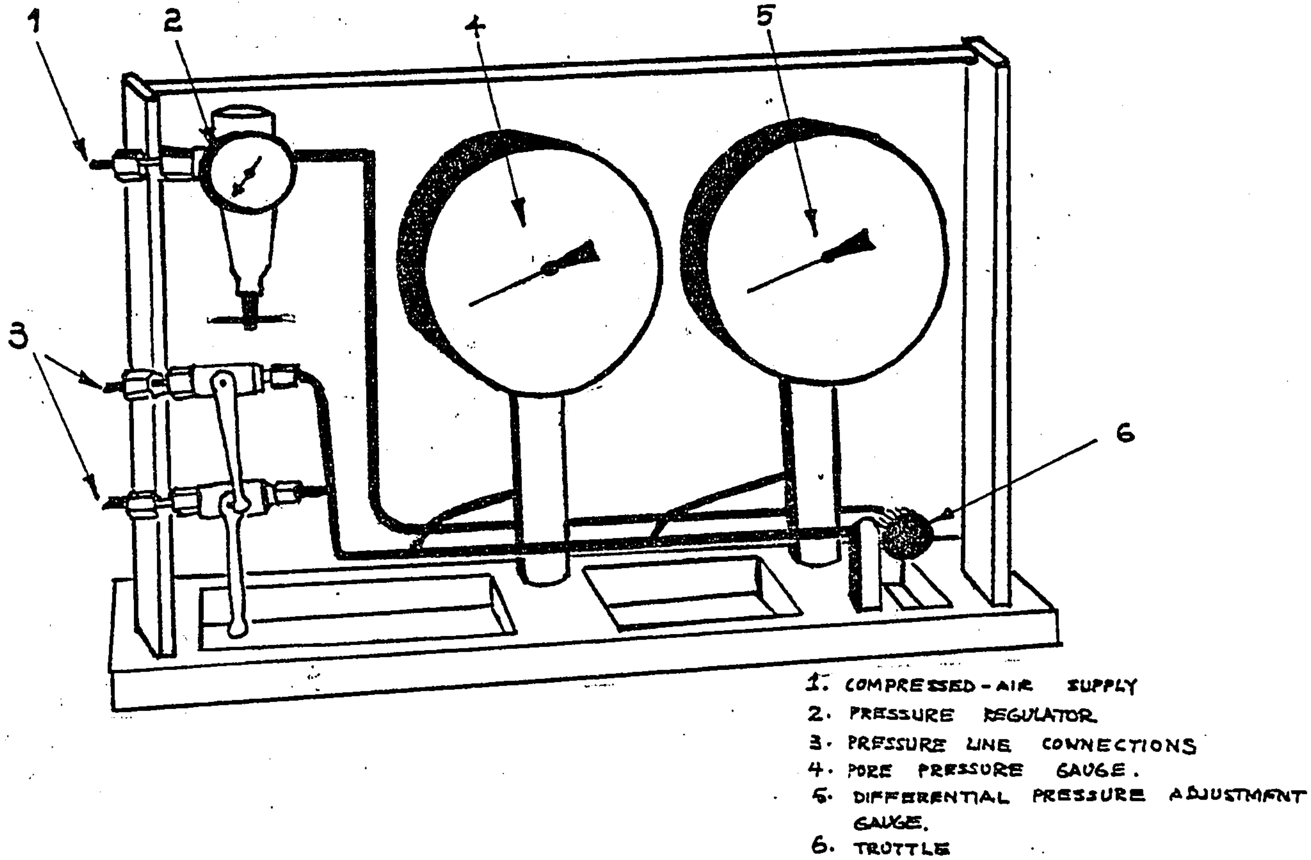

FIGURE : 5.3.3.2(a) READOUT INSTRUMENT FOR PNEUMATIC PIEZOMETER

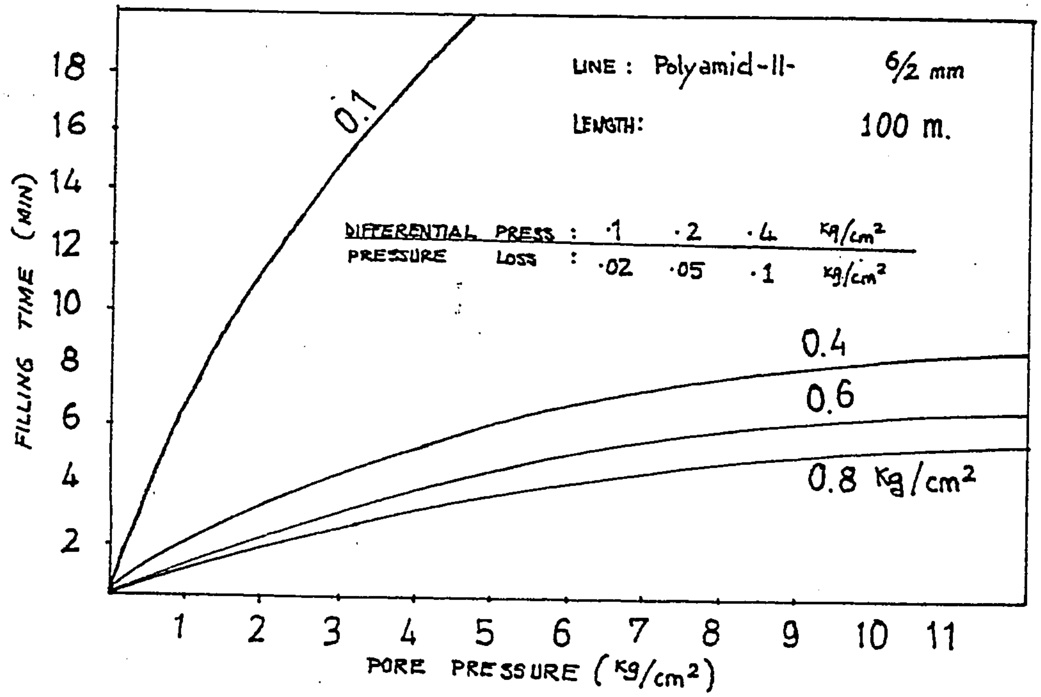

FIGURE : 5.3.3.2(b) A TYPICAL PRESSURE LOSS CALIBRATION CURVE.

Suppose the increase in pore-water pressure sensed by the piezometer = 5 kPa = 0.051 kg/cm^2 = 51 cm of water

Diameter of piezometer tube = 6.35 mm (see Section 5.3.2.) = 0.64 cm

Therefore required volume change = 51 cm x .64 cm = 32.4 cc

Of course, the use of a smaller diameter tube will lower the volume change requirement to respond to the pressure change relatively faster, however with smaller tubes de-airing and capillary action create more problems.

Estimates of the time lags for different piezometers for 90 percent response in a homogeneous soil can be made using Figure 5.3.4.1. This figure taken from Terzaghi and Peck (1967) is based on several experiments by different researchers. For example, it is seen from this plot that for a soil with a permeability coefficient of 10^{-7} cm/sec, the time the Geonor requires for 90 percent response is in the order of 10 days while that for the diaphragm type is less than 15 minutes. It should be remembered, however, that the Geonor type is a lot cheaper, rugged and less complicated to operate and requires no time consuming laboratory calibration.

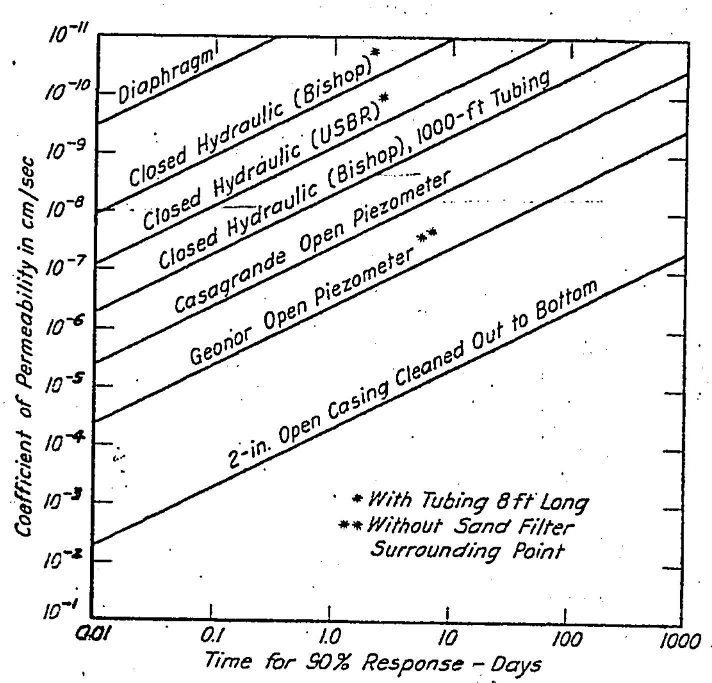

FIGURE 5.3.4.1 APPROXIMATE RESPONSE TIMES FOR VARIOUS TYPES OF PIEZOMETERS (AFTER HVORSLEV, 1951, PENMAN 1961, BROOKER AND LINDBERG, 1965, AND OTHERS). (FROM TERZAGHI AND PECK, 1967).

5.3.5 Installation of Piezometers

Before field installation, both types of piezometers were de-aired following the method suggested by the manufacturers and brought to the site in containers filled with distilled water. For open piezometers a detailed step by step procedure for installation in clay soils is given by Bozozuk (1960). After looking at different possible elevations the depths below the bottom of the raft shown in Figure 5.3.5.1 were chosen. In order to compare the response to a known load by the two types of piezometers, (P-4) and (P-5) were installed at about the same depth, P-5 is a Gloetzl (pneumatic) while P-4 is a Geonor open type. It was originally planned to install all the piezometers, especially the pneumatic ones, before the raft was poured in order to get the pore pressure response to the known weight of the foundation. However, because of shipping delays and also problems encountered during laboratory calibrations, the Gloetzl's were not ready until after the concrete was poured.

All four Geonor piezometers were installed manually by pressing down on the E-rods using pipe wrenches as lever arms (Figure 5.3.5.2). The pneumatic piezometers were pressed down using the "Borros" rack jack previously shown in Figure 5.2.2.3(b), using the readily available metal sleeves as anchors. The E-rods for the Geonor piezometers have threaded caps to protect the inner tubing. Moreover, all the six piezometers are further protected with (5 cm) (2 in) diameter threaded capped CPVS plastic tubing.

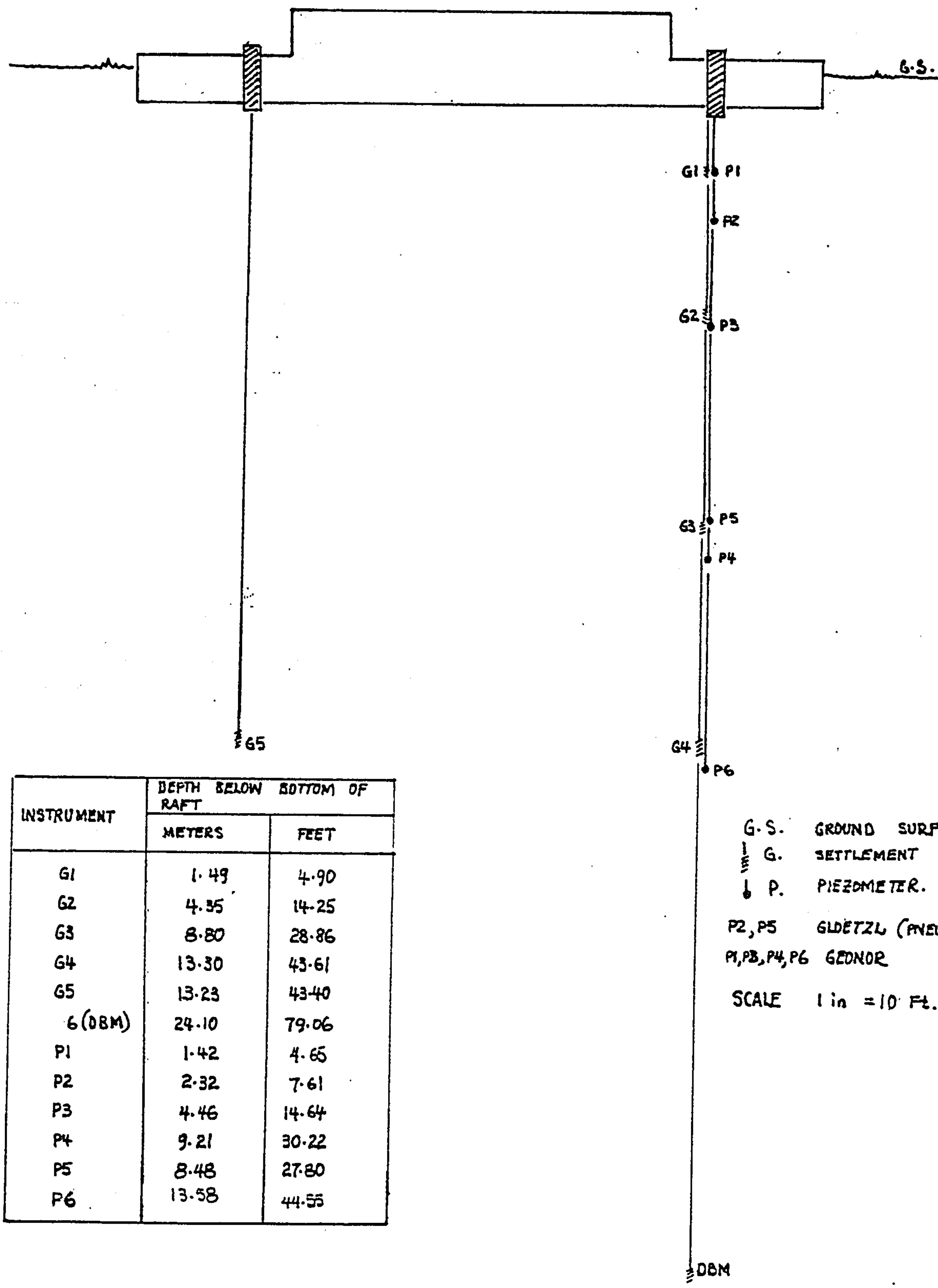

INSTRUMENT	DEPTH BELOW BOTTOM OF RAFT	
	METERS	FEET
G1	1.49	4.90
G2	4.35	14.25
G3	8.80	28.86
G4	13.30	43.61
G5	13.23	43.40
6 (DBM)	24.10	79.06
P1	1.42	4.65
P2	2.32	7.61
P3	4.46	14.64
P4	9.21	30.22
P5	8.48	27.80
P6	13.58	44.55

G.S. GROUND SURFACE
G. SETTLEMENT GAUGE
P. PIEZOMETER.
P2, P5 GLOETZL (PNEUMATIC)
P1, P3, P4, P6 GEONOR
SCALE 1 in = 10 Ft.

FIGURE 5.3.5.1 SECTION THROUGH RAFT.

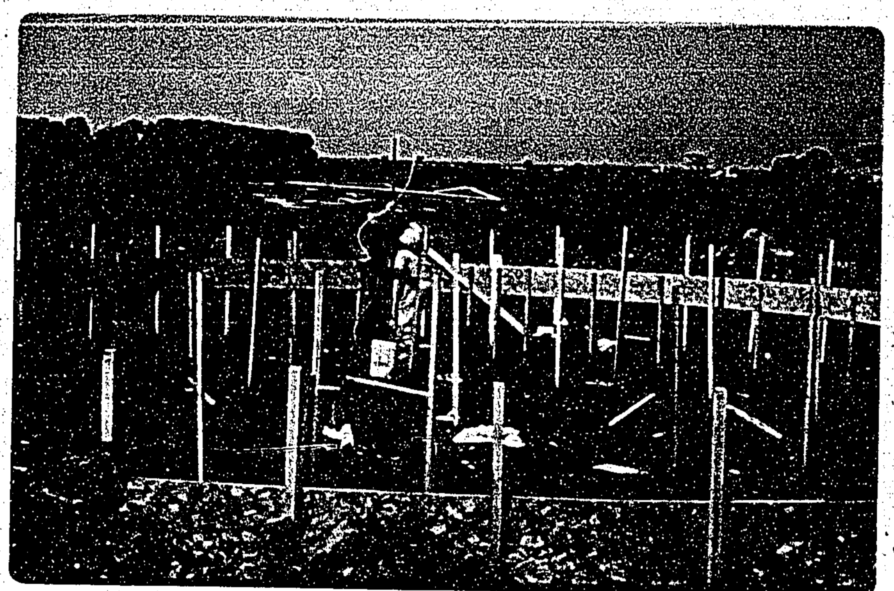

FIGURE 5.3.5.2 GEONOR PIEZOMETER BEING PUSHED DOWN USING PIPE WRENCHES. THE CLAY OFFERED VERY LITTLE RESISTANCE DURING THE MANUAL INSTALLATION.

5.4 Settlement Gauges

5.4.1 Spiral Auger Deep Settlement Gauges and Deep Seated Bench Mark

As the name implies these settlement gauges measure the compression of the soil at different depths below the raft by means of precise dial gauges. The method is illustrated by Figure 5.4.1.1. Here the bracing auger bit welded at the end of a 6.4 mm (1/4 in) steel pipe is lowered through a 25.4 mm (1 in) steel casing already in the ground. Then by turning on the inner pipe the auger bit is advanced further in the soil to the required elevation. The top end of the 6.4 mm (1/4 in) inner tube is machined level, and is provided with a small nylon plug. The head of this plug is made just slightly smaller than the inner diameter of the 'brass gauge seat' so that the inner pipe screw-anchored at the bottom can freely move at top in the vertical direction.

The deep bench mark was installed according to the recommendations given by Bozozuk et al (1962), and has the same detail as the settlement gauges at the top end. The difference between any two dial readings on the bench mark gives the total settlement of the raft. On the other hand, for the other settlement gauges this difference gives the compression of the soil layer between the bottom of the raft and the location of the auger point only. In order to get a fairly good distribution of settlement with depth, the auger points were installed at the depths shown in Figure 5.3.5.1. These depths approximately correspond to those of the four piezometers so that some kind of pore water pressure change with variation of settlement can be observed.

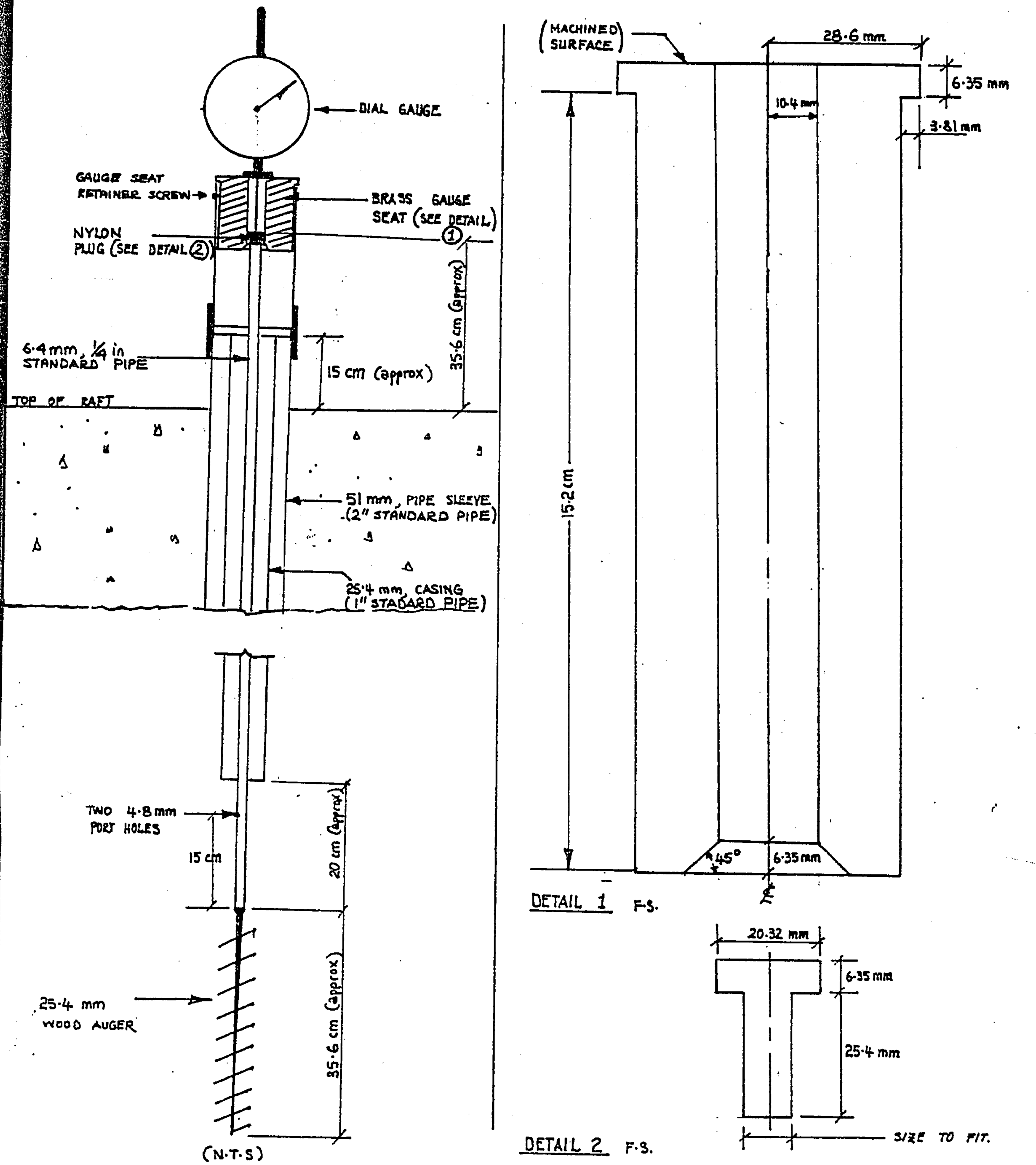

FIGURE 5.4.1.1 DEEP SETTLEMENT GAUGE.

The elevation of the deep bench mark was established using a precise level (WILD N3) and a temporary bench mark which was installed at the beginning of the construction period. This temporary reference datum was made of a 3 m (10 ft) number 9 reinforcing rod and was arbitrarily assigned an elevation of 30.48781 m (100.0000 ft) from which the elevation of the deep bench mark was established at 31.36799 m (102.8870 ft). The location and other details of the temporary bench mark are found in Figures 5.4.1.2(a) and (b).

5.4.2 Installation of Settlement Gauges and Bench Mark

The main requirement during installation of the deep settlement gauges to ensure satisfactory performance, is to keep the casing as clean as possible from any dirt that might interfere with the vertical movement of the inner rod. The following technique was employed successfully: A thin nylon cup (aerosol cover), about the size of the casing is fitted to one end using electrical tape. Then using the 'Borros' rack jack (Figure 5.2.2.3(b)) the casing is pushed through the sleeves down to the required elevation; adding extensions as they are required. To help the nylon cup from being punctured some oil was poured down the casing to apply a downward hydrostatic pressure. Once the required level is reached the inner pipe with the auger bit attached is lowered until it touches the nylon cup. Then using a small wrench, the inner pipe is augered down through the thin nylon cup to the predetermined elevation of the settlement point. Finally, the top piece of the inner tube with the nylon plug, and the

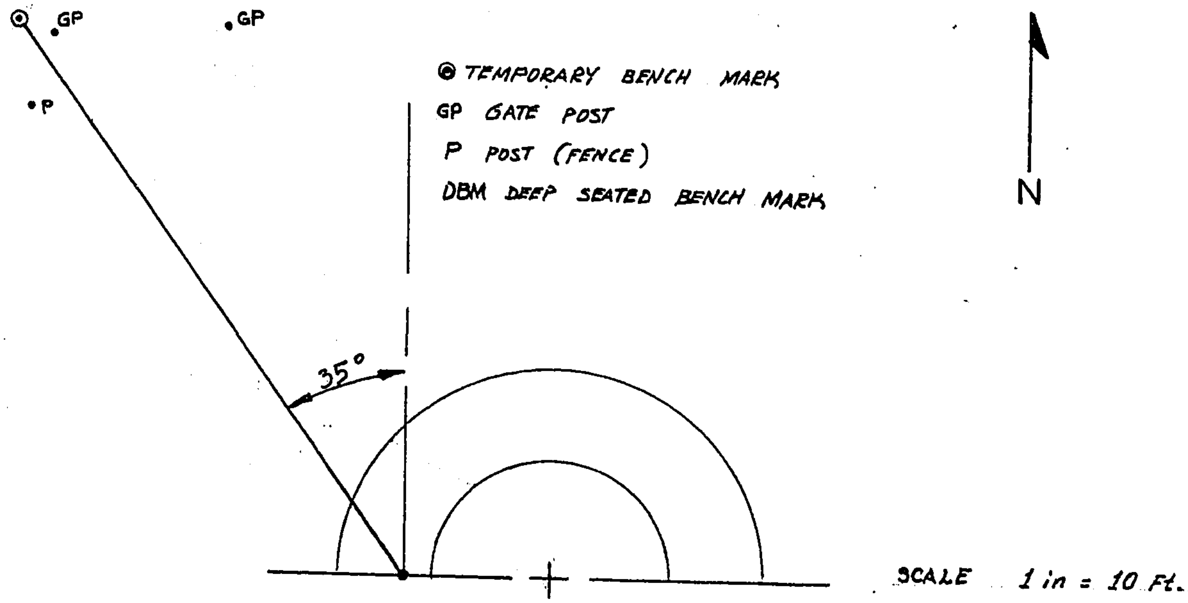

Figure 5.4.1.2(a) Approximate location of temporary benchmark.

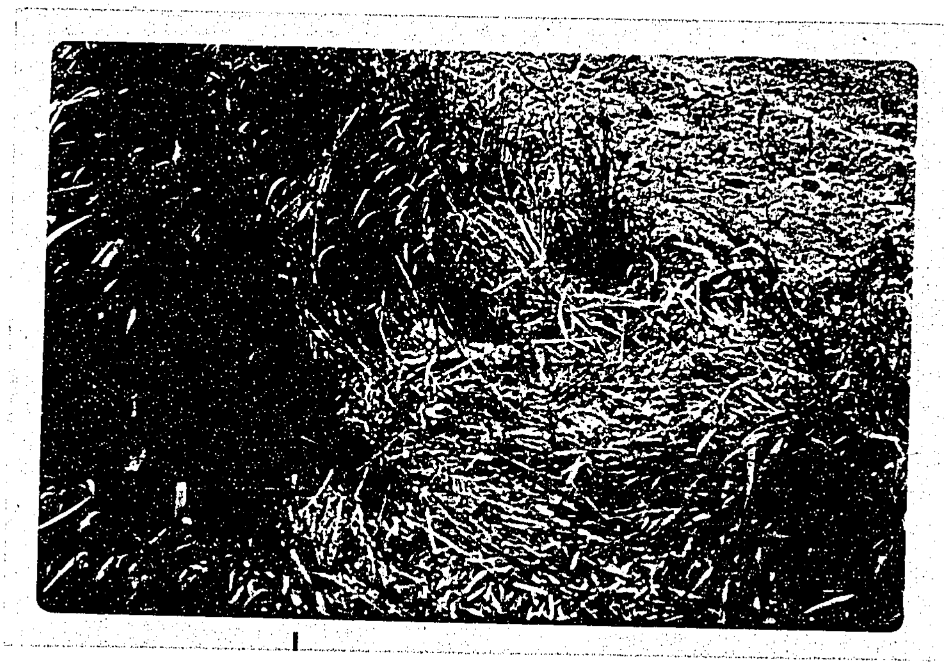

Figure 5.4.1.2(b) Temporary benchmark in the centre of photo. The 51 mm. casing extends to a depth of 1.37 m. and is filled with oil.

'brass gauge seat' are installed.

The 'brass gauge seat' is fastened by means of two retainer screws to the pipe sleeve cast in the raft (see Figure 5.4.1.1). After each reading, the dial gauge is removed and the brass seat is protected with a threaded pipe cap. The protective threaded caps for the settlement gauges and the deep bench mark are shown in Figure 5.2.2.3(b).

5.4.3 Raft Deflection Indicators

There are 24 levelling points, two per radius, located at distances of 4.12 m (13.5 ft) and 6.71 m (22 ft) from the centre at 30 degree intervals around the raft (Figure 5.2.2.1). These are 2.54 cm (1 in) long concrete nails, and their purpose is to give an indication of the raft's distortion. The nails were manually installed with an ordinary hammer to a depth of approximately 2 cm (7/8 in).

5.5 Observations

This section deals with the data collected to the present time and with the accuracy of the instruments used.

The data reported in this thesis are related only to the behaviour of the tower silo during its first loading cycle. It is hoped, however, that in the future the project will generate more valuable information about the long term performance of foundations in Leda Clay subjected to a slow cyclic loading such as this. The building of the new silo was completed on June 21, 1976 about 9 months after the collapse of the old one (Figure 4.1.2).

At the beginning, instruments were read very frequently in accordance with the construction and loading activity at the site. After the last load was put in, which was around the end of summer, field trips were still made but on a less frequent basis until February 4, 1977 when the raft heaved up by 3.15 mm (.125 in) above its end-of-construction elevation due to frost action. Most of the load cells gave readings of zero pressure and some even gave minor negative values. The negative reading has no significance. It can be attributed to a slight change in the prestress since installation or it can also be due to slight error in the initial measurement of the prestress. Moreover, tensile forces normal to the cells due to adfreezing are also suspected. Because of this, the data collection for the thesis was discontinued; although a few more trips were made to check the integrity of the structure.

Other important data that were gathered but not mentioned in the previous sections are: weighing of the haylage, and making of concrete cylinders from the foundation concrete to determine its density and strength parameters. Most of the weighing was done at a nearby quarry owned by Diblee Construction Ltd. and the remaining was carried out using portable scales borrowed from the Ministry of Transportation and Communications of Ontario. The load data together with the moisture content of the haylage is given in Appendix B. In all 21 wagonloads were weighed.

Twelve concrete cylinders were collected, each representing a different batch. To simulate field curing conditions the cylinders were left in a small pit next to the raft (see photograph in Appendix B). In the laboratory, compressive tests were carried out at 7, 14 and 28 days of curing time. On the 28th day, in addition to the compressive strength, splitting tests to determine the tensile strength were also performed. All these data including the calculation of Young's modulus using the ACI (1971) method are given in Appendix B.

Estimated ranges of accuracy for the instrumentation are:

1.	Gloetzl piezometer gauges	±1.0 kPa (±0.14 psi)
2.	Gloetzl load cells	±0.7 kPa (±0.10 psi)
3.	Open piezometers	±1.3 cm (±0.5 in) (±.13 kPa)
4.	Deep settlement gauges	±0.03 mm (±.001 in)
5.	Levelling points	±0.5 mm (±0.02 in)

In the case of the levelling points, the accuracy of the instrument used, which is the Wild N3, is in the order of 0.01 mm under very ideal conditions and using an invar rod. However, because of levelling errors due to the use of an ordinary levelling rod and also since some of the points were damaged by tractor tires and other activity, it is believed the accuracy cannot be better than ±0.5 mm.

The accuracies cited for instruments 1 to 4 are those of the reading devices used in this project. The absolute value of the accuracy was estimated as being half the smallest division on the particular reading device, except in the case of the deep settlement gauge, whose accuracy was simply taken as being the smallest division on the dial.

CHAPTER 6

PRESENTATION OF RESULTS

6.1 Loading Procedure

Within twenty-five days after construction, the structure was subjected to 76 percent of its design bearing pressure of 87.5 kPa (1750 psf). The loading was discontinued for about 30 days until more haylage became available. Then the silo was completely filled; and the pressure estimated from the load cells was 72.5 kPa (1450 psf) which corresponds to 83 percent of the design bearing pressure. This maximum pressure was maintained for a relatively short period only, since gradual unloading for feeding purposes had begun a few days later. The complete loading pattern including the negative pressure due to excavation is illustrated in Figure 6.1.1.

6.2 Contact Pressures

Vertical contact stresses were measured at the locations shown in Figure 5.2.2.1. Since all readings were taken with the read-out instrument on top of the raft, corrections for the hydrostatic effect became necessary. The hydrostatic pressure that is added to the gauge readings is equal to the height of the centre of the gauge above the load cells multiplied by the unit weight of the oil. The distance between the cells and the pressure gauge is equal to 1.24 m (4.07 ft), (see Figure 5.2.2.5). The specific gravity of the oil was determined in the laboratory and the average of three tests gave

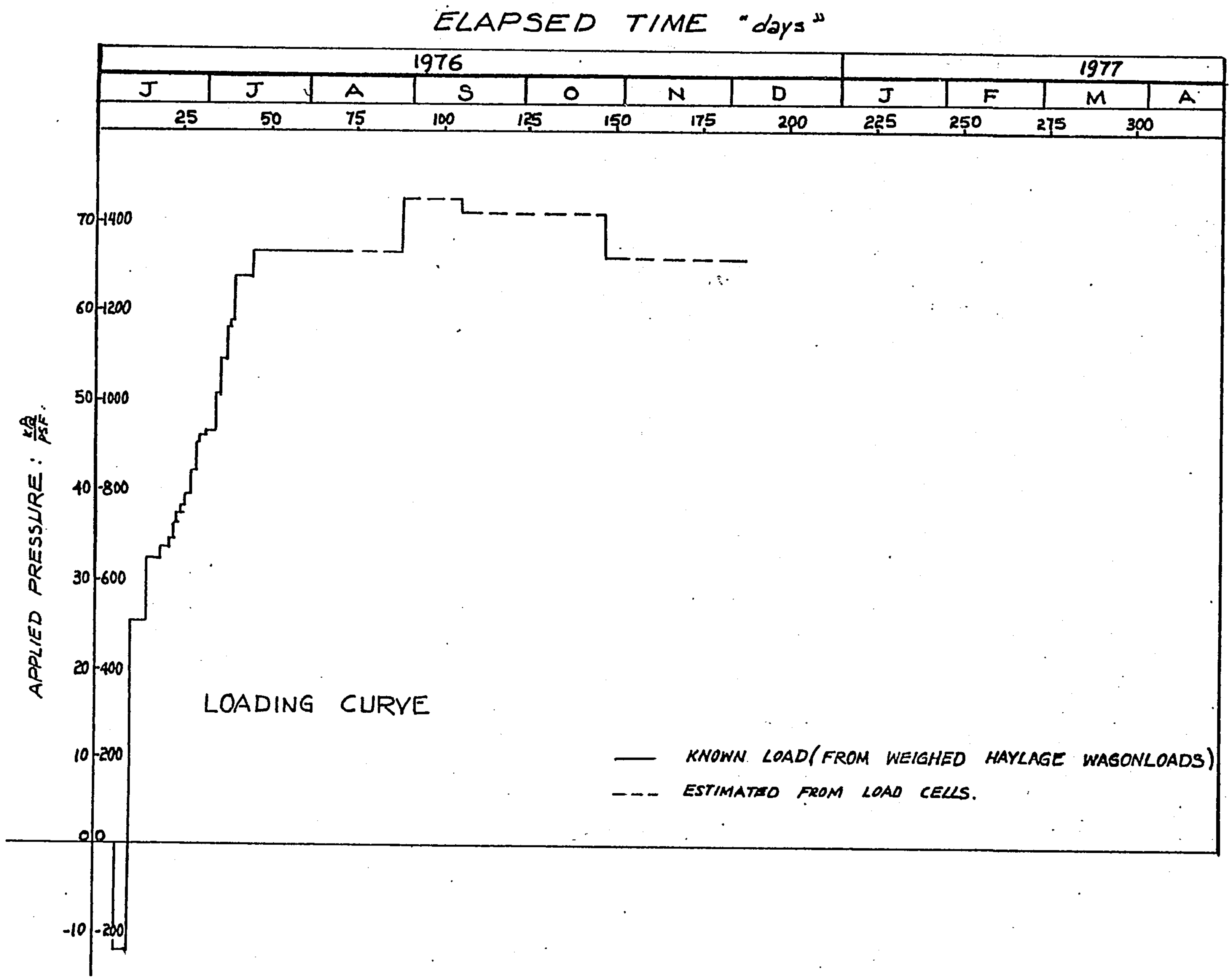

FIGURE 6.1.1. LOADING CURVE

a value of 0.81. According to the manufacturer of the load cells, temperature effects in applications such as this are negligible and therefore no corrections for temperature were applied.

Variation of the contact pressures of the individual cells with time is illustrated in Figure 6.2.1. It is seen from these curves that all the load cells portray a similar pressure increase with time. There is also a close similarity between these curves and that illustrated in Figure 6.1.1 for the average contact pressure.

6.2.1 Observed Vertical Contact Stress Distributions

In order to show the vertical contact stress distribution across the raft, the corrected pressure readings are plotted below each cell and straight line variations assumed between them. These distributions are given in Figures 6.2.1.1 and 6.2.1.2. The figures were drawn by assuming that the load cells on any two rows or strings lie on a common line. The plots are presented for six average applied pressures. It is easily noticed that there is a variation in stress distribution across each row of load cells. The probable reason for this variation as well as comparison with theoretical and experimental work reported in the geotechnical literature will be dealt with in Chapter 7. In this section it is only intended to present the raw data in an understandable format.

6.2.2 Estimation of Silo Load from Load Cell Readings

Total loads from pressure cells were calculated by dividing the footing into five annulie and a small circle at the centre, and

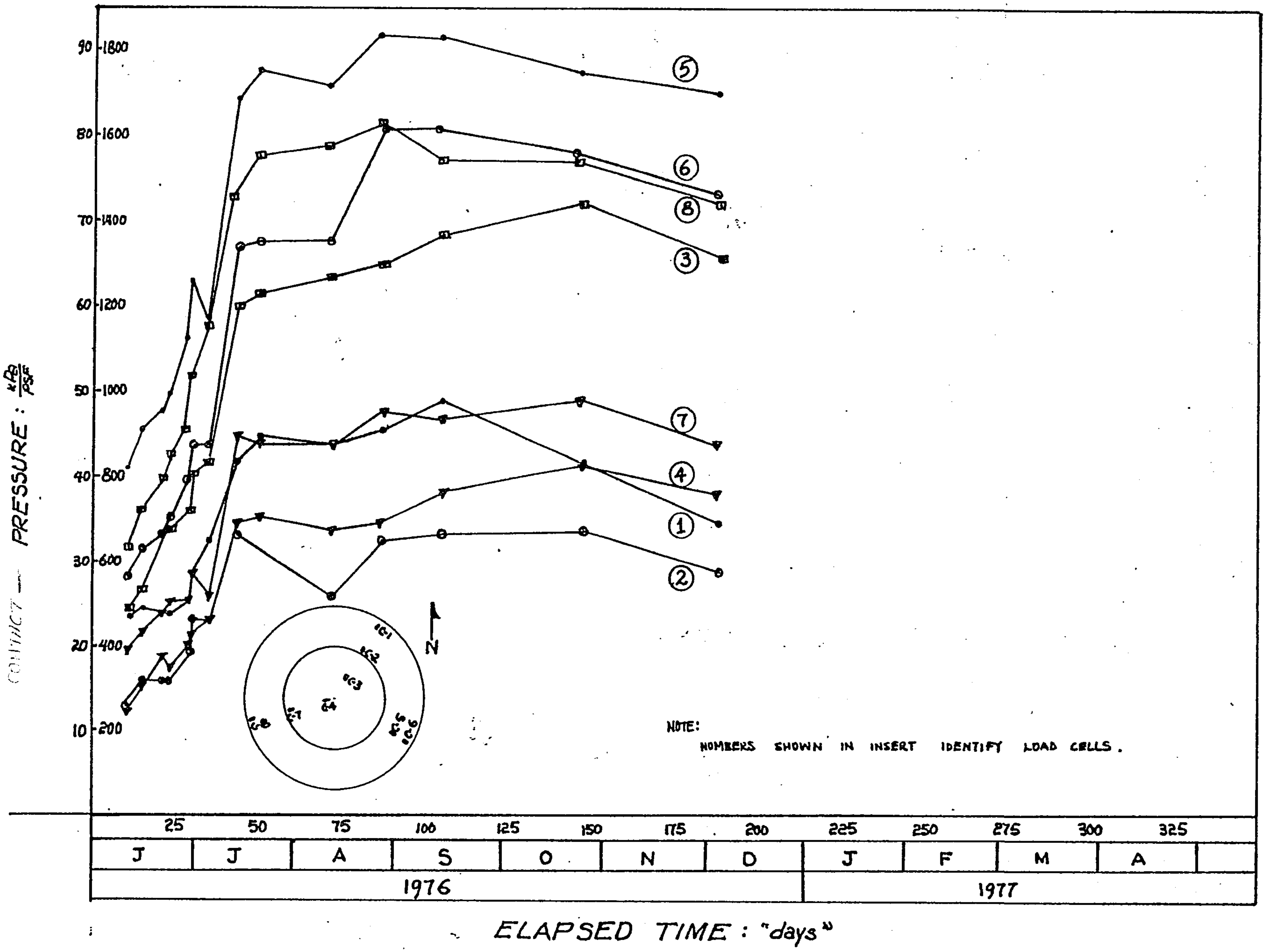

FIGURE 6.2.1 NORMAL CONTACT PRESSURE VS TIME.

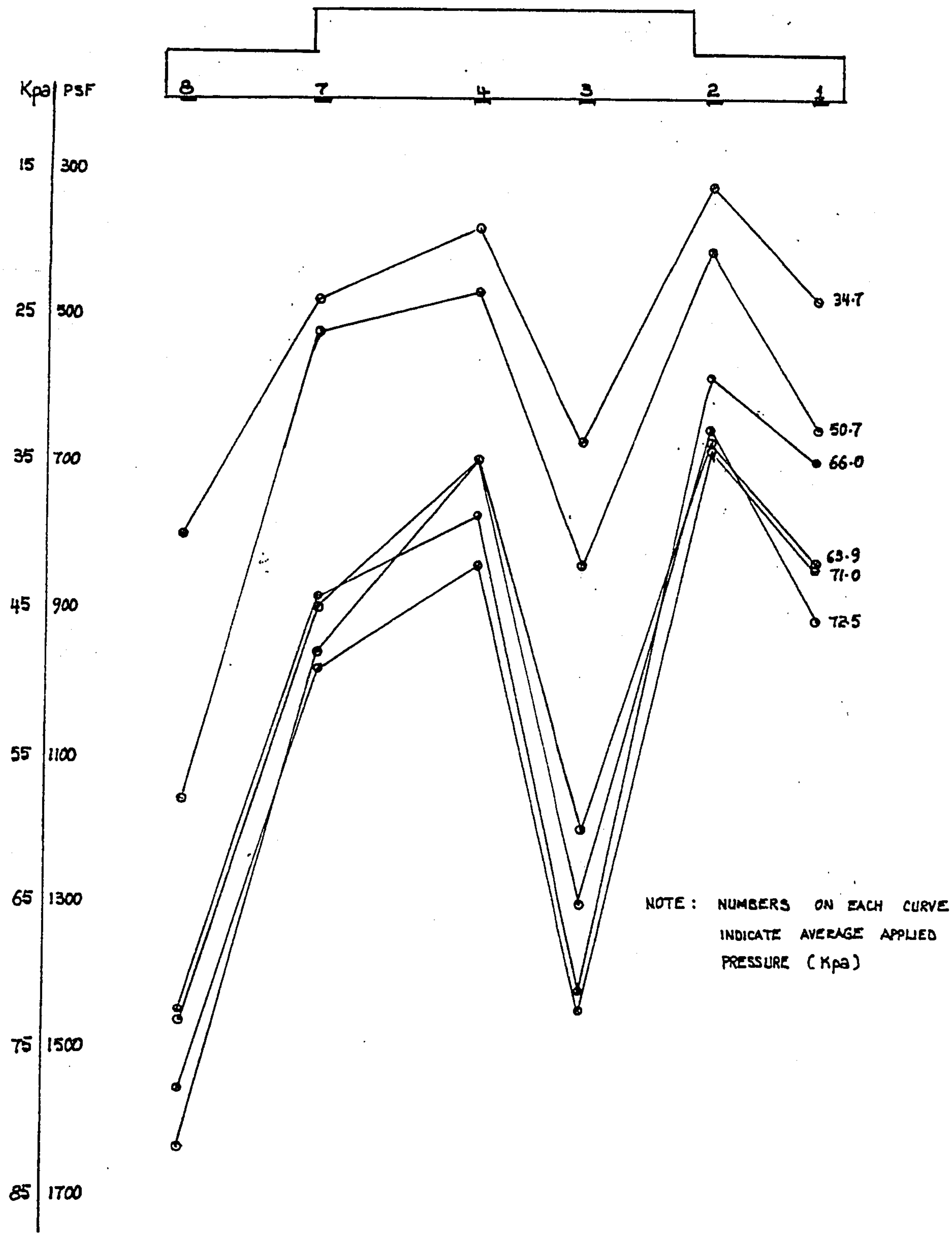

FIGURE: 6.2.1.1. DISTRIBUTION OF NORMAL CONTACT PRESSURE ACROSS CELLS 1,2,3,4,7 & 8

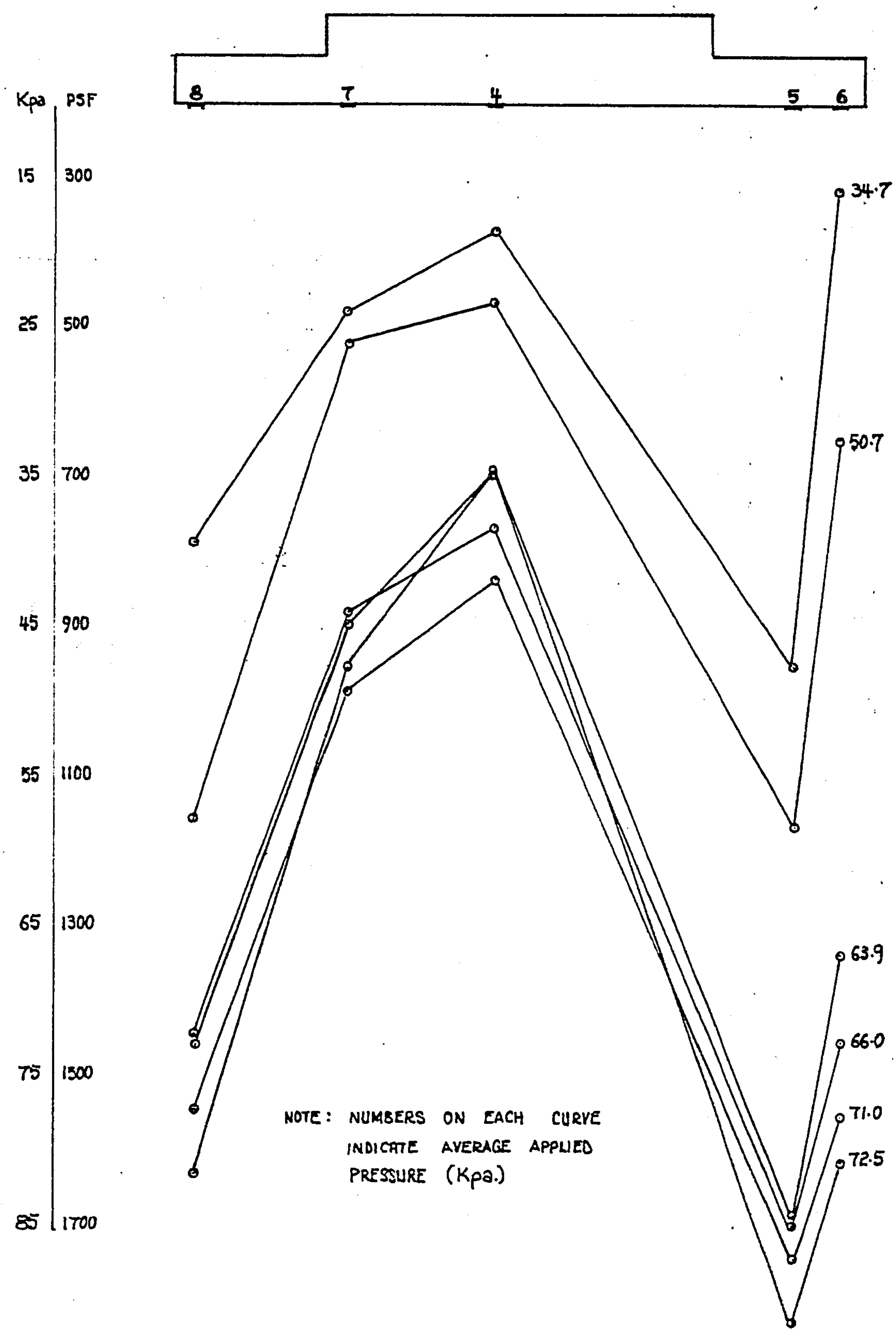

FIGURE 6.2.1.2. DISTRIBUTION OF NORMAL CONTACT PRESSURE ACROSS CELLS 5, 6, 4, 7 & 8

by assuming uniform pressure distribution across each annulus and the central disk. The width of the annulus is taken to be the mid-point distance between successive load cells along any radius, Figure 6.2.2.1. For the outer ring, the average pressure readings of load cells 1, 6 and 8 are used. The values of total silo loads estimated by this method are plotted in Figure 6.2.2.2 against known loads. This plot serves as a field calibration of the cells, so that future load estimates can easily be made from pressure cell readings and the calibration curve. It is found that the load cells underestimate the actual load with an error of approximately 12.3 percent. The field calibration curve (Figure 6.2.2.2) was plotted by assuming that the dead and live loads are accurately known, which is reasonable, since a good number of the wagon loads were weighed. Moreover, the dead weight due to the foundation and the structure are also known with even greater accuracy. The loading record is found in Appendix B.

6.3 Pore-Water Pressure

As mentioned in Section 5.3.5, measurement of pore pressures were carried out with six piezometers installed at different depths. In general the response of the piezometers was not as significant as that of the other instruments. This could be attributed partly to the silty nature of the clay which tends to allow fairly rapid drainage and also to the magnitude of the loads which were considerably smaller than the preconsolidation pressure especially in the crustal zone.

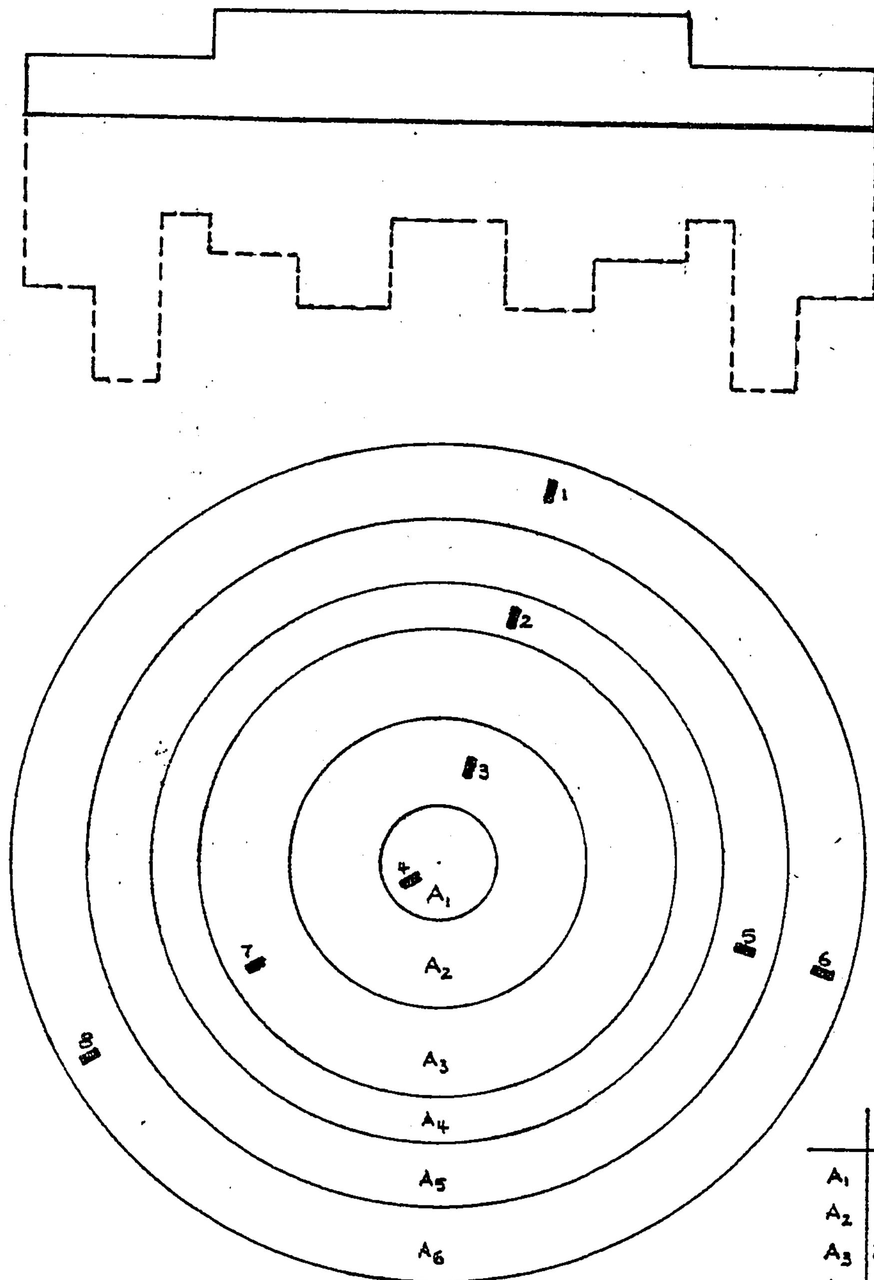

	m^2	Ft^2
A_1	2.63	28.3
A_2	15.14	162.9
A_3	27.86	299.7
A_4	20.08	216.0
A_5	34.24	368.4
A_6	47.89	515.2

NOTE: THE DIMENSIONLESS PRESSURE DISTRIBUTION SHOWN IS BASED ON ACTUAL LOAD CELL READINGS.
A_i = AREA OF A GIVEN ANNULUS
▬ = INDICATES LOCATION

FIGURE: 6.2.2.1 NORMAL CONTACT PRESSURE DISTRIBUTION FOR CALCULATION OF TOTAL LOAD.

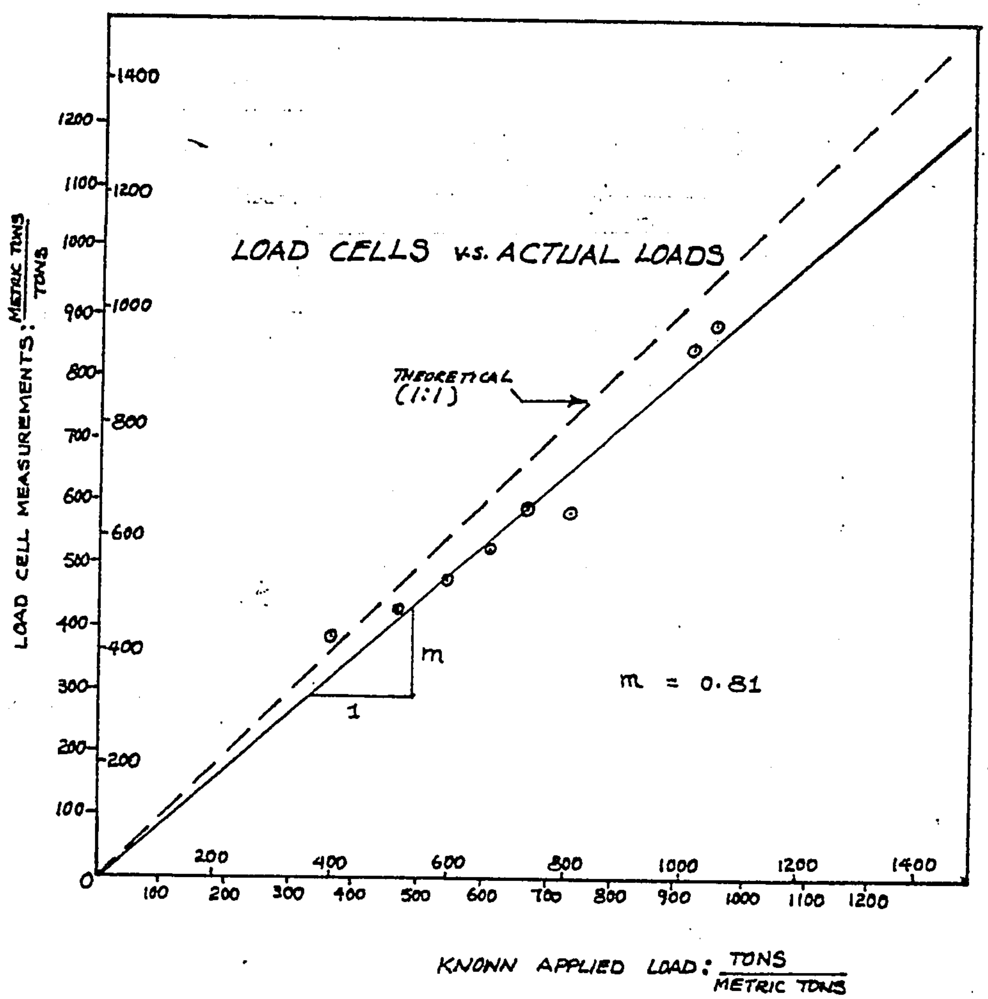

FIGURE 6.2.2.2. GRAPH FOR ESTIMATING SILO LOAD FROM LOAD CELL VALUES

6.3.1 Variation with Load

The variation of pore-water pressure with average applied stress is best shown by referring to Figure 6.3.1.1 which is basically a plot of measured pore-water pressure versus elapsed time. In this graph, the distribution of the average applied pressure with time is also given. The same data is found replotted in the form of excess pore-water pressure against average applied pressure in Figure 6.3.1.2. Excess pore-water pressures are calculated by taking the original ground water level indicated in Figure 6.3.1.1 as a zero datum. For the purpose of clarity, above 60 kPa of applied pressure, only the excess pore-water pressures at the end of the constant loads are plotted.

Although the patterns are somewhat erratic, it can be seen that initially all the piezometers indicate a rise in pore-water pressure with increase in the applied load. It is also noticeable from the above two figures that this initial pore pressure increase is relatively rapid. However, in all cases the maximum pore pressure increase corresponding to a rise in the applied pressure of about 63 kPa is only in the order of a meter of water or approximately 10 kPa of water pressure. This maximum was registered by the pneumatic piezometer, P5 located at a depth of 8.48 m and not by P2 which is installed at a shallower depth of 2.32 m as would be expected from theory.

Theoretically the soil at a shallower depth experiences a greater vertical and horizontal stress increase due to an applied load at the foundation level, than that at a greater depth. Since increase

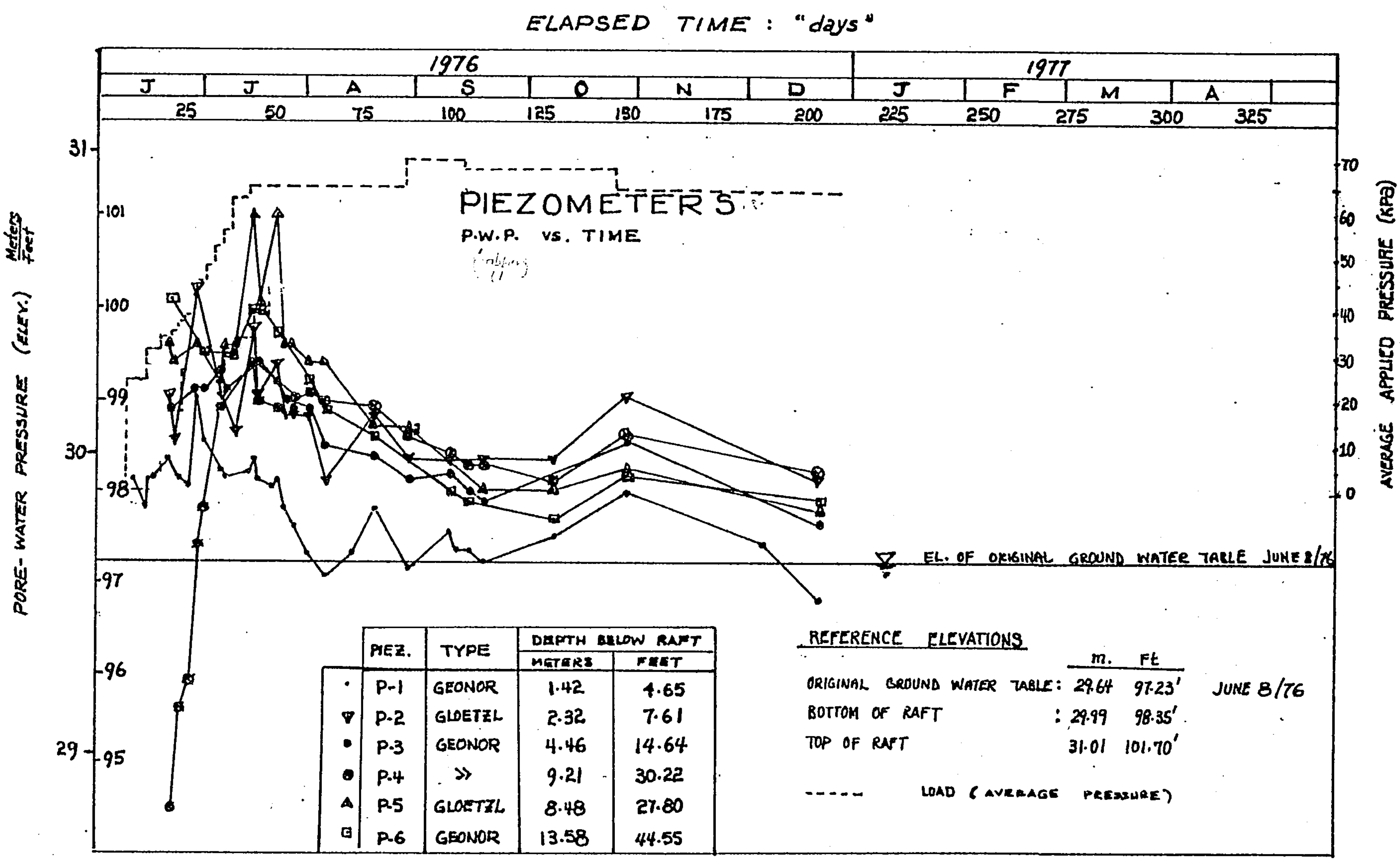

	PIEZ.	TYPE	DEPTH BELOW RAFT METERS	DEPTH BELOW RAFT FEET
·	P-1	GEONOR	1.42	4.65
▽	P-2	GLOETZL	2.32	7.61
•	P-3	GEONOR	4.46	14.64
⊗	P-4	"	9.21	30.22
△	P-5	GLOETZL	8.48	27.80
⊡	P-6	GEONOR	13.58	44.55

FIGURE: 6.3.1.1 VARIATION OF P.W.P. WITH TIME AND WITH AVERAGE APPLIED PRESSURE

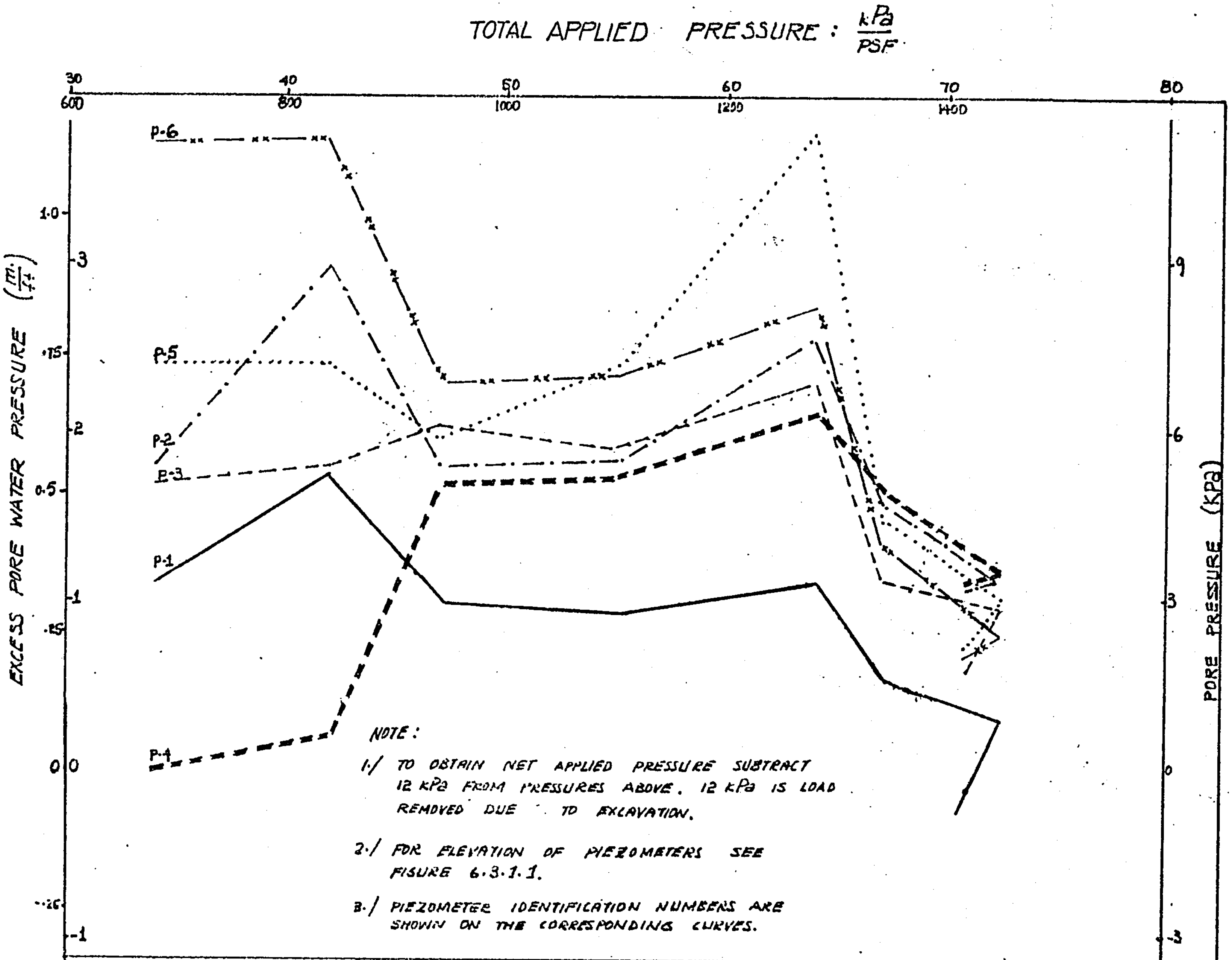

FIGURE 6.3.1.2 EXCESS PORE WATER PRESSURE VS APPLIED LOAD.

in pore-water pressure is a function of these stresses (Skempton, 1954), under ideal conditions the piezometers close to the bottom of the foundation should register higher pore-water pressures. However, since the measured difference is so small and also since at other applied pressure levels P2 indicates higher pressures than P5, the initial behaviour should not be considered as a contradiction to the theory.

It is interesting to note that when the applied pressure is held constant, all piezometer readings drop to lower values. Although the magnitudes of the pressure drops are small, being about 30 cm on the average, they, however indicate that the silty clay drains rather fast. Even though, there is no measured evidence about radial drainage, it is expected radial as well as vertical drainages are taking place. In fact it is probably this additional drainage in the radial direction which is responsible for the low pressure readings by the piezometers.

Calculations of the Skempton's (1954) pore water pressure coefficient from isotropically consolidated undrained (CIU) tests carried out at the NRC, DBR laboratory, show that the coefficient A has a negative value. The coefficient is calculated at sample failure stresses and therefore designated A_f. For the calculation, the coefficient B in Equation 3.6.1 is assumed to be 1, which is valid for a saturated clay. The result of the calculation is shown plotted in Figure 6.3.1.3. From the curve it can be seen that the average A_f for the crust (crust extends to a depth of about 4.5 m) is -0.24 and that for the soft layer is -0.30. These negative values, even though they are calculated at high stress levels, would also cause the pore

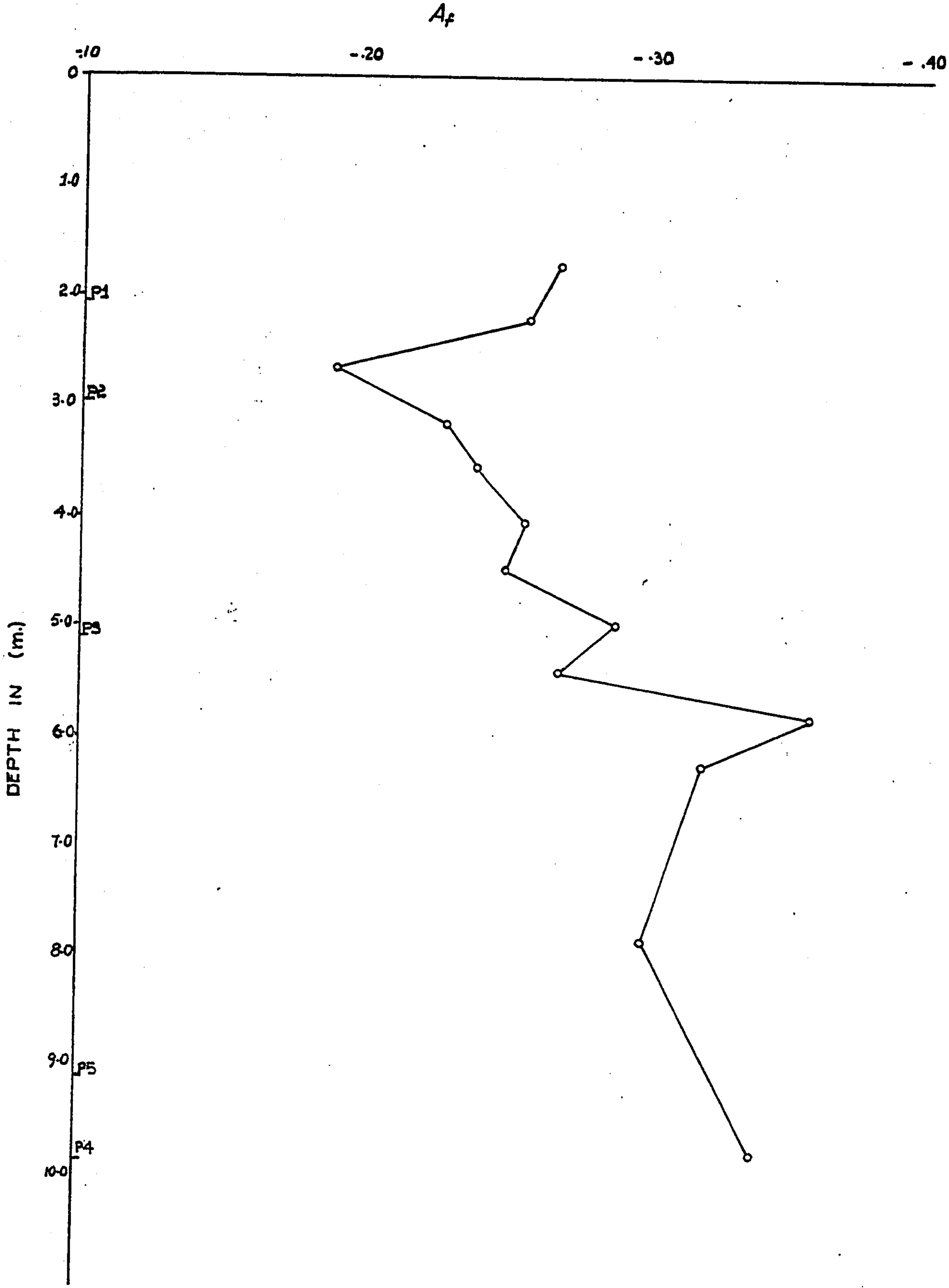

FIGURE 6·3·1·3 DISTRIBUTION OF PORE WATER PRESSURE COEFFICIENTS (A_f) AT SAMPLE FAILURE STRESS LEVEL. CALCULATED FROM CIU TRIAXIAL TESTS.

pressures to be relatively lower than in the case of a normally consolidated clay, thus giving rise to low piezometric readings.

6.3.2 Variation with Time

It is important to observe the magnitude and the rate of pore pressure changes with time to obtain an understanding of the consolidation process. When the magnitude of the applied load varies with time, the change in pore pressure also varies somewhat in phase with the load. This tendency is seen in Figure 6.3.1.1, however, for the purpose of analyzing consolidation settlement, what is more important is the dissipation of the pore pressure under a constant load. As mentioned in the previous section one notes from the figure a gradual drop of pore presure with time when the applied pressure is maintained at 63 kPa. This tendency is repeated when the applied load is increased to an equivalent pressure of about 70 kPa and held constant. However, since none of the loads was held constant for any significant length of time and the pore pressure changes are so small, it is not possible to analyze the pore pressure changes due to consolidation.

6.3.3 Variation with Depth

Because of the small difference in pressure readings between the piezometers at different levels, no attempt was made to make a plot of this variation with depth. A table in Figure 6.3.1.1 lists each piezometer and its depth below the bottom of the raft foundation. From this table and the curves and neglecting piezometers one and three, it is seen that the pore pressure change decreases with depth as is expected from theoretical considerations. Piezometer one always indicates the lowest pressure; this could be due to the high coefficient of permeability afforded by the desiccated and fissured clay layer which allows a quick pressure dissipation path.

6.4 Settlement

Compression of the soil layer directly below the footing was measured with an accuracy of .03 mm (.001 in) by means of a dial gauge and the spiral bit augers installed at four different depths. These instruments were discussed in Chapter 5. All gauges functioned properly except for number 3, whose reading needed some minor adjustment. The applied correction will be discussed in Section 6.4.3.

6.4.1 Variation with Load

In order to study the relationship between applied load and settlement, the total raft displacement and the net pressure are plotted on a common time axis. This plot (Figure 6.4.1.1) shows that up to a pressure of about 55 kPa (1100 psf), the relationship is approximately linear. In fact this linear variation is seen to be more pronounced when the data is replotted with vertical displacement versus net applied pressure and is presented with increased vertical scale as shown in Figure 6.4.1.2. Here in addition to the behaviour of the total compressible layer, the settlement of the soil below each settlement gauge is also presented. It is interesting to note the small creep indicated by all gauges under a constant pressure of about

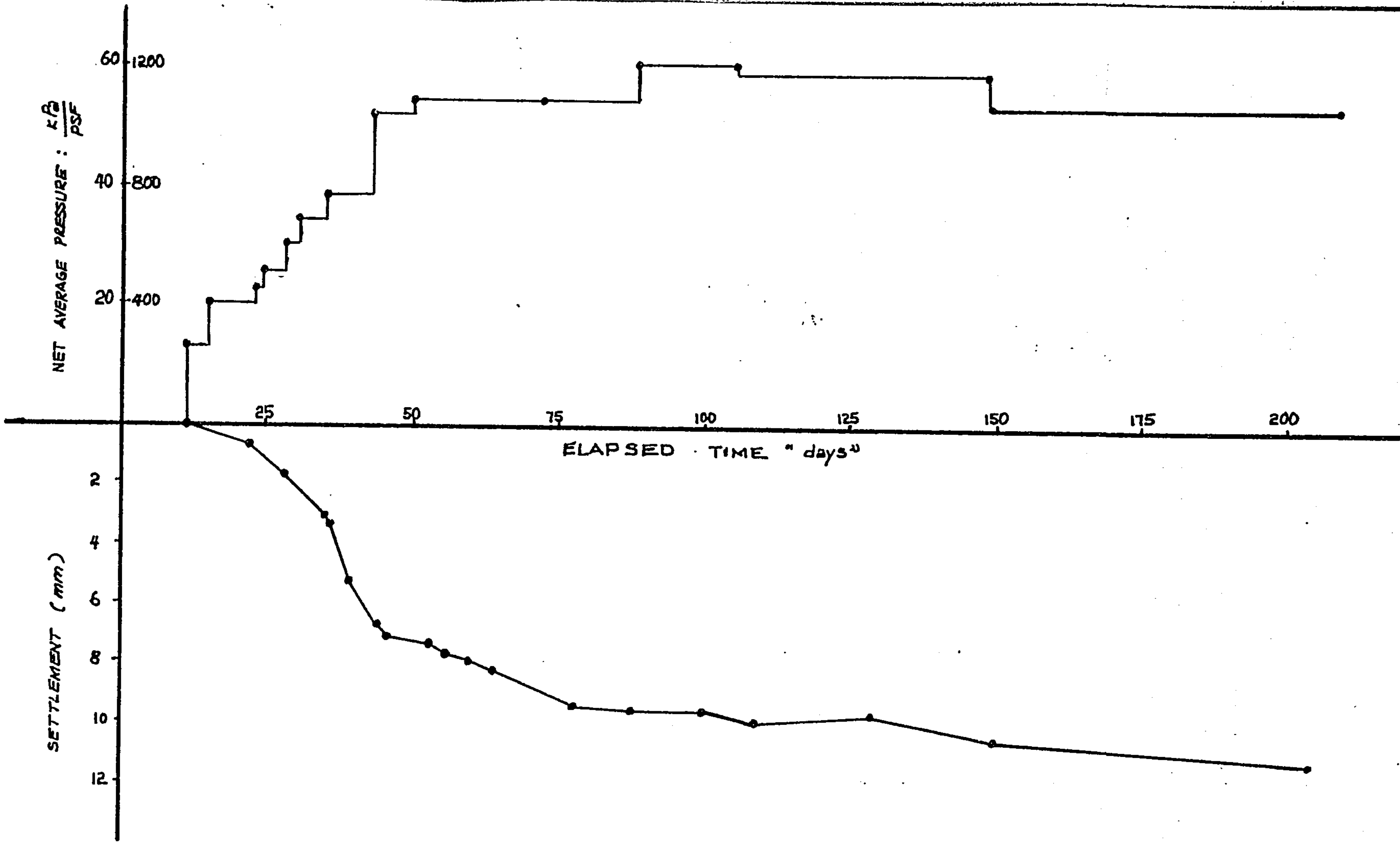

NOTE

NET AVERAGE PRESSURE = Applied load less negative pressure due to excavation.

FIGURE: 6.4.1.1. AVERAGE APPLIED PRESSURE AND TOTAL SETTLEMENT WITH TIME

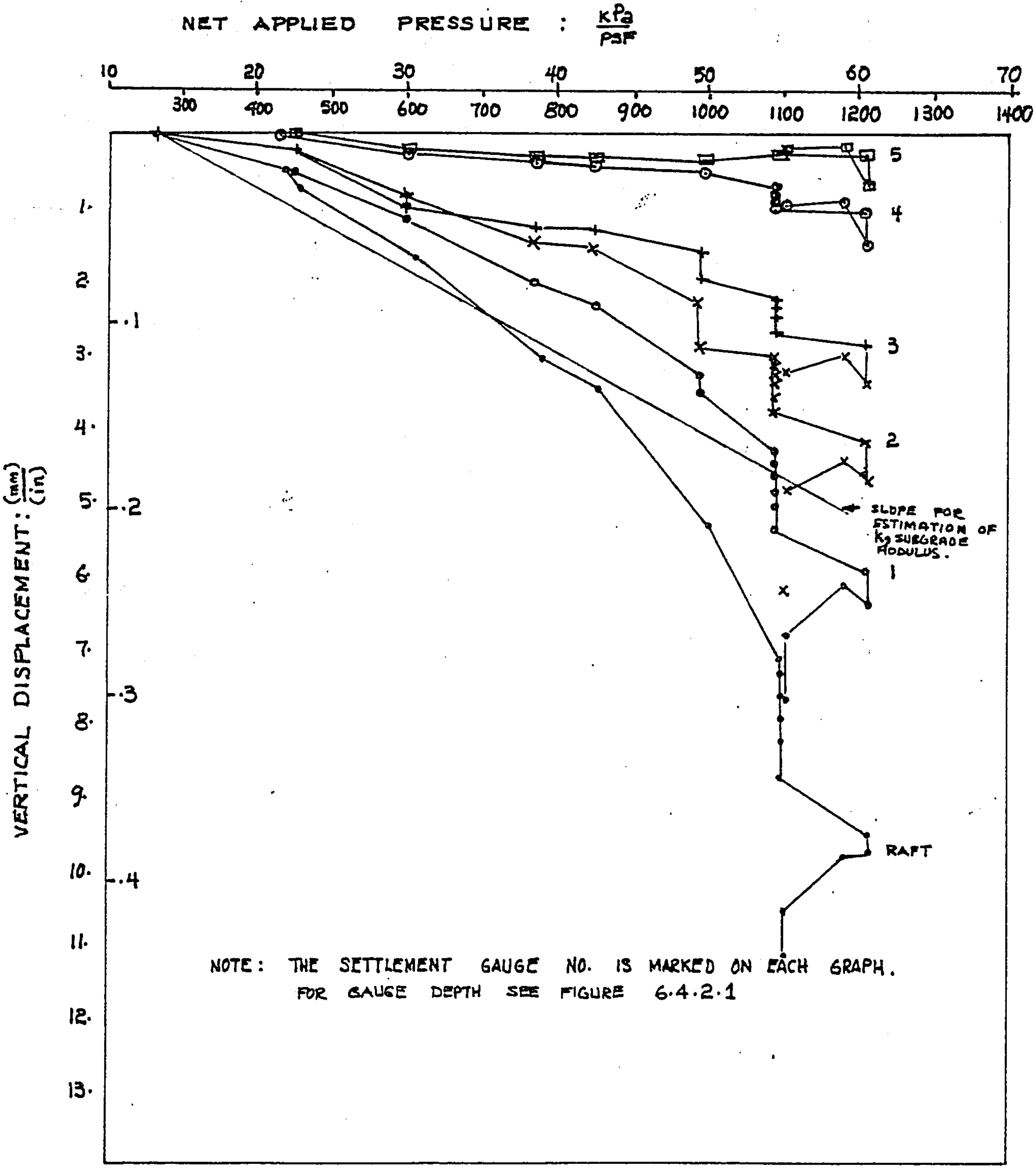

FIGURE: 6.4.1.2. NET APPLIED PRESSURE VS. SETTLEMENT

55 kPa (1100 psf) which was maintained for roughly 30 days. This behaviour will be discussed in Chapter 7 where consolidation settlement is dealt with. The linearity of net pressure versus settlement improves with increasing depth of measuring. This is to be expected since the stress in the soil due to the applied external pressure decreases with depth.

6.4.2 Variation with Time

One method of separating elastic from consolidation settlement is by observing for a reasonable period of time the changes in settlement of the structure under a constant pressure. The required length of time for making the distinction would of course depend not only on the intensity of the applied pressure but also on the coefficient of permeability and the preconsolidation pressure of the soil. In the case of the type of structure this thesis deals with, a constant load is only maintained for a very small length of time and therefore continuous observation under constant pressure is not possible. The variation of settlement with time for the raft foundation was previously given in Figure 6.4.1.1, in this section a more detailed plot for all the sublayers is presented in Figure 6.4.2.1. The only difference between these two figures is the vertical scale. In order to show the settlement of the soil below the deep settlement gauges the displacement scale had to be doubled, otherwise all the data shown in Figure 6.4.2.1 could have been included in Figure 6.4.1.1. It is seen that in all cases, initially the settlement increases

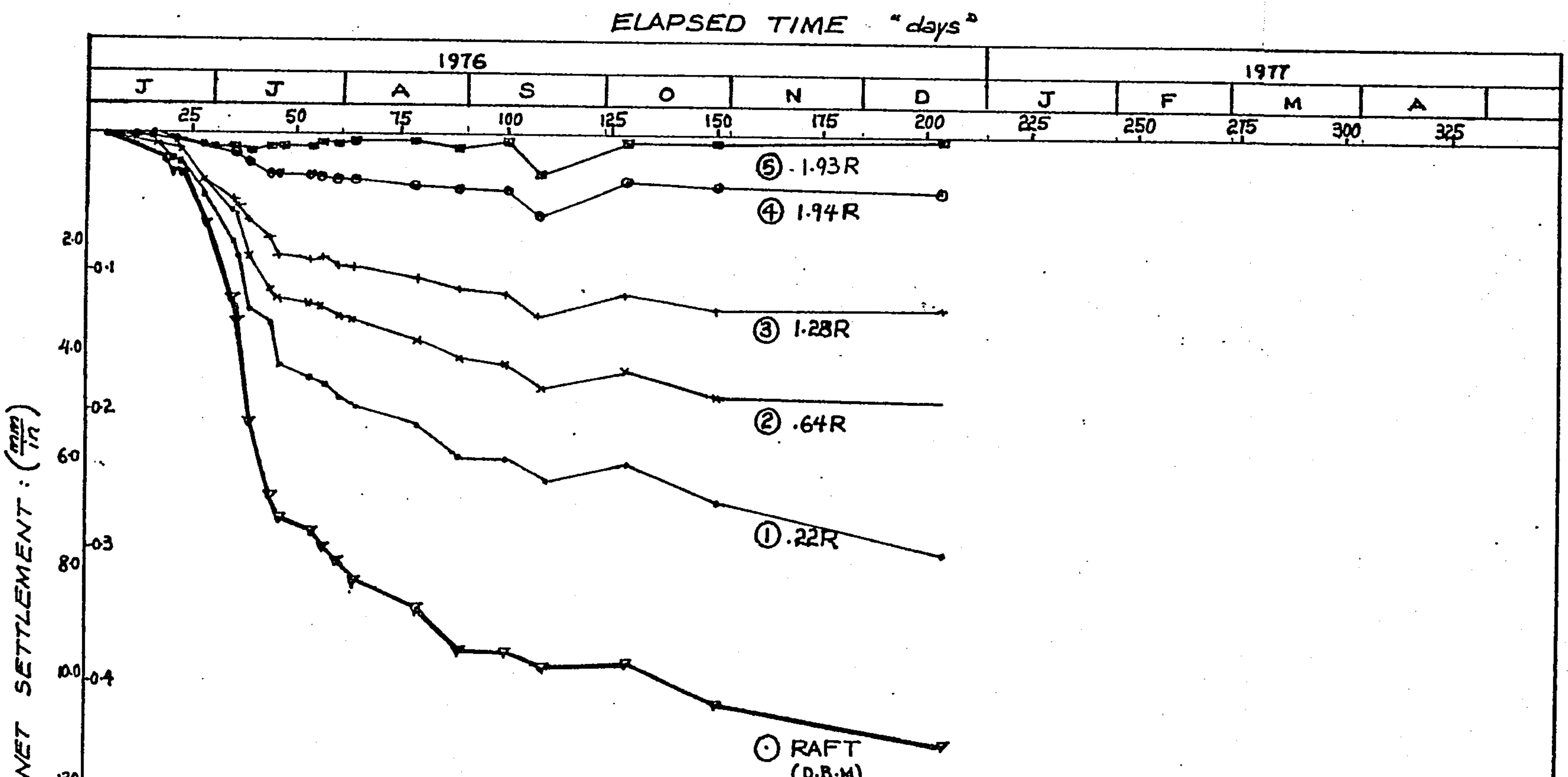

DEEP SETTLEMENT GAUGES

Net Settlement vs. time

Gauge No	Depth below bot. of raft: Feet	Depth below bot. of raft: Meters
1	4.90	1.49
2	14.25	4.35
3	28.66	8.80
4	43.61	13.30
5	43.40	13.23
D.B.M	79.06	24.10

NOTE:
Net settlement is the settlement of clay layer below a given gauge.
D.B.M = deep seated bench mark
R = radius of raft = 6.86 m. (22.5')

NOTE: LAST SET OF POINTS PLOTTED ABOVE ARE READINGS TAKEN ON DEC. 22, 1976. READINGS TAKEN ON FEB. 4, 1976, SHOWED RAFT FROST-HEAVED AND THEREFORE COULD NOT BE PLOTTED AS SETTLEMENTS.

FROST HEAVE DATA.

GAUGE	D.B.M (RAFT)
HEAVE (mm)	3.15

FIGURE: 6.4.2.1 VARIATION OF LAYER SETTLEMENT WITH TIME.

rapidly with time. This is because the corresponding pressure increase is also relatively fast. Once the maximum load is reached which is about 60 kPa (1200 psf), the settlement increase in all cases is very gentle, however, the trend continues even after unloading had started on day 150 shown in Figure 6.4.1.1. All the six curves can easily be approximated with bi-linear graphs having different slopes (rate of settlement).

6.4.3 Variation with Depth

For the purpose of making the discussion more understandable, the distribution of settlement with depth is given plotted in Figure 6.4.3.1. The plots are made for only six loads which had a significant variation in magnitude. Since all gauge readings were made relative to the bench mark, which is assumed to be fixed, it can be seen that the deformation of the soil decays somewhere between the depth of the deepest settlement gauges (Nos. 4 and 5) and the bench mark. A method of estimating this critical depth is to extrapolate the curves until they intersect the relative depth axis as shown in Figure 6.4.3.1 When this is done the approximate critical depth is found to be about 2.5 R. In reality this depth would vary with the magnitude of the net applied pressure, but for the analysis of most practical problems such as this, the error involved in assuming one depth for all pressures is very negligible. This argument is also supported by the fact that about 90 percent of the total settlement takes place in the soil above the deepest settlement gauges which are located at a depth of 1.94 R. Hence, since only 10 percent of the total settlement comes from the

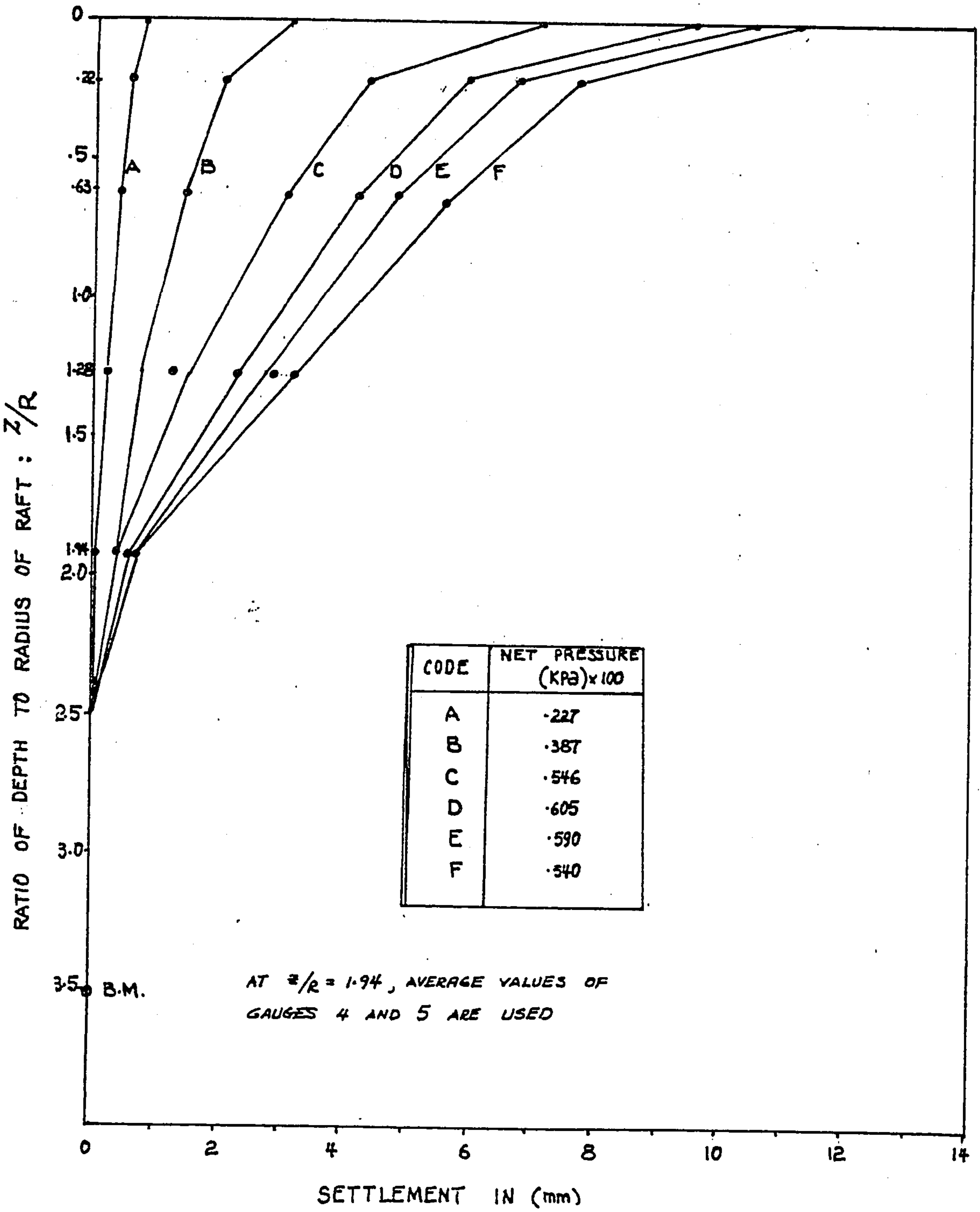

FIGURE 6.4.3.1. DISTRIBUTION OF SETTLEMENT WITH DEPTH

deeper soil, any rational method of estimating the critical depth is likely to give a satisfactory result. The knowledge of the critical depth is important when making calculations to determine the elastic modulus of the soil, which is dealt with in Chapter 7.

Referring to Figure 6.4.3.1 once more, it is easily noticed that the curves for each applied pressure differ slightly. The difference in the shape of the graphs for the minimum and maximum applied pressure is mainly in the top shallow layer extending to a depth of about 0.22R. With increase in the magnitude of the applied load, this layer tends to contribute proportionately more to the total settlement. This is usually an indication that the crust has a ratio of anisotropy greater than unity. This property which was discussed in Chapter 3, gives the soil a relatively large load spreading capacity at a depth close to the foundation. However, laboratory vane tests carried out at NRC, DBR laboratory show the ratio at anisotropy to be very close to one (see Section 6.6.3). Hence, an alternate explanation for the above settlement behaviour could be the closing of fissures. The greater the applied pressure the more the number of fissures that get closed and therefore the more the contribution to settlement by this layer. Bauer et al (1973).

In some of the plots, gauge number 3 gave settlement values close to or even greater than that indicated by gauge number 2, requiring some kind of adjustment. Corrections were made while plotting Figure 6.4.3.1. This is indicated by some plotted points at a depth of 1.28 R, which were not used in the drawing of the graphs.

6.5 Relative Curling of Raft

Upward curling or dishing of the raft foundation was detected by means of precise levelling on 24 concrete nails placed around two circumferences on the raft foundation (Figure 5.2.2.1). Since the central portion of the raft can be assumed to be perfectly rigid, because of its thickness of approximately 2 m, the curling of the raft is just a measure of the upward deflection of the outer 3 m of the raft. This quantity is the difference in elevation changes between the outer and inner settlement points located on a common radius. Under ideal conditions this difference was measured to an accuracy of 0.5 mm. The reasons for this rather low degree of accuracy are given in Section 5.4.

Since the magnitude of these differences is very small no attempt was made to present the data in any kind of graphical form. Instead, the differences between the elevation changes of the outer and inner settlement points for the twelve pairs is presented in Table 6.5.1. It is seen from this table that even under the most severe condition which is probably February 11, 1977, after the raft had heaved up by 3.15 mm (.124 in) above its end of construction elevation, the average curl was only 0.98 mm (.039 in). Average negative values should in theory indicate a downward deflection of the outer edge of the raft which is very unlikely. It can be concluded that since the raft is relatively rigid, the deflections are believed to be too small to be detected with the levelling technique employed.

Date	Average Pressure (kPa)	Relative Deflection Between Pair of Gauges on A Common Radius (cm) 1 / 2	3 / 4	5 / 6	7 / 8	9 / 10	11 / 12	13 / 14	15 / 16	17 / 18	19 / 20	21 / 22	23 / 24	Average Curl of Raft (cm)
1976														
Jun. 28	42.2		.022	-.03		-.002	-.049	-.055	.036	-.007	.026			-.01
Jul. 6	50.7		-.031	.023	.085	.037	.022	.042	.003	.002	-.03			.17
9	60.0		.066	.008	.000	.007	.028	.090	-.055	.013	.087	.116		.36
16	63.0		-.005	.003	-.031	.032	.000	-.053				-.052		-.15
23	66.6		.015	-.003	-.027	.002	-.012	.009	-.001		-.030	-.001	.027	-.05
30	66.6	.219	.026	-.027	.034	.043	.044	.004	.031	.102	.003	.018	.048	.45
Aug. 17	66.6	.002	-.006	.005	.012	.005	-.008	-.004	.110	.000	-.009	-.065	.008	.04
27	72.5	.063	-.006	-.102				.019	-.098	.030	.047	-.031		-.10
Sep. 17	72.5		-.007	.013	-.004	-.007	.022	.013	-.010	-.065	-.019	.012		-.08
1977														
Feb. 11	60.0	.172	.107	-.059	-.033	-.035			.030	.123	.144	.246	.278	.98

Note: On February 11th, raft heaved up by 3.15 mm (.124 in.) above its end-of-construction elevation.

TABLE 6.5.1 Data on Relative Deflection of Raft

6.6 Tests Carried Out at the Laboratory of the National Research Council, Division of Building Research

Some of the test results performed both in the field and in the laboratory have already been mentioned in the various chapters. In this section a brief description of the results of isotropically consolidated undrained (CIU) triaxial tests and oedometer test results will be given. These tests were performed so that estimates of undrained and consolidation settlements can be made using available theories; and to compare these results with field measurements.

6.6.1 Consolidated Undrained Triaxial Tests (CIU)

Thirteen piston samples collected from a depth of 1.73 m (5.67 ft) to 9.76 m (32 ft) were tested under confining stresses equivalent to 75 percent of the effective overburden pressures. This value of K_o = 0.75 was believed to be representative for the deposit. The samples were loaded to failure under a strain rate of 1 percent per hour. Plots of applied pressure versus strain are found in Appendix B. Variation of the pore water pressurs are also plotted on the same sheets with the load versus strain curves. In almost all tests the pore pressure continued to increase after the maximum deviatoric stress occurred, agreeing with Crawford's (1960) observation for the same type of soil. The strain at failure ranges from 5.0 percent for the sample from a depth of 1.73 m (5.67 ft) to 0.6 percent for one from a depth of 4.47 m (14.67 ft). Although the strain at failure fluctuates with depth, there is a strong indication that the crust is less brittle than the underlying firm clay. Secant moduli calculated at a third and half failure stress levels gave an average modulus of 19,900 kPa (2900 psi) and 16,700 kPa (2400 psi) respectively. There is some scatter in the modulus values with depth as indicated in a tabulated form, also in Appendix B. Calculations of Skempton's (1954) pore water pressure coefficient from the CIU data have previously been given in Figure 6.3.1.3.

6.6.2 Standard Oedometer Tests

One way of evaluating the compressibility of a clay deposit is by determining its in situ stress history. This is normally done by conducting a series of consolidation tests. The number of tests that is required for a given project would depend on the thickness of the compressible layer, its consistency with depth and the importance of the project. For most engineering jobs, Leonards (1976) recommends a minimum of one test for each 3 m (10 ft) layer. For this project 12 standard oedometer tests were performed from which the preconsolidation pressures were determined. The spacing of the samples within the depth equal to one diameter is less than that recommended by Leonards (1976). In all tests the average load increment ratio (LIR) is in the order of 0.50, even though there are slight variations. All of the pertinent data including the consolidation curves are given in Appendix B. These consolidation curves have been corrected for machine deflection.

The logarithm of pressures are plotted against strain instead of void ratios as is commonly done. Brumund et al (1976), recommended the use of average strain rather than void ratio for the following reasons:

1. Strains are easier to compute than void ratios.
2. Differences in initial void ratio may cause samples to exhibit quite different plots of void ratio versus stress but almost identical plots of strain versus stress;
3. Settlements are directly porportional to strain, but use of Δe data also requires a knowledge of $(1+e_o)$ which introduces 2 variables, Δe and $(1+e_o)$; and
4. Strain plots are easier to standardize than void ratio plots.

The distribution of the maximum, minimum and the most probable preconsolidation pressure was previously shown in Figure 4.1.4.1. The latest recommended method in obtaining these values is well explained in the paper by Brumund, Jonas and Ladd (1976).

6.7 Stress Increase due to Applied Pressure

Incremental stresses due to the net maximum applied pressure (60.5 kPa) are given in Table 6.7.1. In the calculation both Boussinesq's and Westergaard's stress distributions were considered. The stresses are given below $r/R = 0.67$, which is the radial location of the settlement gauges from the centre of the raft. It is seen that the stress increase using Boussinesq's method decreases less gradually with depth than that given by Westergaard's. The difference in the two stress distributions is due to the difference assumptions inherent in the two theories. Boussinesq assumed a perfectly homogeneous elastic mass; whereas Westergaard considered the homogeneaus elastic

Sample No.	Depth Below Raft(m)	$\Delta\sigma'_z$ (kg/cm^2) at max. net pressure B	W	P'_o kg/cm^2	P_c kg/cm^2	$P'_o + \Delta\sigma_z$	$\frac{P'_o+\Delta\sigma_z}{P_c} \times 100$
197- 1- 1	0.86	0.401	0.515	0.18	1.75	0.695	40
197- 1-13	1.60	0.414	0.483	0.31	1.87	0.793	42
197- 2- 9	2.28	0.418	0.451	0.38	1.10	0.831	76
197- 4- 3	3.80	0.383	0.393	0.51	.84	0.903	108
197- 5-12	5.23	0.337	0.334	0.62	.95	0.954	100
197- 7- 2	6.95	0.284	0.243	0.74	.95	0.983	104
197- 7-12	7.66	0.261	0.211	0.80	1.11	1.011	91
197- 8- 2	8.53	0.233	0.182	0.87	1.05	1.052	100
197- 9- 3	11.73	0.177	0.139	1.11	1.58	1.249	79
197-10- 3	14.78	0.131	0.121	1.34	1.72	1.461	85
197-11-11	18.33	0.097	0.080	1.66	2.67	1.740	65

Note: P_c = probable preconsolidation stress
Stresses are below r/R = .67
B = Boussinesq
W = Westergaard
Maximum net pressure = 60.5 kPa
= .62 kg/cm^2

$\frac{P'_o + \Delta\sigma_z}{P_c}$ calculation based on Westergaard

TABLE 6.7.1 In-situ, incremental and preconsolidation stresses mass to be reinforced by thin, non-yielding, horizontal sheets of negligible thickness. This later assumption was made in an effort to simulate the stratification of real soils.

Table 6.7.1 also gives the effective in situ pressure P_o', the probable preconsolidation pressure P_c and the ratio $\frac{(P_o'+\Delta\sigma_z)}{P_c}$ 100. The last stress ratio gives an indication on how close the incremental stress brings the field stress to the preconsolidation pressure. The same information is indicated on each strain versus log pressure curve in Appendix B as well as in Figure 4.1.4.1.

Even though, in some cases, the field stress due to the incremental load exceeds the probable preconsolidation stress, the differences which are not very significant, are more likely due to errors in the estimation of P_c. Because if indeed P_c was exceeded the resulting settlement would have been much larger.

6.8 Shear Strength Anisotropy Test

Since most elastic theories assume the soil to be isotropic, some kind of measurements are useful to see if indeed the assumption is valid, from at least a practical point of view. Such tests were done at NRC, DBR laboratory at various depths and the results are given in Figure 6.8.1. The tests were done using the Wykeham-Farrance 12.7 x 12.7 mm (0.5 x 0.5 in) laboratory vane and the apparatus shown in Figure 6.8.2. This apparatus is used for holding the sample and measuring the test angles. A zero degree corresponds when the test is done directly through the axis of the 53.98 mm (2-1/8 in) sample and 90 degrees is when the vane is inserted along the side of the sample. Between these limits, tests at any desired angle can be made

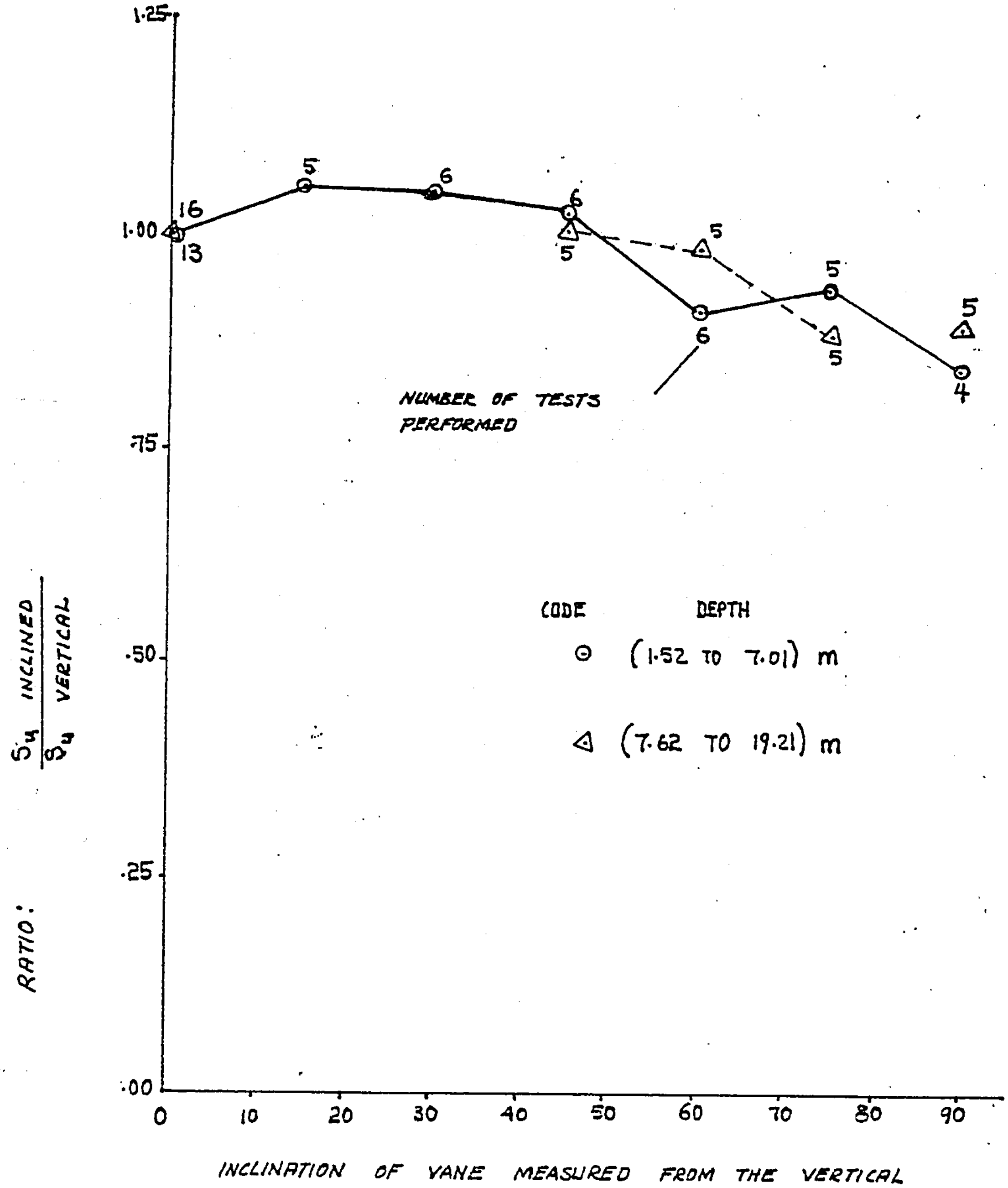

FIGURE: 6.8.1 SHEAR STRENGTH ANISOTROPY
ORIGINAL PLOT PROVIDED BY NRC, DBR.

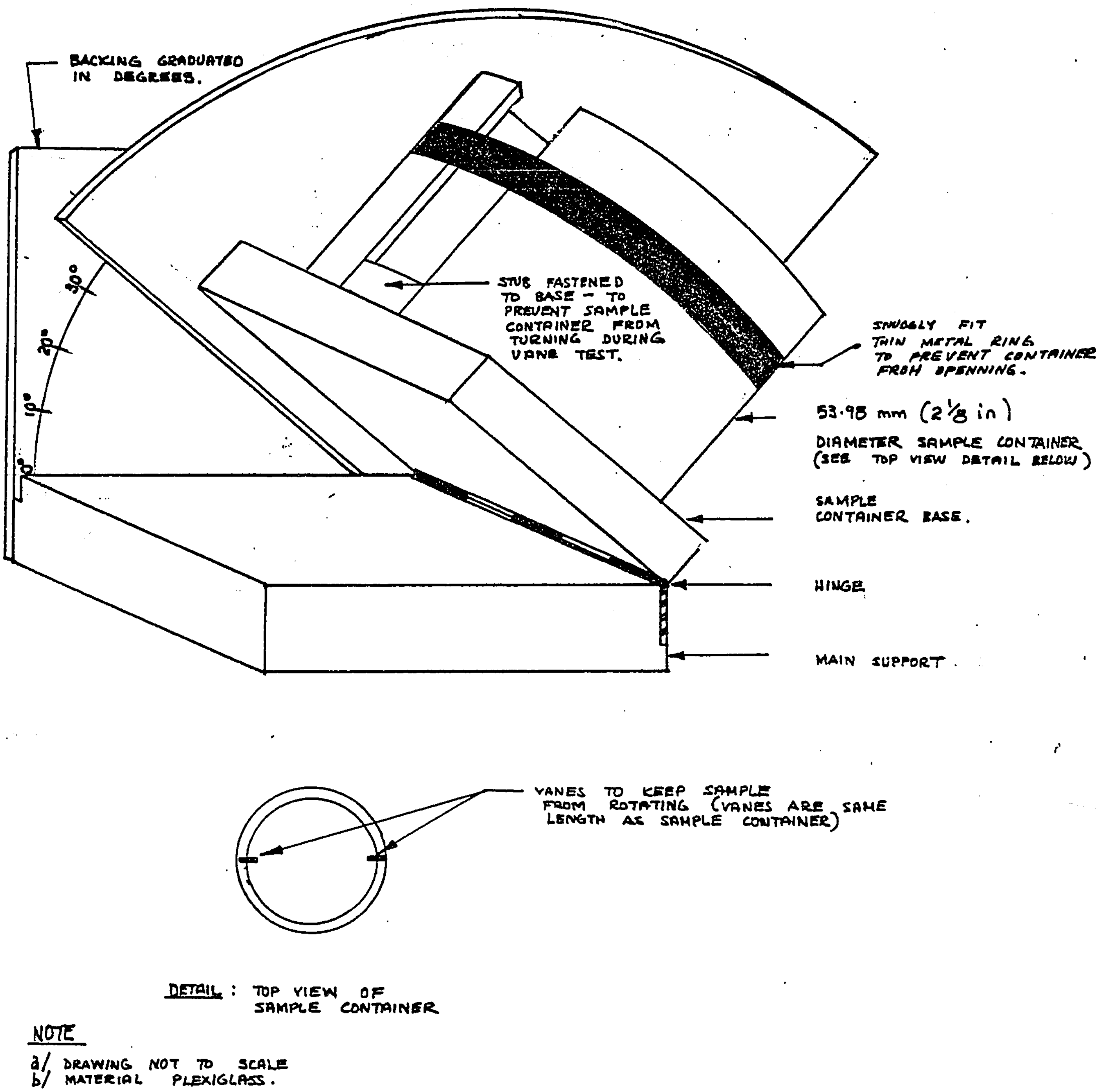

FIGURE 6.8.2 SCHEMATIC DRAWING OF VANE SHEAR STRENGTH ANISOTROPY TESTING APPARATUS, FOR HOLDING TEST SAMPLE AND MEASURING THE TESTING ANGLE. APPARATUS DESIGNED AND BUILT BY NRC, DBR.

in a similar manner. The plot shows that the clay can be considered isotropic for all practical purposes since both at the upper and lower limits the ratios S_u inclined to S_u vertical are close to one.

CHAPTER 7

ANALYSIS AND INTERPRETATION OF RESULTS

7.1 Contact Pressures

7.1.1 Measurements

In Chapter 6, the measured contact pressures were plotted by assuming two rows of load cells to lie on a common diameter (Figures 6.2.1.1 and 6.2.1.2). Comparison of the pressure distribution along each row shows that they are all different. For example, load cells 1, 6 and 8 all located at the same distance away from the centre of the raft, give pressures that vary by relatively large margins. One explanation for this could be the relative upward deflection of the raft at these locations. It was hoped that the settlement points installed on the surface of the raft would indicate these relative displacements, however, as can be seen from Table 6.5.1, this is not clearly indicated due to perhaps levelling errors as the deflections are very small.

Another reason that comes to mind is the effect of wind pressures, especially on such a tall structure, which might tend to tilt it to one side, thus giving rise to uneven pressures on the measuring cells. At the site the strongest wind always blows from the west which is the prevailing direction and where there is no obstruction in its path. Hence, if it had any significant effect*, it would be to increase the stresses in cells 1 and 6 and decrease this

*Wind pressure calculation based on NBC, 1975 (part 4) indicated the maximum increase in contact pressure due to wind to be only about 3 kPa. The reference velocity pressure, q = 0.4 kPa has a level of probability of being exceeded in any one year of 1 in 30. This is equivalent to a pressure generated by a reference wind velocity of 86 km/hr.

in cell 8 (see Figure 5.2.2.1). But field readings give substantially higher values for load cell number 8 than the other two.

During the installation of the load cells, it was observed that the clay surface at the bottom of the excavation was relatively soft at some places and very hard at others, due to exposure to rain and the sun. As the raft would tend to bridge over the load cells that are installed in the wet zones, and thereby cause a reduction in pressure readings in these cells, this condition could be the reason for the different values.

In Chapter 2, it was shown that for an ideal elastic soil, the contact pressure distribution is parabolic with stresses increasing from 50 percent of the average pressure at the centre to a maximum at the edges. If a smooth curve was to be drawn connecting the contact pressures for load cells 8, 7 and 4 (Figure 6.2.1.1), the resulting curve would almost be a parabola. Moreover, it is also interesting to note (Figures 6.2.1.1 and 6.2.1.2) that in almost all cases, the contact pressure readings of load cell number 4 which is very close to the centre of the raft are about 50 percent of the average applied pressure. However, the pressure distribution along the other rows of load cells show very little resemblance to the theory.

7.1.2 Distributions

Since the maximum number of cells per row is only four, any malfunction in any one of them can easily distort the true shape of the contact pressure distribution curve. In fact even if all four work properly, they do not provide enough points to define the expected elasto-plastic curve. A more scientific approach to this problem is to make use of the probability theory to determine the minimum number of cells required to define the curve. A discussion of this technique is given in a recent paper by Phal (1977). Phal finds that for most practical cases the number of cells required is in excess of 20, all installed along one radius.

Unfortunately, in this project because of cost, a total of only 8 load cells were used. Although, these cells were installed along 3 radii, an improvement to the sample size representing the infinite population (all possible points that make up the theoretical curve) is possible by plotting the curves assuming that all 8 cells lie on the same radius. Such plots are shown for 3 applied average pressures in Figure 7.1.2.1. Again, no attempt was made to trace smooth curves through the pressure readings, because of the large number of possibilities. It is the author's opinion that with limited data such as this, drawing smooth continuous curves would serve very little purpose besides hiding the actual data. Mirror images of each distribution are also plotted so that complete contact pressure distributions across the raft are obtained. Distribution curves as predicted by two theories are also traced for the maximum average applied pressure. Based on each method two plots are shown. In the case of Zeevaert's method a second plot incorporating the actual measured edge stress (curve A) was calculated, since the theory based on Equation 2.3.1.6 underestimates the edge stress, resulting in a uniform contact pressure

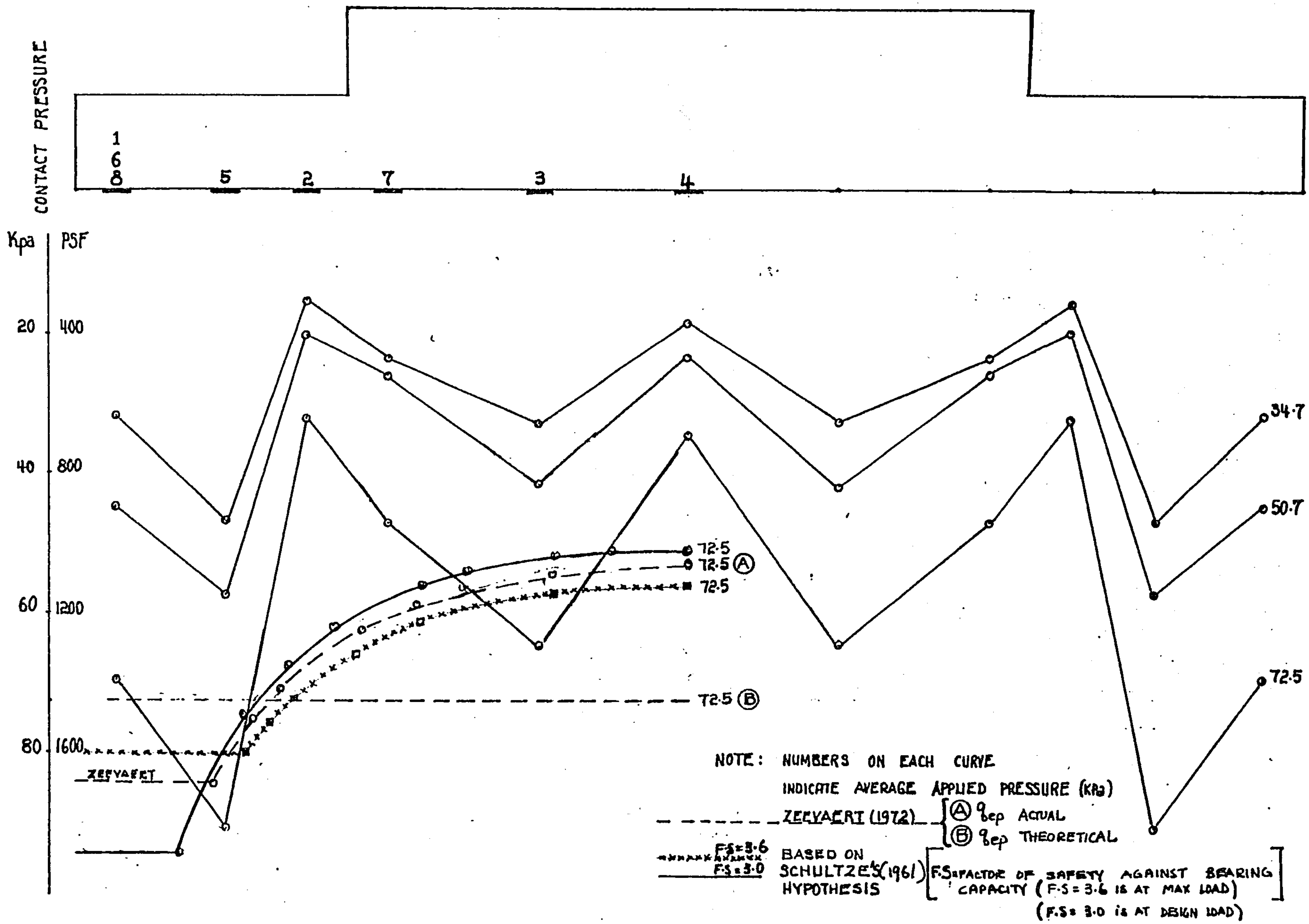

FIGURE 7.1.2.1 *MEASURED AND THEORETICAL CONTACT PRESSURE DISTRIBUTIONS.*

(curve B). Using the method derived on the basis of Schultze's (1961) hypothesis, one curve at the actual factor of safety against bearing capacity, which is 3.6, and another at a factor of safety of 3 are shown. These two curves are similar to curve A based on Zeevaerts method.

There is a large difference between the shapes of the theoretical and actual curves. This is to be expected because of the following reasons: a) as mentioned earlier the number of cells is inadequate, b) both theoretical methods assume a perfectly elastic soil medium, c) the condition of perfect rigidity cannot be satisfied and d) the beds for the cells were not uniform.

Degree of rigidity calculation using Equation 2.2.2 gives a stiffness value, K = 0.59 which when entered in Figure 2.1.1.1 shows that the foundation is close to but not perfectly rigid. If the reinforcement as well as the thicker central portion are taken into consideration a larger K value is possible but not enough to make the raft perfectly rigid. Elastic quantities used in the stiffness calculations are: Poisson's ratios of .15 to .5 for the raft and soil respectively, average secant modulus from the CIU test results corresponding to 0.33 and 0.5 failure deviatoric stresses (see Section 6.6.1) and elastic modulus for concrete derived from the 28th day concrete cylinder tests (Appendix B).

7.1.3 Total Load

One method of checking the accuracy of contact pressure distribution, besides comparing it with the theory is to integrate the curve over the area of the footing and to compare this with the applied vertical load. If the distribution is correct, the condition of statical equilibrium should be satisfied. Such calculations were made for the three distribution curves plotted in Figure 7.1.2.1 and the results show that the average error is in the order of 12 percent. The errors tend to increase with increasing average applied pressure. In all cases the load estimated from the distribution curves is smaller than the actual (see Figure 6.2.2.2).

7.1.4 Comparisons in Literature

The amount of available data from the engineering literature on contact pressure distribution, and especially in Leda Clay is almost non-existent. There have been few measurements done such as that reported by Gaumy (1970) and Eden et al (1973), (see Section 2.5). However, because of the limited number of cells used, the authors of these references were not able to conclude on the shape of the contact pressure distribution curves. They have nonetheless measured edge pressures that are about 2 to 3 times higher than the central pressure. This is also the general trend in this project, except near the very edge of the raft where possibly plastic yielding has reduced the contact stresses.

Another very interesting field measurement is that reported by Takanaka (1971). As described in Section 2.5, contact pressures were measured under a small circular footing of 2 m (6.5 ft) in diameter in a marine clay of high plasticity, high natural water content and also high liquid limit (Figure 2.5.4). Comparison between Figures 7.1.2.1 and 2.5.4 show that there is a striking similarity between the two measurements. The fact that the two marine clays have different properties should not have a very large effect. Although, the agreement between the above two results is not enough to confirm the shape of the pressure distribution, it however makes it safe to conclude that one should not expect to obtain curves similar to those predicted by elastic theory. It appears that sensitive clay soils have a unique contact pressure response, which can only be confirmed by performing a sufficient number of detailed field measurements.

On the other hand, for most design applications, the modified elastic theories such as Zeevaert's (1972) or that derived in Chapter 2 based on Schultze's (1961) hypothesis can be used as good approximation. In the case of Zeevaert's method, however, care should be taken in making an estimate of the edge stress using Equation 2.3.1.6.

One of the important differences between the two methods, lies in the estimation of the edge stress. The edge stress of 71.5 kPa estimated from Equation 2.3.1.6 as proposed by Zeevaert is even smaller than the average stress of 72.5 kPa and therefore cannot be right. Moreover, since the edge stress estimated by Equation 2.3.1.6 is very low, Zeevaert's method resulted in a uniform pressure distribution (see Figure 7.1.2.1), which is contrary to the trend shown by the load cells. The actual edge stress based on the average readings of cells 5, 6 and 8, is 84.5 kPa, which is 15 percent higher than that estimated by Equation 2.3.1.6.

The second method which is based on Schultze's (1961) hypothesis appears to approximate the trend of the contact pressure distribution better. Examination of Figure 7.1.2.1 shows that the edge and central stresses estimated by this method are approximately close to the actual.

Sample calculations to illustrate on how to obtain normal contact pressure distributions using the above two methods follow. The example calculations will be for two of the theoretical curves shown in Figure 7.1.2.1.

7.1.5 Theoretical Calculations

The purpose of this sub-section is to show the calculations for obtaining theoretical contact pressure distributions.

PROBLEM: to find the theoretical normal contact pressure curves.

Foundation = circular silo raft

Diamter of raft = 13.72 m

Average pressure = 72.5 kPa

hence, total load $= \frac{(13.72)^2}{4} \times \Pi \times 72.5$

$= 1.07 \times 10^4$ kN (kilo Newtons)

SOLUTIONS

Method 1(a) Zeevaert's (1972)

a) Calculate edge stress q_{ep}; Zeevaert recommends that for precompressed sensitive clay the minimum value between the average P_c

and that given by Equation 2.3.1.6 should be selected.

$$q_{ep} = 3/2\ s + \sigma_{zD} \qquad 2.3.1.6$$

Assigning 0.41 $\frac{kg}{cm^2}$ = 40.2 kPa for s, (based on vane shear strength profile),

$$\sigma_{zD} = \gamma D = 1860\ \frac{kg}{cm^2} \times 0.61\ m \times \frac{9.8\ m/sec^2}{1000}$$

$$= 11.2\ kPa$$

$\therefore$ q_{ep} = (1.5 x 40.2 + 11.2) kPa

= 71.5 kPa, this is selected according to Zeevaert's method because it is smaller than the average P_c which is about 139 kPa.

b) Calculate r_1 and C_o

$$q_a/q_{ep} = \frac{72.5}{71.5} = 1.01$$

From Figure 2.3.1.1 for q_a/q_{ep} = 1.01, ξ_1 = 0

From which r_1 = 0, hence the distribution is uniform with $p(r)$ = 72.5 kPa.

Therefore for our particular soil properties Zeevaert's method gives a uniform distribution and does not appear to be applicable to shallow foundations in a soil of low shear strength such as the Leda Clay.

<u>Method 1(b)</u> Zeevaert's (1972) - Using Measured Edge Stresses

In order to show the technique for obtaining elasto-plastic contact pressure distribution, calculation will be carried out using the actual edge stress (neglecting cell No. 1) obtained from the average of cells 5, 6 and 8 at applied pressure level of 72.5 kPa. Referring to Figures 6.2.1.1 and 6.2.1.2, the average is:

$$q_{ep} = \frac{1}{3}\,(8.7 + 81.4 + 91.5)\text{kPa} = 84.5 \text{ kPa}.$$

This actual edge stress is 15 percent higher than the theoretical Zeevaert's value.

a) $q_a/q_{ep} = \frac{72.5}{84.5} = 0.86$

From Figure 2.3.1.2 with $q_a/q_{ep} = 0.86$, $\xi_1 = 0.775$

From which $r_1 = 0.775R = 0.775 \times 6.86 \text{ m} = 5.32 \text{ m}$.

Entering Figure 2.3.1.2 with ξ_1, we get $C_o = 0.73$.

b) Distributions

Elastic $(0 \leq \xi \leq 0.73)$: $p(r) = \dfrac{C_o q_a}{\sqrt{1-\xi^2}} = \dfrac{0.73 \times 72.5}{\sqrt{1-\xi^2}}$ (kPa)

Plastic $(0.73 \leq \xi \leq 1.0)$: $p(r) = 84.5$ kPa

The distribution is found in Table 7.1.5.1 and the same data is also plotted in Figure 7.1.2.1.

c) Check Integration

$$\text{Total load} = C_o 2\Pi q_a \int_o^{r_1} \frac{r\,dr}{\sqrt{1-(\frac{r}{R})^2}} + q_{ep}(2\Pi)\int_{r_1}^{R} r\,dr$$

Performing the integration we obtain:

$$\text{Total load} = 2C_o q_a \Pi R[-\sqrt{R^2-r^2}]_o^{5.32} + \Pi q_{ep}[6.86^2 - 5.32^2]$$

After substituting for known quantities:

$$\text{Total load} = (0.58 \times 10^4 + 0.50 \times 10^4) \text{ kN}$$

$$= 1.08 \times 10^4 \text{ kN which is very close to the actual.}$$

<u>Method 2</u>: Derived by author on the basis of Schultze's (1961) hypothesis.

a) Calculate constants C_1 and C_2 using Equations 2.3.2.4(b) and 2.3.2.4(c) respectively.

$$C_1 = (\kappa_1 C N_c + \gamma_1 D N_q)\, \Pi R^2$$

$$C_2 = 4 \Pi R^3 \kappa_2 \gamma_2 N_\gamma$$

For $\emptyset = 0$ condition (saturated and undrained clay), $N_\gamma = 0$, hence $C_2 = 0$.

Since the bearing pressure is less than the ultimate, C_1 should be calculated at some factor of safety. In this example the actual factor of safety of the structure will be used.

$$\text{F.S.} = \frac{q_u}{q_{actual}} = \frac{3(87.5 \text{ kPa})}{72.5\text{kPa}} = 3.6$$

$C = 40$ kPa (average shear strength below raft within a depth of 2/3D)

$\gamma_1 = 1860 \frac{\text{kg}}{\text{m}^3}$ (see Figure 4.1.4.1)

$D = 0.61$ m (depth of foundation)

$$\left.\begin{array}{l} N_q = 1.0 \\ N_c = 5.14 \end{array}\right\} \text{bearing capacity factors}$$

$\kappa_1 = 1.2$ shape factor, circular footing hence,

$$C_1 = \left(\frac{1.2 \times 40 \times 5.14}{3.6} + 1860 \times 0.61 \times 1 \times \frac{9.8}{1000}\right) \Pi R^2$$

$$C_1 = 79.7\ \Pi R^2 \text{ (kilo Newtons)} = 79.7 \times \Pi \times (6.86)^2 = 1.18 \times 10^4 \text{ kN}$$

At this point we note that since $N_\gamma = 0$, the plastic stress at the edge is simply $\frac{C_1}{\Pi R^2} = 79.7$ kPa (see Equation 2.3.2.2)

b) Calculate ξ_1, P_1 and r_1

Equation 2.3.2.6 gives the total load as: $Q = 2\, C_1\, f_{C_1}\, (\xi_1)$

But total load, $Q = 1.07 \times 10^4$ kN (see beginning of problem)

$\therefore\ 1.07 \times 10^4 \doteq 2.36 \times 10^4\, f_{C_1}\, (\xi_1)$

By making a few trials using Figure 2.3.2.2, ξ_1, which satisfies the above equilibrium condition is = 0.72.

From Equation 2.3.2.5 $P_1 = 2\, C_1 \sqrt{1-\xi_1^2}$

$$= 2 \times 1.18 \times 10^4 \sqrt{1-0.72^2} = 1.64 \times 10^4 \text{ kN}$$

also, $r_1 = 0.72 \times 6.86$ m $= 4.94$ m.

c) Distributions

Elastic $(0 \le \xi \le 0.72)$: $p(r) = \dfrac{P_1}{2\Pi R^2 \sqrt{1-\xi^2}}$

Plastic $(0 \le \xi \le 1.00)$: $p(r) = 79.7$ kPa (constant)

For calculation results see Table 7.1.5.1 and Figure 7.1.2.1.

ξ	Contact Pressure p(r) kPa	
	Method 1	Method 2
0	53.0	55.5
0.22	54.3	56.9
0.44	58.9	61.8
0.54	62.9	65.9
0.64	68.9	72.2
0.68	72.2	75.7
0.72	76.3	79.9
0.78	84.5	79.9

Method	r_1	Author
1.	0.78	Zeevaert (1972)
2	0.72	Derived in this thesis based on Schultze's (1961) hypothesis

TABLE 7.1.5.1 Theoretical Normal Contact Pressure Distribution

d) Check Integration

$$\text{Total load} = \int_{o}^{r_1} \frac{P_1(2\Pi r\ dr)}{2\Pi R^2\sqrt{1-\xi^2}} + \int_{r_1}^{R} 79.7\ (2\Pi r\ dr)$$

Using the result of Equation 2.3.2.3 to integrate the first term, we obtain:

$$\text{Total load} = P_1\ [1 - \sqrt{1-\xi^2}]_o^{4.94} + 79.7\Pi[6.86^2 - 4.94^2]$$

Substituting for known quantities:

Total load = $(0.50 \times 10^4 + 0.57 \times 10^4) = 1.07 \times 10^4$ kN, which is exactly the same as the actual.

7.2 Settlement Estimates from Laboratory Test Results

In Chapters 2 and 3, the theory of immediate (elastic) and consolidation settlements were summarized. In this section these theories are used to calculate both the short and long term settlements. The results of these calculations are discussed in the light of the settlement field measurements. Since the settlement gauges below the raft are installed at r/R = .67, and not at the centre, theoretical calculations were made below this point. Calculations are made for two average pressures only since the objective is to show the application of the theories using laboratory data and not to examine the dependency of these calculations on the pressure intensity. The choice of the average pressures for the settlement studies are discussed under each subsection.

7.2.1 Immediate Settlement from CIU Triaxial Test Data

Calculations are made using the CIU plots in Appendix B for 3 Poisson's ratios and assuming the settlement to be contained within the critical depth, which is 2.5 times the radius of the raft (Section 6.4.3). Secant moduli are evaluated at the actual stress levels, which are estimated using Giroud's (1972) tables. Average net pressures of 55 kPa (1100 spf) and 60.5 kPa (1210 psf) are selected; because the first corresponds to the end of what looks like a true undrained settlement (Figure 6.4.1.2) and the second, which is the maximum net applied pressure, was chosen arbitrarily. Although the secant moduli were evaluated for every sample tested, in the settlement calculations larger spacings using the average modulus within the layers were used. Since the lowest sample tested was from a depth of 1.32 R, the soil below this depth is also assumed to be represented by this sample.

The calculations are presented in Tables 7.2.1.1 to 7.2.1.3 inclusive. Inspite of the care taken in sampling, laboratory testing and also in making the calculations, the estimated quantities are considerably larger than actually measured.

Since one of the major source of errors is the assumption that the soil has an infinite thickness, some means of correcting for a finite depth becomes necessary. In order to do this the estimated depth of 30 m (100 ft), (Chapter 4) was assumed to be reliable. Using this depth, using Figure 3.3.2 and assuming a linear relationship between layer thicknesses and total elastic settlement, the correction factors shown in Table 7.2.1.3 were deduced. These factors show that

Sample No	Depth Below Footing z/R	Average net pressure = 55 kPa $\Delta\sigma_z$ kg/cm^2	ε%	$E(\frac{kg}{cm^2})$	Average net pressure = 60.5 kPa $\Delta\sigma_z$ kg/cm^2	ε%	$E(\frac{kg}{cm^2})$
197-1-3	.15	.40	.55	72.7	.45	.65	69.0
197-1-12	.22	.40	.45	88.9	.44	.55	80.0
197-2-2	.28	.40	.25	160.0	.44	.30	146.6
197-2-11	.35	.39	.20	195.0	.43	.20	215.0
197-3-2	.41	.38	.50	76.0	.41	.51	80.4
197-3-11	.49	.35	.25	140.0	.39	.30	130.0
197-4-2	.55	.35	.15	233.3	.38	.15	253.3
197-4-11	.62	.32	.10	320.0	.36	.10	360.0
197-5-2	.68	.31	.20	155.0	.34	.20	170.0
197-5-11	.75	.29	.20	145.0	.32	.20	160.0
197-6-1	.80	.25	.15	166.7	.27	.15	180.0
197-7-3	1.04	.24	.55	160.0	.27	.15	180.0
197-8-10	1.32	.20	.15	133.3	.22	.15	146.7
	*1.91	.12	.15	80.0	.14	.15	93.3

*Assuming sample 197-8-10 applies for z/R > 1.32

TABLE 7.2.1.1 Secant moduli calculated from "CIU" plots

$$\delta = \frac{(1+\nu)q_a R}{E} \{\overline{M}_z + (1-2\nu)\ \overline{M_z^1}\} = \frac{q_a}{E} f(\beta)$$

R = 686 cm

z/R	$\overline{M}_z$	$\overline{M_z^1}$	Layer	Layer Thickness (cm)	ν = .33		ν = .4		ν = .5	
					$f(\beta)_n$	$f(\beta)_n - f(\beta)_{n-1}$	$f(\beta)_n$	$f(\beta)_n - f(\beta)_{n-1}$	$f(\beta)_n$	$f(\beta)_n - f(\beta)_{n-1}$
0.00	.785	.785			960		905		808	
			1	282		104		97		35
.41	.752	.550			856		828		773	
			2	144		99		94		84
.62	.670	.470			757		734		689	
			3	123		53		49		41
.80	.630	.416			704		685		648	
			4	357		139		131		118
1.32	.515	.307			565		554		530	
			5	405		116		113		105
1.91	.413	.233			449		441		425	
			6	405		77		74		70
2.50	.345	.185			372		367		355	

TABLE 7.2.1.2 Calculation of Settlement Influence Factors at r/R = .67, Method after Giroud (1972).

Layer No.	Thickness cm.	q_a = 55 kPa				q_a = 60.5 kPa			
		E_{ave} kg/cm^2	δ (mm)			E_{ave} kg/cm^2	δ (mm)		
			ν= .33	ν=.4	ν=.5		ν=.33	ν=.4	ν=.5
1	282	80.8	7.20	6.74	2.43	74.5	8.60	8.03	2.90
2	144	130.0	4.19	3.98	3.55	130.5	4.59	4.36	3.89
3	123	192.0	1.52	1.41	1.13	206.0	1.56	1.44	1.21
4	357	197.0	3.88	3.66	3.29	218.0	3.86	3.64	3.28
5	405	135.0	4.73	4.61	4.28	150.0	4.67	4.55	4.12
6	405	135.0	3.14	3.02	2.85	150.0	3.11	2.99	2.83
		Sum =	24.66	23.42	17.53		26.39	25.01	18.23
Corrected for rigid base			20.96	18.50	13.50		22.43	19.80	14.04
		Measured	8.80	8.80	8.80		11.2	11.2	11.2

TABLE 7.2.1.3 Calculated Undrained Settlements

larger stress concentrations are created close to the foundation due to the existence of a rigid base. The distribution of this settlement is discussed in Section 7.2.3.

The following calculation shows how these correction factors were obtained. Referring to Figure 3.3.2, the settlement influence factors for the infinite case (r/H=0) and those for the actual case (r/H=0.23) are:

	Influence Factors		Correction
Poisson's Ratio	r/H= 0	r/H=.23	Factor
0.33	1.36	1.15	0.85
0.4	1.32	1.04	0.79
0.5	1.17	0.90	0.77

Then the required correction factor for a given Poisson's ratio is simply the ratio of the influence factor for the rigid case to that for the infinite one.

When these factors are applied to the calculated values, the settlements improve by as much as 23 percent in the case of ν = 0.5 (Table 7.2.1.3). Even with these corrections, the calculated settlements are still larger than the actual probably due to the low modulii values calculated from the CIU triaxial tests. Since field measurements showed drainage occurred during loading of the silo, the moduli from consolidated drained triaxial (CID) tests might simulate the field condition better than the CIU tests done for the project.

7.2.2 Recompression Settlement from Oedometer Test Results

In Chapter 6, piezometer readings showed that the excess pore water pressure increase due to the maximum applied load was too small for any noticeable amount of consolidation settlement to take place in the future. This is because the stress increases due to the maximum applied pressure are within the recompression range of the ε log P curves (see ε log P curves, Appendix B). Moreover, since this structure is not likely to be subjected to a constant load for any significant length of time, a relatively large additional settlement due to consolidation is not expected. However, since the results of the oedometer tests are available, calculations of consolidation settlements are made below, mainly to show the standard method of calculation and also to study the shape of the settlement distribution curves.

Settlement calculations using Westergaard's and Boussinesq's stress distributions were carried out (see Table 7.2.2.1). Since the log pressures are plotted against strain, the calculation of settlement is simple and can be followed by examining Table 7.2.2.1. Once again the stresses were calculated below $r/R = 0.67$.

Normally, one should make a graphical adjustment on all the consolidation plots to estimate the field strain versus log pressure curve. The purpose of performing such a construction is to correct the test results for possible sample disturbance. One such graphical correction known as Schmertmann's method is well explained in Terzaghi and Peck (1967).

Sample No.	Depth Below Raft (m)	Layer Thick-ness (cm)	P'_o $\frac{kg}{cm^2}$	P_c (Prob.) $\frac{kg}{cm^2}$	Westergaard $\Delta\sigma_z$ kg/cm^2	Westergaard $\Delta\varepsilon$	Westergaard ε layer	Westergaard S_{oed} (mm)	Boussinesq $\Delta\sigma_z$ kg/cm^2	Boussinesq $\Delta\varepsilon$	Boussinesq ε layer	Boussinesq S_{oed} (mm)
					Maximum net applied pressure = 60.5 kPa = 0.62 kg/cm^2							
	0.00		0.00		0.620	0.000			0.386	0.000		
		97					0.005	4.9			0.004	3.9
197-1-1	0.97		0.18	1.75	0.515	0.010			0.401	0.008		
		74					0.008	5.9			0.007	5.2
197-1-13	1.71		0.31	1.87	0.483	0.006			0.414	0.005		
		68					0.006	4.1			0.005	3.4
197-2-9	2.39		0.38	1.10	0.451	0.006			0.418	0.006		
		152					0.005	7.6			0.005	7.6
197-4-3	3.91		0.51	0.84	0.393	0.003			0.383	0.003		
		143					0.003	4.3			0.003	4.3
197-5-12	5.34		0.62	0.95	0.334	0.003			0.337	0.003		
		172					0.003	5.2			0.003	5.2
197-7-2	7.06		0.74	0.95	0.243	0.002			0.284	0.002		
		71					0.002	1.4			0.002	1.4
197-7-12	7.77		0.80	1.11	0.211	0.002			0.261	0.002		
		87					0.002	1.7			0.002	1.7
197-8-2	8.64		0.87	1.05	0.182	0.002			0.233	0.002		
		320					0.002	6.4			0.002	6.4
197-9-3	11.84		1.11	1.58	0.139	0.002			0.177	0.002		
		306					0.002	6.1			0.002	6.1
197-10-3	14.90		1.34	1.69	0.121	0.001			0.131	0.001		
		230					0.001	2.3			0.001	2.3
197-11-11*	17.20		1.50	2.67	0.080	0.000			0.097	0.000		
							Total	49.9			Total	47.5
							Corrected for 3-D	44.9				42.8

*Critical depth

TABLE 7.2.2.1 Consolidation Settlements from Oedometer Tests

Based on the above principle a simple correction to account for sample disturbance was carried out by taking the slope of the unloading curve between P'_o and $P'_o + \Delta\sigma_z$, for the settlement calculation. It is seen from Table 7.2.2.1 that the total settlements of over 40 mm are very large, especially when this is added to the elastic settlement previously calculated as suggested by Skempton (1954). A multiplying correction factor of 0.90 for 3-dimensional effect obtained from Figure 3.6.1 reduces the estimated settlements by 10 percent. But in spite of this correction the values are still far too high. The correction is obtained by entering Figure 3.6.1 with an average OCR = 2.5.

The settlement estimate based on Boussinesq's stress distribution theory gives a better value when both theories incorporate the critical depth. This is because in the shallower layer close to the footing, Westergaard's method gives a much higher stress concentration than that of Boussinesq. Moreover, it should be borne in mind that Westergaard's method assumes a flexible footing. Comments on the distribution of these calculated settlements are made below.

7.2.3 Distribution of Settlement from CIU and Oedometer Test Results

For the purpose of comparison, the calculations given in Tables 7.2.1.3 and 7.2.2.1 are plotted in Figure 7.2.3.1 together with the actual distribution, all at the maximum net applied pressure. In the case of the oedometer test results to a depth of z/D = 0.75 Westergaard's theory indicates larger compression in this layer than that given by Boussinesq. The reason for this has already been

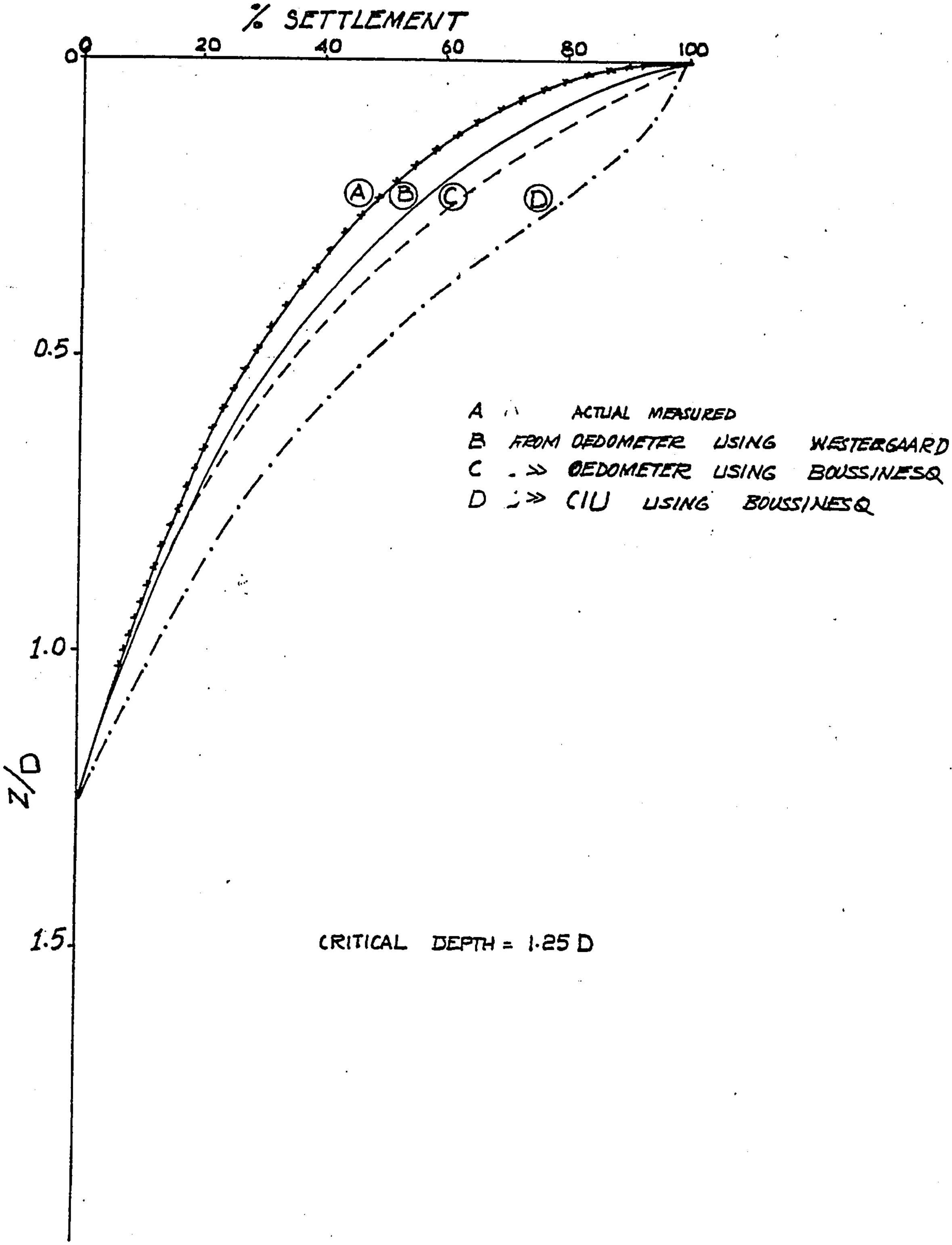

FIGURE 7.2.3.1 SETTLEMENT DISTRIBUTIONS FOR SILO RAFT AT MAXIMUM NET APPLIED PRESSURE. (MEASURED AND CALCULATED)

explained in the previous section. However, all the three curves based on calculations, overestimate the contribution of the lower layer to the total settlement than is the case. One can safely conclude that none of the elastic theories should be expected to give the same distribution as the actual even though in this case the oedometer results appear to approximate the actual distribution better. However, this could just be a coincidence since there is always some subjective judgement involved in correcting the ε log P curves for sample disturbance. The distribution obtained from the CIU test results has very little similarity with the actual case. As pointed out in Section 7.2.1, CID triaxial tests might have been more appropriate.

7.3 Distribution of Settlement with Depth

In this section the distribution of percent settlement with depth is calculated for various applied pressures and the result compared to similar calculations done for the plate and square footing settlement data from another site introduced in Section 3.8. By percent settlement it is meant that the compression of the soil below each deep settlement gauge is expressed as a fraction of the total settlement measured.

To eliminate the dimensional variable, R the percent settlements are plotted against z/R. Further, since the distribution will be plotted for various applied average pressures, to make the comparison easier, the pressures are expressed as multiples of the weighted average vane shear strength, S_w below each footing or plate; thus making all the parameters independent of R and S_w. The calculation of the weighted shear strength values, S_w, for the square footings, the test plates and for the large circular raft are given in Tables 7.3.1(a) to 7.3.1(d) inclusive. For the circular raft and the square footings the shear strength from the foundation to bedrock is considered since this depth is always less than 6R; however, for the small test plates the calculation is done for a layer of only about 6 times the radius of the plates since their influence is limited to this depth. However, in all cases when a reference is made to q/S_w ratios, it should be noted that the pressure q refers to the net applied pressure.

The weighted vane shear strength decreases as the elevation of a footing or a plate decreases. This is due to the influence of the higher shear strength in the upper layers. The S_w for the silo raft is the lowest, since the layer is much thicker and therefore the influence of the desiccated crust is small.

7.3.1 Percent Settlement with Depth for Circular Raft

To avoid any influence due to creep with time, calculations are done for pressure intensities below 55 kPa (1100 psf). At this pressure there was only a small creep or consolidation settlement as shown in Figure 6.4.1.2.

The curves given in Figure 7.3.1.1 for the four pressure intensities considered have similar shapes under all q/S_w ratios. As mentioned in Section 6.4.3 gauge number 3 located at z/D = .64 had

Footing or Plate	Size m	Size ft	Elev m	Elev ft	Depth, Z Below Footing (m)	S_u (kg/cm^2) at z	Change in Depth Δz (m)	$\bar{S}_u$ For Δz	$\Delta z \bar{S}_u$	Weighted Average for Layer $S_w = \frac{\Delta z \bar{S}_u}{\Sigma \Delta z}$
Test Footing	3.1	10	85.7	281.0	0.0	2.70				
					.5	2.10	.5	2.60	1.30	
					1.0	1.60	.5	1.90	.95	
					1.5	1.20	.5	1.40	.70	
					2.0	.90	.5	1.05	.52	
					2.5	.70	.5	.85	.43	
					3.0	.55	.5	.63	.32	
					4.0	.42	1.0	.49	.49	
					5.0	.35	1.0	.39	.39	
					6.0	.35	1.0	.35	.35	
					7.0	.40	1.0	.38	.38	
					8.0	.45	1.0	.43	.43	= 0.78 (kg/cm^2) = 76.4 kPa
M-17	2.9	9.5	85.4	280	0	2.10	.5	1.90	.95	
0-19	3.5	11.5	»	»	.5	1.60	.5	1.40	.70	
					1.0	1.20	.5	1.05	.52	
					1.5	.90	.5	.85	.43	
					2.0	.70	.5	.63	.32	
					3.0	.42	.5	.49	.49	
					4.0	.35	1.0	.39	.39	

TABLE 7.3.1(a) Calculation of Weighted Average Shear Strength

Footing or Plate	Size m	Size ft	Elev m	Elev ft	Depth, Z Below Footing (m)	S_u (kg/cm^2) at z	Change in Depth Δz m	$\bar{S}_u$ For Δz	$\Delta z \bar{S}_u$	Weighted Average for Layer $S_w = \frac{\Delta z \bar{S}_u}{\Sigma \Delta z}$
M-17	2.9	9.5	85.4	280						
O-19	3.5	11.5	»	»	5.0	.35	1.0	.35	.35	
					6.0	.40	1.0	.38	.38	
					7.0	.45	1.0	.43	.43	= 0.71 kg/cm^2
										= 69.6 kPa
CC-12	4.1	13.5	84.2	276	0	1.20	.5	1.05	.53	
					.5	.90	.5	.80	.40	
					1.0	.70	.5	.63	.31	
					1.5	.55	.5	.49	.25	
					2.5	.42	1.0	.39	.39	
					3.5	.35	1.0	.35	.35	
					4.5	.35	1.0	.38	.38	
					6.5	.45	1.0	.43	.43	= 0.47 kg/cm^2
										= 46.1 kPa
EE-7	3.7	12.3	83.2	273	0	.70	.5			
GG-8	4.0	13.0	»	»	.5	.55	1.0			
					1.5	.42	1.0			
					2.5	.35	1.0			
					3.5	.35	1.0			

TABLE 7.3.1(b) Calculation of Weighted Average Shear Strength

Footing or Plate	Size m	Size ft	Elev m	Elev ft	Depth, z Below Footing m	S_u (kg/cm^2) at z	Change in Depth Δz m	$\overline{S}_u$ For Δz	$\Delta z \overline{S}_u$	Weighted Average for Layer $S_w = \frac{\Delta z \overline{S}_u}{\Sigma \Delta t}$
EE-7	3.7	12.3	83.2	273						
GG-8	4.0	13.0	>>	>>	4.5	.40	1.0	.38	.38	
					5.5	.45	1.0	.43	.43	= 0.43 kg/cm^2
										= 42 kPa
Plates										
V2/1	.46	1.51	83.8	274.9	0	1.0				
V2/2			83.9	275.1	.25	.90	.25	.95	.24	
					.50	.80	.25	.85	.21	
					.75	.55	.25	.68	.17	
					1.00	.45	.25	.50	.13	
					1.50	.35	.25	.40	.20	= 0.63 kg/cm^2
										= 61.7 kPa
Plates										
V3/1	.46	1.51	82.6	270.9	0	.50				
V3/2			82.5	270.8	.25	.40	.25	.45	.49	
					.50	.38	.25	.39	.10	
					.75	.38	.25	.38	.10	
					1.00	.40	.25	.39	.10	
					1.50	.35	.50	.38	.10	= 0.59 kg/cm^2
										= 57.8 kPa

TABLE 7.3.1(c) Calculation of Weighted Average Shear Strength

Footing or Plate	Size m	Size ft	Elev m	Elev ft	Depth, z Below Footing m	S_u (kg/cm^2) at z	Change in Depth Δz m	$\bar{S}_u$ For Δz	$\Delta z \bar{S}_u$	Weighted Average for Layer $S_w = \frac{\Delta z \bar{S}_u}{\Sigma \Delta z}$
Silo	13.7	45	107	325						
Raft					1.5	.55	1.50	.55	.83	
					4.3	.42	2.87	.44	1.26	
					8.8	.32	4.50	.33	1.49	
					13.3	.38	4.50	.38	1.71	
					17.1	.49	3.80	.49	1.86	= 0.42 kg/cm^2 = 41 kPa

TABLE 7.3.1(d) Calculation of Weighted Average Shear Strength

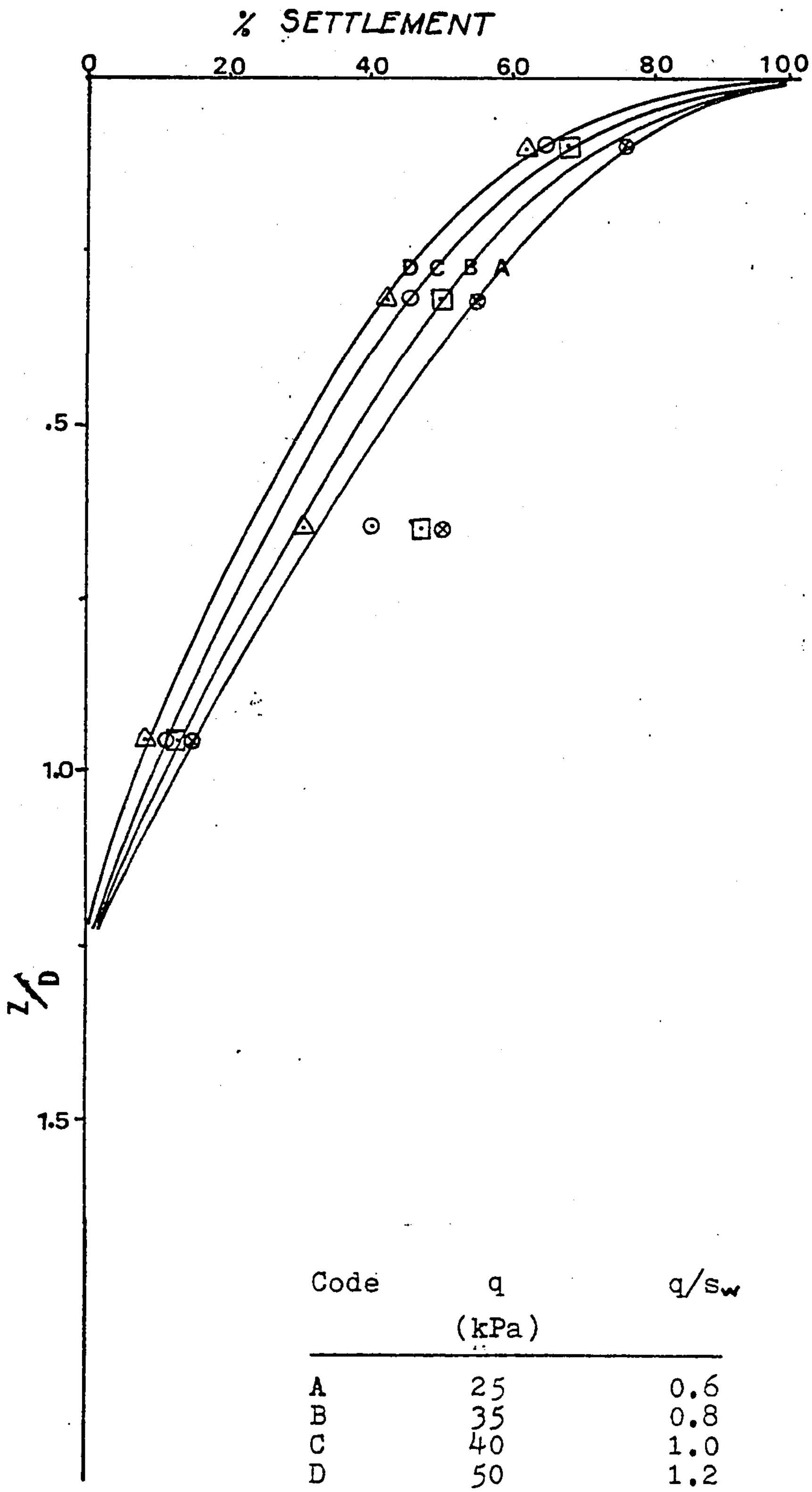

Code	q (kPa)	q/s_w
A	25	0.6
B	35	0.8
C	40	1.0
D	50	1.2

$s_w = 41$ kPa

FIGURE 7.3.1.1 SETTLEMENT DISTRIBUTIONS FOR SILO RAFT (MEASURED) to be corrected or neglected since it gives larger settlements than indicated by the gauge located at z/D = .32, which is not possible. In this case since there were enough other points it was easier to neglect these points while drawing the curves. The plots show that as q/S_w increases the individual curves shift to the left indicating a decrease in the settlement contribution by the lower layers. In other words as q/S_w increases the shallow layer close to the raft contributes proportionately more to the total settlement. Once again the critical depth which corresponds to zero percent settlement is seen to be around 1.25 D. To facilitate comparison with other similar data and because the curves for all prssure intensities are fairly close together, the average curve for all q/S_w values is plotted in Figure 7.3.1.2.

7.3.2 Percent Settlement with Depth for Test Plates and Square Footings

The original load settlement data for four test plates, a square test footing and five building footings all in Leda Clay were introduced in Section 3.8. In this section the percent settlement with depth for these foundations is presented.

7.3.2.1 Percent Settlement with Depth for Test Plates

Here only settlements which are thought to be elastic are considered. For all the four plates an attempt was made to obtain curves for at least four pressure intensities, but in some cases the settlements at low pressure levels were found to be very small and

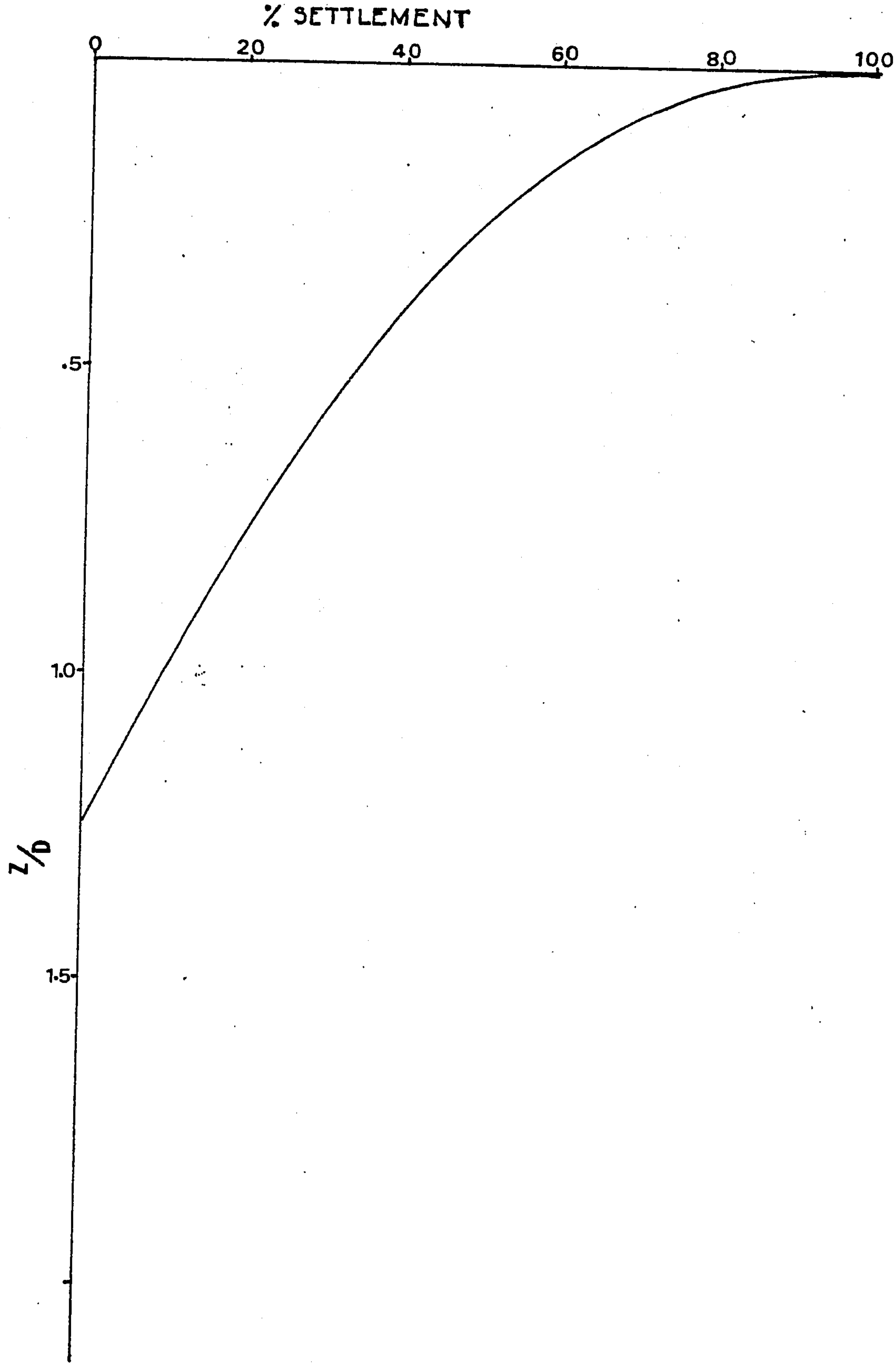

FIGURE 7.3.1.2 AVERAGE SETTLEMENT DISTRIBUTION FOR SILO RAFT

erratic. Therefore, as shown in Figures A6 to A9, except for plate V3/2 all the plots have curves for only three pressures. A quick examination of the distributions would indicate that the curves do not fall in a similar pattern as the silo raft curves as q/S_W varies. However, the settlement distributions for the different pressure intensities all lie fairly close together. Therefore, to simplify comparison the average curve for each plate test is plotted in Figure 7.3.2.1.1.

The settlement distribution for all the plates are very similar, although the curve for V3/2 is slightly different. The critical depth corresponding to zero percent settlement is seen to vary within a narrow margin of 1.7D to 2.2D with an average of about 2D. As mentioned in Section 3.8, the settlement gagues were not below the centre of the plates but at a distance of $r/R = 0.5$ from the centre.

7.3.2.2 Percent Settlement with Depth for Square Footings

For all footings, settlements were measured near the centre and at the very edge of the footing. Initial calculations showed that the settlement data for the test footing at the edge were somewhat erratic and hence for this footing only the settlements beneath the centre were considered. However, for the actual building footings, since the two sets of settlement data for each footing are similar, the average of these are considered. The location of the settlement gauges as well as the load settlement curves are given in Section 3.8.

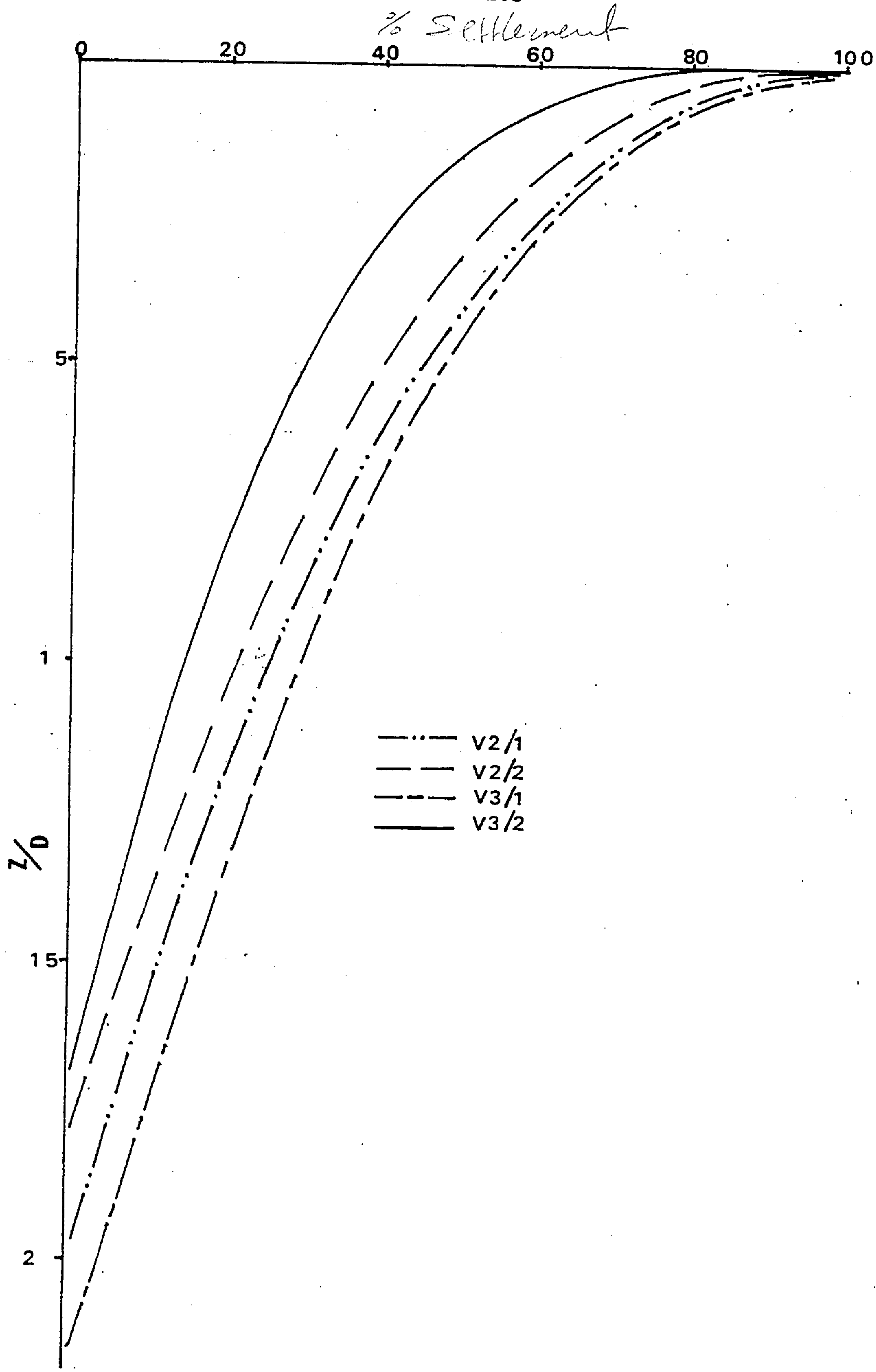

FIGURE 7.3.2.1.1 AVERAGE SETTLEMENT DISTRIBUTIONS FOR FLATES.

For the test footing the linear portion of the settlement data up to a pressure level of 250 kPa (5000 psf) is used. Similarly, for the interior footings, only the load settlement curves to the end of construction (prior to the occupation of the building) are considered. The effects of consolidation or creep with time are therefore not included in the analysis.

The percent settlement distribution curves for all the above mentioned footings are presented in Figures A10 to A15. Again, since all of the six footings showed little difference in settlement distribution as q/S_w varied, it was thought preferable to plot the average distribution curve for each footing for comparison. Such calculations were carried out and the results are found plotted in Figure 7.3.2.2.1. It can be seen that the distributions follow a very similar pattern except for footing EE-7 which is at the same elevation as GG8. This behaviour in EE-7 can only be attributed to error in the settlement gauge reading at a depth equal to $z/B = 1.14$. Neglecting EE-7 the critical depth for all the square footings appears to lie between 1.75 B to 2.20 B giving an average value of about 2B. This is in agreement with the range of critical depth for most soils reported by Shvets and Kulchitski (1970), which varies from 1.5 to 2.0 D.

7.3.3 Comparison of Settlement Distribution of Different Sized Foundations

The comparison to be made is between the average distributions for the large circular raft, the square footings and the test plates. Further, these actual measured distributions are compared to theoretical

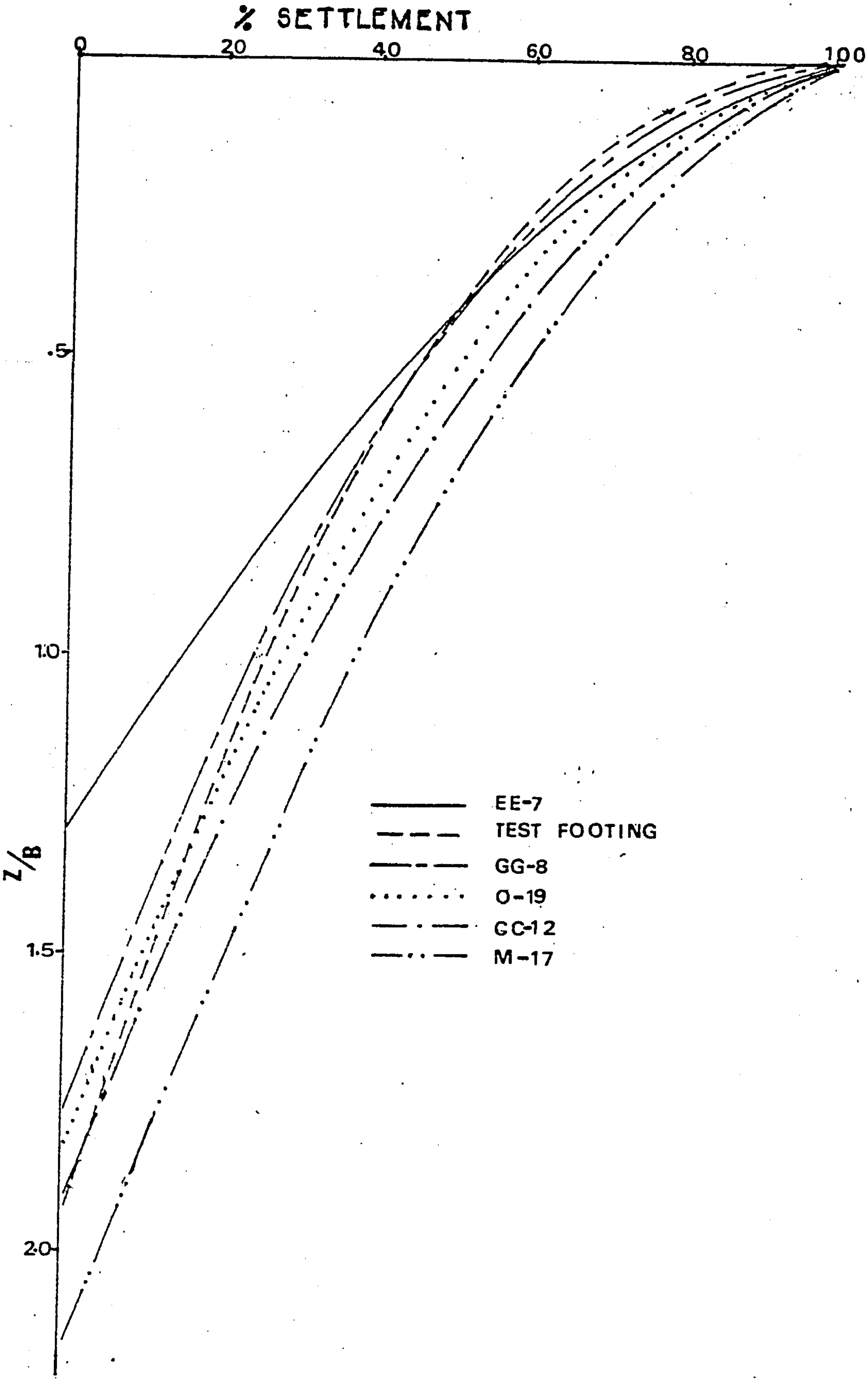

FIGURE 7.3.2.2.1 AVERAGE DISTRIBUTIONS OF SETTLEMENT FOR ALL SQUARE FOOTINGS.

curves. The main purpose for the comparison is to examine if the size of footing has a significant effect on the behaviour of the soil. Previously it was found out that the magnitude of q/S_w does not have a very noticeable effect on the shape of the percent settlement with depth distributions for all the foundation sizes.

In order to do this analysis a further averaging of the curves for all the plates and another for all the square footings was made. Figure 7.3.3.1 compares the settlement distribution of all the foundations. The curves for the square footings and the plates are very identical and intercept the ordinate at the same critical depth. The circular raft, however, starts out following a similar pattern as the other two to a depth of about 0.4 D, after which it follows a different slope until it cuts the ordinate at a shallow depth of 1.25 D. The shape of the distributions are, however, similar. One apparent reason for the slight difference is the relatively low q/S_w value the silo raft is subjected to, which is in the order of only 1.2 as compared to 3 to 5.1 for the plates and the footings. The argument is, that the higher the q/S_w, the higher the applied pressure and therefore the deeper the pressure bulb penetrates into the soil, giving rise to a deeper critical depth. Another possible reason for the shallow critical depth shown by the silo raft could be due to the existence of a hard clay layer immediately below depth 1.25 D. The preconsolidation stress for the oedometer sample obtained at a depth of 19.05 m from the original ground or (at 1.38 D below the bottom of the raft) is 2.67 kg/cm^2. This value which is even higher than the

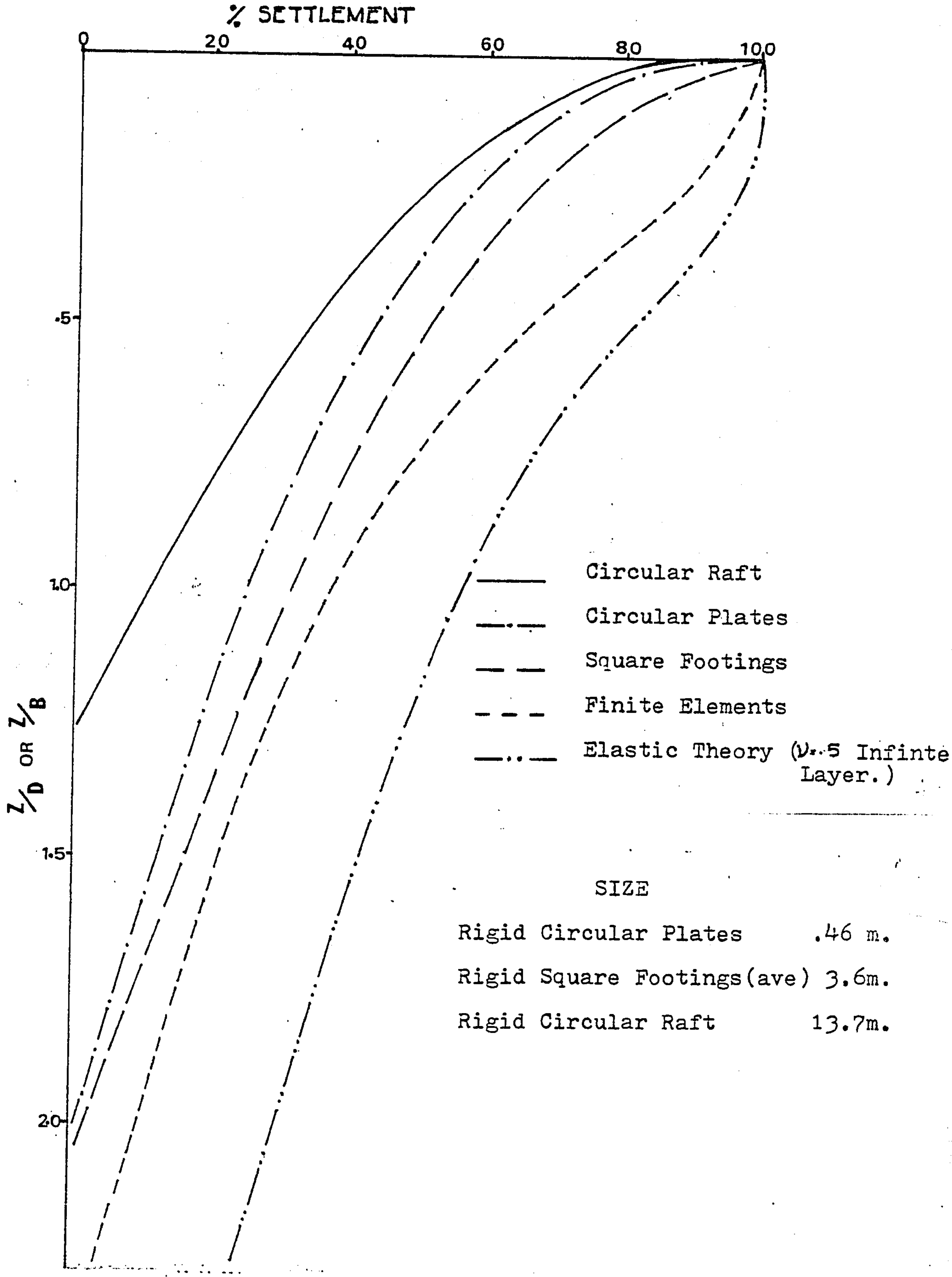

FIGURE 7.3.3.1 AVERAGE DISTRIBUTIONS OF SETTLEMENT FOR ALL FOUNDATION ELEMENTS (Plates, Footings & Raft.)

maximum P_c in the crust, (1.87 kg/cm^2) led the writer to believe that the soil below this depth is relatively incompressible, giving rise to a shallower critical depth.

The fact that most of the settlement is confined to a shallower layer could not be due to closing of fissures as concluded by Bauer et al (1973) since some of the foundations are below the fissured crust and yet show the same distribution. It cannot be due to crustal anisotropy either since laboratory vane tests (see Section 6.8) show the soil to be fairly isotropic. Hence, it can be concluded that the observed behaviour is a characteristic of the soil and does not depend on the size of the footing.

As shown in Figure 7.3.1.1, elastic theory based on the assumption of an infinite layer overestimates the contribution to the total settlement by the lower layers.

On the other hand the finite element model reported by Wroth (1977) appears to be somewhat more realistic than the simple elastic theory. The finite element analysis was done to simulate a circular raft having a thickness of 0.91 m (3 ft) and a diameter of 21 m (69 ft) resting on London clay. The concrete was assigned the properties E = 25 Mpa, ν = 0.15 and the soil E = 27 Mpa and ν = .49. All these values except for the diameter of the footing are similar to the raft on Leda Clay considered in this thesis. Hence, a computer model employing the finite element analysis seems more reliable than simple elastic theory although it too overestimates the settlement at depth.

In this section it was learned that:

- the shapes of the settlement distribution curves are independent of q/S_w.
- Size of foundation has very little effect on the distribution of settlement.
- q/S_w level may slightly affect the critical depth; the larger the q/S_w the larger this depth.
- Settlement distributions are different than predicted by elastic theory because of the non-linear behaviour of the soil.
- The similarity in the settlement distributions shown by the three different foundation elements appears to be a characteristic of the soil.
- Figure 7.3.3.1 indicates that for most designs a critical depth of 2 D would give satisfactory estimates of settlement. This agrees with the findings of Shvets et al (1970), who considered a wide range of variable soil types; they found this depth to vary between 1.5 to 2 D (see Section 3.7).

7.4 Undrained Modulus from Settlement Data

For the purpose of this discussion, the undrained modulus is defined as the deformation modulus of the soil when the major part of settlement is due to undrained shear deformation only. This definition does not rule out the possibility of some consolidation settlement occurring even during the construction and initial loading of the structure, which was observed in this project. Knowledge of the field undrained modulus is very useful since it is more reliable than laboratory results; assuming that the settlement measurements and the calculations to obtain these values have been properly made.

For most foundations founded on clay deposits, the working pressures are kept well below the preconsolidation pressure of the clay and undrained shear deformation combined with a small amount of recompression is responsible for all or a major part of the settlement of the foundations. The importance to the practicing engineer of having field measurements of this parameter cannot therefore be over emphasized.

In the following paragraphs, the results of calculations of the undrained modulus for various pressure levels and also at different depths below the foundation are introduced. The field moduli are presented as multiples of the average shear vane strength, S_u for the particular sub-layer. Moreover, to eliminate the variables q and S_w (which is the weighted average shear strength with z/R = 6 below the foundation), q is expressed in terms of S_w.

Such a plot for 6 layers is given in Figure 7.4.1 for the silo raft. The moduli at various pressure levels are calculated using Equation 3.5.1 and these values are divided by the corresponding average vane shear strength value for the layer. The result is separate variations of E_u/S_u curves for each layer defined by the location of the settlement gauges. It should be noted that S_u is the average shear strength for the layer whereas S_w is the weighted shear strength for the whole layer. For sample calculation see Section 7.5.3.

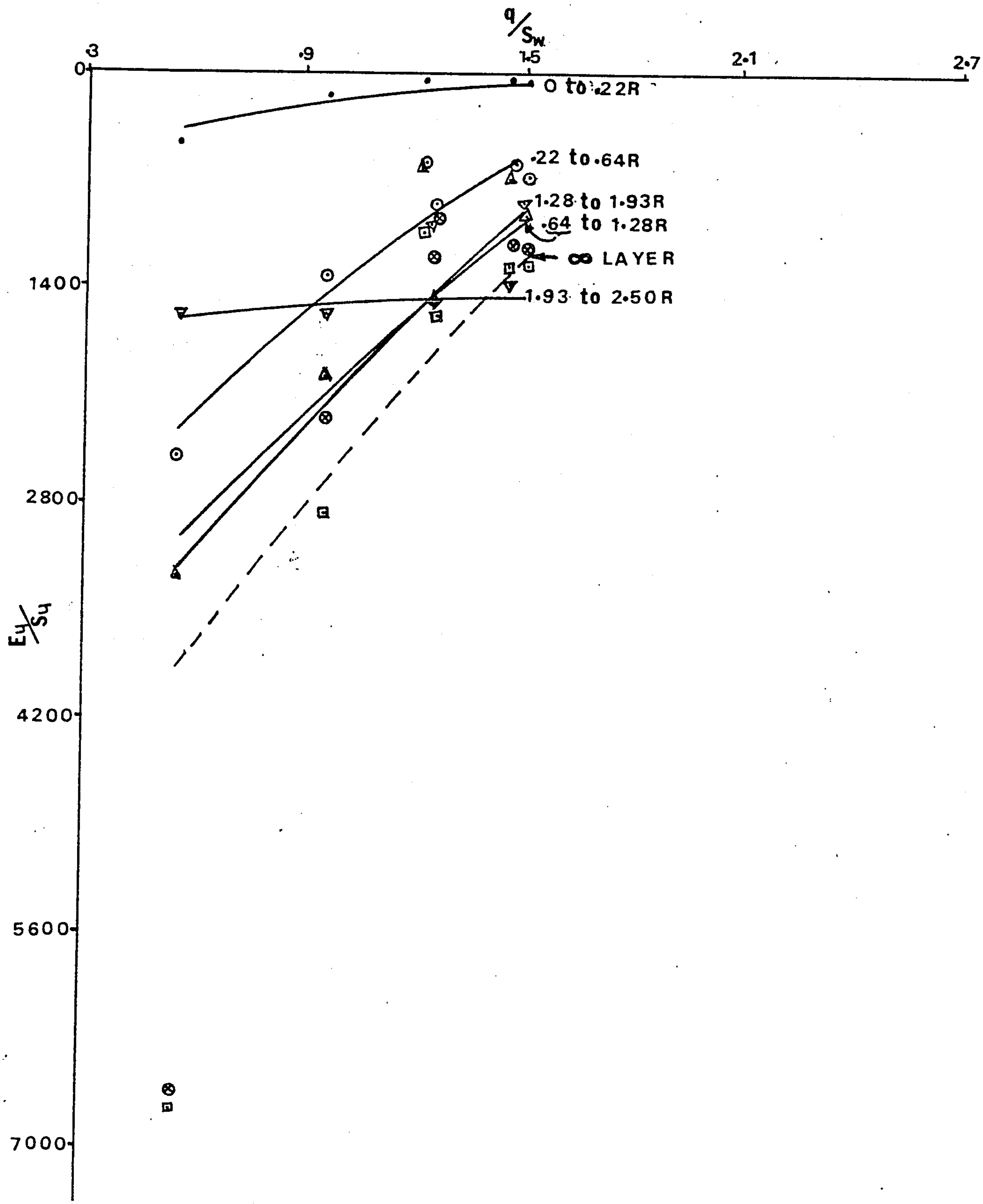

FIGURE 7.4.1 DISTRIBUTION OF E_u/S_u WITH q/S_w WITHIN SOIL LAYERS BELOW RAFT. (tower silo)

The figure reveals that there is some overlapping between some of the curves in the lower layers. It is easily seen that the points at low values of q/S_w are very scattered, except for the first layer close to the footing. On the other hand, all the points above q/S_w larger than 1.36 are crowded together, this indicates that if there were more points between $q/S_w = 1.36$ and 1.51, the curves would probably be more horizontal as in the upper layer. The high and erratic E_u/S_u values indicated by the lower gauges for the lower layers can be attributed to the very small settlements recorded in these layers. Since the settlements are small, they tend to be affected by instrument and reading errors. Since the assumption of an infinite depth is often used for settlement calculations, a plot of E_u/S_u based on this assumption is also included. It should be noted that since the maximum q/S_w value is only 1.51, the silo is not loaded even to its allowable bearing pressure which should correspond to $q/S_w = 2$.

7.4.1 Variation of E_u/S_u with Load

Examination of Figure 7.4.1 shows that for all layers, the E_u/S_u value decreases as q/S_w increases. Theoretically, if a material is perfectly elastic, the elastic modulus should be a constant regardless of the magnitude of the applied stress, provided that the applied stress is kept below that which would cause plastic deformation. The stress dependency of the undrained modulus indicates that the soil possesses a non-linear load settlement behaviour as is the case with most soils.

7.4.2 Variation of E_u/S_u with Depth

Examination of the curves in Figure 7.4.1 indicates that with the exception of the layer between 1.28R and 2.5R, the E_u/S_u value increases with depth at all q/S_w levels. Below $q/S_w = 1.36$, the points are very erratic due to the small settlements. However, for most designs, engineers are interested in the range of $q/S_w = 2$, which corresponds to an allowable bearing capacity with a factor of safety of 3.

The layer between 1.28 R and 2.5 R appears to be more compressible than the layer above it, even though the vane shear strength values do not vary. This sudden drop in the modulus for this particular layer is also indicated by the secant moduli calculated at 33 and 50 percent of the maximum deviatoric stresses (sample 197-8-10, Appendix B). This probably indicates the existence of a thin soft sub-layer within this layer, not detected by the field vane shear results.

The increase in the E_u/S_u values with depth shown by the other layers does not necessarily imply that the lower layer has a greater stiffness than the one above it, since all layers are not subjected to similar stress levels. In fact, it is possible that the layer close to the foundation could be stressed beyond its elastic limit, thus indicating a smaller E_u/S_u value than actual.

The analysis in this section has shown that:

a) the ratio E_u/S_u appears to decrease with increase in q/S_w and also with depth. However, at low q/S_w levels the results are erratic and therefore cannot be relied upon.

b) the increase in E_u/S_u with depth does not imply a stiffer soil below. This resulted because at lower levels elastic theory appears to overestimate the stress increases.

7.5 Comparison of E_u/S_u Ratios with Other Values for a Similar Clay

In Chapter 3, the results of D'Appolonia's (1971) analysis and also the detailed load settlement data at Algonquin College carried out by the Geotechnical Group of the University of Ottawa were introduced. In the sub-sections to follow, the results presented in Section 7.5 will be compared with the above data and some conclusions reached.

7.5.1 Comparison with Information Derived from Test Plates and Square Footings at the Algonquin College Site

Calculations of E_u/S_u values were carried out for two plate tests, the test footing and 3 building footings. The analysis for the other two plates and two building footings are not included since they have very similar load settlement data to the ones chosen for the analysis. The two plate tests analyzed are V2/1 and V3/1 and the building footings include M-17, CC-12 and G-8, all at different elevations. The distribution of E_u/S_u for each plate and footing plotted against q/S_w is found in Figures A-16 to A-21. Because of the relatively high q/S_w values compared to that for the circular raft the q/S_w scale is doubled; but the ordinate remains unchanged.

Examination of these plots show that, they are not all similar. However, they have a number of common features which are:

a) in all cases E_u/S_u increases with depth under a given q/S_w ratio except for plate V3/1 where there is some overlapping; b) they all show a decrease in E_u/S_u as the pressure level increases with the exception of footing CC-12. Since soil is not a perfectly uniform material, some variation is to be expected even if the footings were founded at the same site. This makes a detailed comparison with the results for the circular raft difficult. Hence, to simplify the analysis, it was decided to examine two additional plots: one for comparing the E_u/S_u distributions when the layer is assumed to be infinite and a second plot considering the layer extending to a depth 2R. The reason for selecting a depth of 2R is because in all cases; circular raft, square footings and the plates, 70 to 90 percent of the settlement is confined within this layer, see Figure 7.3.3.1. In the case of the square footings, the equivalent radius, R_e is calculated using the equation: (Bauer et al, 1973)

$$R_e = 2\sqrt{\frac{A}{\Pi}} \qquad 7.5.1.1$$

where A = area of the square footing.

In the discussion to follow, R will be used for all footings, raft and plates.

7.5.1.1 Comparison of E_u/S_u Values when the Assumption of an Infinite Layer is Made

As mentioned earlier, the assumption of an infinite layer is often made during settlement calculations. Hence, even if the theory is not always valid, it can still be used to estimate settlements reliably provided that the modulus to be used is calculated from accurate field measurements. Figure 7.5.1.1.1 shows, the distribution of E_u/S_u for the raft, the four square footings and the test plates. Because the E_u/S_u values for the raft at low pressure levels were very erratic, they were not included in the plot. In order to accommodate all of the cases, the horizontal scale had to be double that for the raft in Figure 7.4.1, this is why in Figure 7.5.1.1, the curve for the raft is rather short.

Even though the curves have different shapes it is seen that the effect of q/S_w or the stress level in the infinite case is not significant. As mentioned previously, most foundations are designed for q/S_w of about 2 or less. For this pressure level, E_u/S_u is found to vary between 500 and 1500 with an average value of 1000. However, when all the stress levels are considered, the range of E_u/S_u is seen to be between 350 and 1550 with an average of 950. Hence, for most elastic settlement calculation in Leda Clay a value of $E_u/S_u = 1000$ appears to be reasonable regardless of the size of the foundation. For the silo raft, this will give $E_u = 411$ kg/cm^2 (5800 psi) compared to the values from the CIU test data, which range between 167 to 199 kg/cm^2 (2360-2810 psi) (see summary of CIU tests, Appendix B). It should be borne in mind that the above conclusion holds true only for stress levels less than the preconsolidation pressure.

7.5.1.2 Comparison of E_u/S_u values when the Soil to a Depth of 2R is Considered

As outlined earlier, it is within the depth 2R below the foundation that most of the compression in Leda Clay appears to be

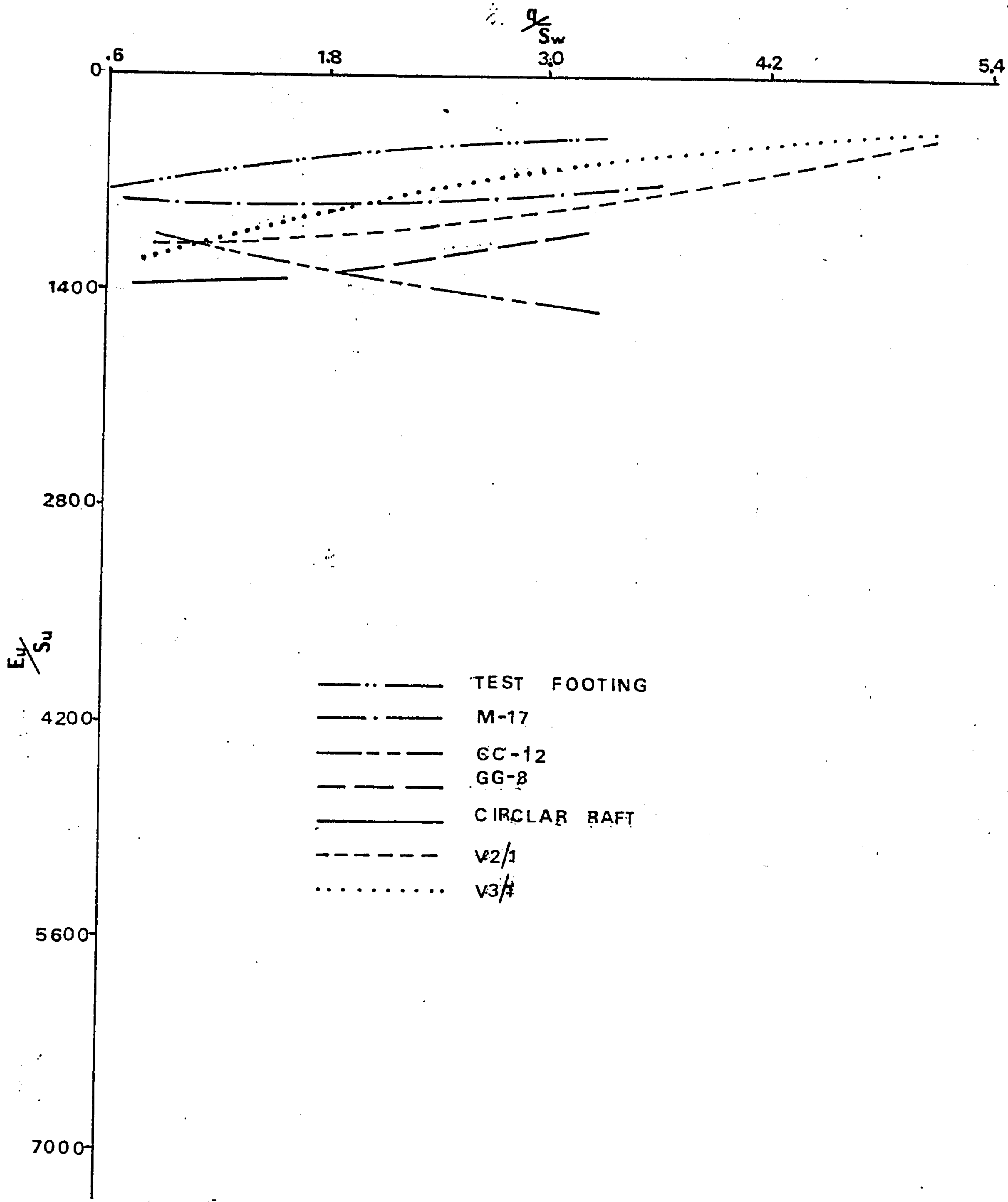

FIGURE 7.5.1.1.1 DISTRIBUTION OF E_u/S_u WITH q/S_w WHEN THE SUBSOIL IS ASSUMED TO HAVE INFINTIE THICKNESS. (Circular raft, Square footings, & Test plates.)

taking place. The distribution of E_u/S_u within a depth 2R below the raft, the footings and plates are presented in Figure 7.5.1.2.1. Once again for pressure levels less than the preconsolidation pressure, the distribution of E_u/S_u are more or less horizontal, hence do not indicate a big dependency on the q/S_w ratio. However, in this case both the upper and lower bounds of the E_u/S_u envelope are very much smaller than for the infinite case. The range of E_u/S_u for q/S_w less than or equal to 2 is between about 200 and 1050, giving an average of about 630. A simple explanation for the difference between the above average E_u/S_u and that for the infinite layer case follows.

Examination of Equation 3.2.2 shows that, elastic settlement is directly proportional to the thickness of the soil considered and is inversely proportional to the modulus. Then, it is obvious that back calculation of E_u from settlement data should yield a higher value when an infinite layer depth is considered.

7.5.2 Comparison of E_u/S_u with Results in the Literature

Perhaps the most detailed work on the correlation of the undrained modulus to the shear strength is that presented in a paper by D'Appolonia et al (1971). After examining a number of case records the authors have found that E_u/S_u decreases with an increase in the OCR, the plasticity index and the applied stress ratio (Figure 3.8.3.1). Because of this dependency on a number of variables, it is difficult to assign a single value for all clay deposits. However the authors give a safe range of values for design applications. For example, in the

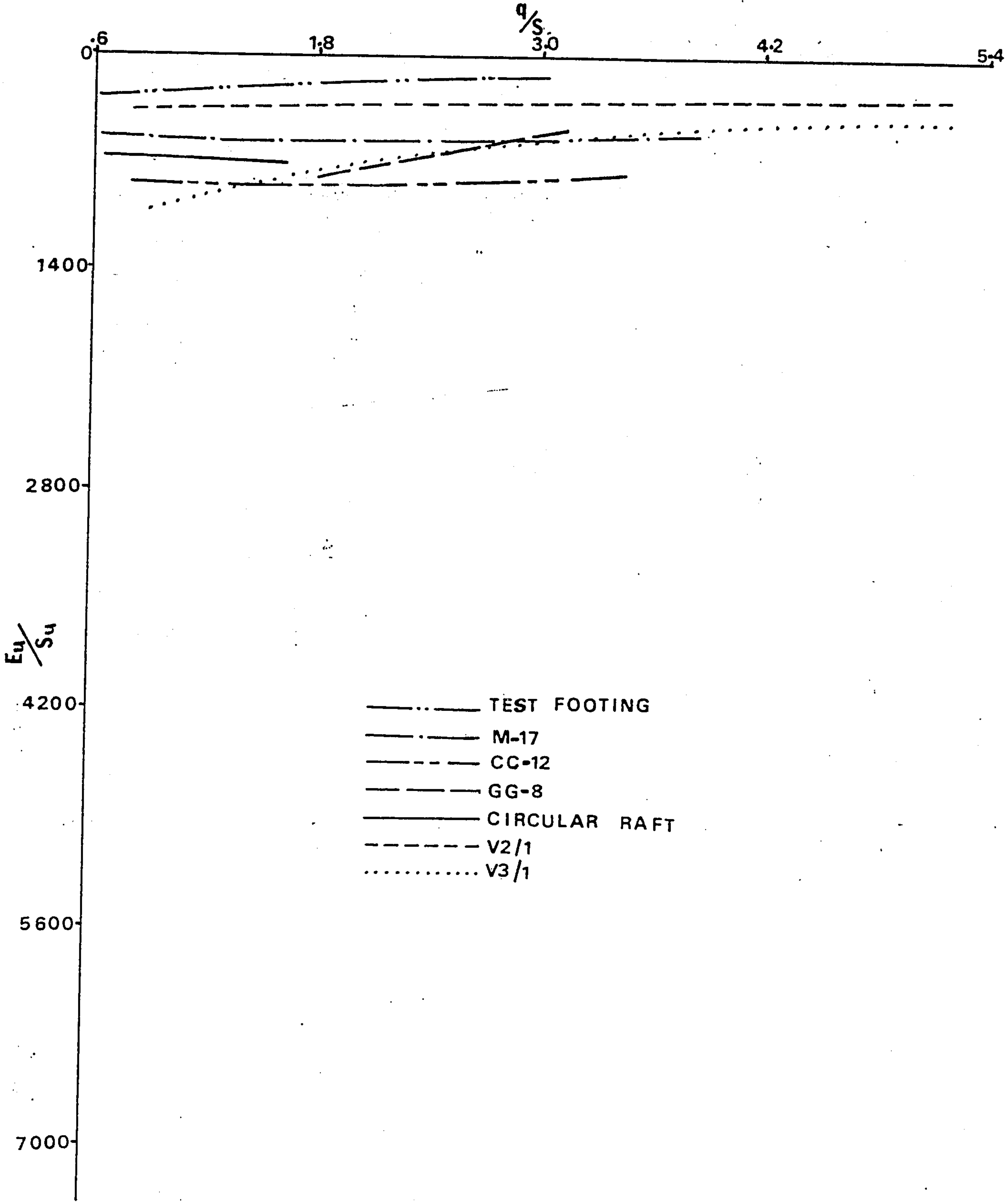

FIGURE 7.5.1.2.1 DISTRIBUTION OF E_u/S_u WITH q/S_u WITHIN THE DEPTH 2R BELOW THE BOTTOM OF RAFT, FOOTINGS & PLATES. (For square footings R is the equivalent radius)

case of inorganic clay of moderate to high sensitivity and with PI of less than 30 percent, the recommended range is 1000 to 1200. This description approximately fits the soil at hand. D'Appolonia et al's (1971) calculations are based on average shear strength values within a depth equal to the diameter or the width of the footing and also on the assumption that elastic solutions for the semi-infinite layer are applicable. The above range with an average of 1100 is in close agreement with an average of 1000 found for the infinite layer case (Section 7.5.1.1). Hence, as mentioned in the previous section, an average value of 1000 for the Leda Clay seems very reasonable, when the assumption of infinite layer is made.

7.5.3 Calculation of E_u/S_u

In this section a sample calculation is presented to show how a typical distribution of E_u/S_u for a given layer is obtained.

Problem: to obtain the distribution for the first layer (0 to 0.22R) in Figure 7.4.1

Data: From Figure 6.4.3.1, load settlement data for the layer extending to a depth of 0.22R below the raft is as follows: (the loads selected are exact measured loads, S_w = 41 kPa)

q(kPa)	22.6	38.7	59.6	60.5
q/S_w	0.6	0.9	1.3	1.5
δ(mm)	0.2	1.02	2.79	3.61

Average vane strength, S_u for the layer = 56.8 kPa

= 0.58 kg/cm^2

Solution: From Equation 3.5.1 and Poisson's ratio of 0.5,

$$E = \frac{1.5R\ q\ \overline{M}_z}{\delta} \quad , \quad R = 686 \text{ cm}$$

From Giroud's (1972) table below r/R = 0.67, linear interpolation gives the following $\overline{M}_z$ values.

z/R	0	0.22
$\overline{M}_z$	0.785	0.762

∴ ΔM_z for layer = 0.785 - 0.762 = 0.023

Then assigning E_u to E and substituting for all known quantities:

$E_u = 24 \frac{q}{\delta}$ dividing by S_u, then

$E_u/S_u = 41.4 \frac{q}{\delta}$, δ should be in (cm)

The calculation results for the above data are:

q/S_w	0.6	0.9	1.3	1.5
E_u/S_u	477	160	83	71

These are four of the six values plotted in Figure 7.4.1

7.6 Subgrade Modulus

Although, the theory of subgrade reaction is not very accurate, it is still used quite extensively for the design of footings, pavements and even large raft foundations. Since the concept will still be used for some time to come, it was thought appropriate to give some range of values for the Leda Clay in the Ottawa area. As mentioned in Section 2.5, one of the drawbacks of the method is that it gives a uniform pressure distribution when applied to rigid footings.

Both Terzaghi's (1955) and Bowles' (1977) methods will be used to calculate k for the rigid raft. In the first case, the linear portion of the net pressure versus settlement curve (Figure 6.4.1.2) is approximated by a straight line, the slope of which is taken as the subgrade modulus. In the second method, the empirical formual (Equation 2.5.3) which is a function of the allowable bearing pressure is used. The results of the calculations are:

According to Terzaghi's (1955) method, $k = \dfrac{30\ \text{kPa}}{2.9\ \text{mm}}$

$$= 10400\ \frac{\text{kN}}{\text{m}^3}$$

$$= 66\ \text{kcf}$$

Using Bowles' (1977) method: $k = 120\ (87.5\ \text{kPa})$

$$= 10500\ \frac{\text{kN}}{\text{m}^3}$$

$$= 67\ \text{kcf}$$

It appears that both methods give similar results. In the next section, the modulus of subgrade reaction values from other sources are compared with the above calculated results.

7.6.1 Subgrade Modulus from Other Sources

Subgrade moduli were calculated for the test plates and the five square footings using Bowles' (1977) method. This method is chosen since it gives quick results and also takes the shear strength of the soil into consideration. The results of the calculations are given in Table 7.7.1.1. The values have a range of: 10440 - 18960 $\frac{kN}{m^3}$ (67 - 121 kcf). It is seen that the footings and the plate closer to the surface have higher subgrade moduli; perhaps due to the effect of the crust. Since the result for the tower silo also falls at the bottom end of the range, it appears that the above range of values of subgrade modulus can safely be used for most foundation designs in Leda Clay. Generally, for soft to firm clay most designers assume a uniform contact pressure, hence there are no published values of subgrade modulus available. However, for all clays with unconfined compressive strength, q_u < 200 kPa (4 ksf) Bowles (1977) gives a range of 11800 - 23600 $\frac{kN}{m^3}$ (75 - 150 kcf). He also points out that the above range is to be used as a guide only. His values are reasonable compared to values found here as his are for stiff clay while the Leda Clay is probably not as stiff.

Fortunately, moments in rigid isolated footings subjected to concentrated central loads are not very sensitive to large errors in the estimation of the subgrade modulus. For example, in the case of a circular raft, the assumption of uniform pressure underestimates the moments by 18 percent and for a rigid strip footing this error is about 27 percent (Zeevaert, 1972). With the high safety factor usually employed, these errors are not usually significant.

It is appropriate to mention, however, that in the case of a large raft subjected to several concentrated loads, the difference

Plate or Footing	Weighted Shear Strength, S_w (kg/cm^2)	Allowance Bearing Pressure, q_a (kPa)	$k=120\ q_a$ $\frac{kN}{m^3}$	k (kcf)	Foundation depth from original ground (m)
V2/1	.63	128	15400	98	2.50
V3/1	.59	119	14300	91	3.70
T.F.	.78	158	19000	121	0.60
M-17	.71	144	17300	110	0.93
O-19	.71	144	17300	110	0.93
CC-12	.47	95	11400	73	2.10
GG-8	.43	87	10400	67	3.07
Raft	.41	87.5	10400	67	0.61

Sample Calculation:

Consider V2/1

$$q_u = S_w N_c = 6.2 \times 0.63 \frac{kg}{cm^2} = 3.9 \frac{kg}{cm^2} = 382 \text{ kPa}$$

$$q_a \quad q_u/3 = 382/3 \qquad = 128 \text{ kPa}$$

from Equation 2.4.3

$$k = 120\ q_a \ = \ 15400 \text{ kPa}$$

TABLE 7.7.1.1 Calculation of Subgrade Modulus using Bowles' (1977) Formula in shear and bending moments may be important for different assumptions of subgrade modulus. Consequently, the foundation structural analysis and economy may be affected.

CHAPTER 8

CONCLUSIONS AND RECOMMENDATIONS

8.1 General

This chapter summarizes the important findings of the research project. It also includes important conclusions and recommendations for future work. The conclusions and recommendations are based on data derived from this project and from the geotechnical literature. The main topics dealt with are: normal contact pressures, settlement distributions and the range of E_u/S_u (ratio of undrained modulus to average vane shear strength) values for the Leda Clay of the Ottawa region.

8.2 Summary

As mentioned in Chapter 1, initially the research proposal was to instrument a standard concrete silo with a ring foundation having a factor of safety of 3. However, for the reason given in Chapter 1, instead of the ring footing, a large rigid circular raft with a diameter of 45' (14.6 m) was constructed. This led the research work to the study of the performance of a rigid raft in Leda Clay. This project was made available through, the National Research Council, Division of Building Research, which carried out the field and laboratory soil investigation to explore the cause for the overturning of an older silo. The foundation for the new instrumented silo was constructed about 6 m away from the disturbed crust caused by the overturning of the old silo.

To study the performance, 8 load cells to measure normal contact pressures, 2 pneumatic and 4 open standpipe piezometers, 5 deep seated settlement gauges, a deep seated bench mark and 24 levelling points were carefully installed.

The field and laboratory soil investigations as well as the instrumentation made the following analysis possible:

a) distributions of normal contact pressures under a rigid circular raft.

b) theoretical settlement calculations and distributions from CIU triaxial and standard oedometer tests.

c) actual distribution of settlement with depth and the determination of the critical depth of settlement.

d) the distribution of E_u/S_u ratios.

All these analysis were also compared where possible to theoretical and other measured values cited in the geotechnical literature.

In particular the settlement data from four plate load tests and six square footings all in the Leda Clay of Ottawa were analyzed and the results compared with that for the rigid circular raft. The data from these plate and footing instrumentations all conducted by the Geotechnical Group of the University of Ottawa made the study of the effect of foundation size on the distribution of settlement possible. The range of foundation elements studied covers most foundation sizes used in practice. This range includes 46 cm diameter plates, square footings with average size of 3.6 m and the large circular raft with a diameter of 14.6 m. The conclusions to follow apply only to pressure levels less than the preconsolidation pressures.

8.2.1 E_u/S_u Values

8.2.1.1 For foundation designs in Leda Clay of the Ottawa area with a factor of safety of 3 against bearing failure, the following ranges of E_u/S_u values are applicable, for all foundations within the size range of 0.46 to 13.7 m in diameter:

a) When the soil below the foundation element to a depth of 6R or bedrock (whichever is the smallest) is considered, E_u/S_u ranges between 500 and 1500 with an average value of 1000. This agrees closely with an average of 1100 suggested by D'Appolonia et al (1971) for a similar soil.

b) Within the depth 2R below the foundation E_u/S_u varies between 200 and 1050 with an average of 630. For a square footing, R is the equivalent radius of a circular footing having the same area as the square one.

8.2.1.2 The ratio of E_u/S_u appears to decrease with an increase in q/S_w. This applies when the soil below the foundation element is divided into layers. However, the rate of decrease varies from one soil layer to another in a rather erratic manner especially at low q/S_w values. In the case where the soil layer is assumed to be infinite in thickness or when the layer extending to a depth of 2R is considered, the influence of q/S_w on the magnitude of E_u/S_u for a given foundation element is very small.

8.2.1.3 The increase in E_u/S_u with depth indicated by calculations for all the foundation elements, should not be taken as an indication of a stiffer soil below. This calculated increase occurs because at lower levels elastic theory appears to overestimate the stress increases.

8.2.2 Distribution of Settlement with Depth

8.2.2.1 Figure 7.3.3.1 indicates that for most designs a critical depth of 2D would give satisfactory estimates of settlement. This finding agrees with that of Shvets and Kulchitskii (1970), who made load tests in a wide range of variable soil types and found a critical depth envelope varying from 1.5 to 2D.

8.2.2.2 The amount of settlement within the soil layer extending to a depth of 2R is between 70 to 90 percent of the total settlement for all foundation elements considered. Hence for most foundations within the size range studied here, settlement calculations assuming that 80 percent of the total is within this layer, will give reliable results.

8.2.2.3 Elastic theories when used with CIU triaxial and oedometer test results underestimate the contribution to the total settlement by the shallow layer near the footing. However, when the critical depth is taken into account the oedometer calculations give distributions that approximate the actual somewhat better. For example, the component of settlement in the layer above $z/D = 0.5$ as a percentage of the total from the various distributions is as follows (Figure 7.2.3.1):

1) actual for silo raft = 71 percent
2) recompression settlements from oedometer tests based on the following stress distribution theories are
   a) Westergaard's = 63 percent
   b) Boussinesq's = 67 percent
3) Immediate settlement from CIU triaxial, with Boussinesq's stress distribution theory = 55 percent

Therefore, the distribution due to oedometer test recompression settlement approximates the actual better than that calculated from CIU triaxial tests. However, this agreement is probably partially due to the method of correcting the oedometer curves used in the calculations.

8.2.2.4 Even though the silo raft indicates a shallower critical depth of 1.25D, than the other foundation elements which have a critical depth of 2D, it can be concluded that the shapes of the distribution curves are identical. These settlement distributions are therefore independent of the size of the foundation element as well as of the magnitude of the loading. The shape of the curves from the elastic theories are different and overestimate the compression of the lower layers. A finite element model reported for a similar raft by Wroth (1977) indicates that this technique can be designed to simulate the actual distribution better than elastic theory. The difference between the actual distribution and that predicted by elastic theory is probably mainly due to the non-linear response of the soil to external pressure.

8.2.2.5 The fact that all foundation elements located both in the desiccated crust and below it show the same shape of distribution curves, implies that the distribution is a characteristic of the soil. Hence, the relatively larger compression of the top layer cannot be due to closing of fissures as suggested by Bauer et al (1973). Also, it cannot be due to crustal anisotropy; since laboratory vane tests indicate the soil to be fairly isotropic.

8.2.3 Total Settlement

8.2.3.1 Settlement readings were taken frequently for 232 days [June 22, 1976 to February 4, 1977], no additional readings were taken after February 4 since the raft frost heaved up by 3.15 mm from its end-of-construction elevation. A few days earlier, December 22, 1976, piezometer readings indicated an average excess pore water pressure of only about 8 cm (3 in) and therefore it was felt that future settlements due to consolidation would be very small. The total settlement of 11.2 mm recorded on December 22, 1976 probably includes some consolidation settlement due to the recompression of the soil, however the piezometers showed little pore pressure build up as the load was applied and therefore the settlement appears to have been mainly elastic in nature.

8.2.3.2 Calculations based on secant moduli obtained from CIU triaxial tests, overestimate the settlement. The best estimate obtained is that corresponding to $\nu = 0.5$, which is 14.04 mm as opposed to an actual settlement of 11.2 mm. Since in the calculation, the critical depth and the effect of a rigid base are accounted for, the main reason for the discrepancy can only be the low moduli calculated from CIU triaxial tests. It is believed that, for such clays which drain rather fast CIU triaxial test is not applicable since it does not simulate the field condition. CID triaxial tests simulating the field rate of drainage might be more appropriate.

8.2.3.3 Settlement calculations from oedometer tests due to recompression, even when the critical depth is considered, are very large and therefore not applicable. The calculated values after making correction for 3-dimensional effects are 44.9 and 42.8 mm using Westergaard's and Boussinesq's stress distribution theories respectively.

8.2.4 Contact Pressure Distribution

8.2.4.1 At the maximum applied pressure of 72.5 kPa, the contact pressures below the centre and at the edge of the silo raft were 35 and 84.5 kPa, respectively. The stress at the centre agrees with the prediction of elastic theory, being about 50 percent of the average pressure. Near the edge elastic theory predicts infinite stress and therefore is not applicable.

8.2.4.2 Zeevaert's elasto-plastic theory underestimates the edge stress and shows a uniform contact pressure distribution. It does not apply to shallow foundations in soils with low shear strengths such as the Leda Clay studied in this project. On the other hand, the theory derived in this thesis on the basis of Schultze's (1961) hypothesis gives 55 and 80 kPa below the centre and the edge respectively. These quantities are in reasonable agreement with the actual values. Hence for most rigid foundation designs in Leda Clay this later method appears to be applicable.

8.2.4.3 To make a detailed study of contact pressure distribution in the field, the minimum number of cells required should be decided on the basis of probability theory. By this it is meant that the sample size (number of distinct contact pressure measurements) representing the population (infinite number of points that define the actual contact pressure curve) should be determined using statistical theory. A discussion of this technique dealing particularly with contact pressure measurements is given in a recent paper by Phal (1977). According to Phal, for typical clay soils a minimum number of at least 20 cells is required; all installed along one radius. Therefore, the 8 load cells used in this project were not enough to clearly define the true normal contact pressure curve.

8.2.4.4 When installing load cells in Leda Clay, it is important that the soil immediately under each cell has the same consistency, since the footing will have a tendency to bridge over cells located in softer areas. This is believed to be the cause for the low reading given by cell no. 1 which is installed near the edge of the raft. Possible methods of providing a uniform bedding under all cells are: (a) by ensuring that the soil at the bottom of the excavation is fairly uniform, and (b) immediately after excavation protecting the locations of the cells from wetting due to external water and also from desiccation.

8.2.5 Subgrade Modulus

The subgrade modulus calculated from the load settlement data for all foundation elements ranges between 10440 to 18960 $\frac{kN}{m^3}$ (67 to 121 kcf) with a mean value of 14700 $\frac{kN}{m^3}$ (93.6 kcf). The author feels that this mean value can be safely applied to most isolated footing designs in Leda Clay. The above range compares reasonably well with that suggested by Bowles for stiff clays which is 11800 to 23600 $\frac{kN}{m^3}$ (75 to 150 kcf) with an average of 17700 $\frac{kN}{m^3}$

(113 kcf). It should be borne in mind, however, the concept of subgrade modulus is not very reliable compared to actual contact pressure distributions. For example, for rigid footings, the theory of subgrade modulus gives a uniform contact pressure and therefore it is incorrect.

8.2.6 Recommendations for further work

Based on the findings in this project and the literature survey, the author would like to suggest the following tasks for further research work.

8.2.6.1 More foundations with different stiffness and shape should be instrumented so that a narrower and therefore more reliable E_u/S_u range for all types of foundations is available. This can be done without very expensive instrumentation by installing one simple settlement gauge (similar to those used in this project) at a depth equal to the width or diameter of the foundation plus one reliable bench mark. From a number of such inexpensive, and yet, very valuable instrumentations the E_u/S_u values within the depth D or B and also for the whole deposit can be deduced, since the field vane shear strength of the soil is usually known.

8.2.6.2 When making any settlement calculation for footings resting on a relatively deep deposit of clay, some means of estimating the depth of the active zone of settlement is required so that the result of the calculation will be more reliable. The critical depth for a given deposit can probably be deduced from the distribution of the field vane shear strength values; this, however, can only be confirmed by studying case histories or by performing further instrumentation work.

8.2.6.3 More sophisticated mathematical formulae that consider the non linear behavior of soils are needed.

8.2.6.4 A few carefully planned normal contact pressure distribution measurements are needed. From such detailed work, the author believes a more reliable elasto-plastic contact pressure model can be formulated using numerical methods such as regression analysis.

REFERENCES

Barden, L., 1963, "Stresses and Displacements in Cross-anisotropic Soil", Geotechnique, 13:3, 198-210.

Bauer, G.E., Scott, J.D. and Shields, D.H., 1973, "The Deformation Properties of a Clay Crust", Proc. 8th ICSMFE, 1:31-38.

Bauer, G.E., Shields, D.H., McRostie, G.C. and Scott, J.D., 1976, "Predicted and Observed Footing Settlements in a Fissured Clay", Proc. Conf. on Performance of Building Structures, Vol. 1, 287-302, Glasgow.

Borowicka, H., 1936, "Influence of Rigidity of a Circular Foundation Slab on the Distribution of Pressures Over the Contact Surface", Proc. I, ICSMFE, 1:31-35.

Bozozuk, M., 1960, "Description and Installation of Piezometers for Measuring Pore-Water Pressures in Clay Soils", BRN (Building Research Notes).

Bozozuk, M., Johnston, G.H. and Hamilton, J.J., 1962, "Deep Bench Marks in Clay and Permafrost Areas", ASTM, STP 322, pp.265-279.

Bowles, J.E., "Foundation Analysis and Design", McGraw-Hill Inc., N.Y., First Edition, 1968; Second Edition 1977.

Brown, P.T., 1969(a), "Numerical Analysis of Uniformly Loaded Circular Rafts on Elastic Layers of Finite Depth", Geotechnique, Vol. 19, pp.301-306.

Brown, P.T., 1969(b), "Numerical Analysis of Uniformly Loaded Circular Rafts on Deep Elastic Foundations", Geotechnique, Vol. 19, pp.399-404.

Brumund, W.F., Jonas, E., Ladd, C.C., 1976, "Estimating In-situ Maximum Past (Preconsolidation) Pressure of Saturated Clays From Results of Laboratory Consolidometer Tests", Transp. Res. Board Spec. Rep., No. 163, pp.4-12.

Building Code Requirements for Reinforced Concrete (ACI 318-71), Section 8.3, 7th Printing, August 1975.

Burmister, D.M., 1956, "Stress and Displacement Characteristics of a Two Layer Rigid Base Soil System: Influence Diagrams and Practical Applications", Proc. H.R.B., Vol. 35, pp.773-814.

Carrier III, W.D., and Christian, J.T., 1973, "Rigid Circular Plate Resting on a Non-homogeneous Elastic Half-Space", Geotechnique, 23:1:67-84.

Chin, F.K., 1969, "Size and Load Effect on Settlement of Footings in Clay", Proc. 7th ICSMFE, 53-57.

Crawford, C.B., 1960, Discussion, "Proceedings A.S.C.E., Research Conference on Shear Strength of Cohesive Soils", Boulder, Colo., pp.1080-1086.

Crawford, C.B. and Eden, W.J., 1965, "A Comparison of Laboratory Results with In-Situ Properties of Leda Clay", Proc. VI ICSMFE, 1:31-35.

Davis, E.H. and Poulos, H.G., 1968, "The Use of Elastic Theory for Settlement Prediction Under Three-Dimensional Conditions", Geotechnique, 18:67-91.

D'Appolonia, D.J., Poulos, H.G. and Ladd, C.C., 1971, "Initial Settlement of Structures on Clay", Proceedings of A.S.C.E., SMID, pp.1359-1377, Discussion, M.L. Calhoon. 98 [SM3, No. 8751] 306-8 Mr. 72; Reply 99 [SM4, No. 9639]: 343-4 Ap. 73.

Eden, W.J., 1960, "Field Studies on the Consolidation Properties of Leda Clay", Proc. Fourteenth Canadian Soil Mechanics Conference, 107.

Eden, W.J., McRostie, G.C. and Hall, J.S., 1973, "Measured Contact Pressures Below Raft Supporting a Stiff Building", Canadian Geotechnical Journal, Vol. 10.

Fransham, P.B. and Gadd, N.R., 1976, "Geological and Geomorphological Controls of Landslides in Ottawa Valley, Ontario", paper submitted to the 29th Canadian Geotechnical Conference, Vancouver, B.C.

Fransham, P.B., Gadd, N.R. and Carr, P.A., 1976, "Sensitive Clay Deposits and Associated Landslides in Ottawa Valley", Open File 352, GSC, Ottawa.

Gadd, N.R., 1975, "Geology of Leda Clay", 4th Guelph Symposium on Geomorphology, GSC Library MGF 9S98 4th.

Gadd, N.R., 1971, "Pleistocene Geology of the Central St. Lawrence Lowland", Memoir 359, Geological Survey of Canada.

Gadd, N.R., 1962, "Surficial Geology of Ottawa Map - Areas Ontario and Quebec", 31G/S, Geological Survey of Canada, Department of Mines and Technical Surveys, Paper 62-16, 1962, 4 pages.

Gaumy, Y., 1970, "Etude du Tassement Immediat D'une Semelle Carree Reposant sur une Argile Sensible", M.A.Sc. Thesis, University of Ottawa, Ottawa (unpublished).

Giroud, J.P., 1972, Mecanique des Sols: Table pour le Calcul des Fondations. Tome 1, Tassement, Dunod, Paris.

Hanna, A.J., 1976, "Deformation Characteristics of Soil", M.A.Sc. Thesis, University of Ottawa, Ottawa (unpublished).

Hanna, T.H., 1973, "Foundation Instrumentation", First Edition, Trans Tech. Publications.

Hooper, J.A., 1974, "Analysis of a Circular Raft in Adhesive Contact with a Thick Elastic Layer", Geotechnique, 24, pp.561-580.

Huang, Y.H., 1968, "Stresses and Displacements in Nonlinear Soil Media", ASCE, JSMFD, 94:SM1:1-19.

Janbu, N., Bjerrum, L. and Kjaernsli, B., Norwegian Geotech. Inst. Publ. 16, Oslo, 1966, pp.30-22 (in Norwegian).

Jumikis, A.R., "Settlement Tables for Centrally Loaded, Rigid Circular Footings on Multilayered Systems", Eng. Res. Bull. No. 54, Rutgers University, New Jersey.

Karrow, P.F., 1960, "Canadian Pleistocene Marine Clays", Proc. Fourteenth Canadian Soil Mechanics Conference, 94.

Kenney, T.C., 1964, "Sea Level Movements and Geological Histories of the Post-Glacial Marine Soils at Boston, Nicolet, Ottawa and Oslo", Geotechnique, 14:3:203.

Leonards, G.A., 1976, "Estimating Consolidation Settlements of Shallow Foundations on Overconsolidated Clay", Transp. Res. Board Spec. Rep. No. 163, pp.13-16.

Malyshev, M.V., Zaretsky, Y.K., Shirokov, V.N. and Cheremikh, V.A., "Interaction of Rigid Foundations with a Base that Deforms Nonlinearly", Proc. VIII, ICSMFE, Moscow, USSR, August 1973, Vol. 1.3, pp.155-159.

Mitchell, R.J., Sangrey, D.A. and Webb, G.S., 1972, "Foundations in the Crust of Sensitive Clay Deposits", ASCE Conf. on Performance of Earth and Earth Supported Structures, Vol. 1, Pt. 2, 1051-1072.

Parkes, E.W., 1956, "A Comparison of the Contact Pressures beneath Rough and Smooth Rafts on an Elastic Medium", Geotechnique 6, No. 4, 183-189.

Phal, P.J., 1977, "Testing the Shape of Contact Pressure Curves", ASCE, JGTD, Vol. 103, pp.798-803.

Poulos, H.G., 1967b, "The Use of the Sector Method for Calculating Stresses and Displacements in an Elastic Mass", Proc. 5th Australia-New Zealand Conf. Soil Mech.

Poulos, H.G., 1968, "The Behavior of a Rigid Circular Plate Resting on a Finite Elastic Layer", Institution of Engineers, Australia, Civil Engineering Trans., Oct.

Raymond, G.P. and Wahls, H.E., 1976, "Estimating 1-Dimensional Consolidation, Including Secondary Compression of Clay Loaded from Overconsolidated to Normally Consolidated State", Transp. Res. Board Spec. Rep. No. 163, pp.17-23.

Schiffman, R.L., 1969, "The Influence of Adhesion on the Stress and Displacement in an Elastic Half-Space", Highway Research Record No. 283.

Schultze, E., 1961, "Distribution of Stress Beneath a Rigid Foundation", Proc. 5th ICSMFE, pp.807-813.

Selvadurai, A.P.S., 1976, "The Response of a Rigid Circular Plate Resting on an Idealized Elastic-Plastic Foundation", Int. J. Mech. Sci., Vol. 18, pp.463-468.

Shvets, V.B. and Kul'chitskii, G.B., 1970, "Experimental Investigation of the Depth of Compressed Soil Foundation Stratum Under a Plate", Soil Mechanics and Foundation Engineering, No. 1.

Shirokov,V.N., Solomin, V.I. and Zareckij, J.K., 1970, "State of Stress and Displacements of Non-linear Semi-infinite Soil Mass Beneath a Rigid Circular Footing", Soil Mechanics and Foundation Engineering 12, No. 1, pp.2-5.

Skempton, A.W., "The Pore Pressure Coefficients A and B", Geotechnique, Vol. 4 (1954), p.143.

Skempton, A.W. and Bjerrum, L., 1957, "A Contribution to the Settlement Analysis of Foundations on Clay", Geotechnique 7, No. 4, 168-178.

Skopec, J., 1961, "The Influence of Foundation Depth on Stress Distribution", Proc. 5th ICSMFE, Vol. 1, 815-818.

Stefanoff, G. and Krastilov, G., 1973, "Evaluation of the Active Zone of Settlement", Proc. VIII, ICSMFE, 1:3, 249-251.

Sutherland, H.B. and Lindsay, J.A., 1961, "The Measurement of Load Distribution under Two Adjacent Column Footings", 5th ICSMFE, pp.829-835.

Terzaghi, K. and Peck, R.B., 1967, "Soil Mechanics in Engineering Practice", John Wiley and Sons, Inc., New York.

Terzaghi, K., 1955, "Evaluation of Coefficients of Subgrade Reaction", Geotechnique, Vol. V, pp.297-326.

Townsend, D.L., Sangrey, D.A. and Walker, L.K., 1969, "The Brittle Behaviour of Naturally Cemented Soil", Proc. VIII, ICSMFE, 1:411-417.

Wroth, C.P., 1976, "Response of the Structure to Foundation Movements", Performance of Building Structures, Vol. 2, Discussion pp.499-502.

Vesic, A.B., 1961, "Beams on Elastic Subgrade and the Winkler Hypothesis", 5th ICSMFE, pp.845-850.

Zeevaert, L., 1972, "Foundation Engineering for Difficult Subsoil Conditions", VanNostrand Reinhold Company, N.Y., pp.216-242.

APPENDIX A

MISCELLANEOUS INFORMATION

ADDITIONAL ALGEBRAIC STEPS USED IN THE DERIVATION OF CONTACT PRESSURE DISTRIBUTION FOR A RIGID CIRCULAR FOOTING

From static force equilibrium it is given in the section that,

$$\frac{Q}{2} = \frac{V + T}{2}$$, where V and T are integrals to be evaluated here

$$\frac{V}{2} = \Pi \int_{o}^{r_1} \frac{P_1}{2\Pi R} \frac{r}{\sqrt{1-(\frac{r}{R})^2}} dr$$

After making some algebraic substitutions, the integration simplifies to:

$$\frac{V}{2} = [-\frac{P_1}{2} \sqrt{1-(\frac{r}{R})^2}]_{o}^{r_1} = \frac{P_1}{2} [1- \sqrt{1-\xi_1^2}] \qquad \text{a.1}$$

Similarly

$$\frac{T}{2} = \frac{1}{2} \int_{r_1}^{R} [\kappa_1 cN_c + \gamma_1 DN_q + 4R\kappa_2 \gamma_2 N_\gamma (1- \frac{r}{R})] \, 2\Pi r \, dr$$

In order to perform this integration, the pressure intensities at r_1 and R should be known; and noting these as q_1 and q_2 respectively (Figure 2.3.2.1) we can write,

$$\frac{T}{2} = \frac{1}{2} \int_{r_1}^{R} [q_1 - m(r-r_1)] \, 2\Pi r \, dr$$

where $m = \frac{q_1 - q_2}{R - r_1}$ is the slope of the trapzoidal distribution.

Performing the integration we get,

$$\frac{T}{2} = \Pi \left[\frac{q_1 r^2}{2} - m\frac{r^3}{3} + mr_1 \frac{r^2}{2}\right]_{r_1}^{R}$$

Further operation and substitution of ξ_1 for $\frac{r_1}{R}$ results

$$\frac{T}{2} = \Pi \left\{\frac{q_1 r^2}{2}\left[1 - \xi_1^2\right] - \frac{R^2(q_1-q_2)}{3}\left[\frac{1-\xi_1^2}{1-\xi_1}\right] + \frac{R^2(q_1-q_2)}{2}\left[\xi_1+\xi_1^2\right]\right\} \quad \text{a.2}$$

Evaluating q_1 and q_2 using the Prandtl and Buisman formula (Equation 2.3.2.1) and substituting in the above equation we get after further algebraic simplification,

$$\frac{T}{2} = \frac{C_1}{2}(1-\xi_1^2) + \frac{C_2}{6}\left[3(1+\xi_1)(1-\xi_1)^2 - 2(1-\xi_1^3) + 3(1-\xi_1)(\xi_1+\xi_1^2)\right] \quad \text{a.3}$$

but $\frac{Q}{2} = \frac{V}{2} + \frac{T}{2}$

By eliminating P_1 from Equation a.1 (see Equation 2.3.2.5) and adding the result to Equation a.2 the final result given by a.3 is obtained. The value of $Q/2$ as a function of ξ is given in Equation 2.3.2.6.

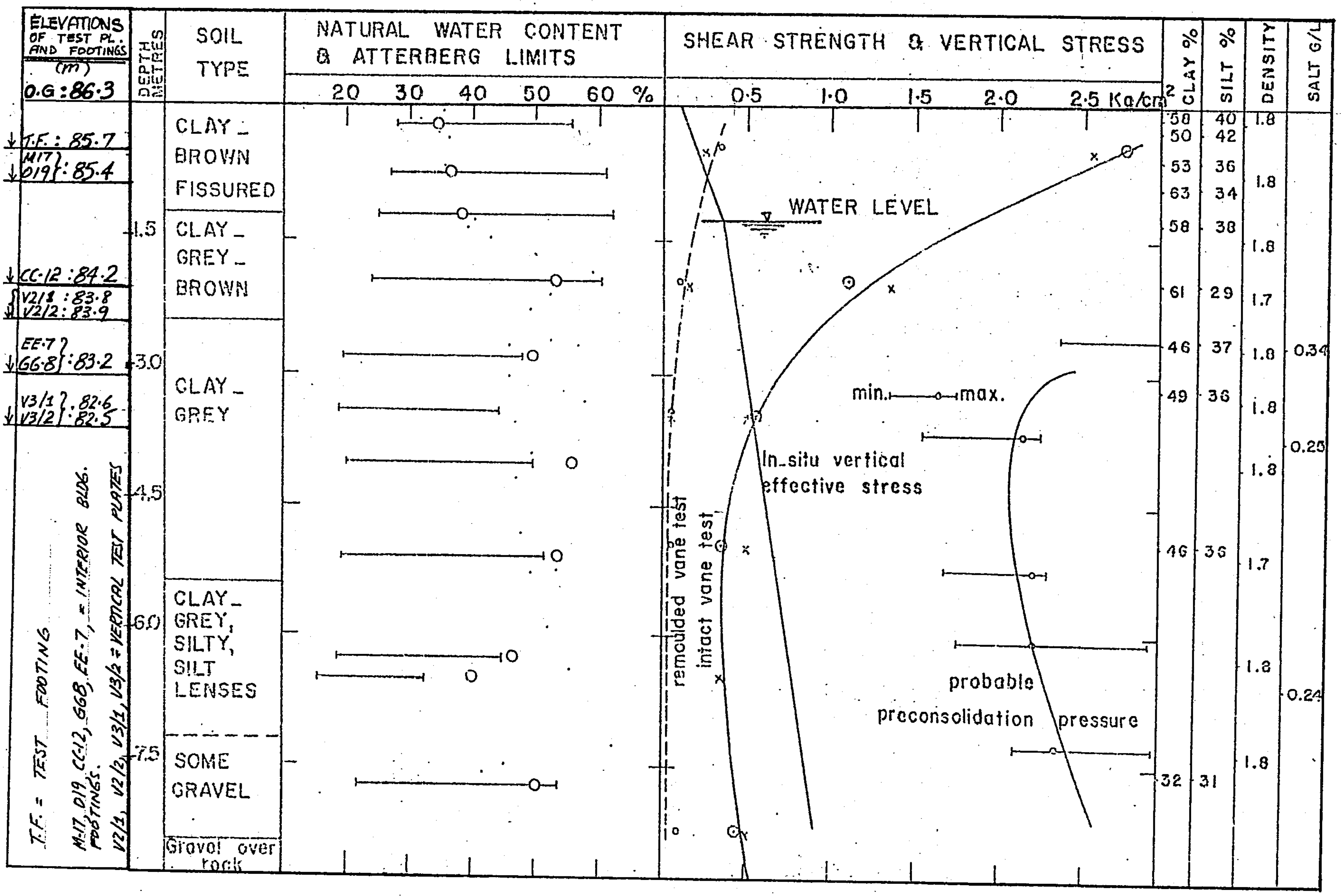

FIGURE - A1 SUBSOIL PROFILE (AFTER GAUMY, 1970) -

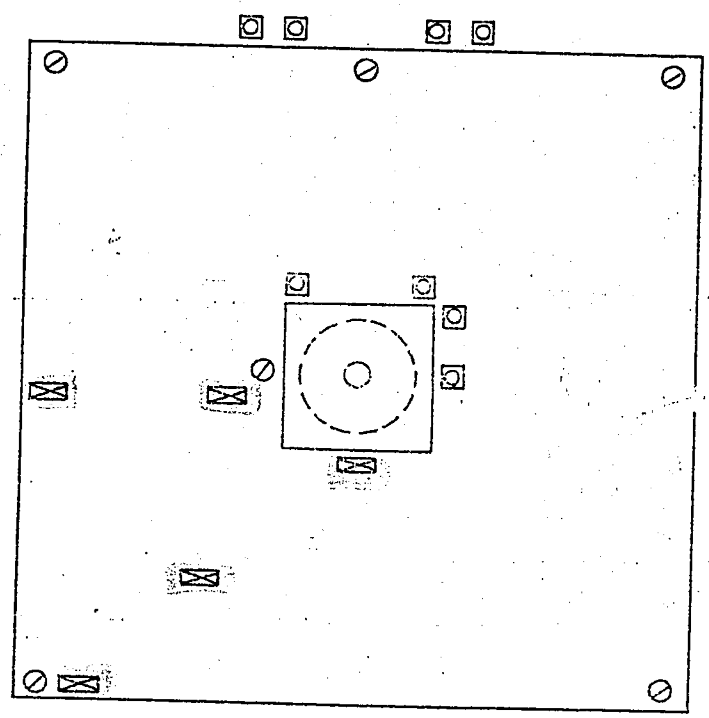

⊘ DIAL GAUGE ON TOP OF FOOTING

⊡ DIAL GAUGE ABOVE REFERENCE POINTS AT DEPTH.

⊠ CONTACT PRESSURE CELLS

FIGURE -A2 . PLAN VIEW OF 3·1 x 3·1 m RIGID FOOTING (AFTER GAUMY , 1970)

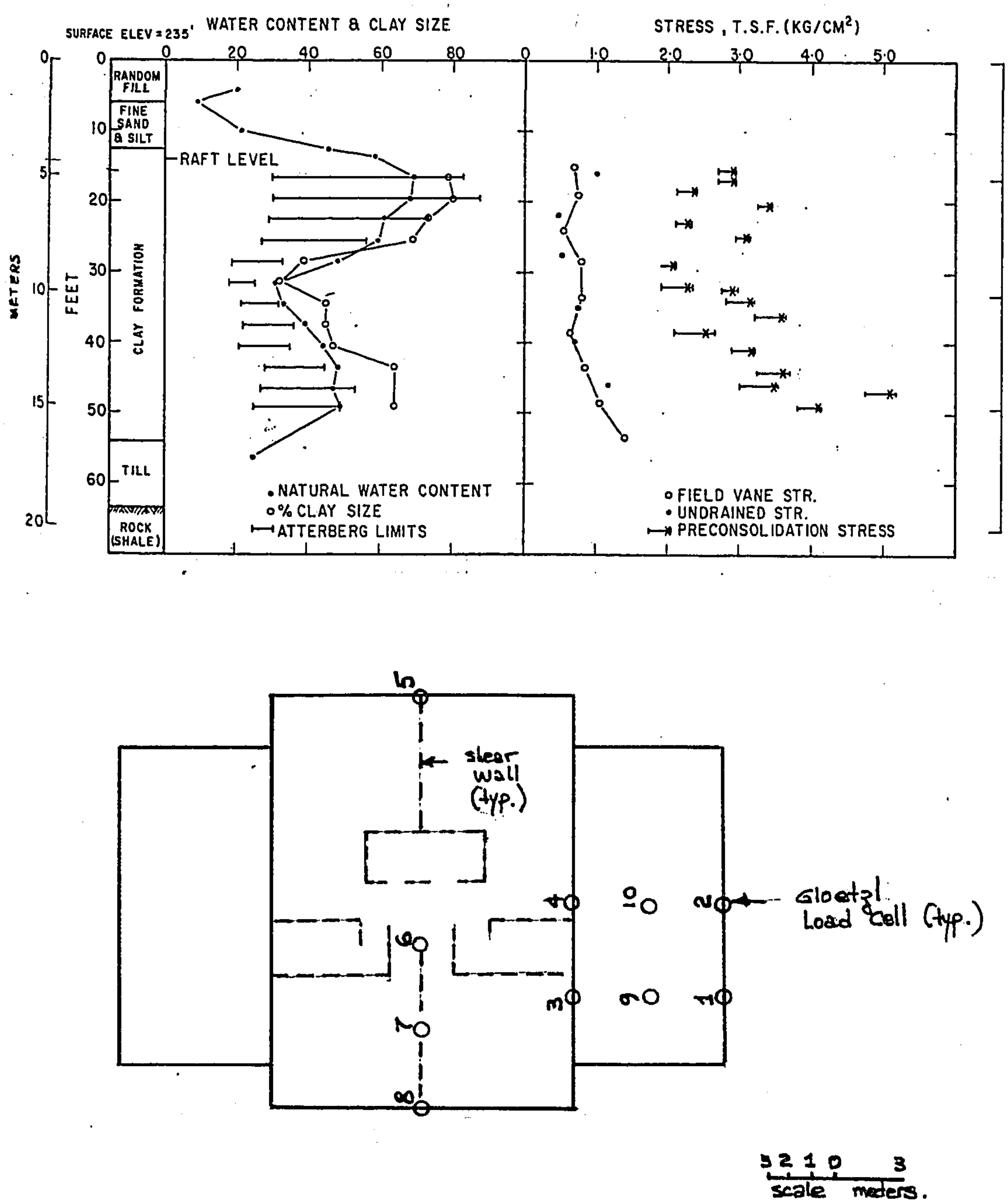

FIGURE A3 SOIL PROFILE & LAYOUT OF LOAD CELLS

AFTER EDEN et al. (1973)

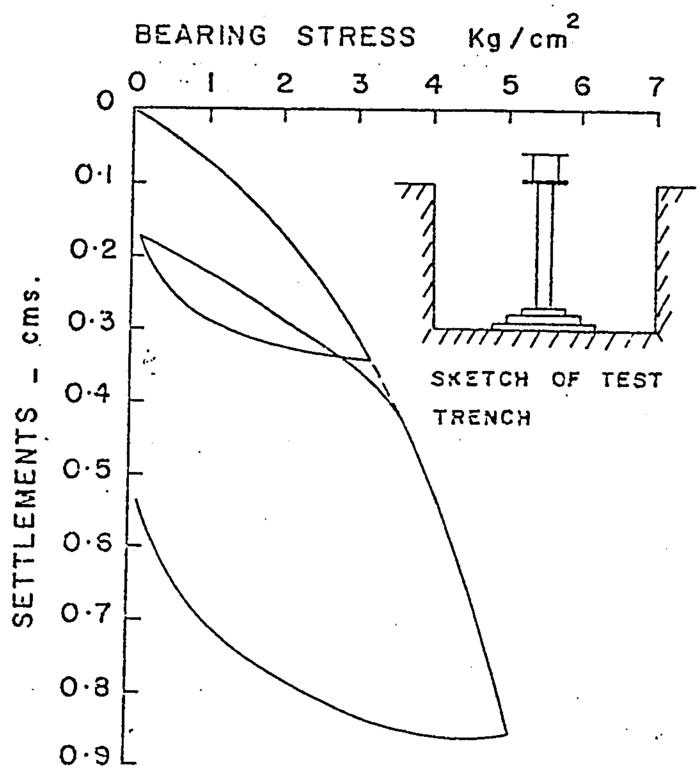

FIGURE A4 LOAD_SETTLEMENT CURVE
FOR PLATE LOADING TEST #1 (V2/1)

AFTER BAUER et al. (1973)

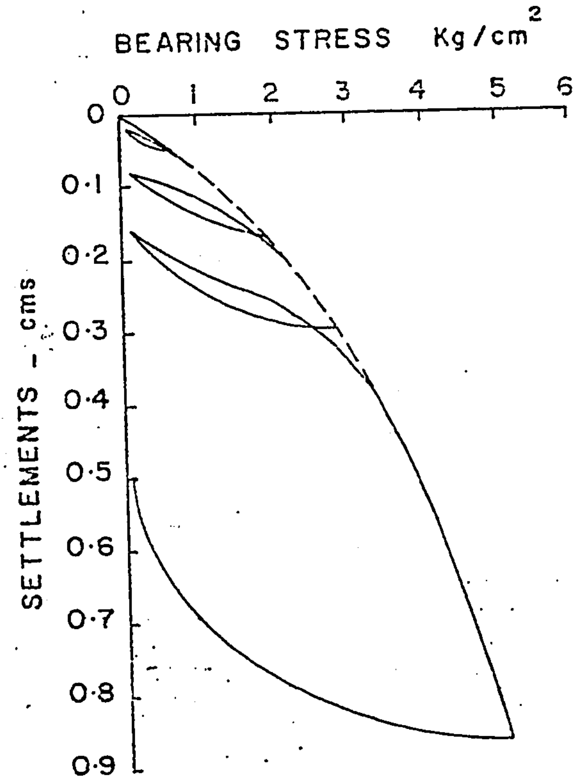

FIGURE A5 LOAD_SETTLEMENT CURVE FOR PLATE LOADING TEST #2 (V2/2).

AFTER BAUER et al. (1973)

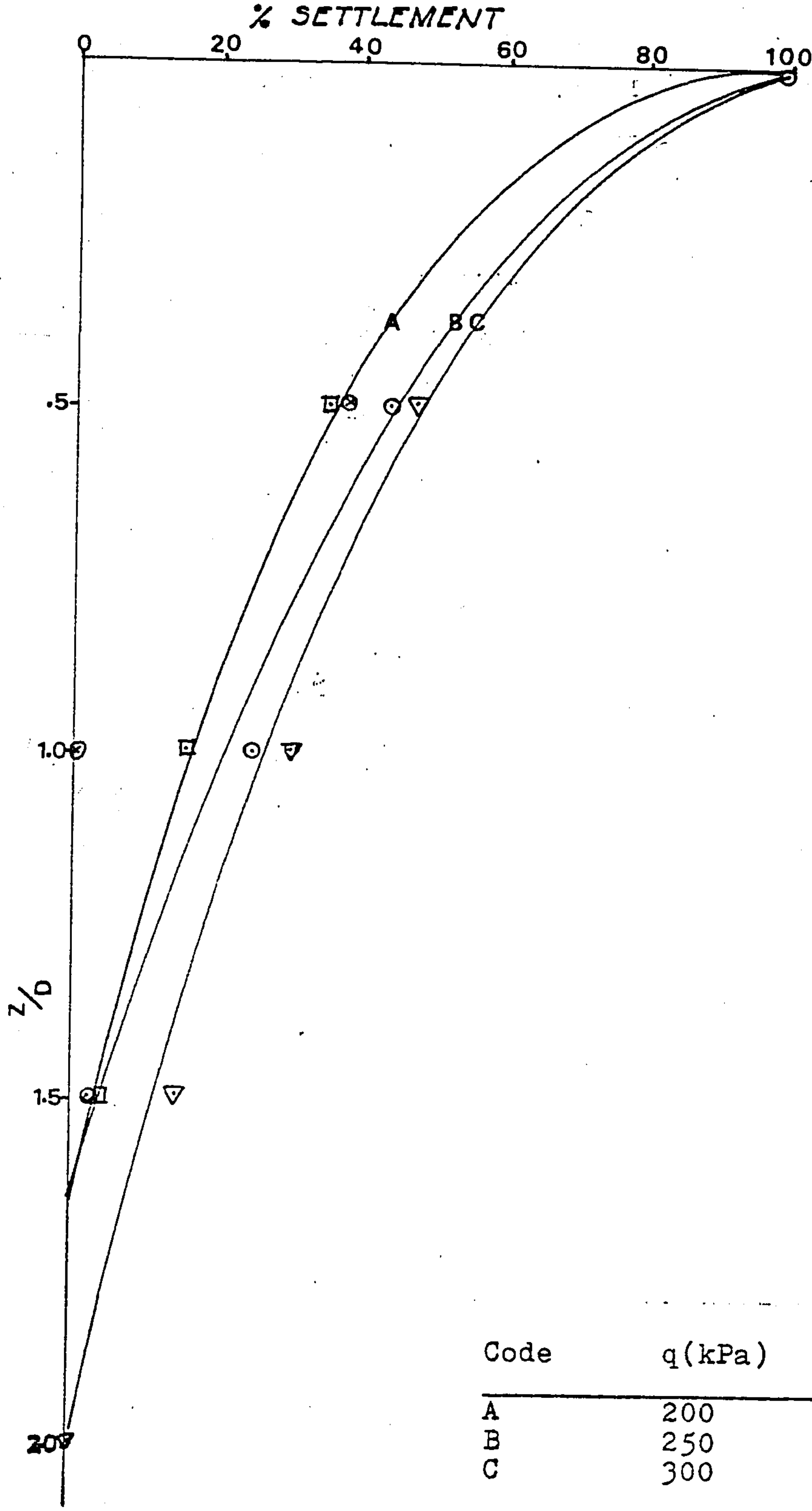

Code	q(kPa)	q/s_w
A	200	3.2
B	250	4.0
C	300	4.8

s_w = 61.7(kPa)

FIGURE A6 DISTRIBUTIONS OF SETTLEMENT FOR PLATE V2/1

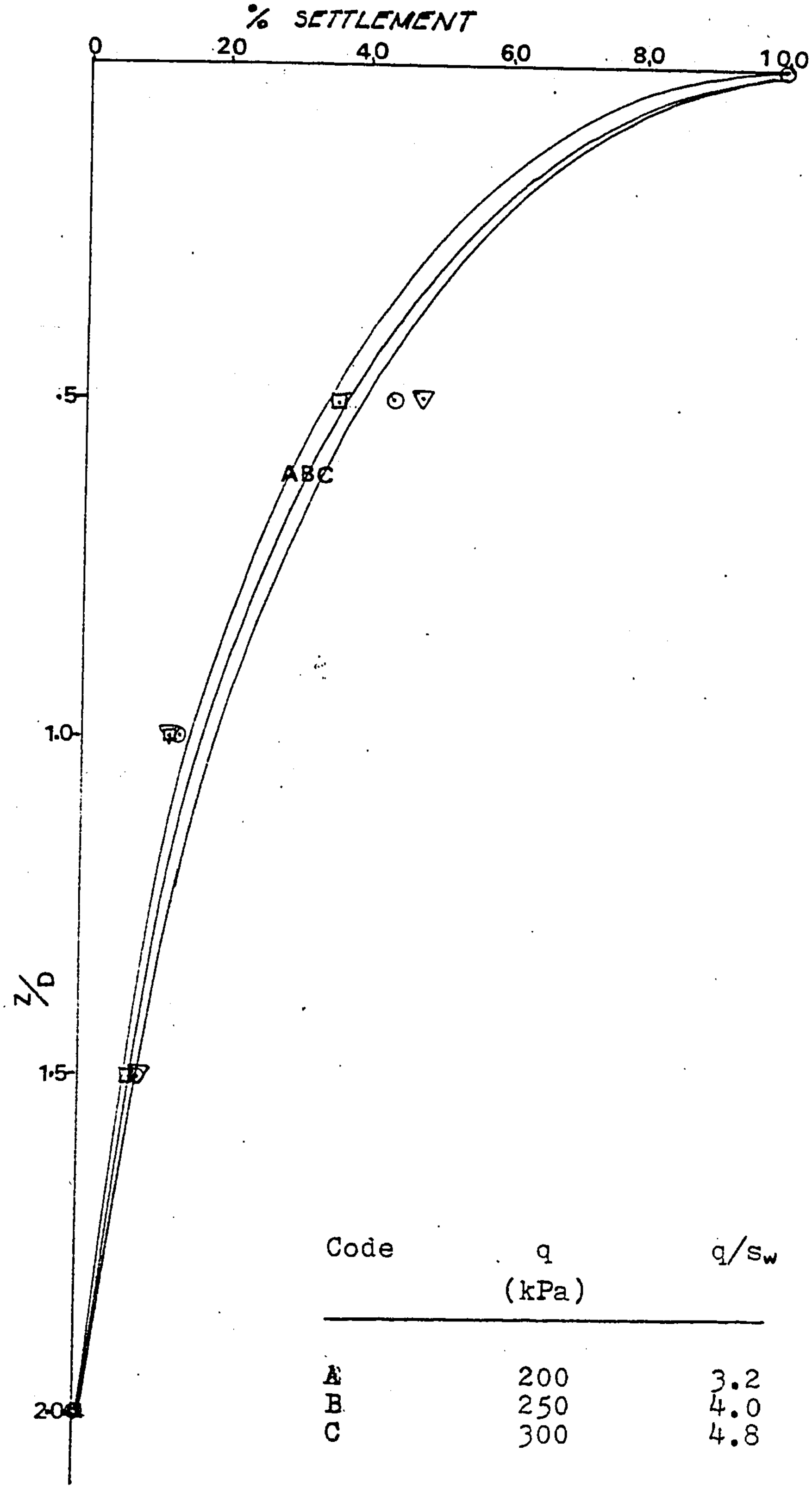

Code	q (kPa)	q/s_w
A	200	3.2
B	250	4.0
C	300	4.8

$s_w = 61.7$ kPa

FIGURE A7 DISTRIBUTIONS OF SETTLEMENTS FOR TEST PLATE V2/2

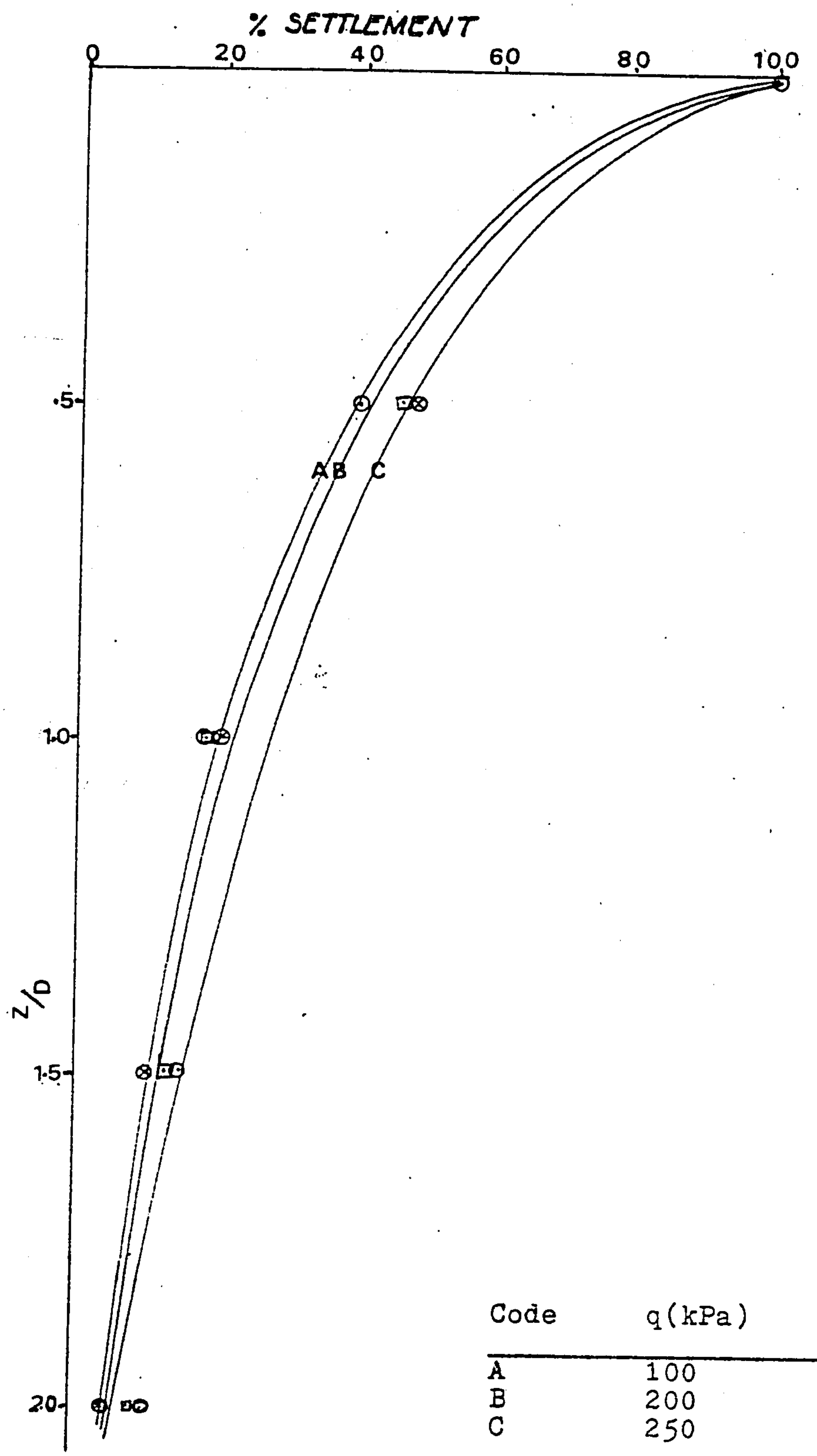

Code	q(kPa)	q/s_w
A	100	1.7
B	200	3.4
C	250	4.3

$s_w = 57.8$ (kPa)

FIGURE A8 DISTRIBUTIONS OF SETTLEMENT FOR PLATE V3/1

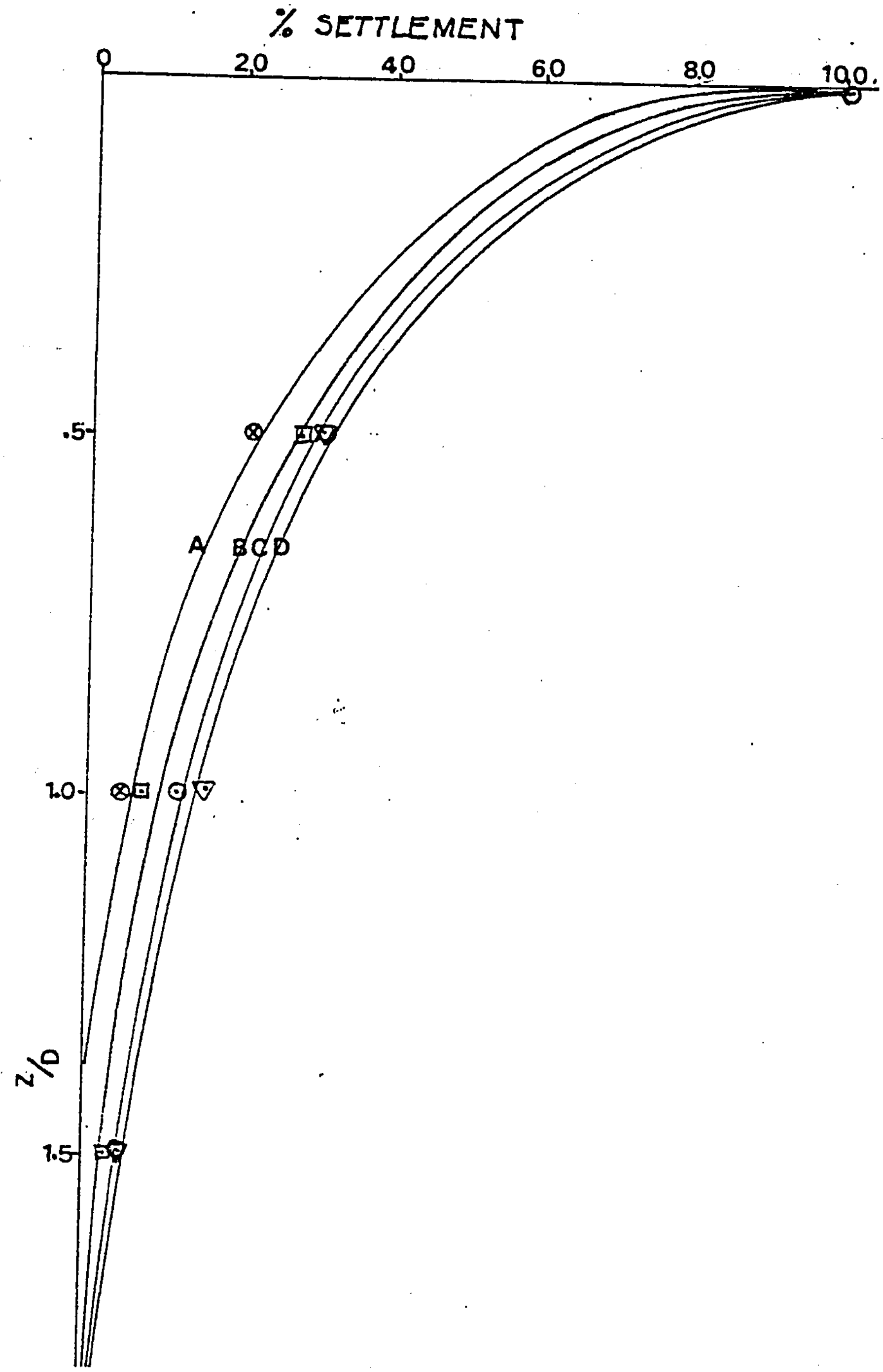

Code	q(kPa)	q/s_w
A	100	1.7
B	200	3.4
C	250	4.3
D	275	4.7

$s_w = 57.8$ (kPa)

FIGURE A9 DISTRIBUTIONS OF SETTLEMENT FOR PLATE V3/2

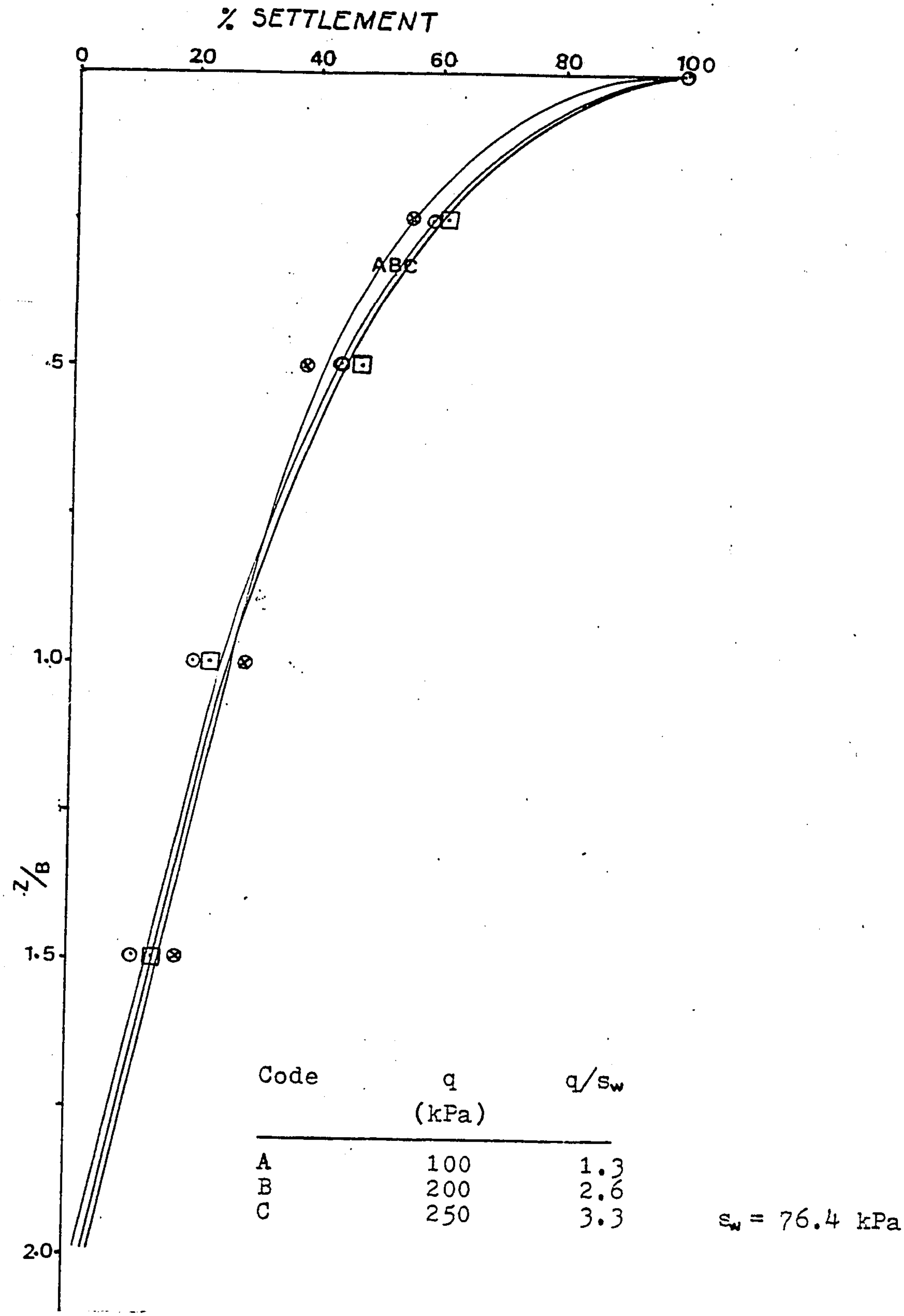

FIGURE A10 SETTLEMENT DISTRIBUTIONS FOR TEST FOOTING

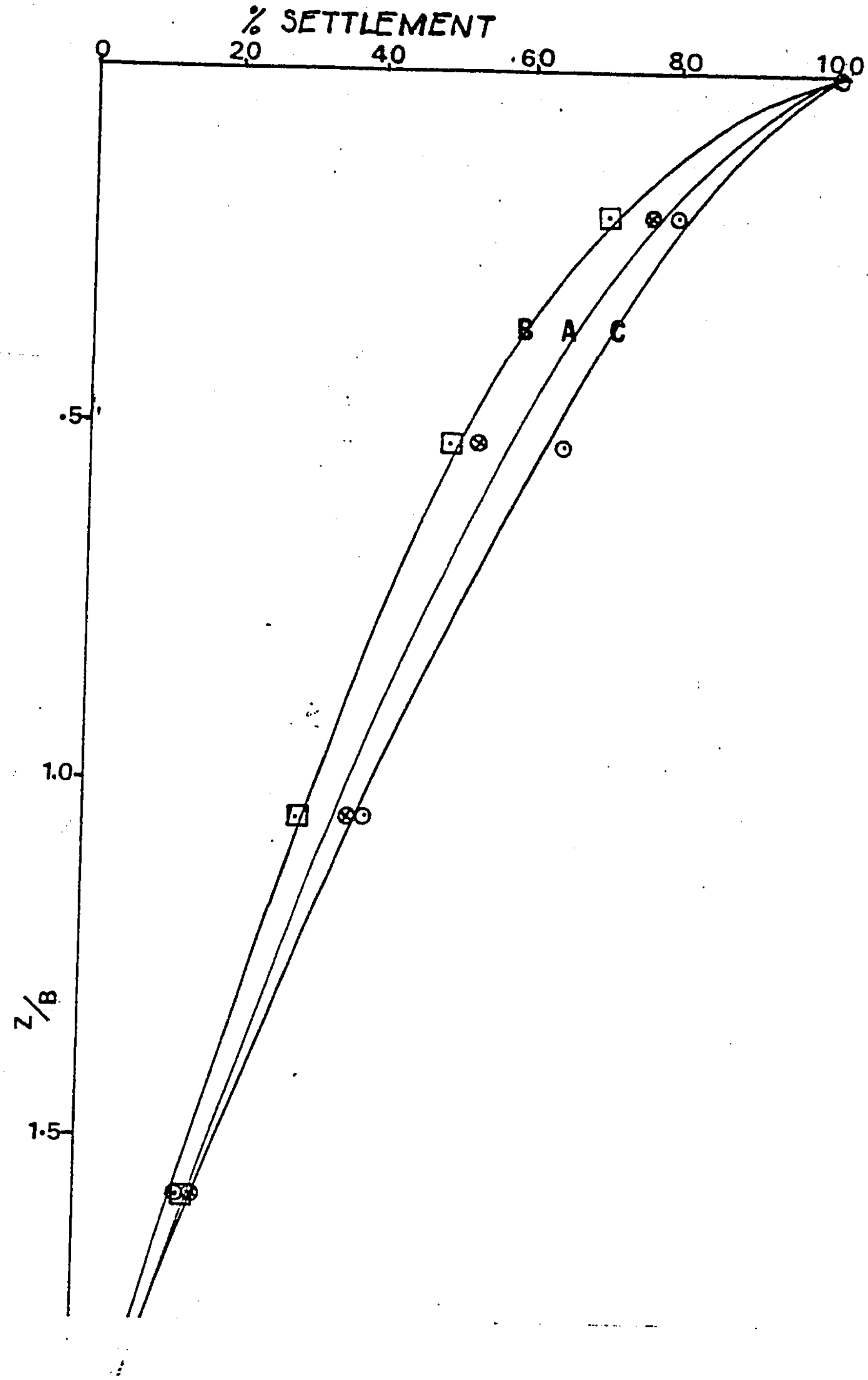

Code	q(kPa)	q/s_w
A	83	1.2
B	166	2.4
C	266	3.9

s_w = 69.6(kPa)

FIGURE A11 DISTRIBUTIONS OF SETTLEMENT FOR FOOTING M-17

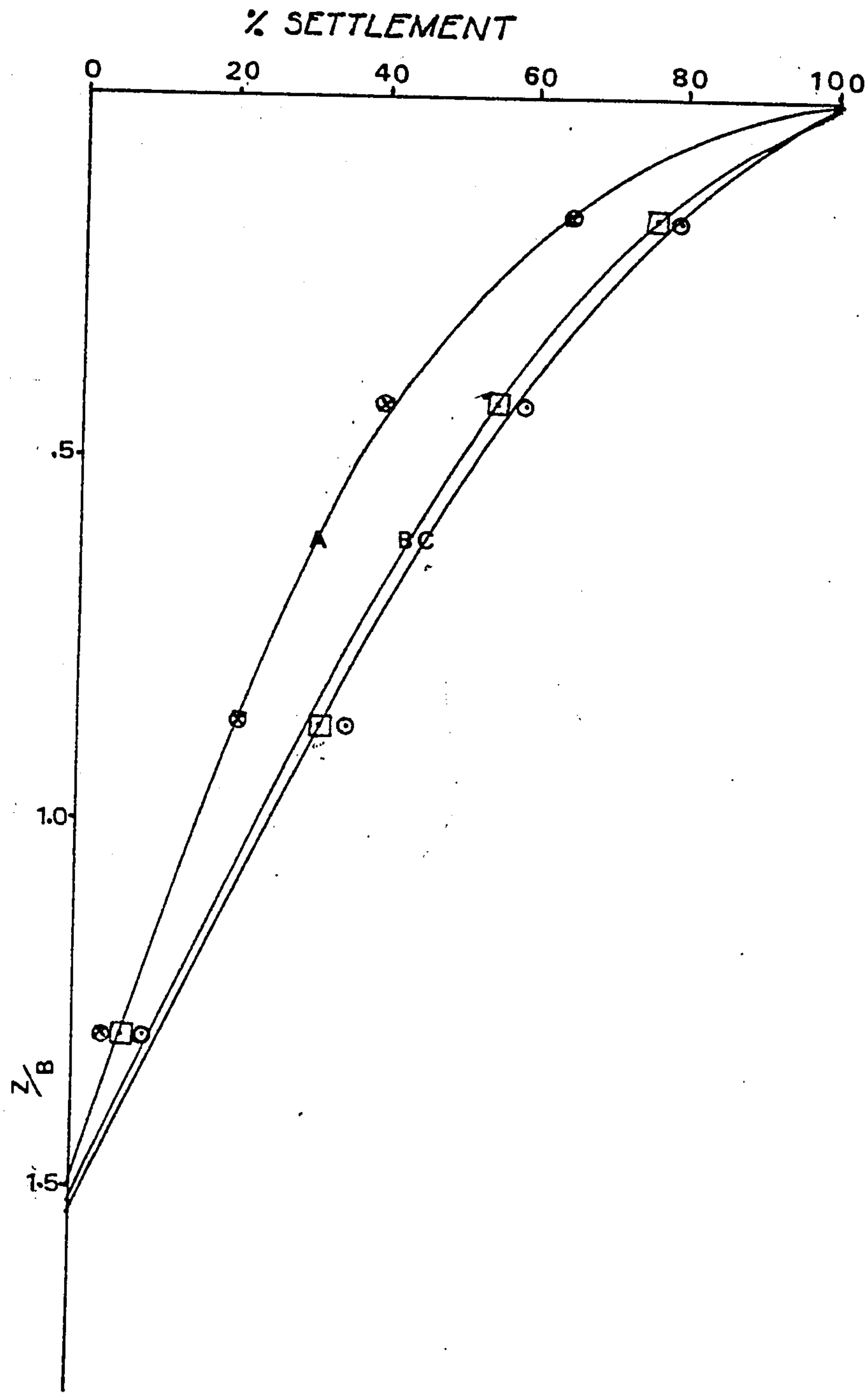

Code	q(kPa)	q/s_w
A	94	1.3
B	198	2.7
C	217	3.0

s_w = 69.6(kPa)

FIGURE A12 DISTRIBUTIONS OF SETTLEMENT FOR FOOTING 0-19

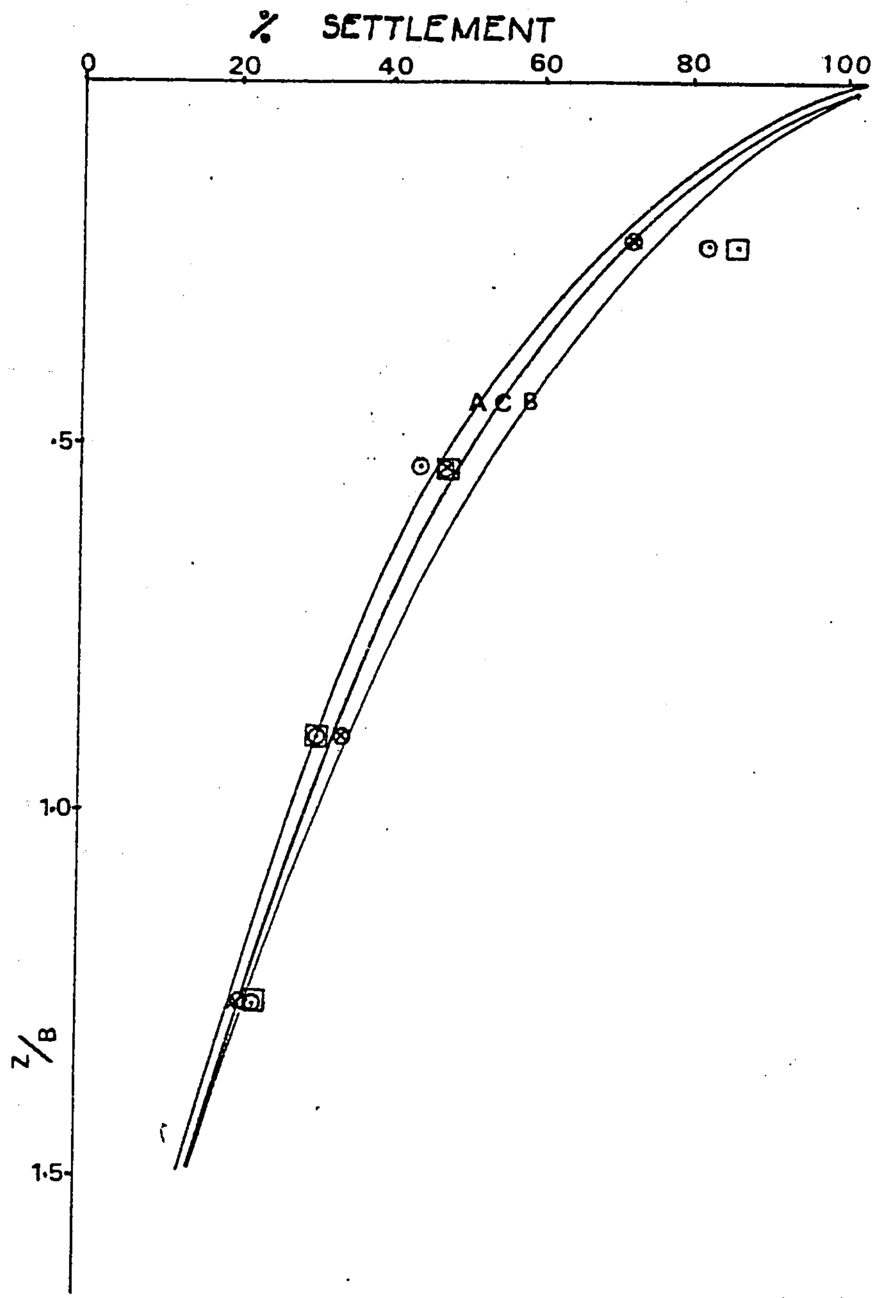

Code	q(kPa)	q/s_w
A	69	1.5
B	137	2.9
C	158	3.4

s_w = 46.1(kPa)

FIGURE A13 DISTRIBUTIONS OF SETTLEMENT FOR FOOTING CC-12

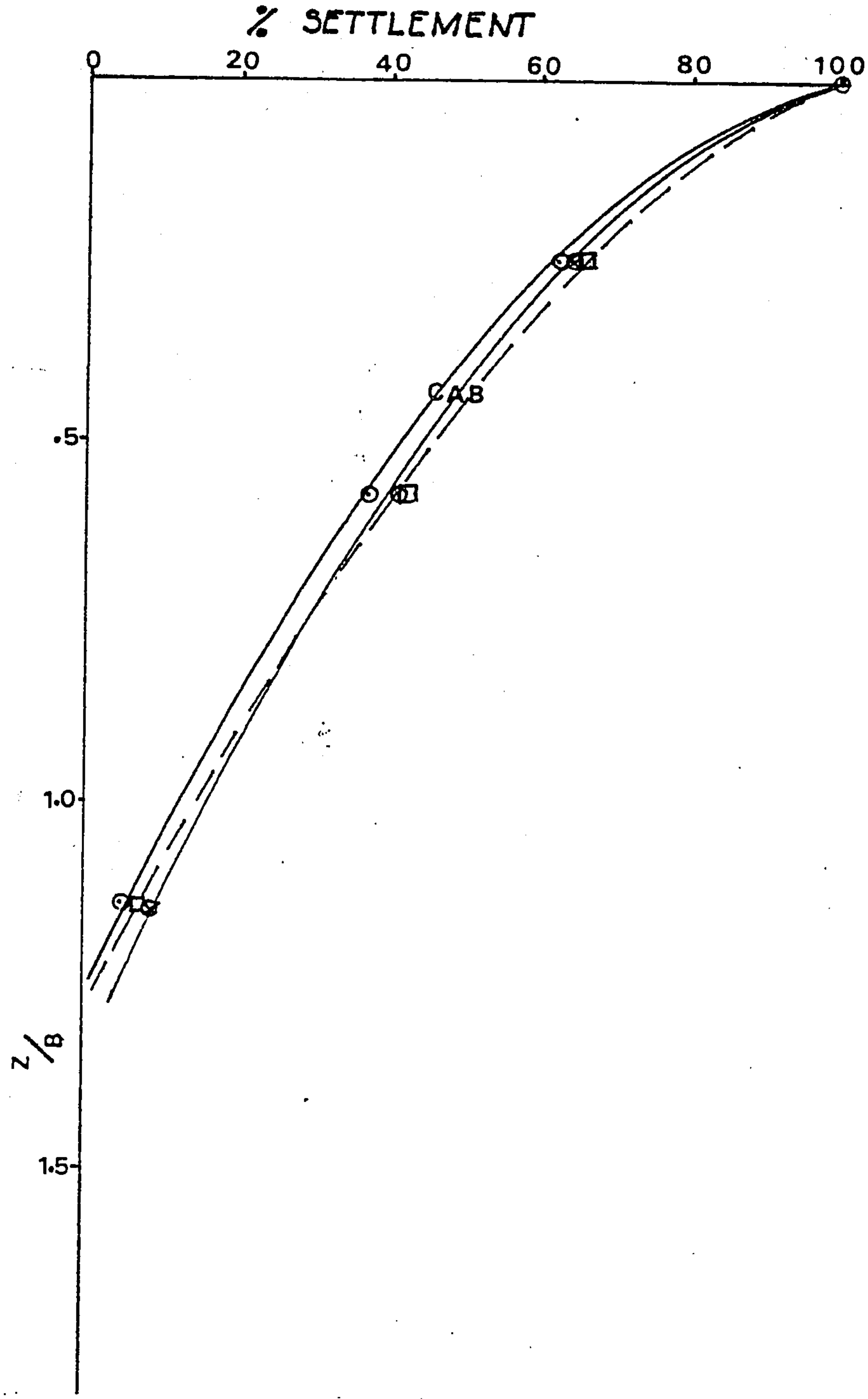

Code	q(kPa)	q/s_w
A	80	1.9
B	112	2.7
C	124	3.0

s_w = 42(kPa)

FIGURE A14 DISTRIBUTIONS OF SETTLEMENT FOR FOOTING EE-7

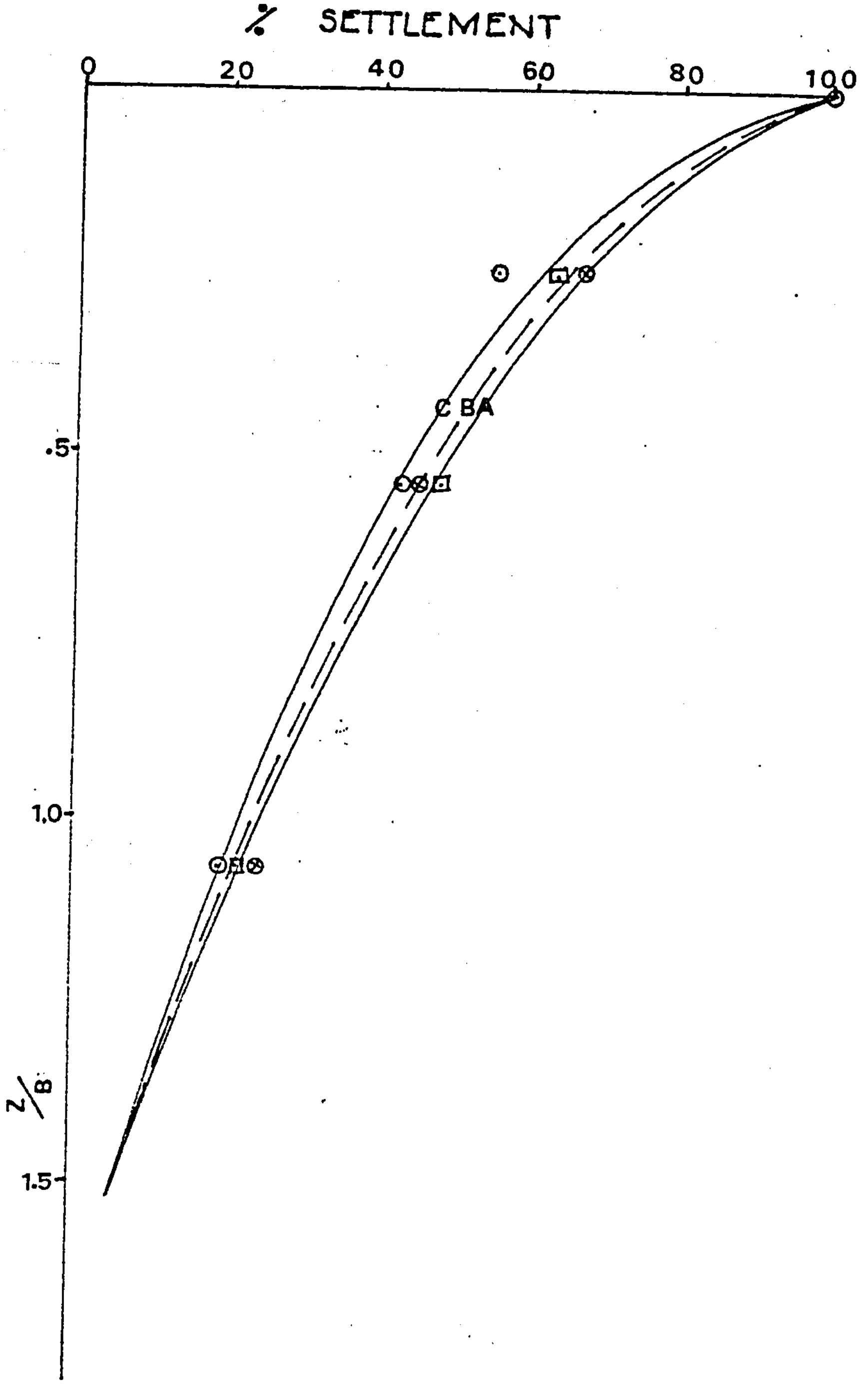

Code	q(kPa)	q/s_w
A	79	1.9
B	106	2.5
C	128	3.1

s_w=42(kPa)

FIGURE A15 DISTRIBUTIONS OF SETTLEMENT FOR FOOTING GG-8

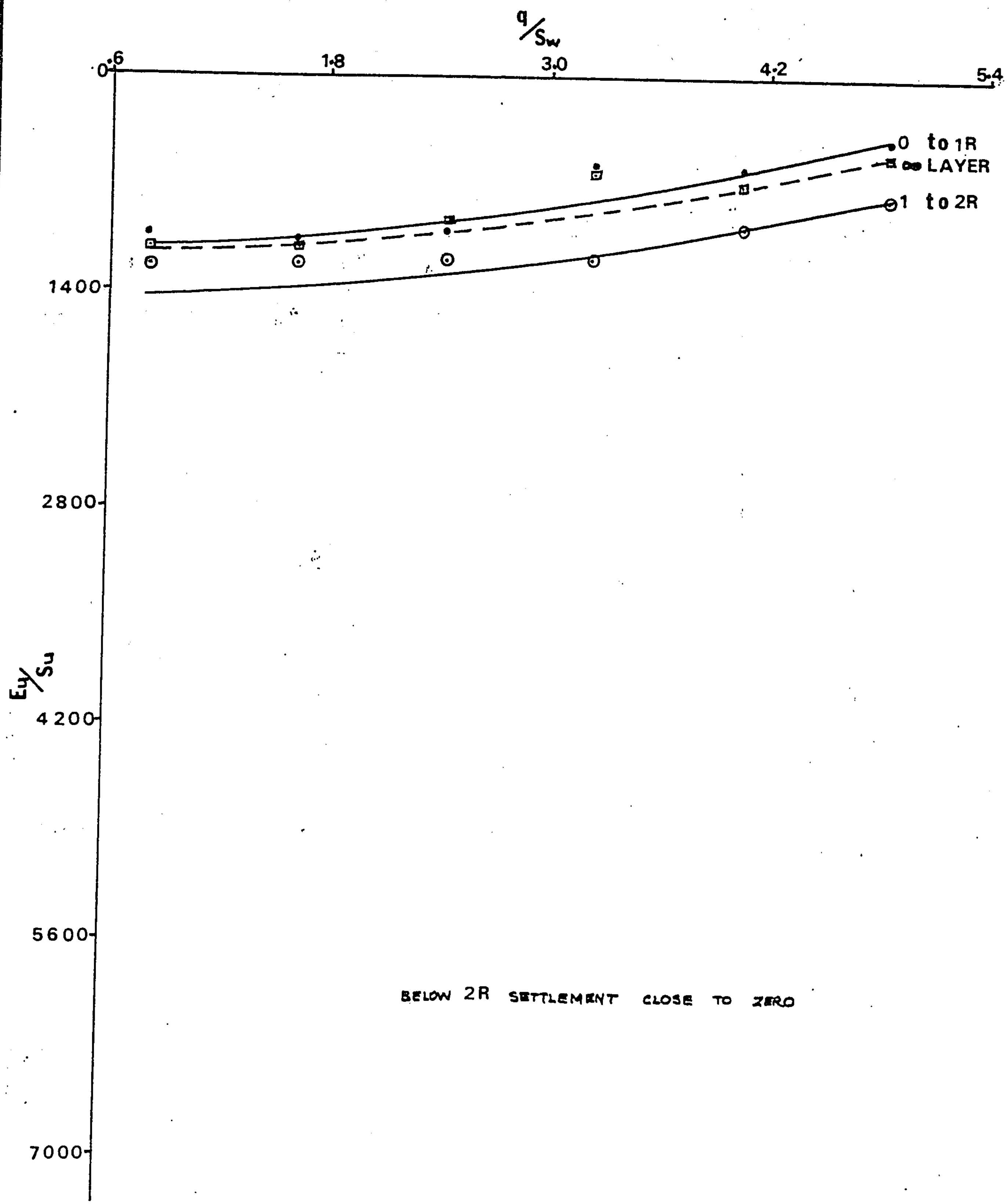

FIGURE A16 DISTRIBUTION OF E_u/S_u WITH q/S_w WITHIN SOIL LAYERS BELOW TEST PLATE V2/1 (Algonquin College), Based on Hanna's(1976) data

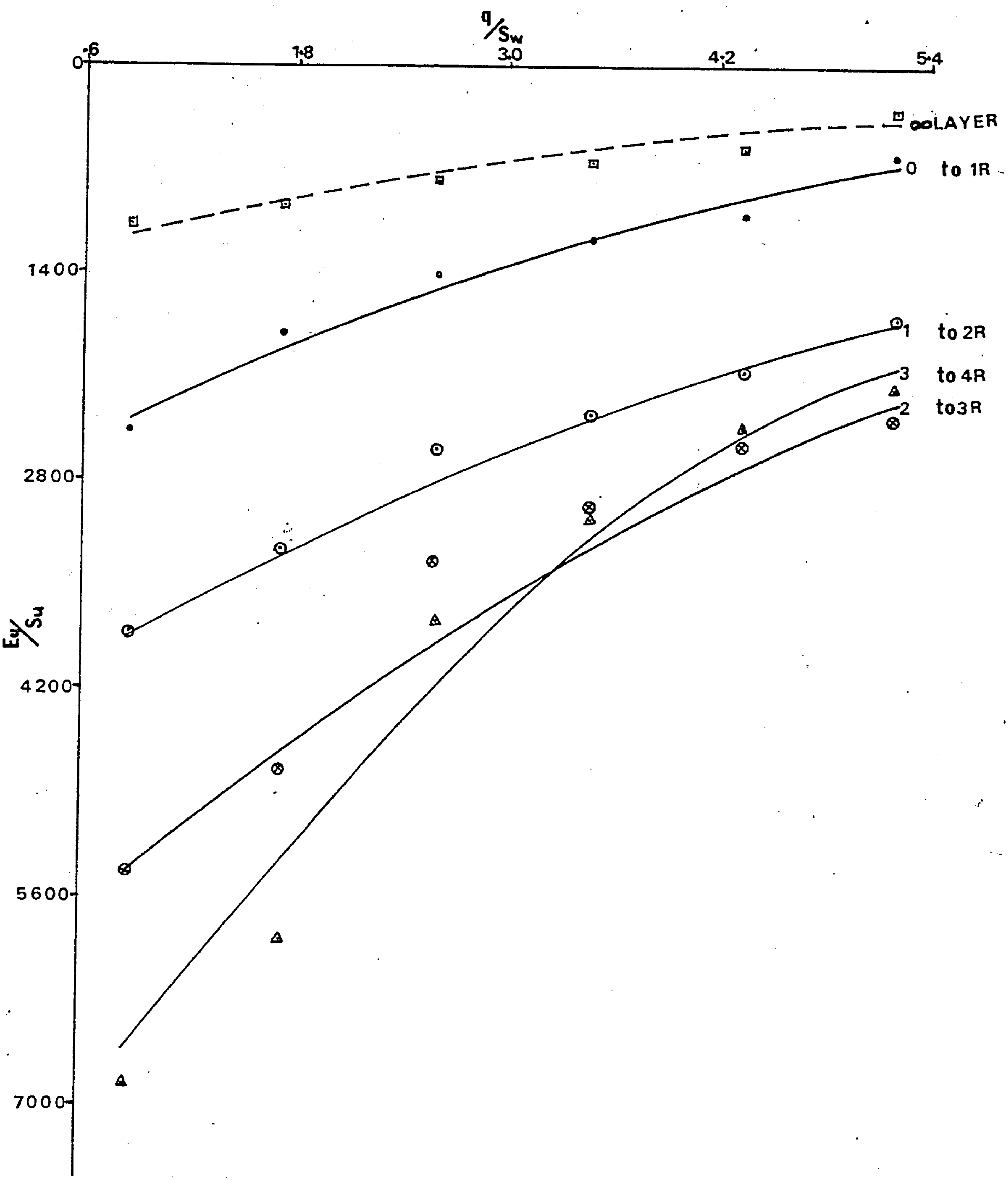

FIGURE A17 DISTRIBUTION OF E_u/S_u WITH q/S_w WITHIN SOIL LAYERS BELOW TEST PLATE V3/1 (Algonquin Colllege), Based on Hanna's (1976) data.

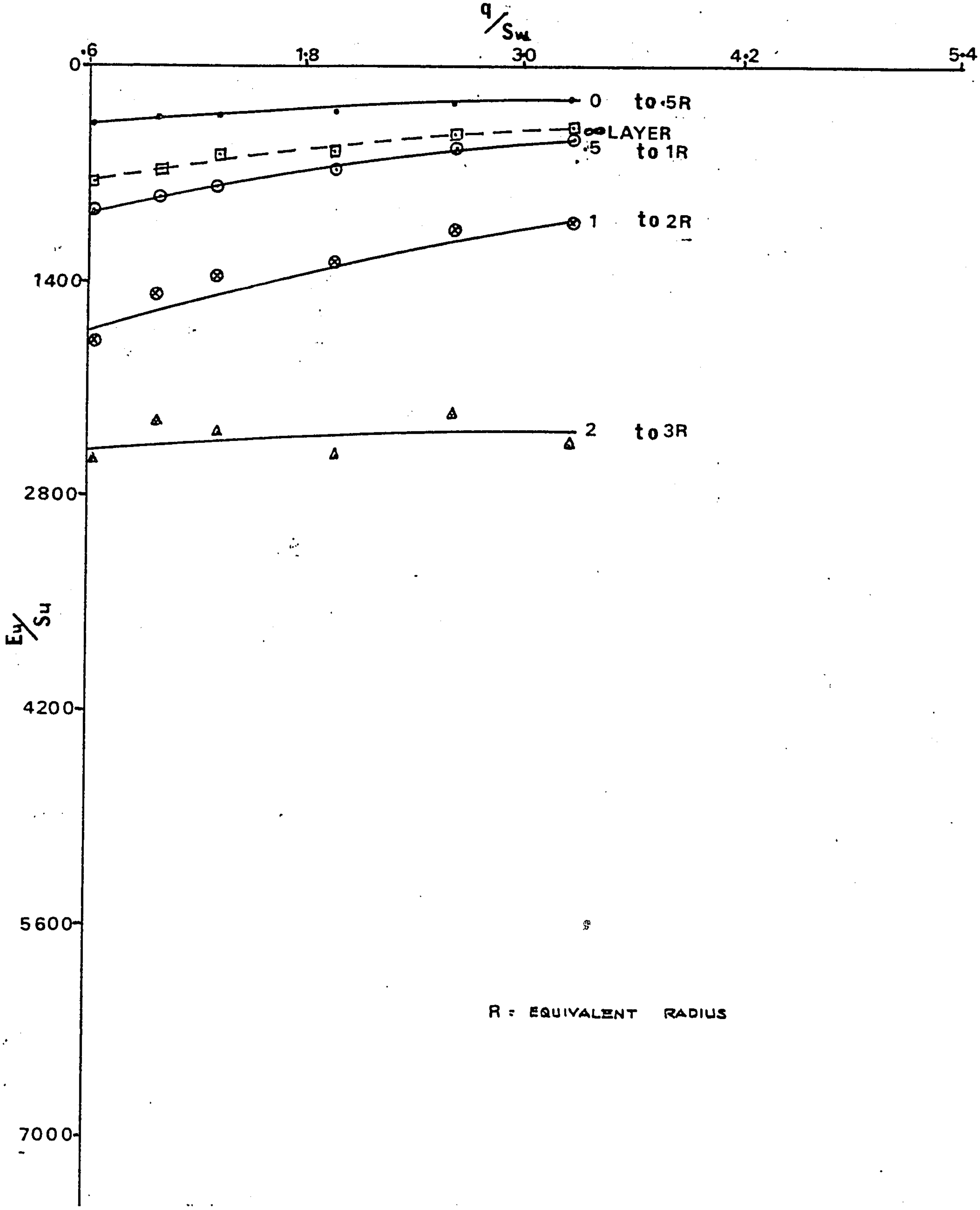

FIGURE A18 DISTRIBUTION OF E_u/S_u WITH q/S_w WITHIN SOIL LAYERS BELOW TEST FOOTING (Algonquin College)

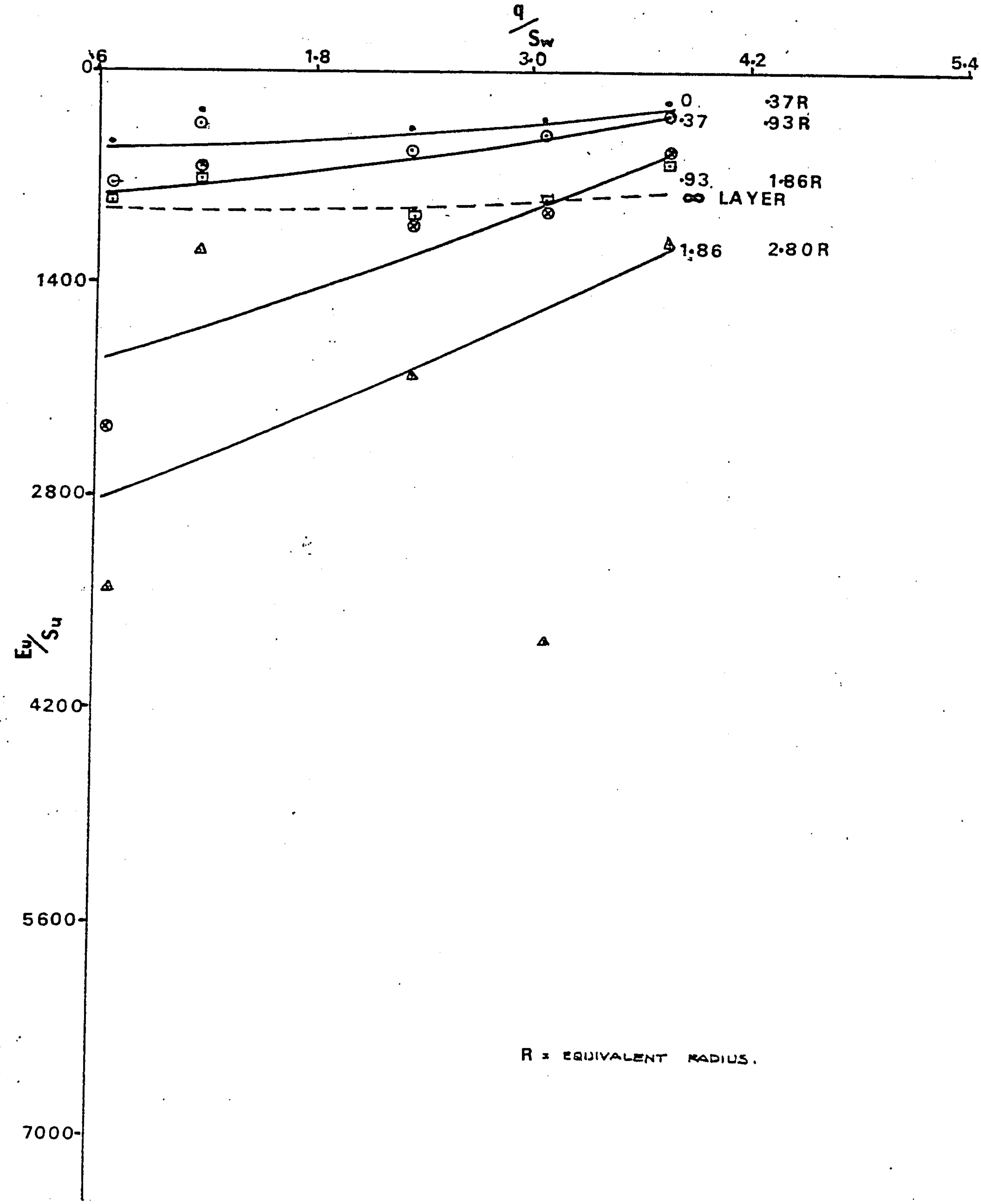

FIGURE A19 DISTRIBUTION OF Eu/Su WITH q/Sw WITHIN SOIL LAYERS BELOW FOOTING M-17. (Algonquin Colllege)

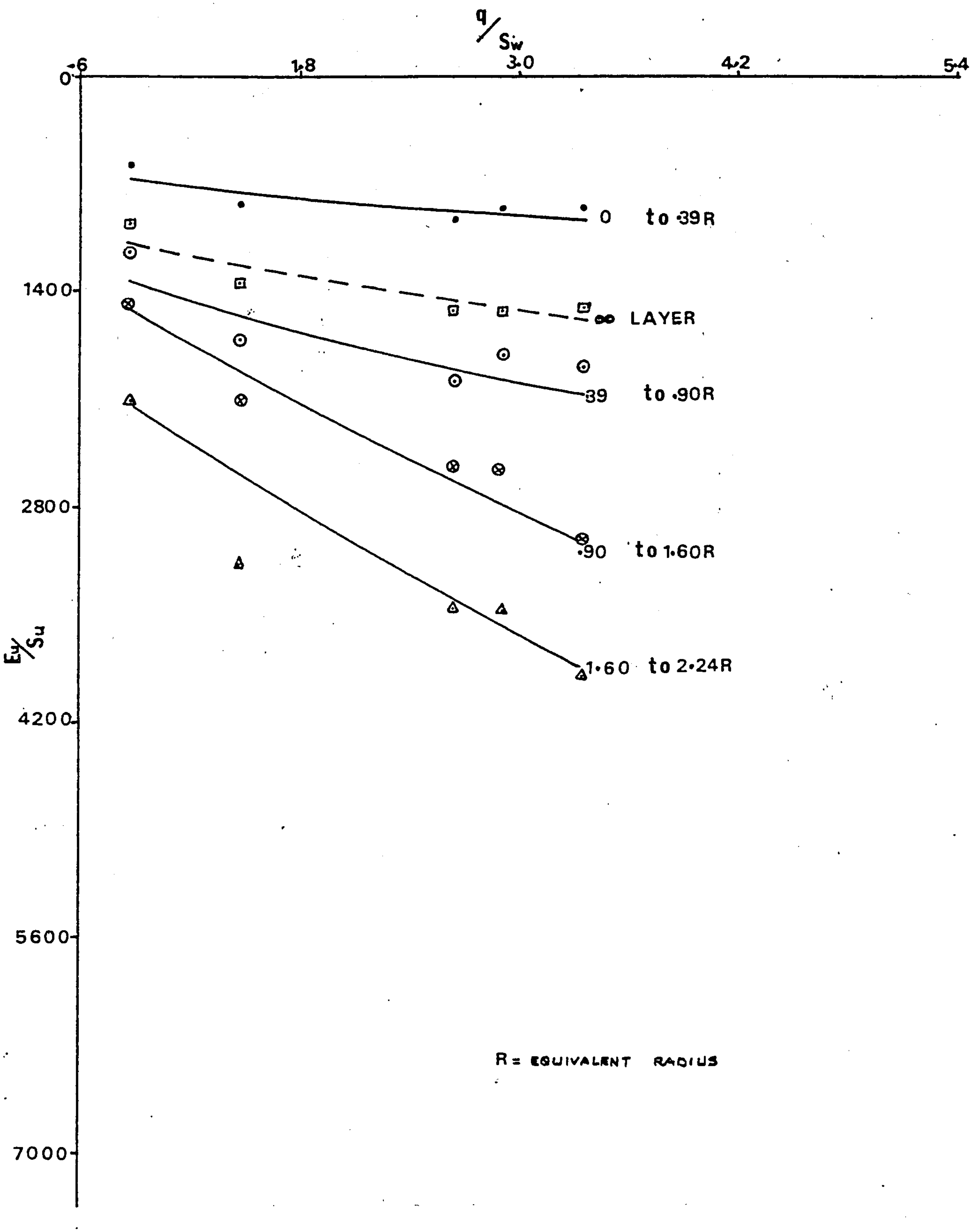

FIGURE A20 DISTRIBUTION OF E_u/S_u WITH q/S_w WITHIN SOIL LAYERS BELOW FOOTING CC-12. (Algonquin College)

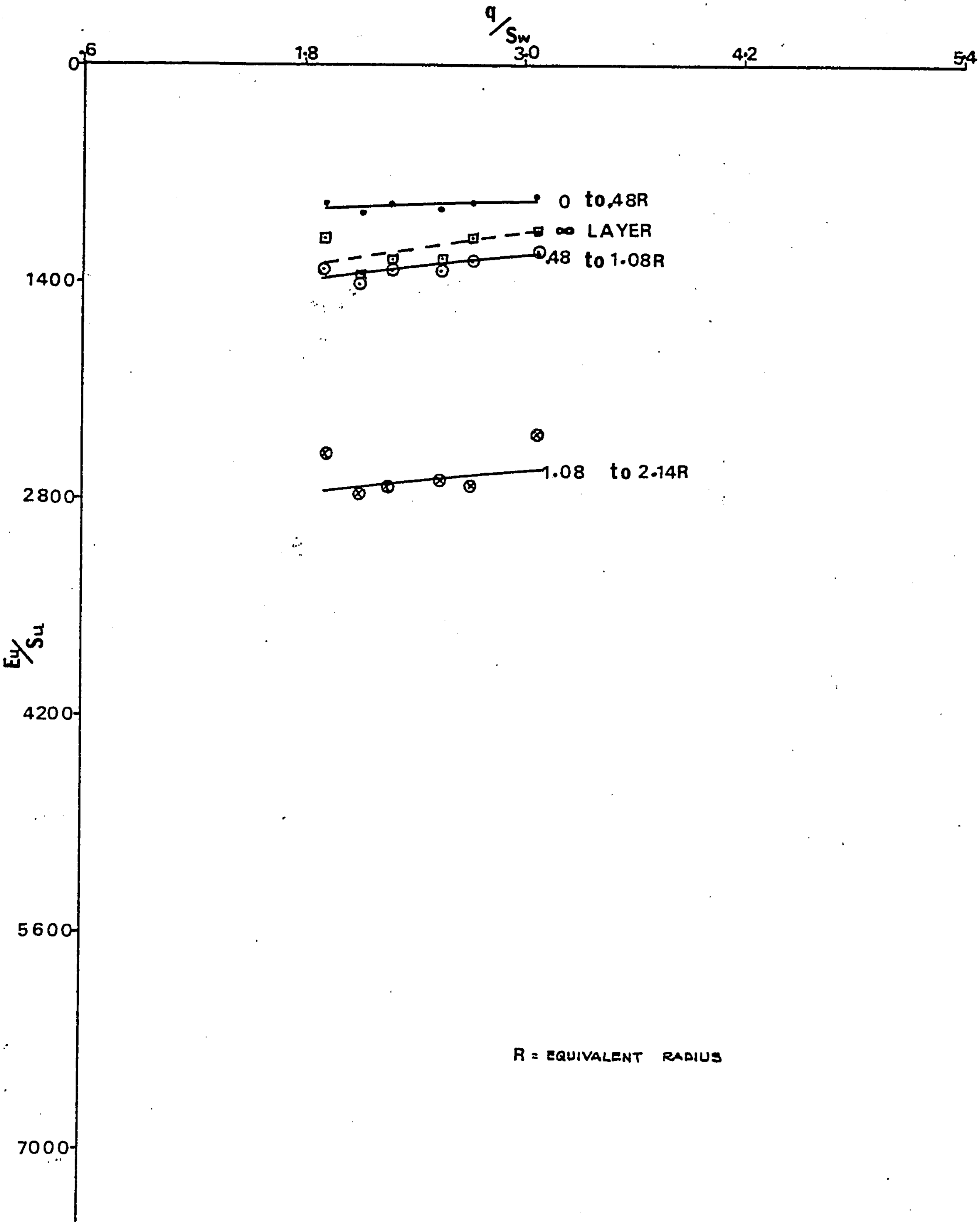

FIGURE A21 DISTRIBUTION OF E_u/S_u WITH q/S_w WITHIN SOIL LAYERS BELOW FOOTING GG-8 (Algonquin College), Based on Hanna's (1976) data.

APPENDIX B

LABORATORY TEST RESULTS

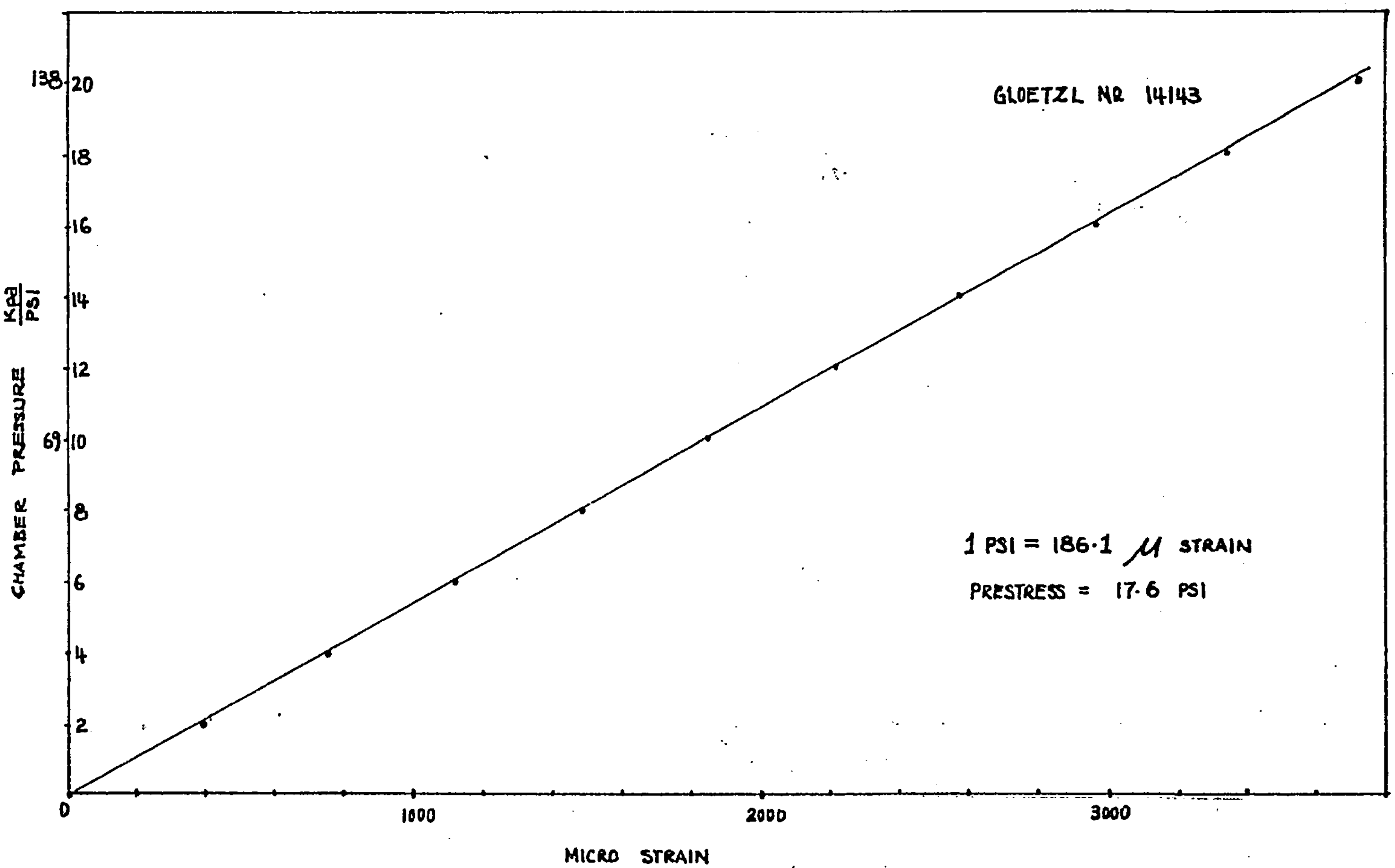

FIGURE: B1 CALIBRATION OF LOAD CELL NO. 1

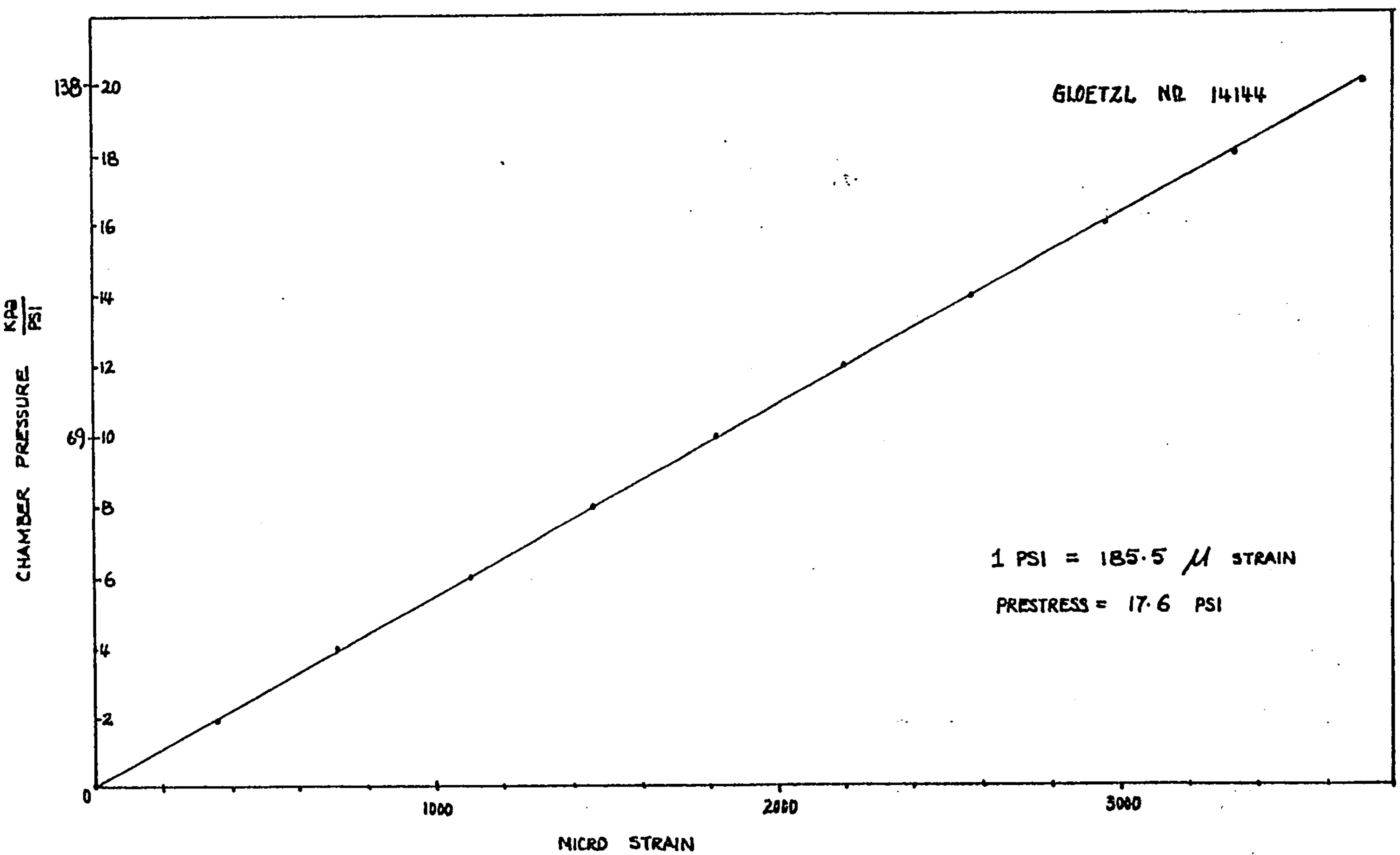

FIGURE: B2 CALIBRATION OF LOAD CELL NO. 2

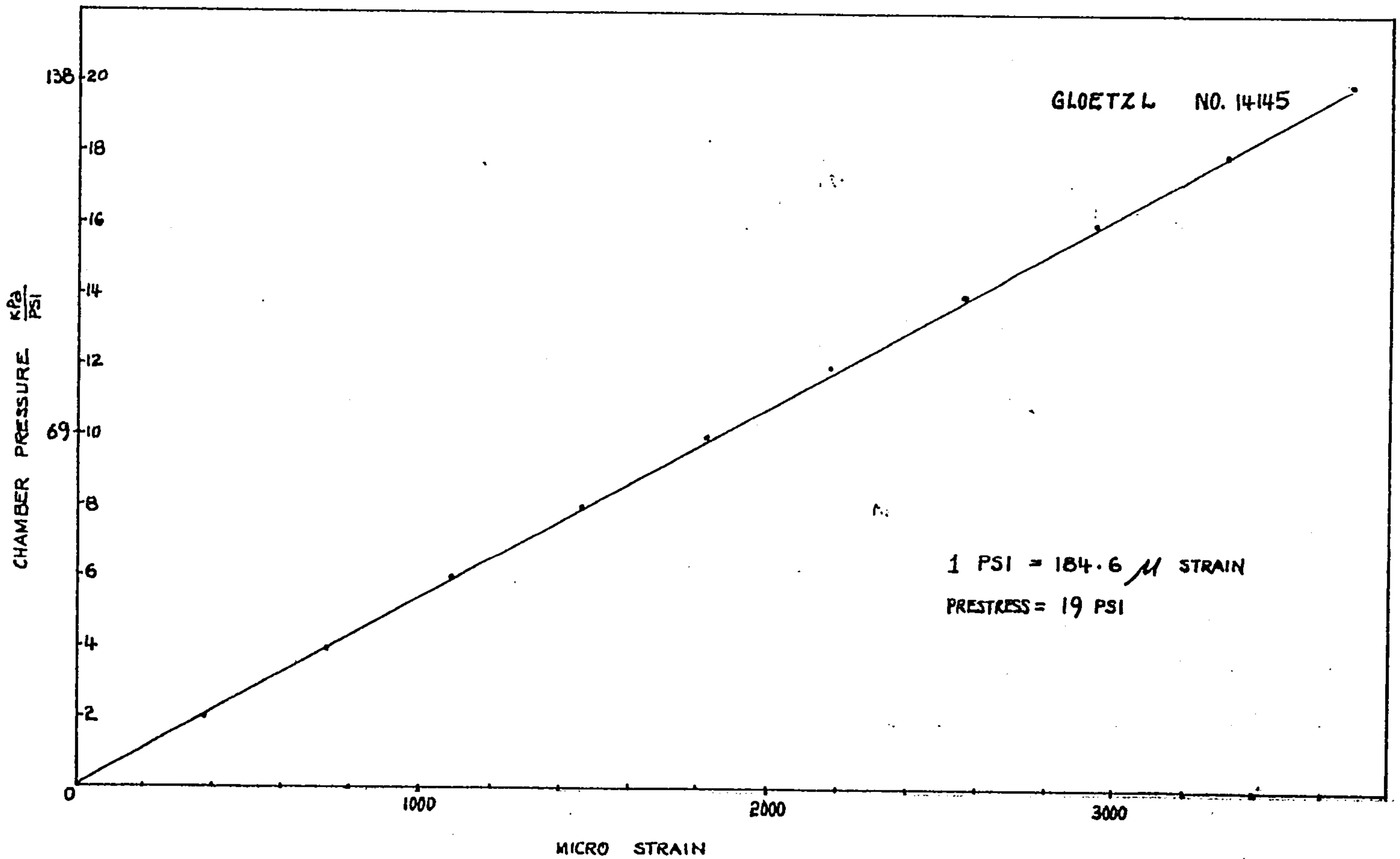

FIGURE: B3 CALIBRATION OF LOAD CELL NO. 3

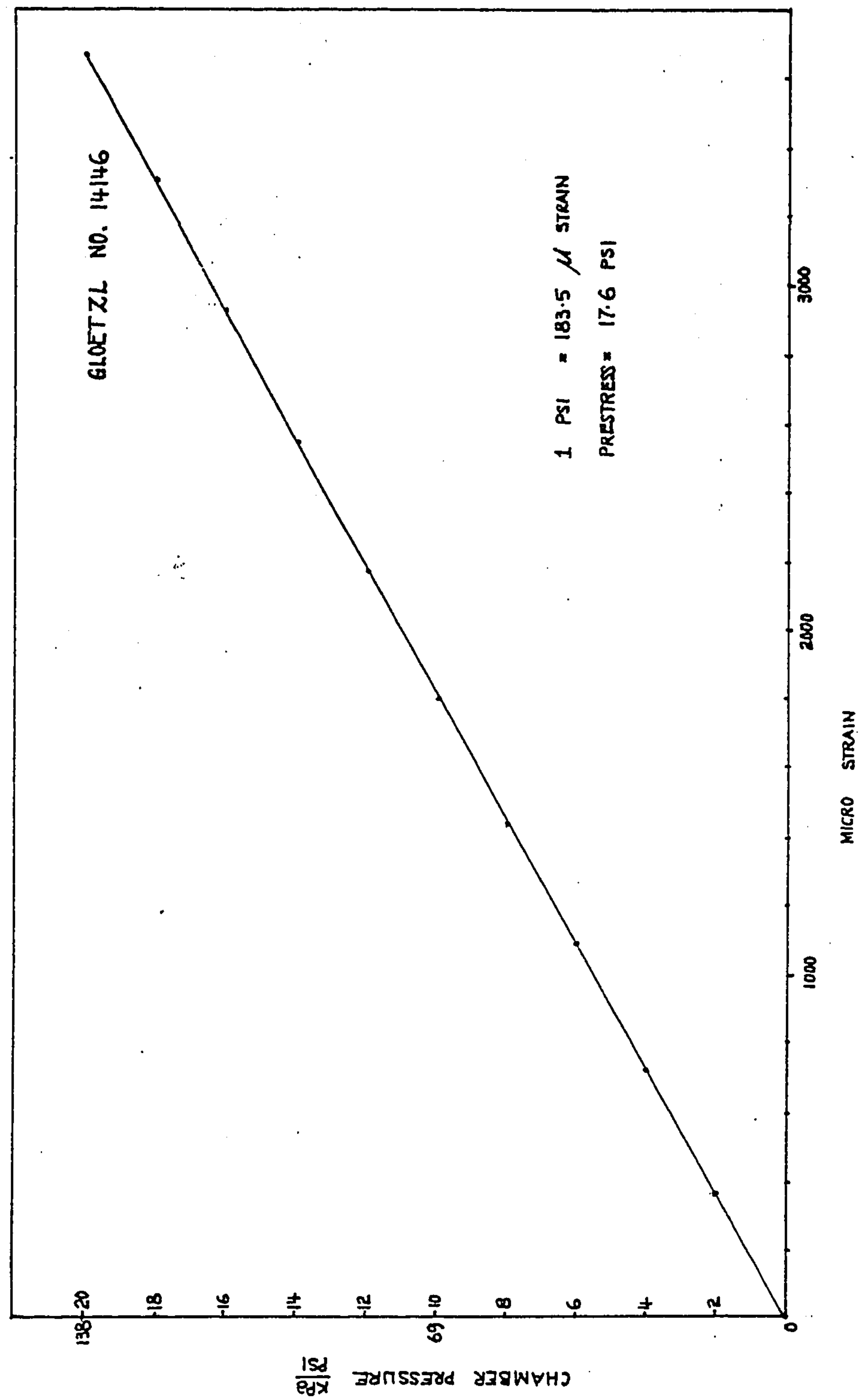

FIGURE: B4 CALIBRATION OF LOAD CELL NO. 4

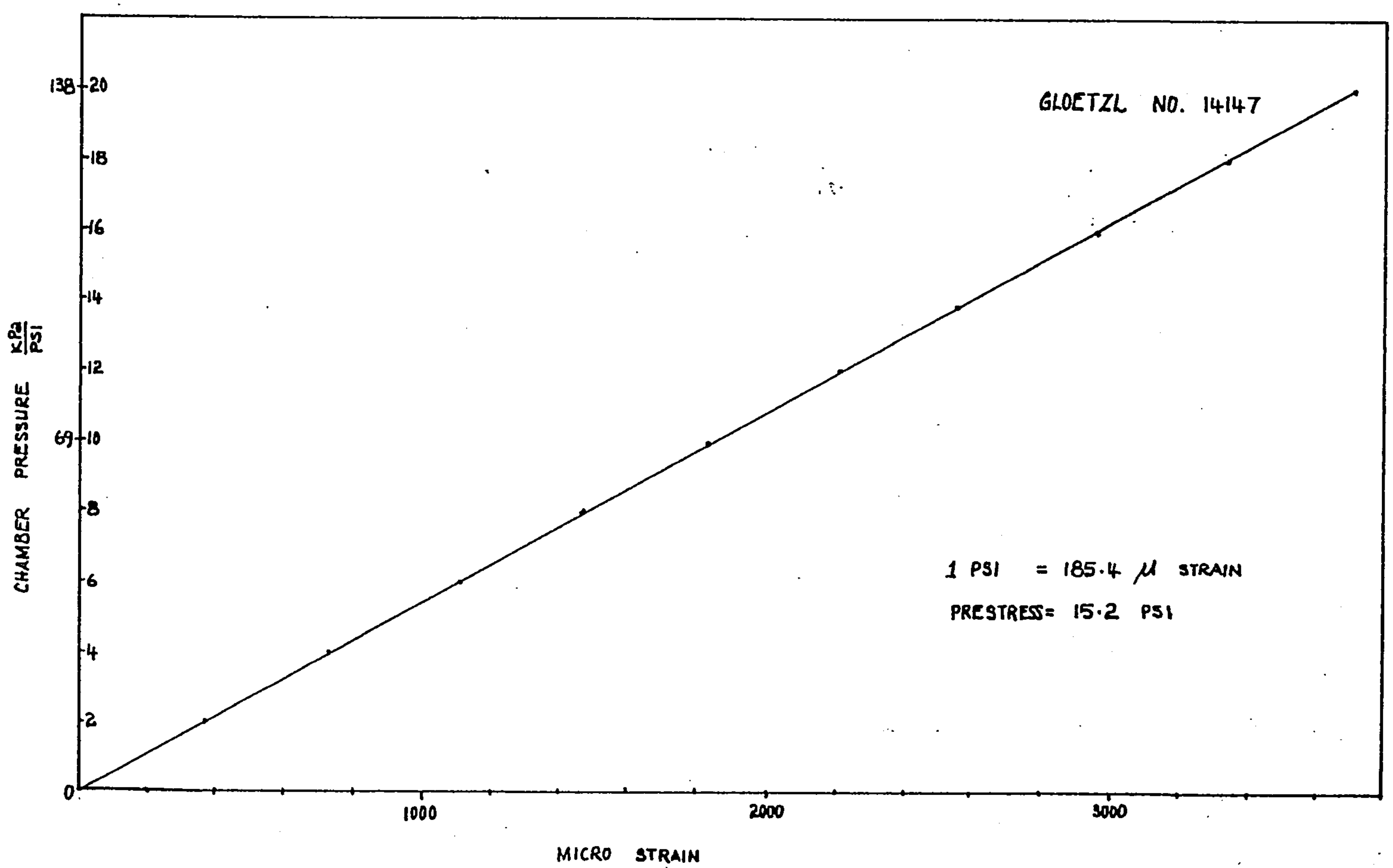

FIGURE: B5 CALIBRATION OF LOAD CELL NO.5

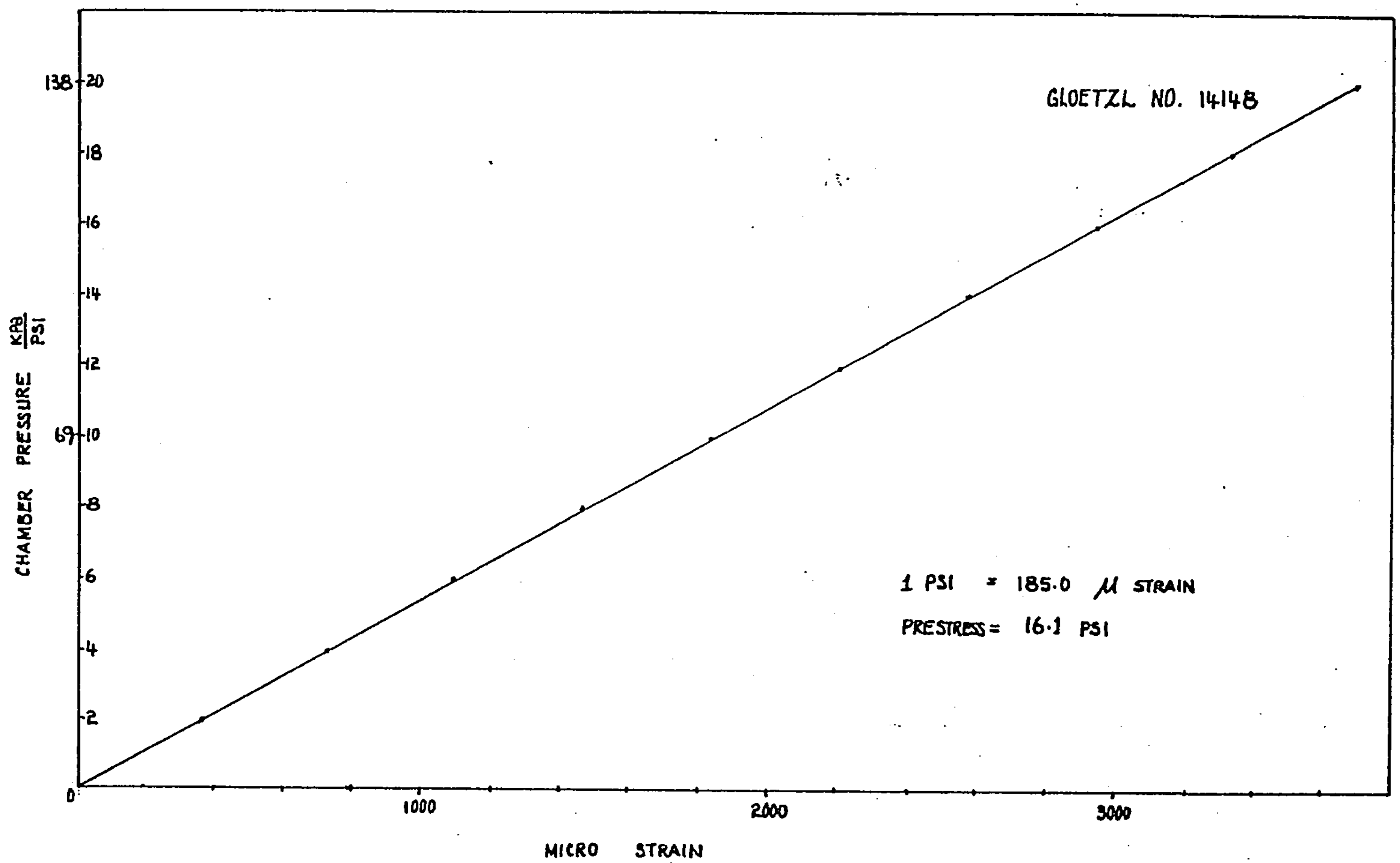

FIGURE: B6 CALIBRATION OF LOAD CELL NO. 6

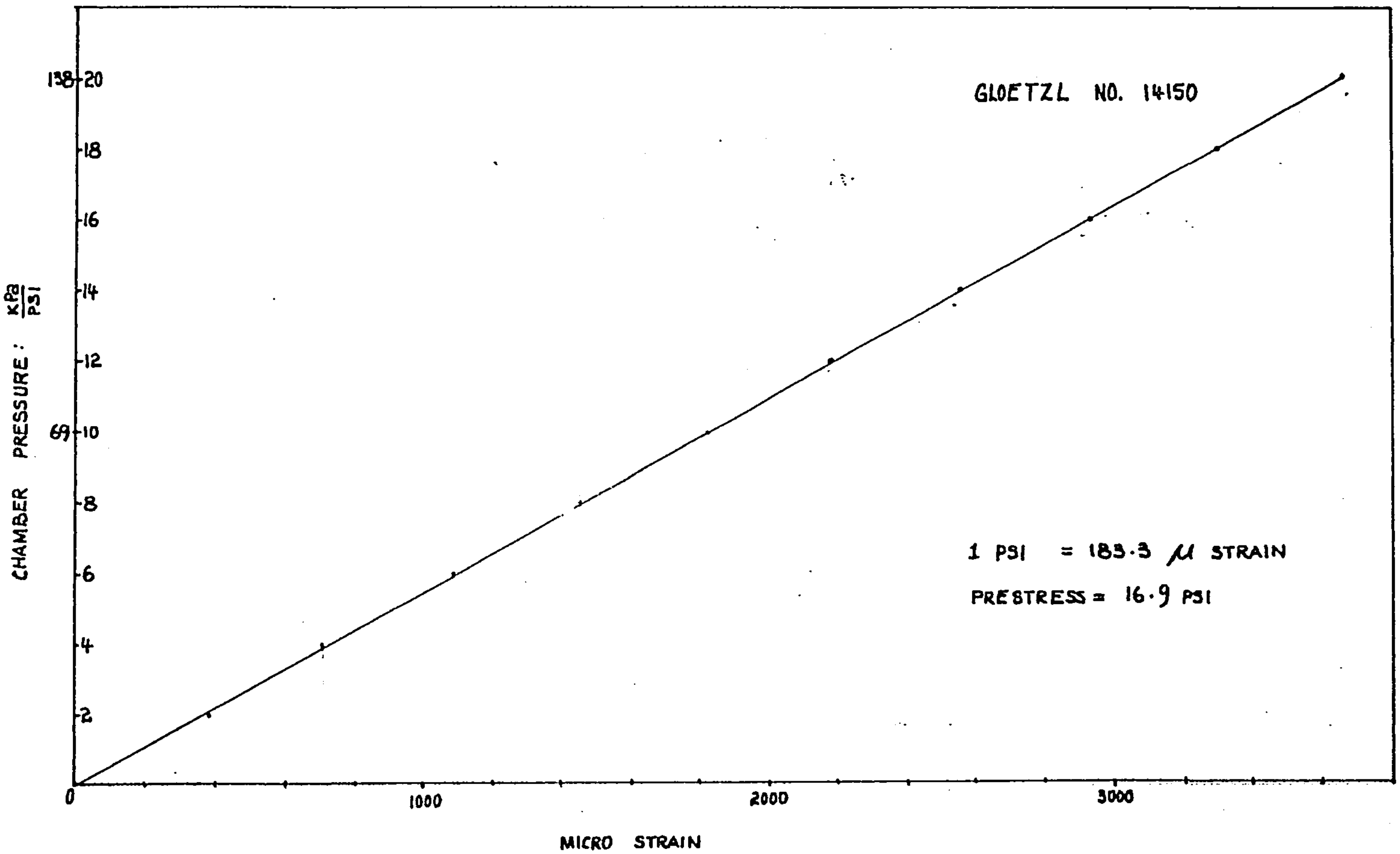

FIGURE: B7 CALIBRATION OF LOAD CELL NO. 7

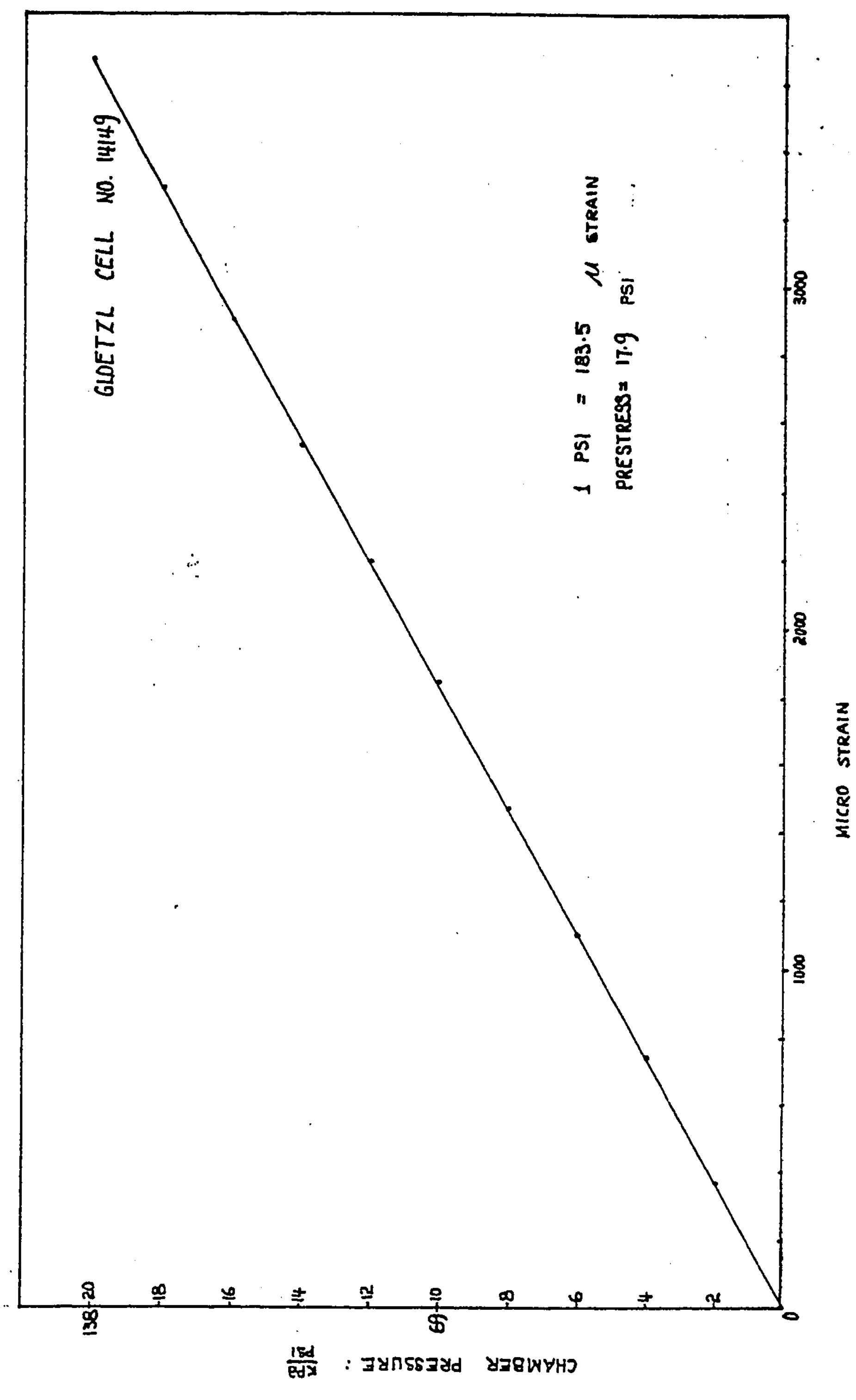

FIGURE: B8 CALIBRATION OF LOAD CELL NO. 8

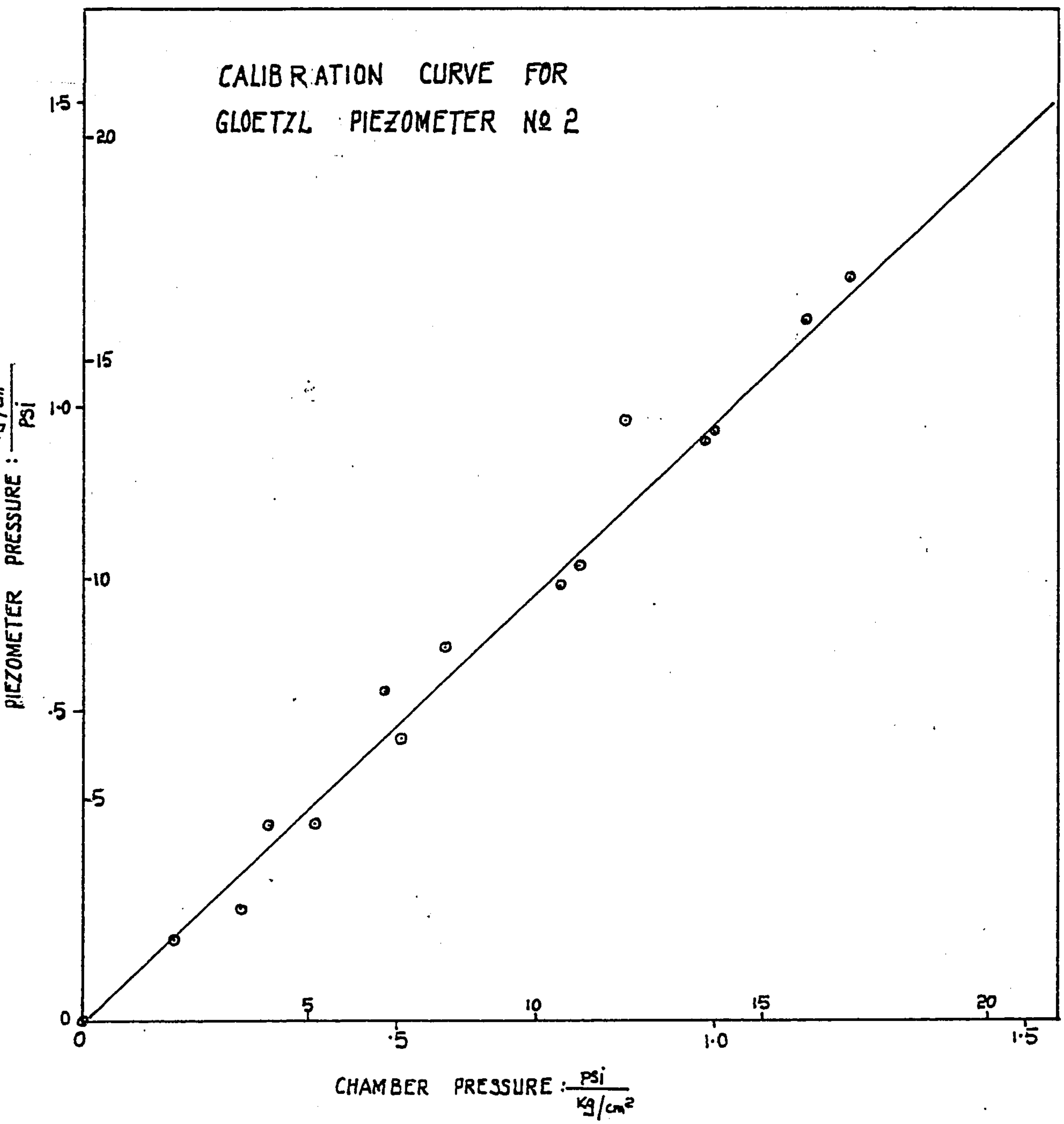
CALIBRATION CURVE FOR
GLOETZL PIEZOMETER No 2
PIEZOMETER PRESSURE : Kg/cm²
psi
1·5
20
15
1·0
10
·5
5
0
CHAMBER PRESSURE : psi
Kg/cm²
0
5
·5
10
15
1·0
20
1·5

FIGURE: B9

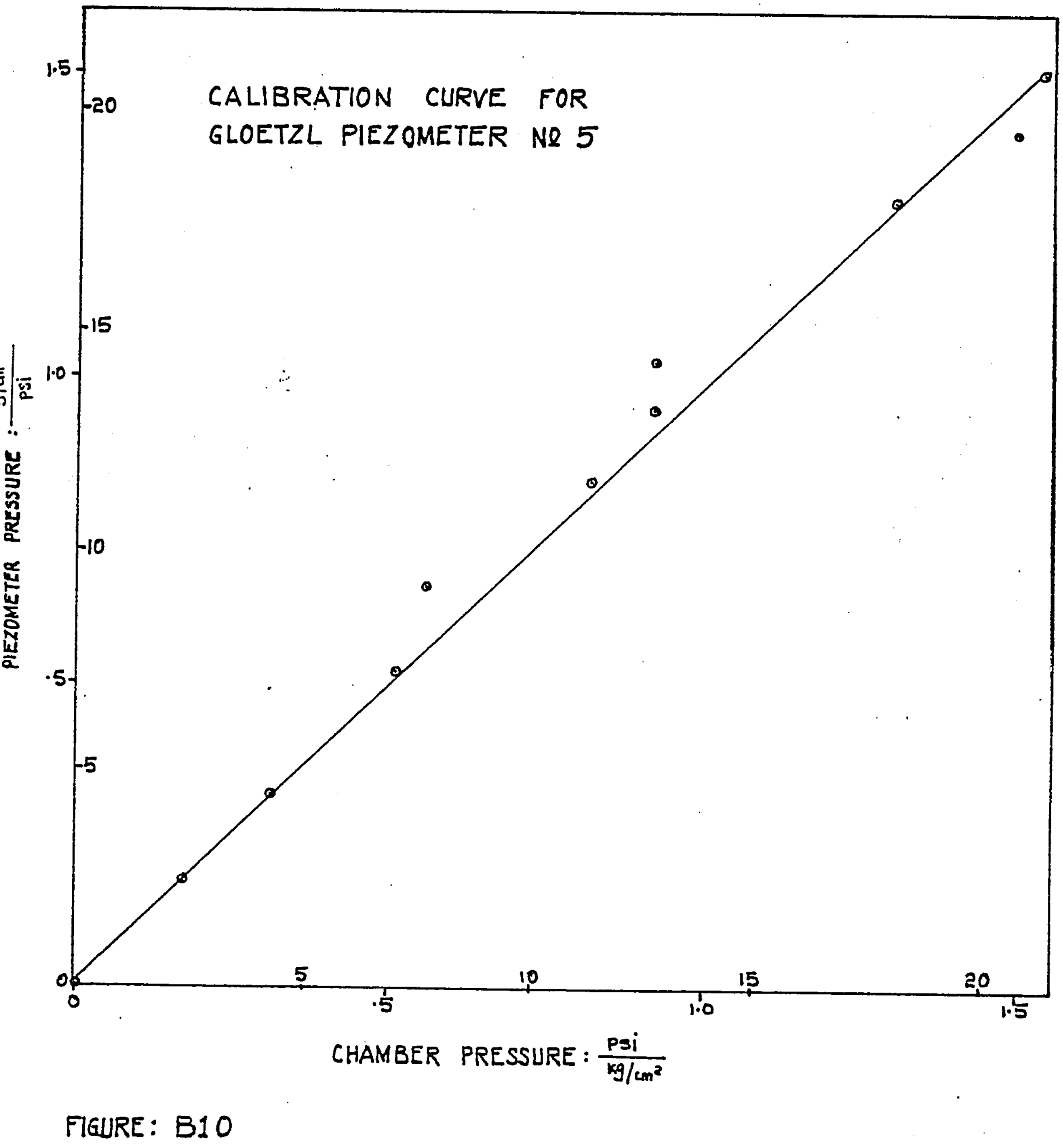
CALIBRATION CURVE FOR
GLOETZL PIEZOMETER NO 5
PIEZOMETER PRESSURE : Kg/cm² / psi
CHAMBER PRESSURE : psi / Kg/cm²
0
·5
1·0
1·5
5
10
15
20

FIGURE: B10

Date 1976	No. of Wagon Loads	Cumulative	Percent Moisture of Hay	Weights (kg)	
				Wagon No	Tare + Load
Jun. 23	7	7	46.0	1	5736
24	7	14	45.0		4909
25	4	18	44.5		5168
26	6	24	44.0		5282
28	13	37	40.6		4382
29	15	52	35.6		4591
30	5	57	*52.2		5341
Jul. 2	1	58	*60.0		4955
5	21	79	30.5		
6	19	98	35.3	2	4882
7	18	116			4818
8	4	120			4282
9	14	134			4768
10	10	144			5055
15	13	157	Loading Stopped Temporarily		4818
					5227
Aug. 17		Unloading Started			
27	28			3	4909
Sep. 3	2				4350
4	1				5473
10	6				4182
Oct. 4	4				5646
28	33	Silo Full			6736

Average Weights

Wagon No.	No. of Times Weighed	Tare		Average Load		Remarks
		kg	lbs	kg	kg	
1	8	2113	4650	2880	6335	To find tonnage in silo, W from total number of wagon loads, N, proceed as follows:
2	7	2136	4700	2700	5939	
3	6	2136	4700	3063	6738	

$$W = \frac{N}{21x1000}(2880x8+2700x7+3063x6)$$

$$W = 2.87\ N \text{ (metric tonnes)}$$

TABLE B-11 Loading Record

CIU TEST SUMMARY

Sample No.	Depth (m)	w%	Density kg/m^3	σ_3 kg/cm^2	ε_f%	$(\Delta u)_f$ kg/cm^2	$(\sigma_1-\sigma_3)_f$	A_f	Modulus kg/cm^2 1/3 Pt.	Modulus kg/cm^2 1/2 Pt.	
197-1-3	1.73	39.5	1,800	.283	5.0	.070	.787	-0.27	104	87	
197-1-12	2.23	34.9	1,900	.278	2.4	.092	.730	-0.26	120	92	
197-2-2	2.64	38.2	1,900	.309	1.5	.152	.822	-0.19	245	164	
197-2-11	3.15	41.6	1,780	.341	.76	.172	.736	-0.23	250	230	
197-3-2	3.56	40.4	1,790	.368	2.0	.190	.742	-0.24	200	78	
197-3-11	4.06	41.5	1,780	.393	1.7	.210	.696	-0.26	192	139	
197-4-2	4.47	43.2	1,780	.416	.6	.220	.772	-0.25	311	283	
197-4-4	4.98	45.4	1,740	.457	.7	.220	.830	-0.29	280	244	
197-5-2	5.39	48.4	1,740	.470	.96	.256	.800	-0.27	192	190	
197-5-11	5.89	45.9	1,750	.502	1.1	.262	.662	-0.36	157	151	
197-6-1	6.20	48.3	1,760	.515	1.45	.290	.700	-0.32	230	167	
197-7-3	7.83	53.1	1,730	.605	1.0	.340	.890	-0.30	200	194	
197-8-10	9.76	52.9	1,720	.722	2.2	.930	.859	-0.34	171	154	
									199	167	Average Modulus

Note: ε_f = strain at failure

Depths shown are from original ground surface.

$$A_f = \frac{(\Delta u - \sigma_3)_f}{(\sigma_1 - \sigma_3)_f}$$

TABLE B-12

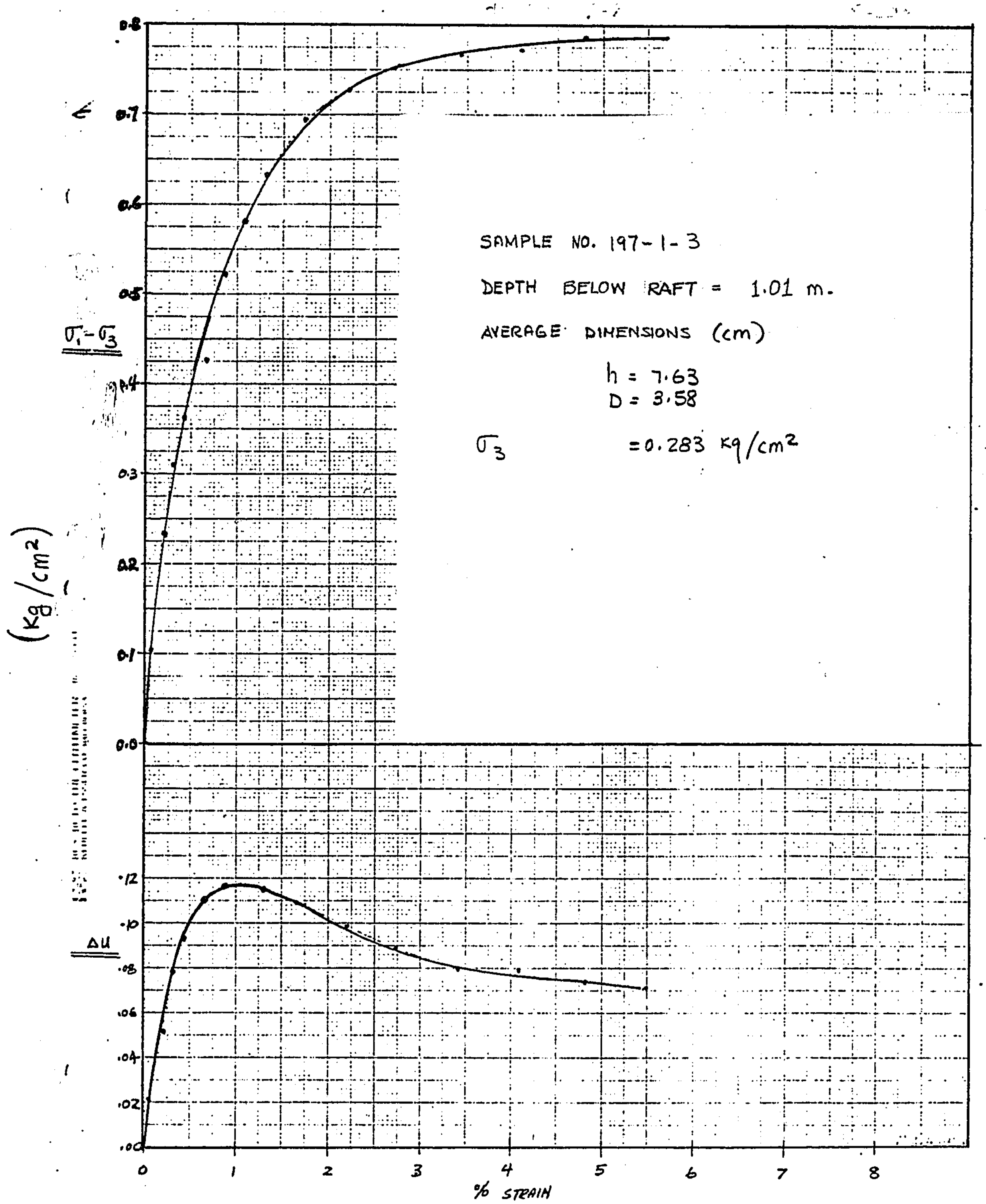
SAMPLE NO. 197-1-3
DEPTH BELOW RAFT = 1.01 m.
AVERAGE DIMENSIONS (cm)
h = 7.63
D = 3.58
σ3 =0.283 kg/cm²
σ1-σ3
(kg/cm²)
ΔU
0.8
0.7
0.6
0.5
0.4
0.3
0.2
0.1
0.0
.12
.10
.08
.06
.04
.02
.00
0
1
2
3
4
5
6
7
8
% STRAIN

FIGURE B-13

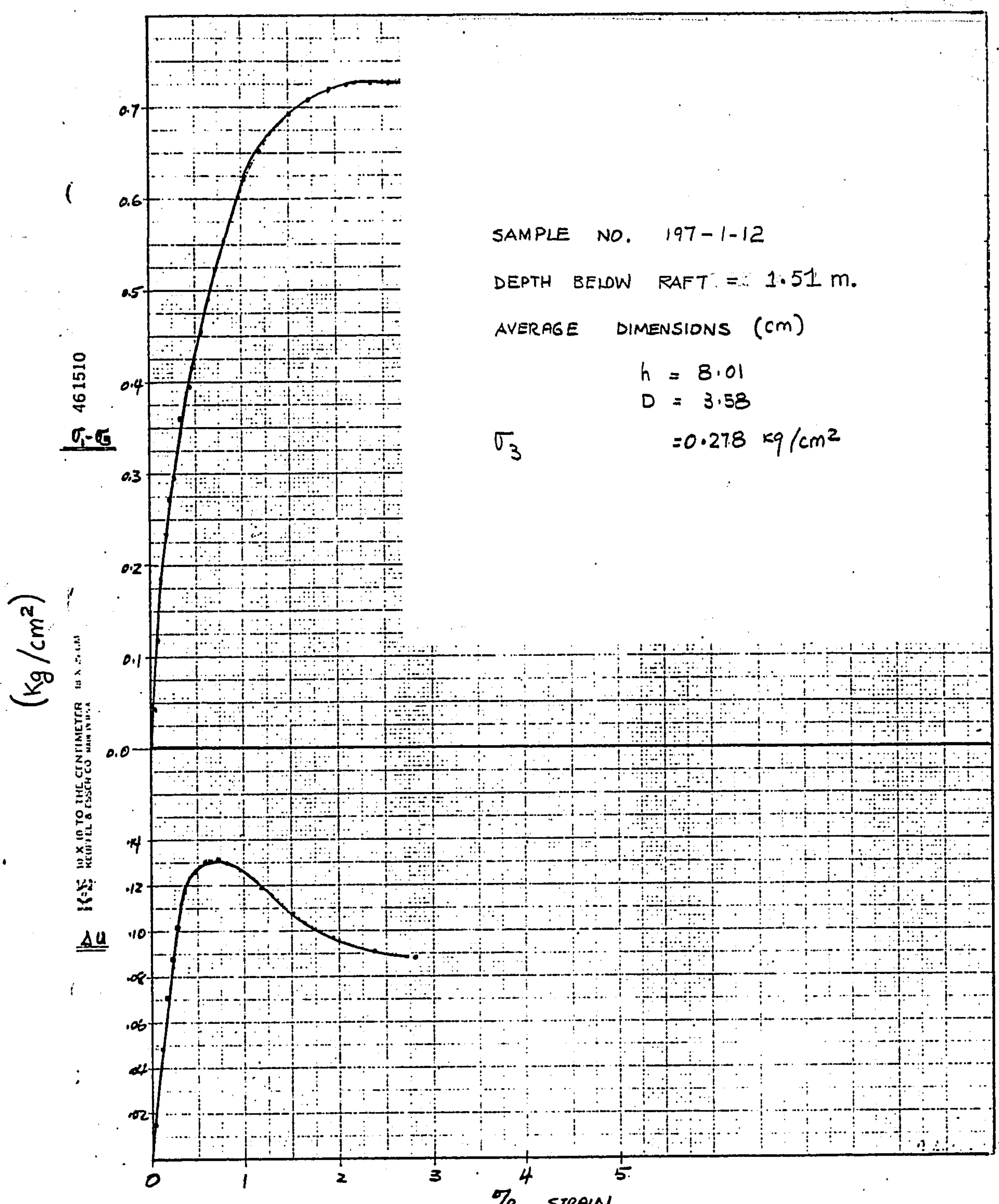
SAMPLE NO. 197-1-12
DEPTH BELOW RAFT = 1.51 m.
AVERAGE DIMENSIONS (cm)
h = 8.01
D = 3.58
σ3 = 0.278 kg/cm²
σ1-σ3
Δu
(kg/cm²)
% STRAIN
0
1
2
3
4
5
0.0
0.1
0.2
0.3
0.4
0.5
0.6
0.7
.02
.04
.06
.08
.10
.12
.14
461510

FIGURE B-14

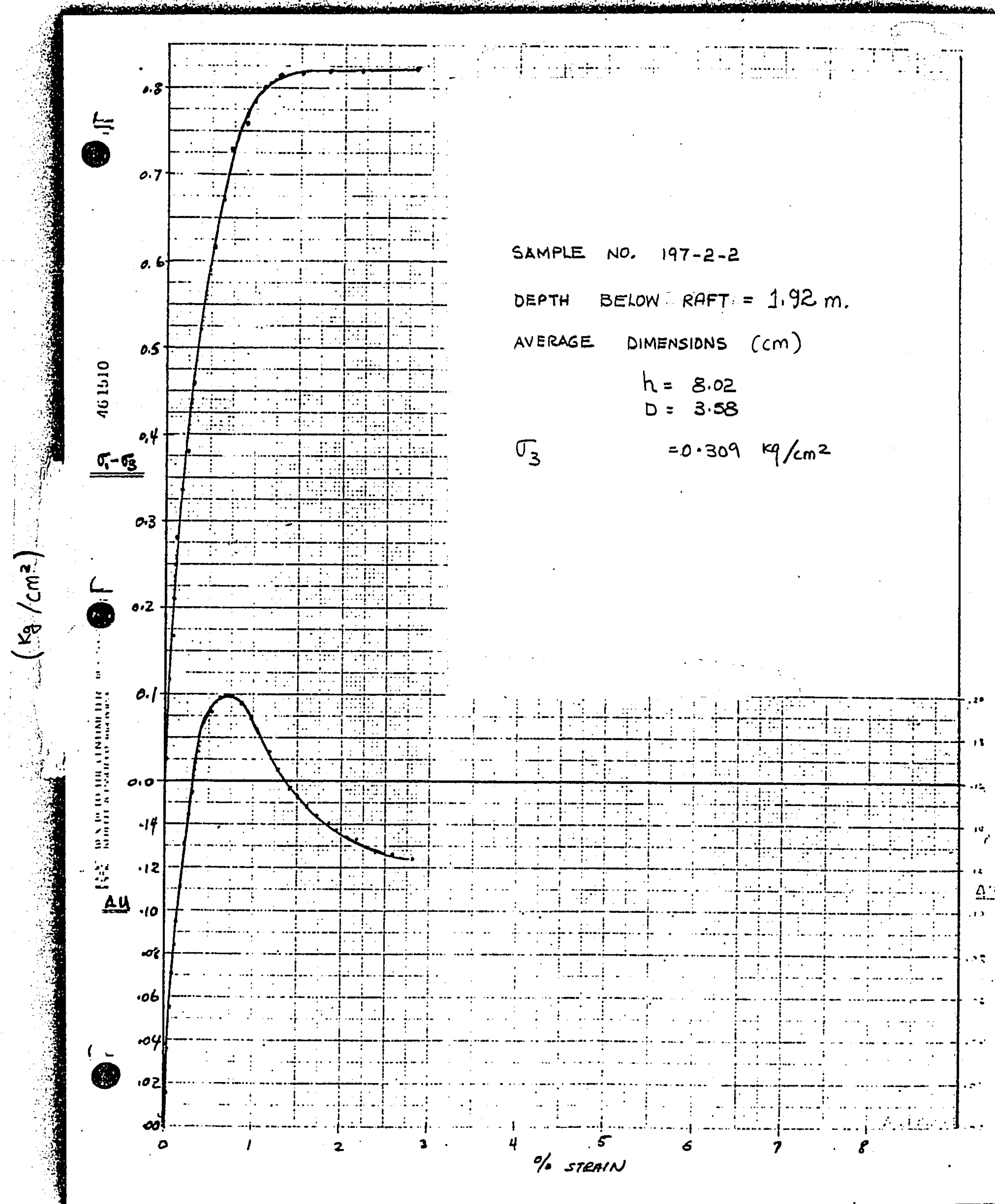
SAMPLE NO. 197-2-2
DEPTH BELOW RAFT = 1.92 m.
AVERAGE DIMENSIONS (cm)
h = 8.02
D = 3.58
σ3 =0.309 kg/cm²
σ1-σ3
(kg/cm²)
ΔU
% STRAIN
0.8
0.7
0.6
0.5
0.4
0.3
0.2
0.1
0.0
.14
.12
.10
.08
.06
.04
.02
.00
0
1
2
3
4
5
6
7
8

FIGURE B-15

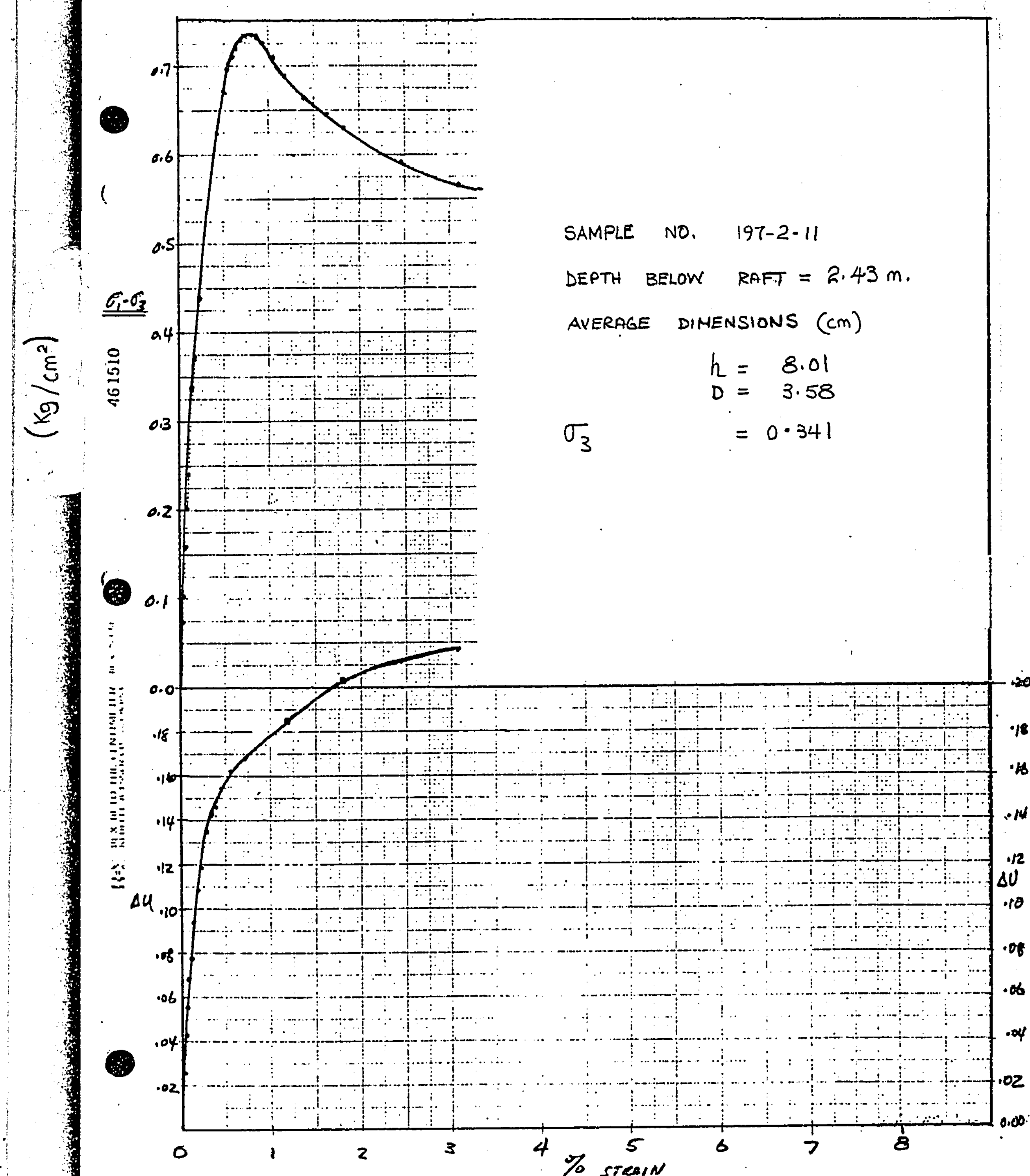
SAMPLE NO. 197-2-11
DEPTH BELOW RAFT = 2.43 m.
AVERAGE DIMENSIONS (cm)
h = 8.01
D = 3.58
σ3 = 0·341
σ1-σ3
(Kg/cm²)
ΔU
% STRAIN
0
1
2
3
4
5
6
7
8

FIGURE B-16

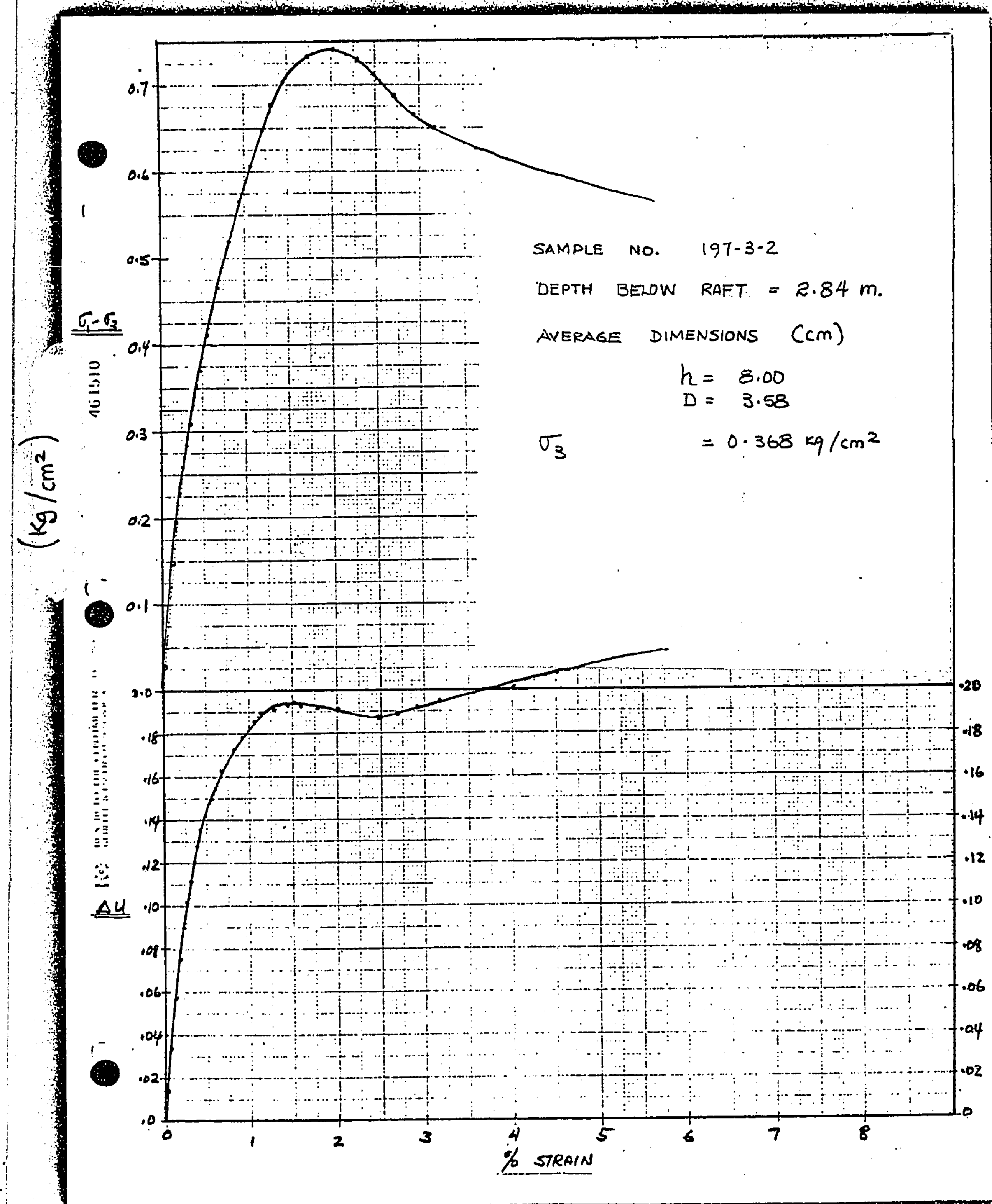
SAMPLE NO. 197-3-2
DEPTH BELOW RAFT = 2.84 m.
AVERAGE DIMENSIONS (cm)
h = 8.00
D = 3.58
σ3 = 0.368 kg/cm²
σ1 - σ3
(kg/cm²)
ΔU
% STRAIN
0.7
0.6
0.5
0.4
0.3
0.2
0.1
0.0
.18
.16
.14
.12
.10
.08
.06
.04
.02
.0
.20
0
1
2
3
4
5
6
7
8

FIGURE B-17

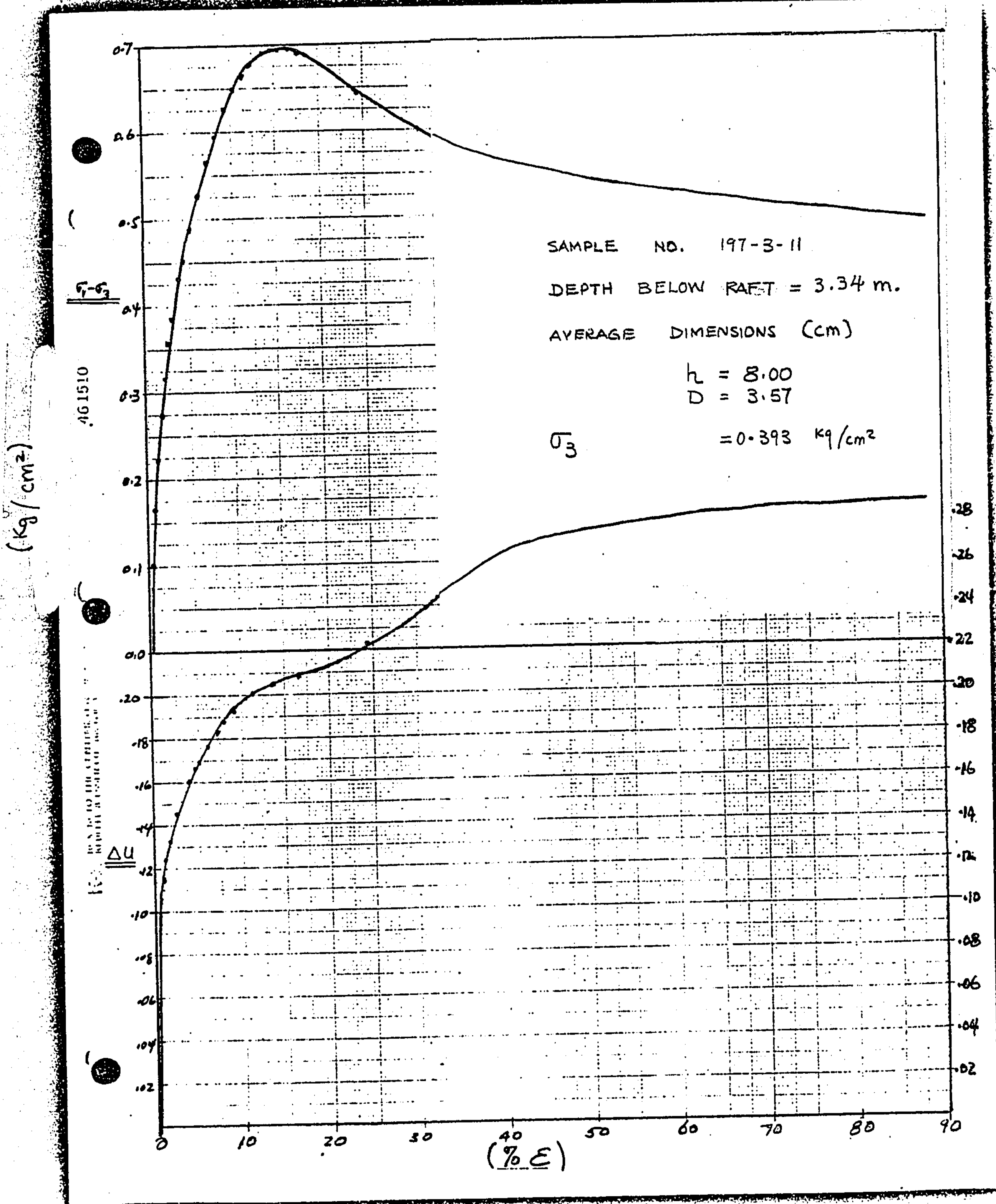

SAMPLE NO. 197-3-11
DEPTH BELOW RAFT = 3.34 m.
AVERAGE DIMENSIONS (cm)
h = 8.00
D = 3.57
σ3 =0.393 Kg/cm²
σ1-σ3
(Kg/cm²)
Δu
(% ε)

FIGURE B-18

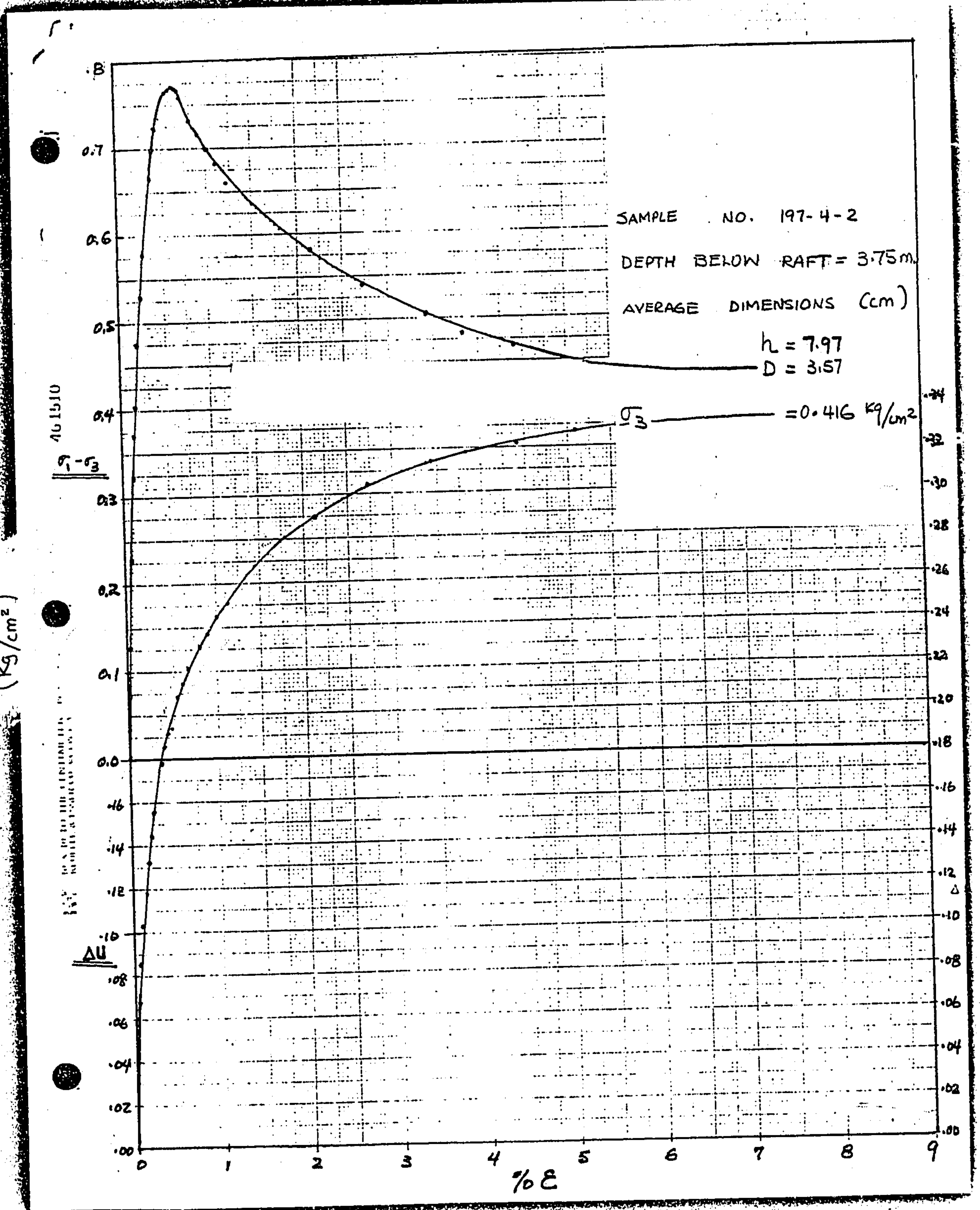
SAMPLE NO. 197-4-2
DEPTH BELOW RAFT = 3.75m.
AVERAGE DIMENSIONS (cm)
h = 7.97
D = 3.57
σ3 = 0.416 kg/cm²
σ1 - σ3
ΔU
(Kg/cm²)
% ε
.8
0.7
0.6
0.5
0.4
0.3
0.2
0.1
0.0
.16
.14
.12
.10
.08
.06
.04
.02
.00
0
1
2
3
4
5
6
7
8
9

FIGURE B-19

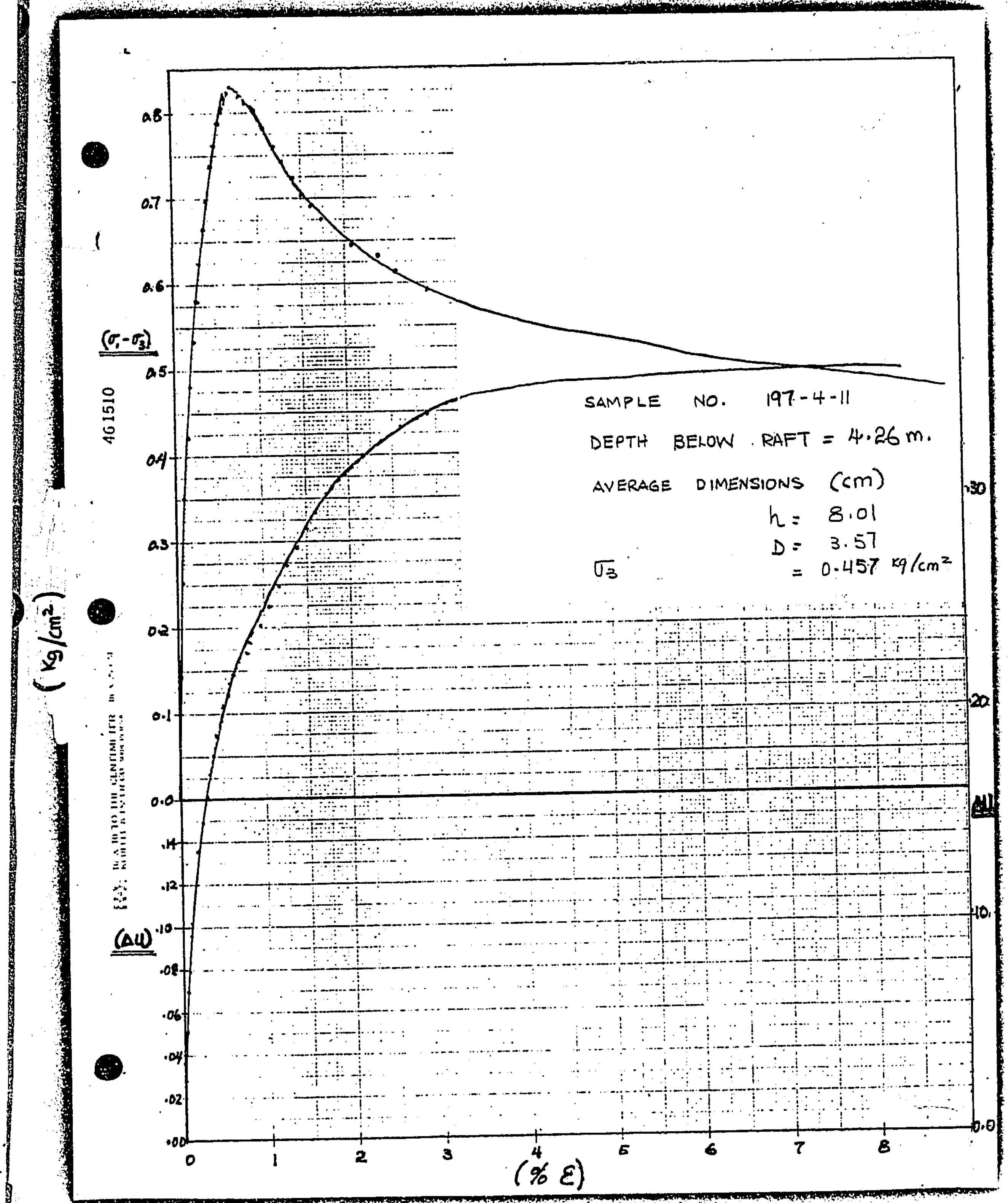

0.8
0.7
0.6
$(\sigma_1 - \sigma_3)$
0.5
0.4
0.3
0.2
0.1
0.0
.14
.12
.10
(Δu)
.08
.06
.04
.02
.00
(Kg/cm²)
4G1510
0
1
2
3
4
5
6
7
8
(% ε)
30
20
10
0.0
Δu
SAMPLE NO. 197-4-11
DEPTH BELOW RAFT = 4.26 m.
AVERAGE DIMENSIONS (cm)
h = 8.01
D = 3.57
σ3 = 0.457 kg/cm²

FIGURE B-20

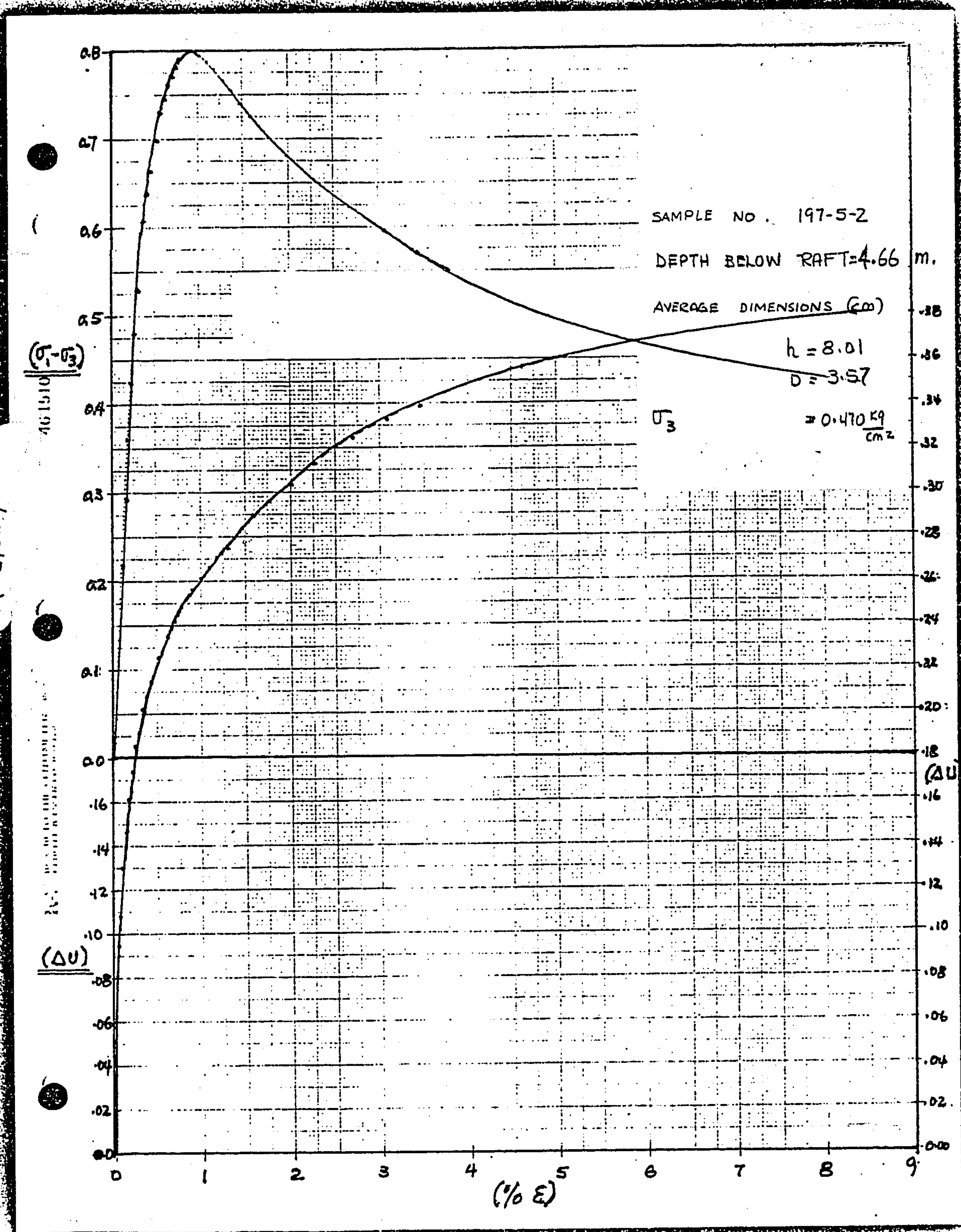
SAMPLE NO. 197-5-2
DEPTH BELOW RAFT=4.66 m.
AVERAGE DIMENSIONS (cm)
h = 8.01
D = 3.57
σ_3 = 0.470 kg/cm²
$(\sigma_1-\sigma_3)$
(kg/cm²)
(ΔU)
(ΔU)
(% ε)
0 1 2 3 4 5 6 7 8 9

FIGURE B-21

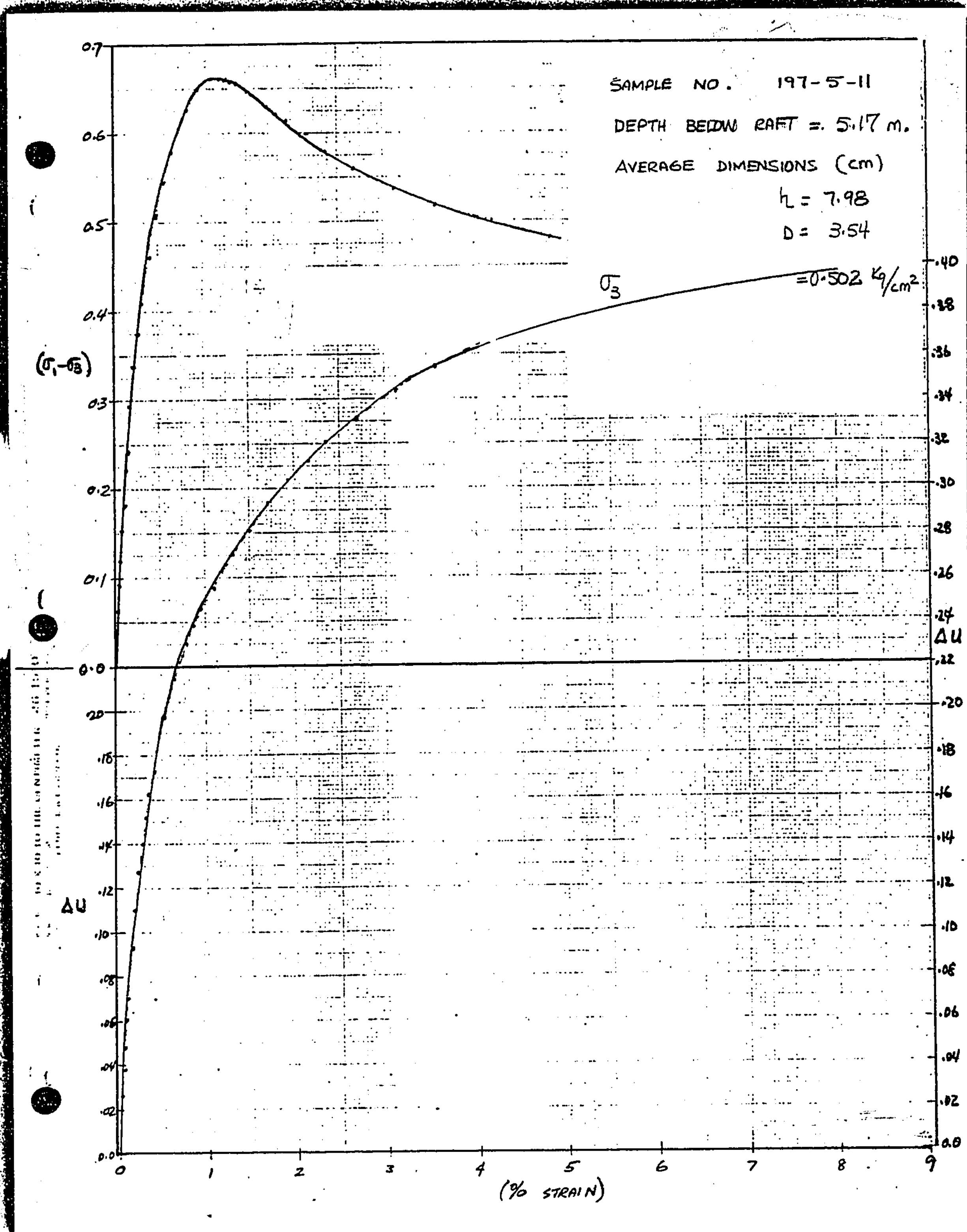
SAMPLE NO. 197-5-11
DEPTH BELOW RAFT = 5.17 m.
AVERAGE DIMENSIONS (cm)
h = 7.98
D = 3.54
σ_3
= 0.502 Kg/cm²
(σ_1-σ_3)
(Kg/cm²)
ΔU
ΔU
(% STRAIN)
0
1
2
3
4
5
6
7
8
9
0.7
0.6
0.5
0.4
0.3
0.2
0.1
0.0
.20
.18
.16
.14
.12
.10
.08
.06
.04
.02
0.0
.40
.38
.36
.34
.32
.30
.28
.26
.24
.22
.20
.18
.16
.14
.12
.10
.08
.06
.04
.02
0.0

FIGURE B-22

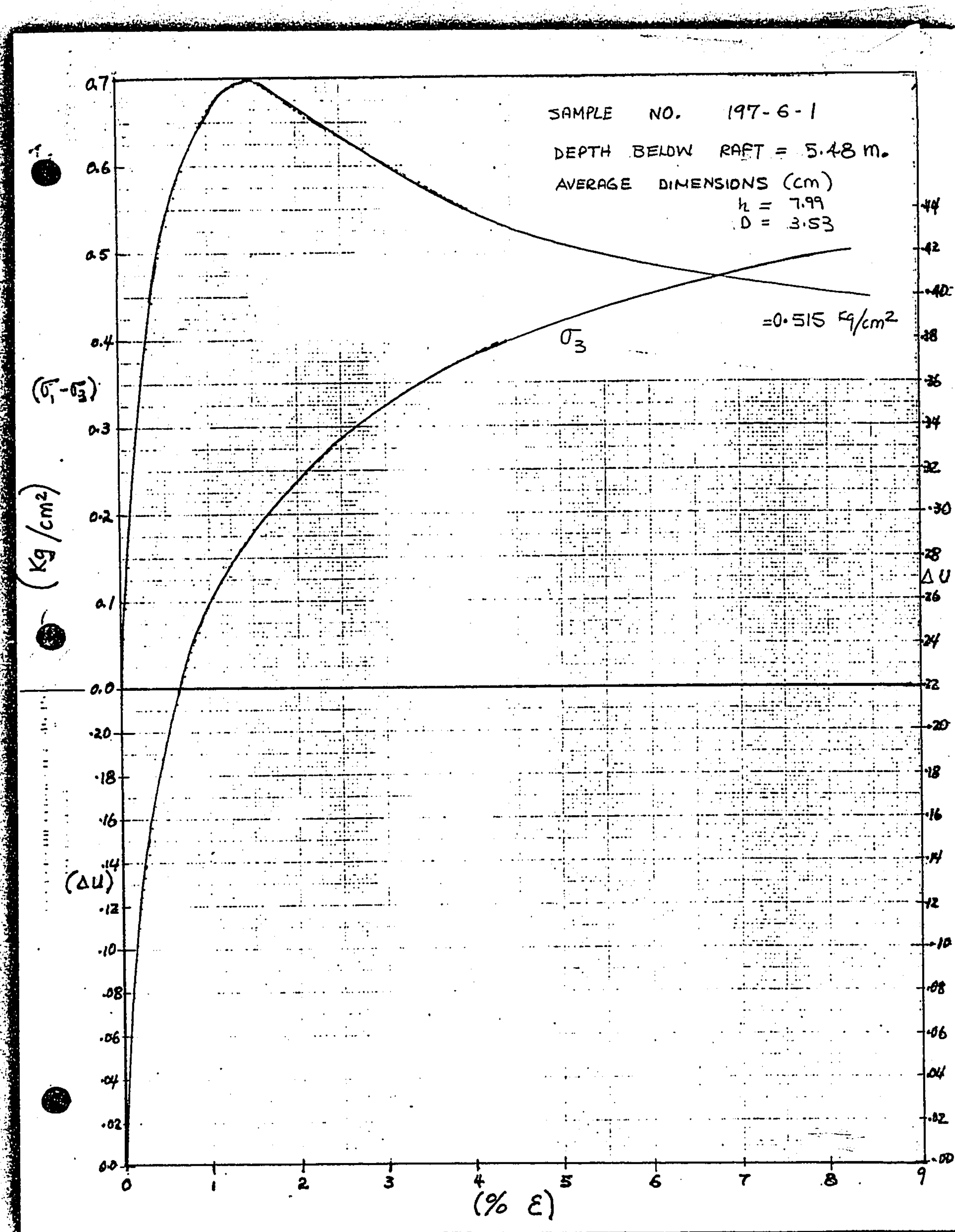

SAMPLE NO. 197-6-1
DEPTH BELOW RAFT = 5.48 m.
AVERAGE DIMENSIONS (cm)
h = 7.99
D = 3.53
=0.515 Kg/cm²
σ3
(σ1-σ3)
(Kg/cm²)
(Δu)
ΔU
(% ε)

FIGURE B-23

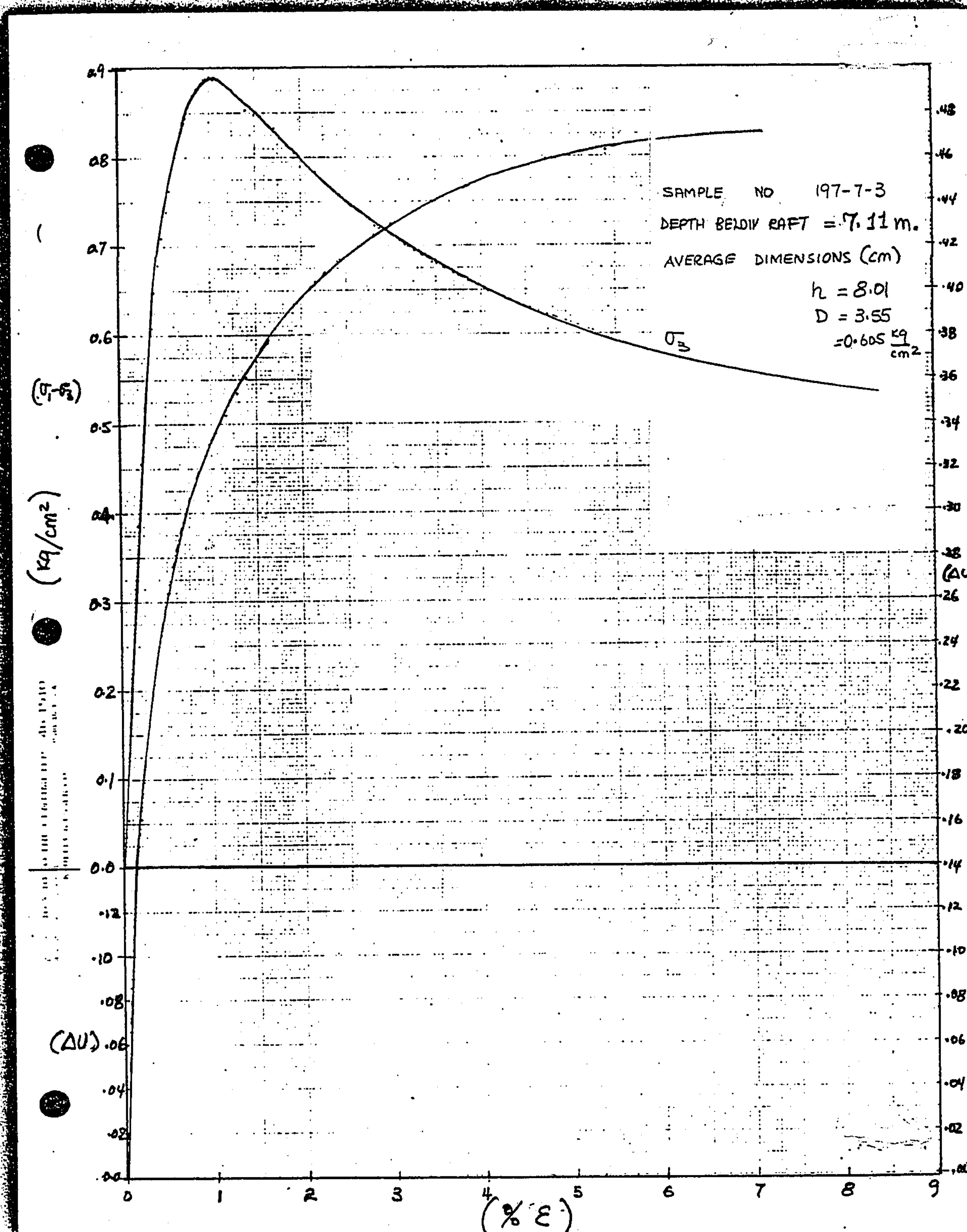
SAMPLE NO 197-7-3
DEPTH BELOW RAFT = 7.11 m.
AVERAGE DIMENSIONS (cm)
h = 8.01
D = 3.55
=0.605 kg/cm2
σ3
(σ1-σ3)
(kg/cm²)
(ΔU)
(% ε)

FIGURE B-24

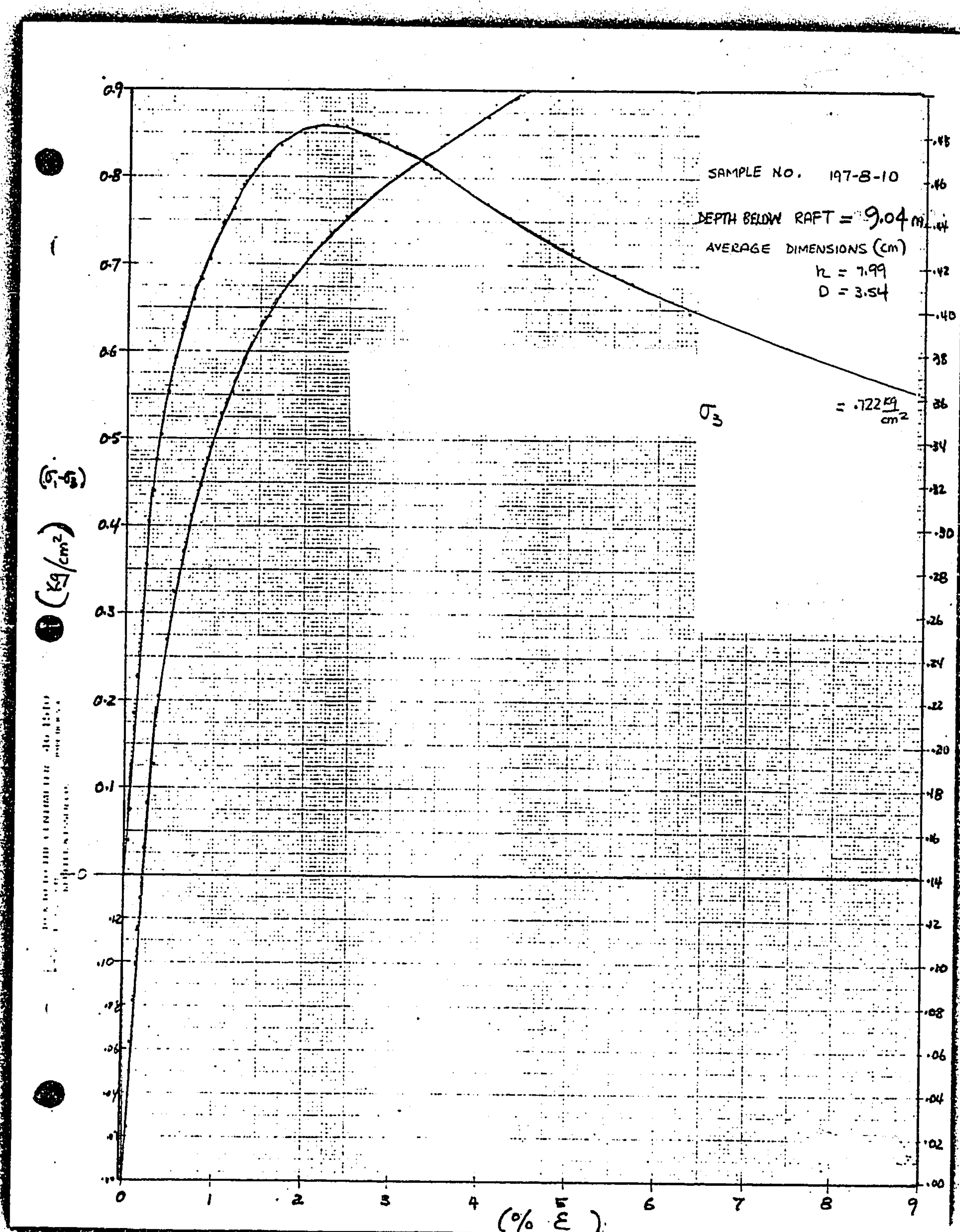
SAMPLE NO. 197-8-10
DEPTH BELOW RAFT = 9.04 m
AVERAGE DIMENSIONS (cm)
h = 7.99
D = 3.54
σ_3 = .722 kg/cm²
(σ_1-σ_3) (kg/cm²)
(% ε)

FIGURE B-25

OEDOMETER TEST SUMMARY

Sample No.	Depth (m)	w%	Size, cm, cm^2		$P_c (kg/cm^2)$			P_o (kg/cm^2)	e_o
			Height	Area	Min	Prob	Max		
197- 1- 1	1.58	36.35	2.03	20.11	1.16	1.75	1.93	.31	1.036
197- 1-13	2.32	29.59	2.01	20.11	1.00	1.87	2.08	.39	.844
197- 2- 9	3.00	48.78	2.00	20.02	.95	1.10	1.12	.45	1.395
197- 4- 3	4.52	40.66	2.01	20.11	.75	.84	.87	.57	1.155
197- 5-12	5.95	48.79	2.00	20.02	.86	.95	.96	.67	1.381
197- 7- 2	7.67	50.15	1.99	20.07	.79	.95	.97	.80	1.435
197- 7-12	8.38	57.68	1.99	20.07	.97	1.11	1.15	.86	1.613
197- 8- 2	9.25	58.94	2.00	20.02	.93	1.05	1.08	.922	1.636
197- 9- 3	12.45	63.10	2.01	20.11	1.49	1.58	1.60	1.163	1.775
197-10- 3	15.50	50.90	2.01	20.03	1.51	1.72	1.76	1.38	T 1.446
197-10- 3	15.50	50.98	1.99	20.06	1.43	1.58	1.61	1.38	B 1.448
197-11-11	19.05	60.37	2.00	20.06	2.44	2.67	2.73	1.62	1.729

Ave. Diameter of Samples = 5.05 cm (1.99 in.)

Notes: T, B, stand for top and bottom of test specimen from the same 15.25 cm, (6 in.) sample.
Depths shown are from original ground surface.

TABLE B-26

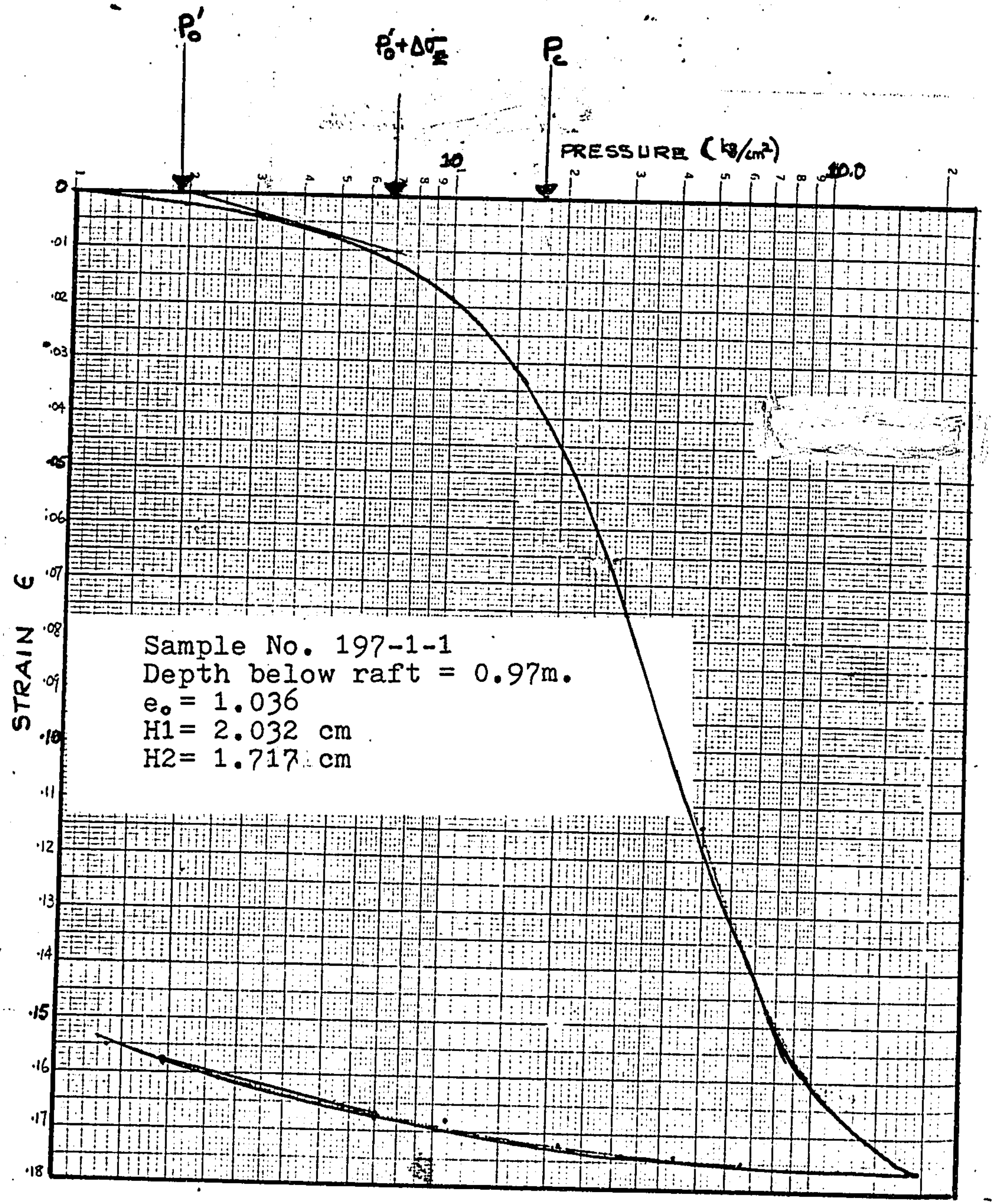

P_o'
$P_o'+\Delta\sigma_z$
P_c
PRESSURE (kg/cm²)
10
10.0
STRAIN ε
Sample No. 197-1-1
Depth below raft = 0.97m.
e_o = 1.036
H1= 2.032 cm
H2= 1.717 cm

FIGURE B-27

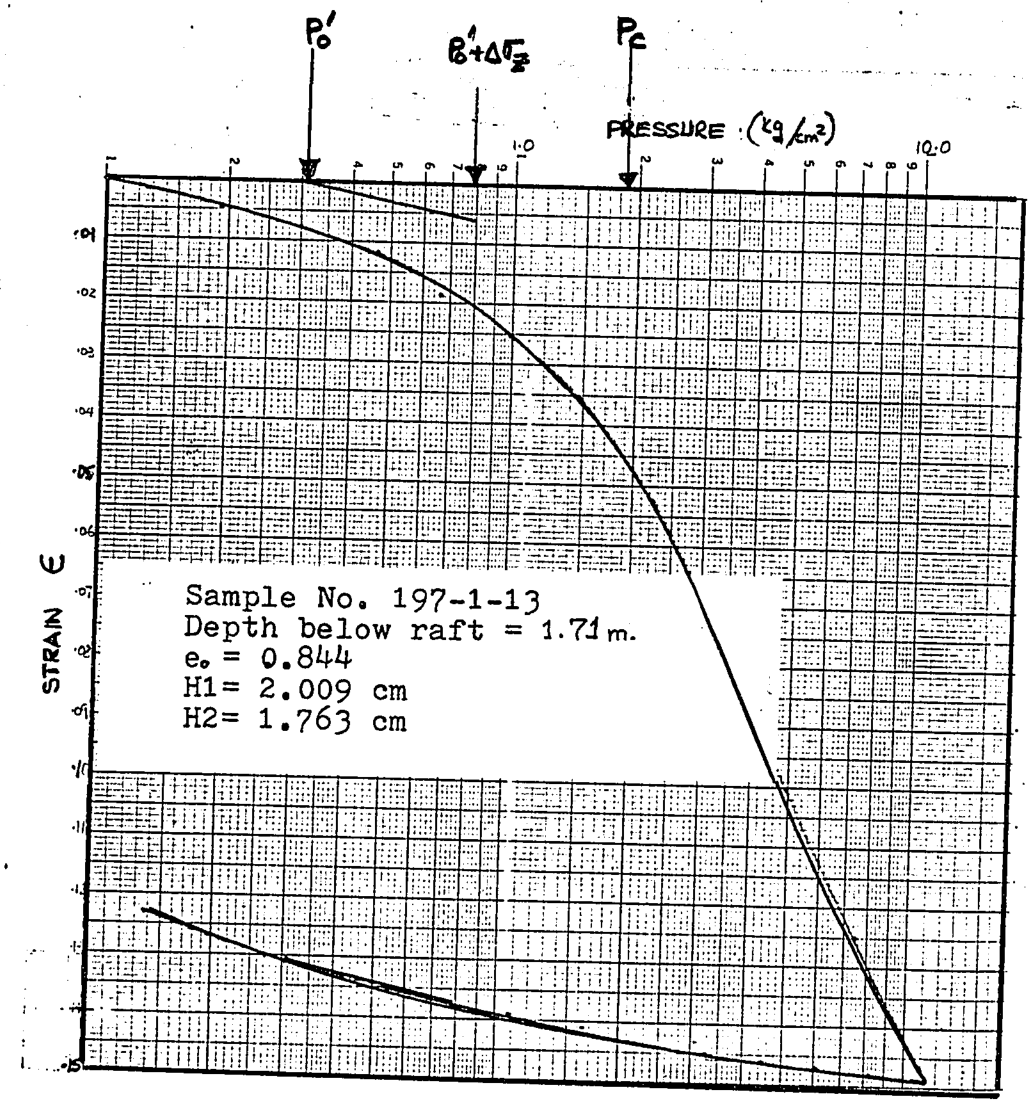

P_o'
$P_o'+\Delta\sigma_z$
P_c
PRESSURE : (kg/cm²)
1.0
10.0
STRAIN ∈
Sample No. 197-1-13
Depth below raft = 1.71 m.
e₀ = 0.844
H1= 2.009 cm
H2= 1.763 cm

FIGURE B-28

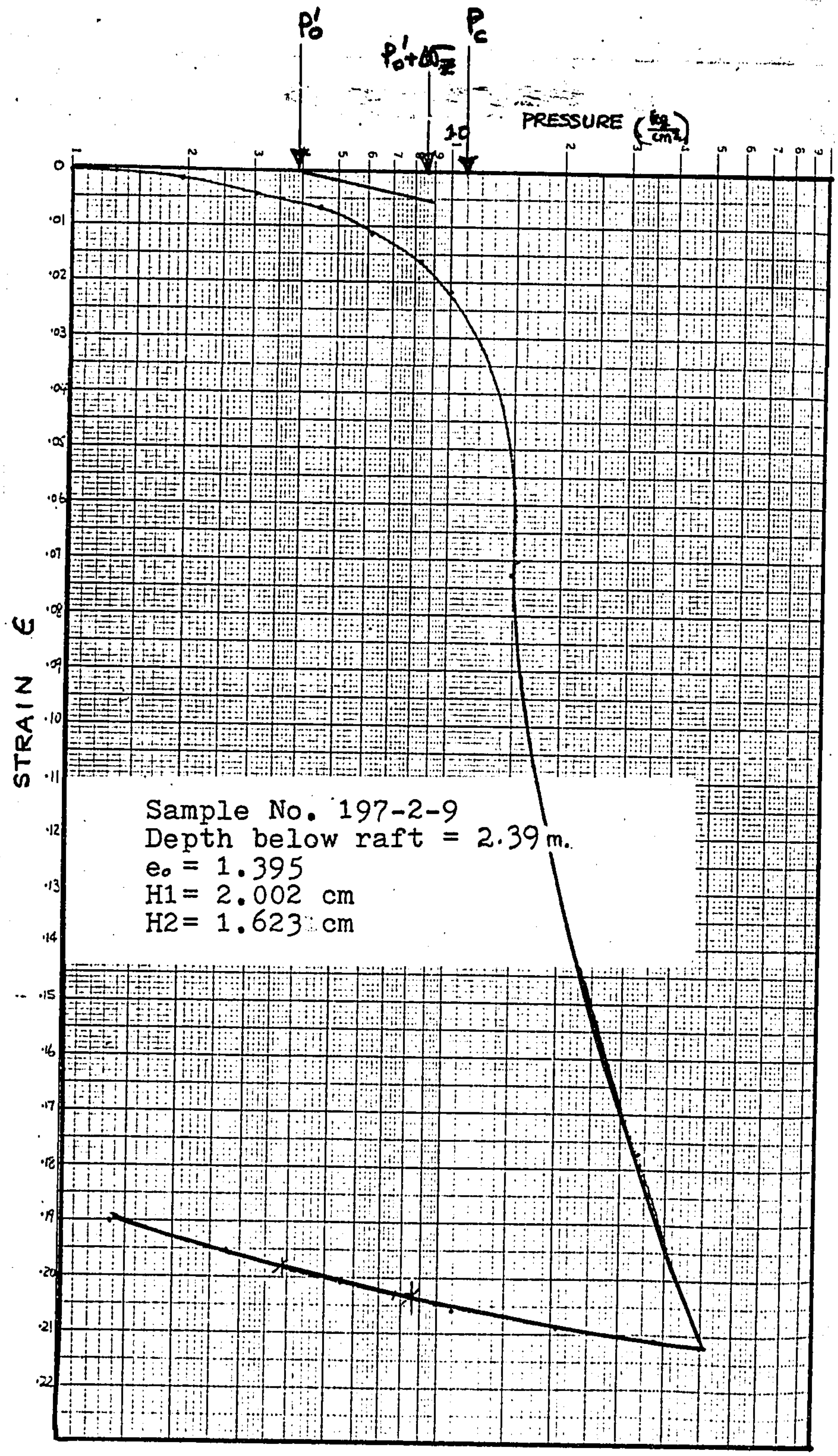
P_o'
$P_o'+\Delta\sigma_z$
P_c
PRESSURE (kg/cm²)
STRAIN ε
Sample No. 197-2-9
Depth below raft = 2.39 m.
e₀ = 1.395
H1= 2.002 cm
H2= 1.623 cm

FIGURE B-29

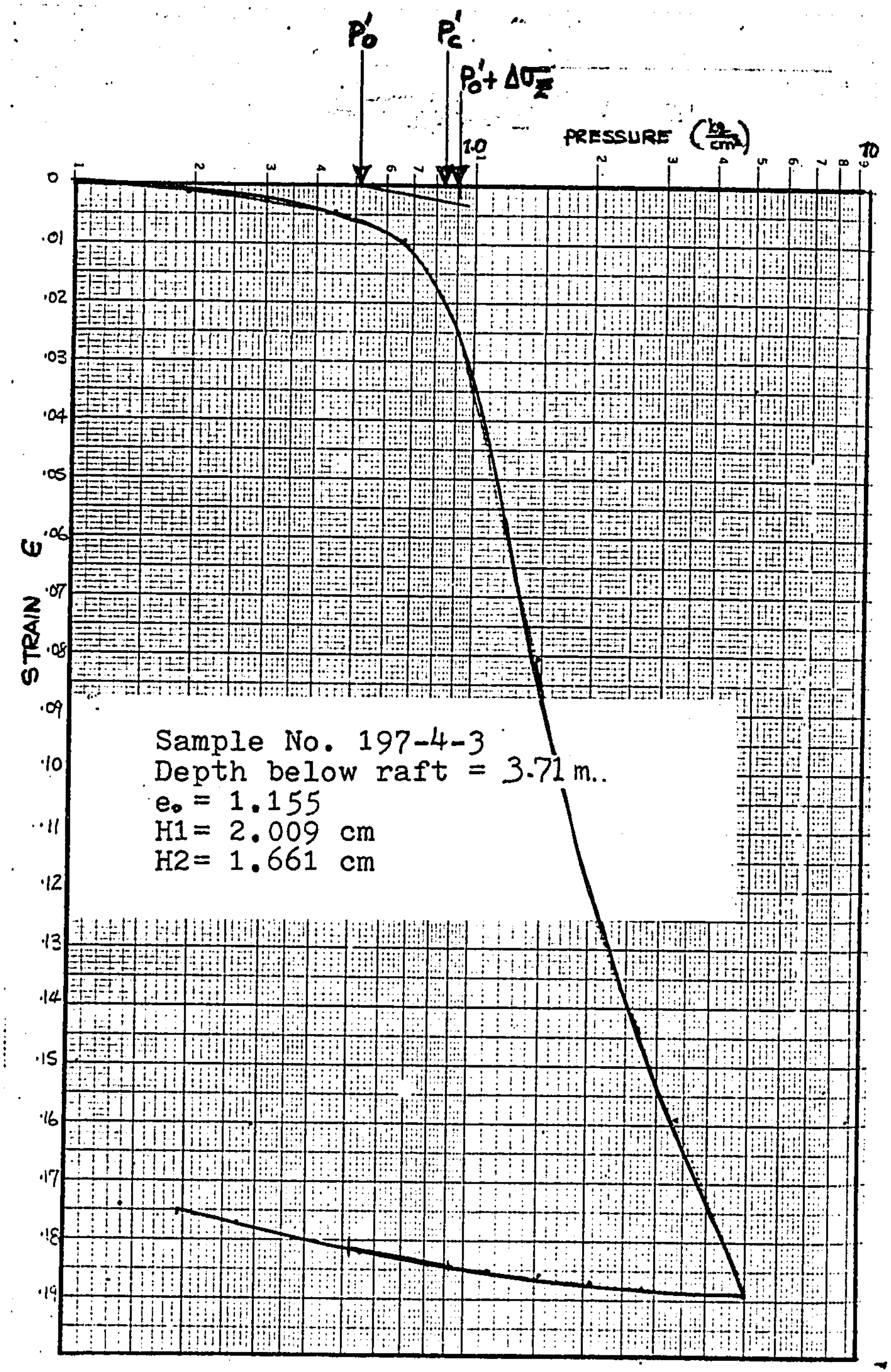
P'o
P'c
P'o + Δσz
PRESSURE (kg/cm²)
1.0
10
STRAIN ε
Sample No. 197-4-3
Depth below raft = 3.71 m.
e₀ = 1.155
H1= 2.009 cm
H2= 1.661 cm

FIGURE B-30

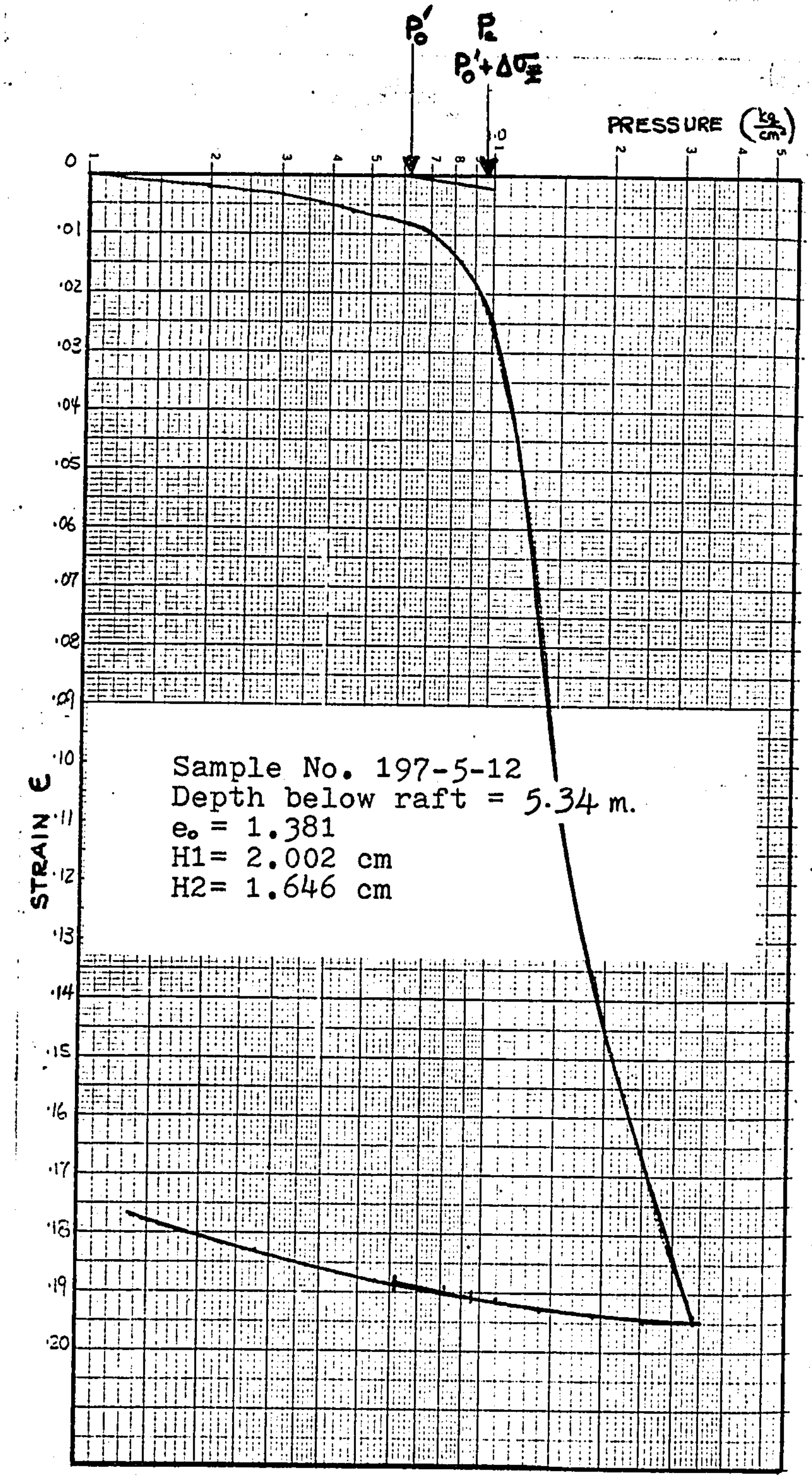

P_o'
P_c
$P_o' + \Delta\sigma_z$
PRESSURE (kg/cm²)
STRAIN ε
0
·01
·02
·03
·04
·05
·06
·07
·08
·09
·10
·11
·12
·13
·14
·15
·16
·17
·18
·19
·20
Sample No. 197-5-12
Depth below raft = 5.34 m.
e₀ = 1.381
H1= 2.002 cm
H2= 1.646 cm

FIGURE B-31

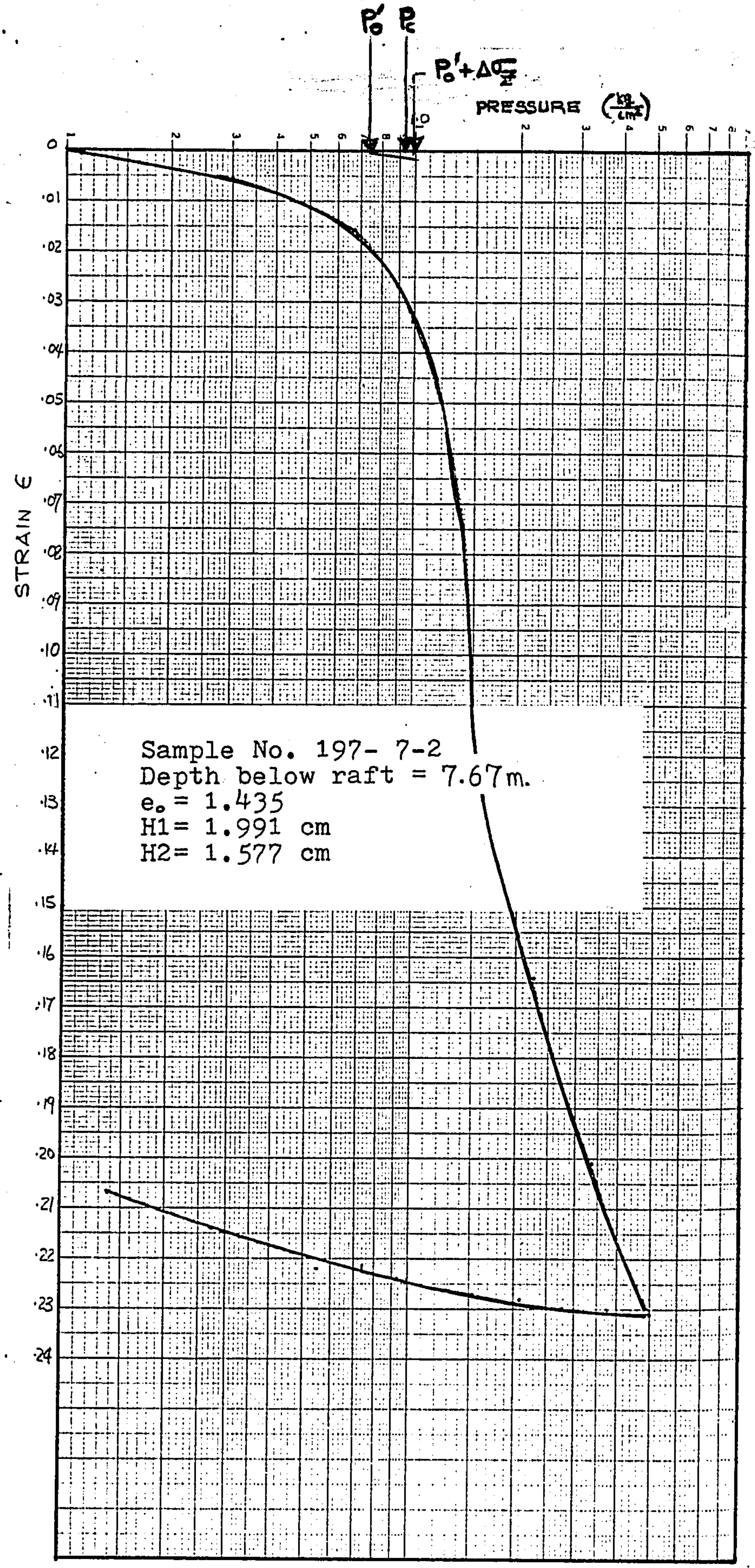
P'o
Pc
P'o+Δσz
PRESSURE (kg/cm²)
STRAIN ϵ
Sample No. 197- 7-2
Depth below raft = 7.67m.
e₀= 1.435
H1= 1.991 cm
H2= 1.577 cm

FIGURE B-32

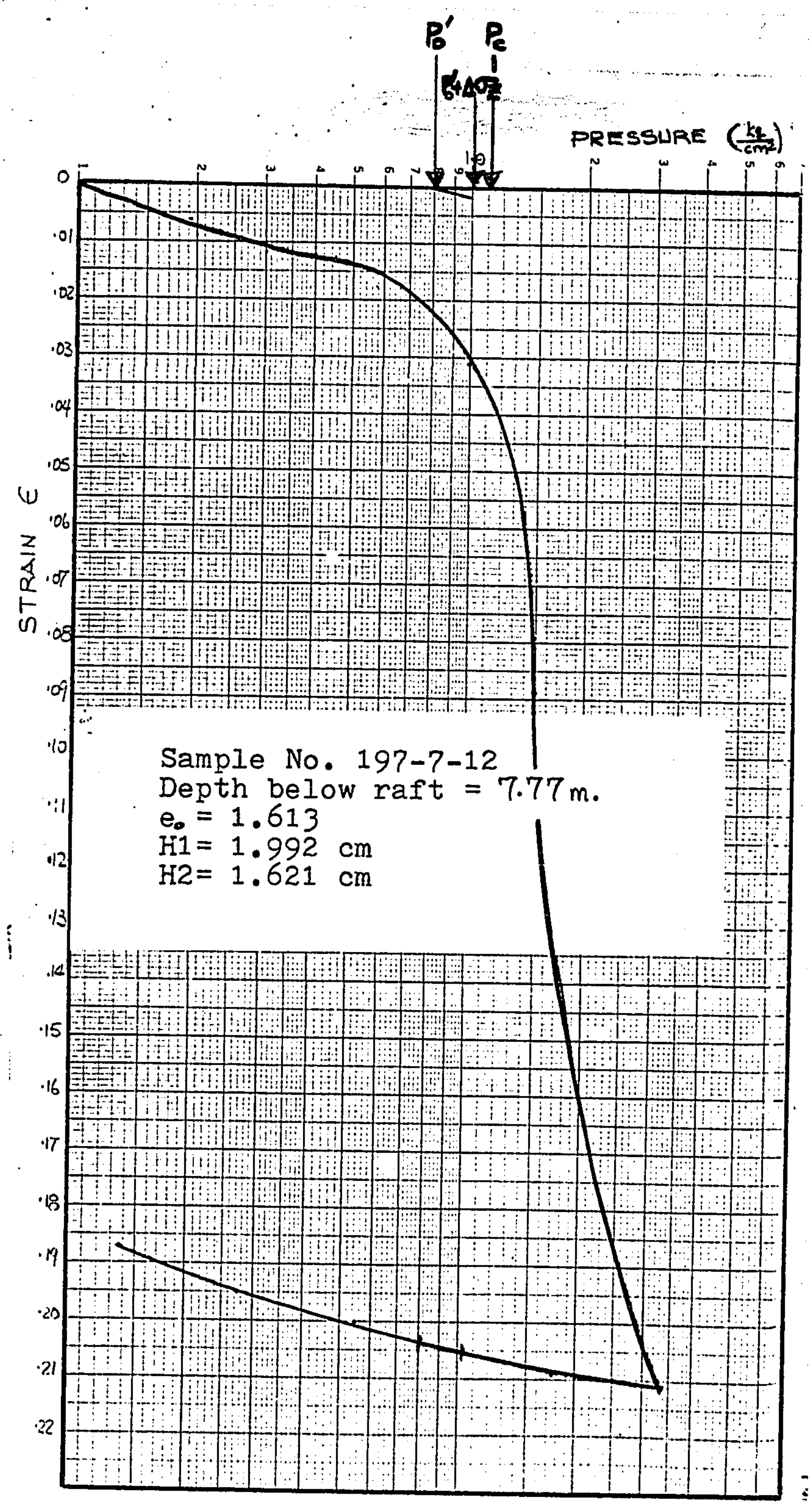
PRESSURE (kg/cm²)
STRAIN ε
Sample No. 197-7-12
Depth below raft = 7.77 m.
e₀ = 1.613
H1= 1.992 cm
H2= 1.621 cm

FIGURE B-33

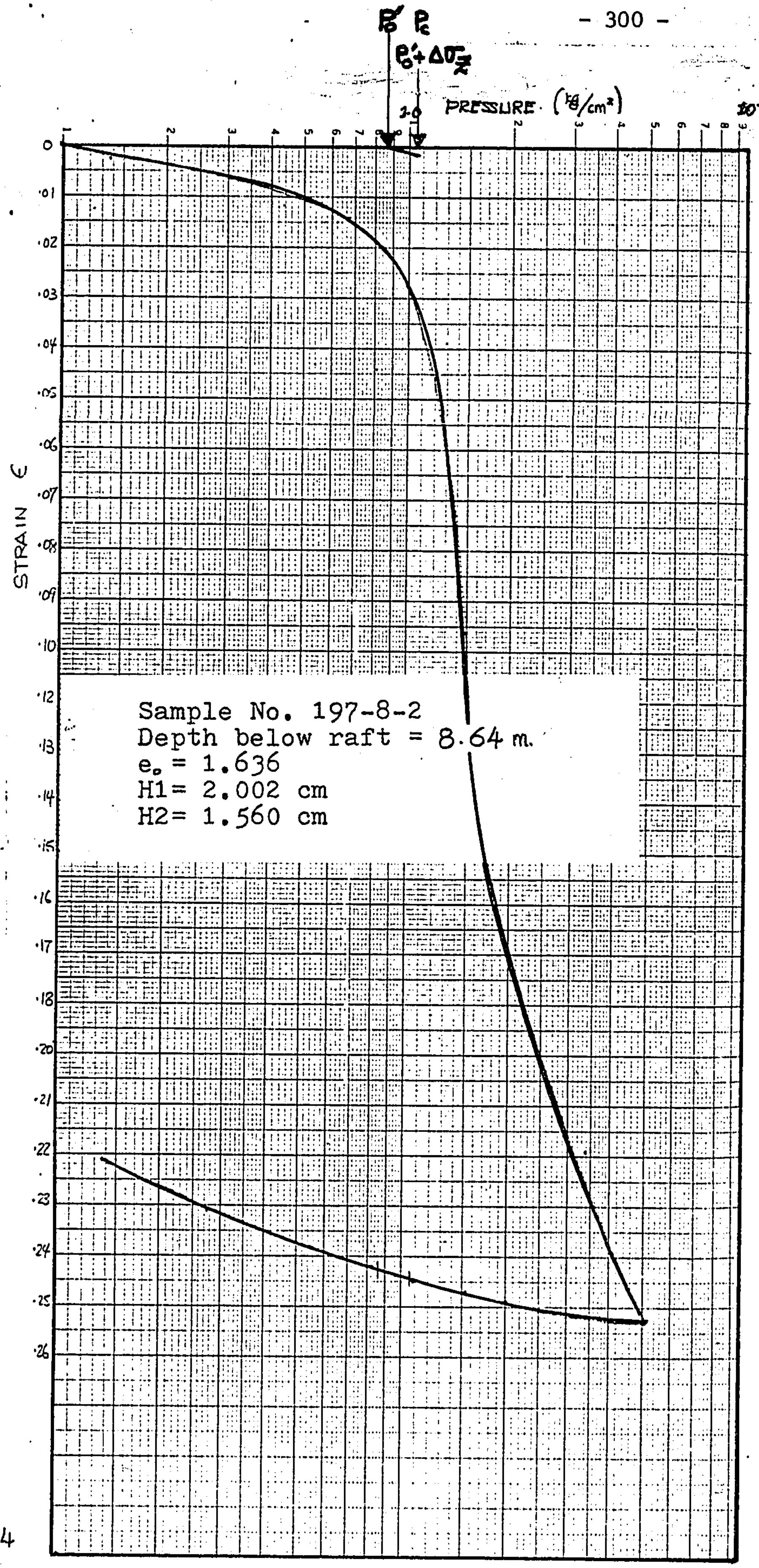
PRESSURE (kg/cm²)
STRAIN ε
Sample No. 197-8-2
Depth below raft = 8.64 m.
e₀ = 1.636
H1= 2.002 cm
H2= 1.560 cm

FIGURE B-34

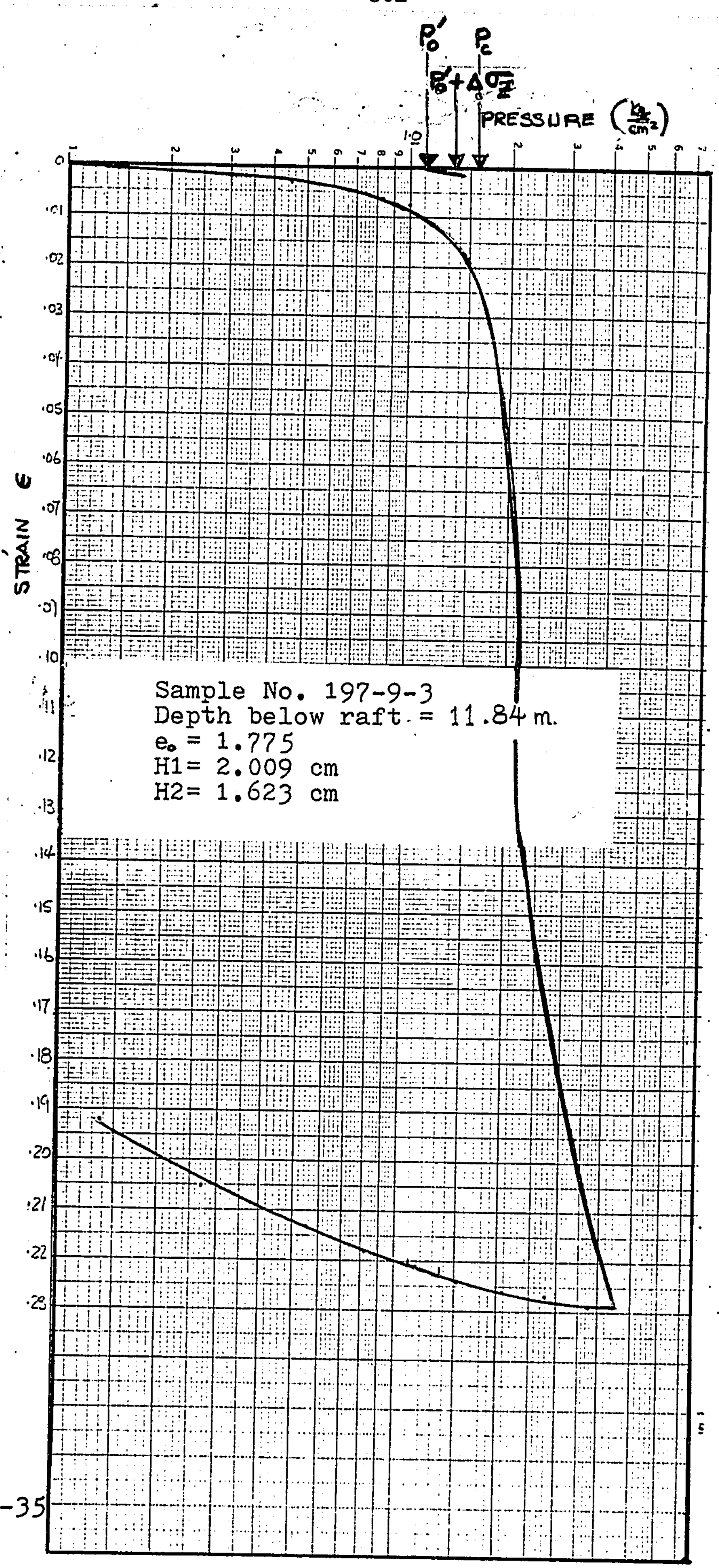
P_o'
P_c
$P_o' + \Delta\sigma_z$
PRESSURE $\left(\frac{kg}{cm^2}\right)$
STRAIN ϵ
Sample No. 197-9-3
Depth below raft = 11.84 m.
e_o = 1.775
H1= 2.009 cm
H2= 1.623 cm

FIGURE B-35

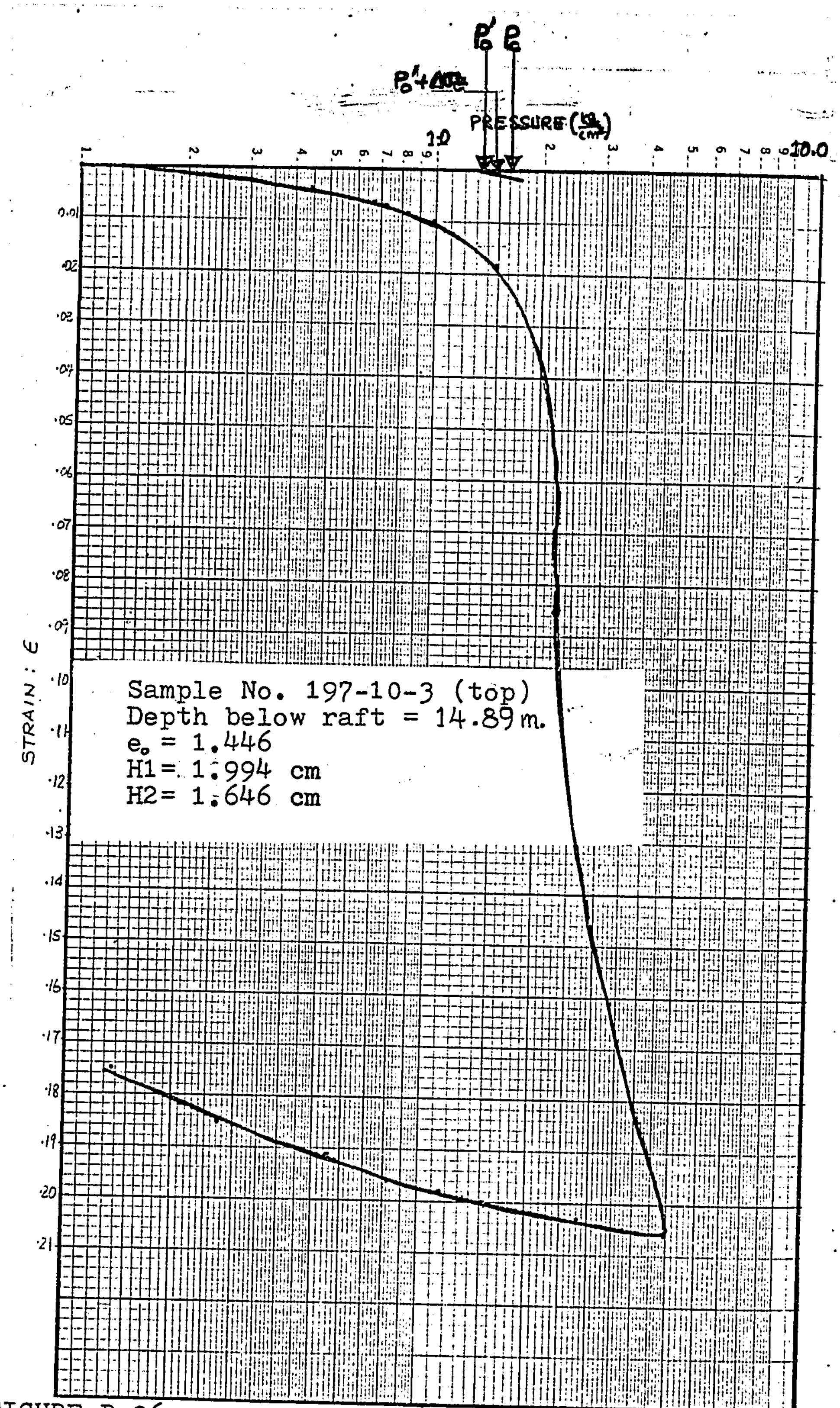

$P_o' + \Delta\sigma$
P_o' P_c
PRESSURE (kg/cm²)
1.0
10.0
STRAIN : ε
Sample No. 197-10-3 (top)
Depth below raft = 14.89 m.
e_o = 1.446
H1 = 1.994 cm
H2 = 1.646 cm

FIGURE B-36

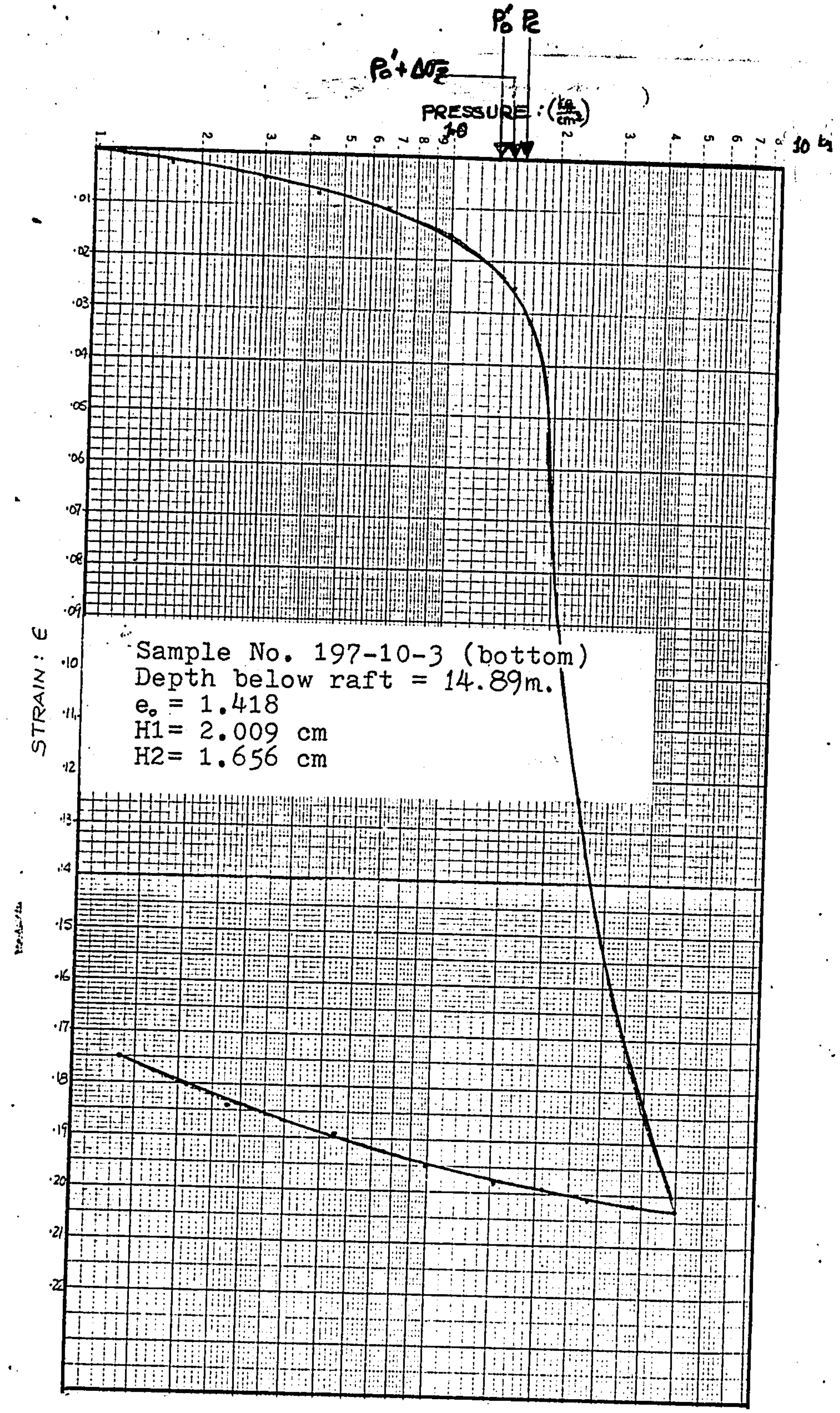
P_o' P_c
$P_o'+\Delta\sigma_z$
PRESSURE : ($\frac{kg}{cm^2}$)
1.0
10
STRAIN : ε
Sample No. 197-10-3 (bottom)
Depth below raft = 14.89m.
e_o = 1.418
H1= 2.009 cm
H2= 1.656 cm

FIGURE B-37

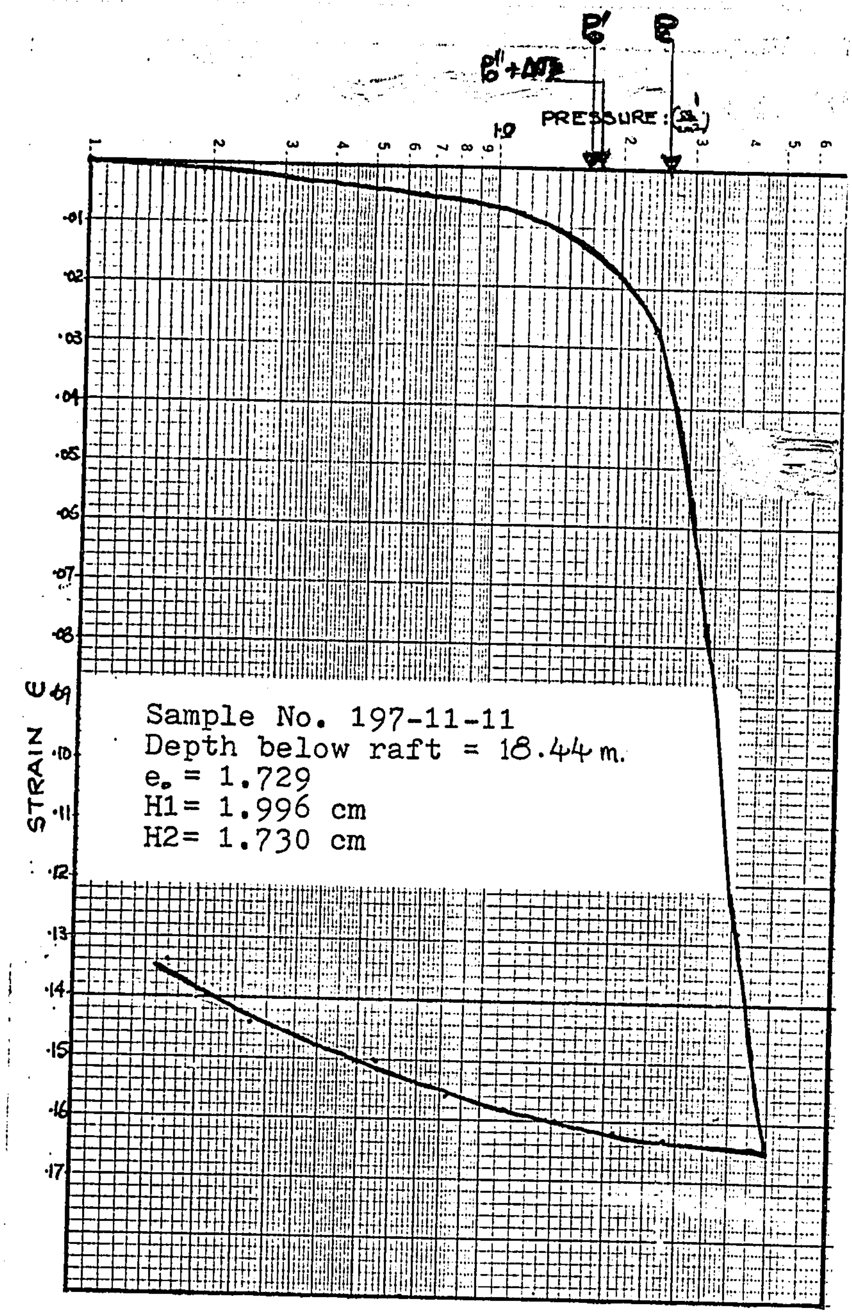
PRESSURE
STRAIN ε
Sample No. 197-11-11
Depth below raft = 18.44 m.
e_o = 1.729
H1= 1.996 cm
H2= 1.730 cm

FIGURE B-38

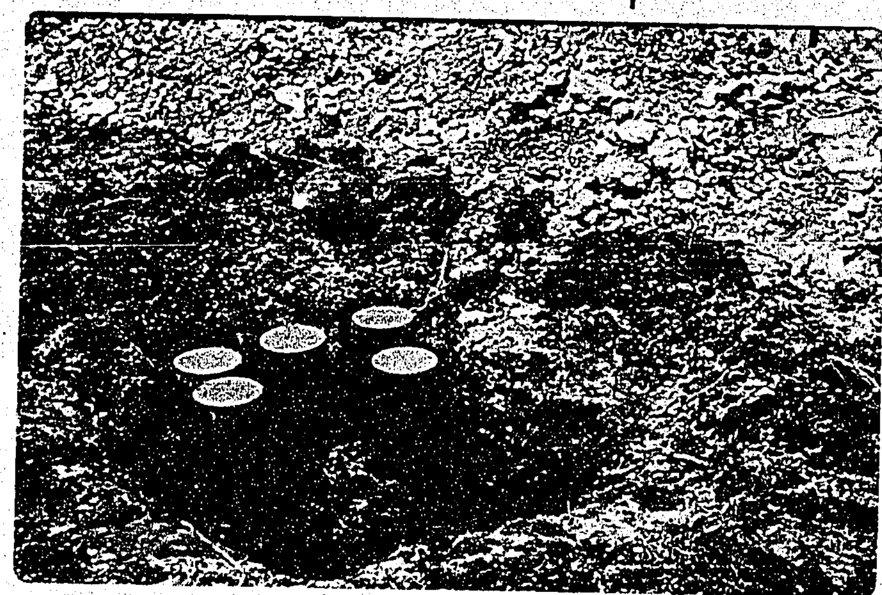

CONGRETE CYLINDERS CURED UNDER SITE CONDITIONS

LABORATORY TEST RESULTS

Curing Time (Days)	Compressive Strength f_c ($\frac{psi}{Mpa}$)			Young's Modulus E ($\frac{psi}{Mpa}$)			Tensile Strength f_t ($\frac{psi}{Mpa}$)		
	1	2	3	1	2	3	1	2	3
7	($\frac{2900}{20.0}$)	($\frac{2759}{19.0}$)	($\frac{2447}{16.9}$)	-	-	-	Stress units are psi and Mpa		
14	x	($\frac{2652}{18.3}$)	($\frac{2830}{19.5}$)	-	-	-			
28	($\frac{3180}{21.9}$)	($\frac{3610}{24.9}$)	($\frac{3470}{23.9}$)	3.42×10^6 2.5×10^4	3.64×10^6 2.5×10^4	3.57×10^6 2.5×10^4	($\frac{390}{2.7}$)	($\frac{473}{3.3}$)	($\frac{394}{2.7}$)

Cylinder Size: D = 6", L = 12"

Average u.w., γ = 150 pcf

$f_t = \frac{2P}{\Pi LD}$; where P = splitting load

$E = \gamma^{1.5}\ 33\ \sqrt{f_c}$ (ACI 318-71)

FIGURE B-39